Instabilities in Sixth Order Cahn-Hilliard Type Equations

Boyle, Benedict

Award date:
2017

Awarding institution:
University of Bath

Instabilities in Sixth Order Cahn-Hilliard Type Equations

submitted by

Benedict Boyle

for the degree of Doctor of Philosophy

of the

University of Bath

Department of Mathematical Sciences

September 2016

Summary

This thesis is mostly concerned with understanding the multiplicity and geometric structure of asymptotic patterns that arise from the Cauchy problem for the equations

$$u_t = \Delta^3 u \pm \Delta^m \left(|u|^{p-1}u\right), \quad p > 1,\ m = 1, 2,$$

posed on the whole of $\mathbb{R}^N$. Higher order PDEs have become a popular research area over the last two decades but sixth order equations are still less common and less well understood than related equations of fourth order. Sixth order parabolic models continue to arise in various physical contexts, so understanding their behaviours is a matter of increasing importance.

We dedicate two chapters to the case $m = 1$. In Chapter 2, we study the equation with negative sign, which is unstable and allows for solutions that blow up in finite time. In Chapter 4, we study the positive sign case, which is stable. The bulk of our results here concern so-called *self-similar* solutions, and we describe and categorize them as extensively as we can over a variety of parameter ranges. Our approach comprises a mix of rigorous analysis, careful numerics and asymptotic approximations.

Chapter 5 addresses both the positively and negatively signed $m = 2$ case. We again focus on self-similar solutions, which demonstrate a complete departure from the lower-order theory.

Chapter 3 details an adaptive numerical scheme suitable for simulating a wide class of sixth order parabolic PDEs. Based on earlier work for second and fourth order equations, it uses a robust collocation scheme over a grid whose mesh points can be made to move according to features of the solution as they develop. This is used at various points throughout the thesis to better understand aspects of the main problem.

Acknowledgments

My thanks go to my supervisors Dr Jonathan Evans and Professor Victor Galaktionov for their support, patience and enthusiasm. They have introduced me to a fascinating world of mathematics and I have much enjoyed learning from them, about subjects both on and off topic. I am also indebted to the ESPRC, without whose funding I would not have been able to embark on this at all, and to the Maths department at large for providing a welcoming and stimulating environment.

Thank you also to my examiners Ilia Kamotski and Roger Moser, whose careful scrutiny and constructive comments have allowed me to make a number of improvements to this thesis.

I am glad to have had the the chance to be surrounded by so many bright and interesting people, both amongst the staff and students. I have been given useful counsel on this project by Chris Budd, Alistair Spence, Johannes Zimmer, Melina Freitag, and Euan Spence, and I am very grateful to all of them. Extra thanks must go to Euan for the time he let me stay at his house when they found a bomb near mine, and for his moral support and good company. I have also been delighted to discuss life and mathematics with James Roberts, Maren Eckhoff, Matt Pressland, Doug Shanks, Horacio González, Hüseyin Koçak and various other denizens of 4W.

Thanks especially to Francis Lane, Acyr Locatelli and Istvan Redl. My PhD experience would have been unfathomably poorer without them to drink coffee, argue, commiserate and misbehave with.

I would also like to thank my non-maths friends, especially Bigtopp et. al., who I miss dearly. When this is finished I hope I will have fewer excuses to not see them. Likewise my family, on whose support I have always been able to count. Enormous thanks to Mum, Dad and Joe, Malcolm, Charles and Isabel.

Equally enormous thanks to the Blackburns and Mairs for their relentless

hospitality wherever in the world they are.

Marina, I could do nothing but say thank you for the next hundred years and I doubt that would quite cover it.

Contents

List of Figures

Chapter 1

Introduction and Background

1.1. Motivation - Cahn Hilliard Type Equations

1.1.1. The Model and Comments on Higher-Order Equations: This research project focuses on sixth-order, semilinear parabolic evolution equations of the form

$$u_t = \Delta^3 u \pm (-\Delta)^m \phi(u), \quad m = 1, 2 \tag{1.1.1}$$

where $\phi(u)$ is some nonlinear function of u, typically of the form $\phi(u) = |u|^{p-1}u$, $p > 1$. This and all other model equations discussed in the introduction concern the evolution of some scalar function $u : \Omega \times I \to \mathbb{R}$, where $\Omega \subset \mathbb{R}^N$ is a spatial domain and $I \subset \mathbb{R}$ is a finite or infinite period of time. We usually take Ω to be the whole of $\mathbb{R}^N$ as we are interested in asymptotic behaviours, either as $t \to \infty$ or approaching some finite 'blow-up' time, and as such we want to only account for behaviours due to the equation itself without extraneous contributions from the geometry of the domain.

These models are connected with various physical applications, which we will briefly survey; the last few decades have seen interest in higher models increase as they have been found to be a good fit for a number of phenomena poorly approximated by more classical second order parabolic PDE. From our perspective, they are worthy of study precisely because of this unclassicality: at higher order many of the tools that have been used so successfully in the second order theory are no longer effective.

In particular, the maximum/comparison principle (see [58] and [64] or almost any PDE textbook for details) no longer applies and so solutions can have interior global maxima and minima, and we cannot control the L^∞ norm of a solution by its values on the parabolic boundary. This blocks one avenue for easily establish-

ing existence/uniqueness results, although is arguably a greater loss in terms of our ability to deduce qualitative properties of solutions. For instance, for some equations it is possible to prove radial symmetry of solutions with the maximum principle in conjunction with the *Aleksandrov Reflection Principle* [3] see e.g.[91] for a notable example. It also underpins the *Sturmian Intersection Theory* [83] which gives information on the number of sign changes of a solution in terms of the number of sign changes on the parabolic boundary and is often employed in determining the number of intersections of an arbitrary solution with a known family, providing detailed restrictions on behaviour. We could fill the rest of these pages with the versatility of the maximum principle alone!

Another very common technique in PDE theory is to derive an ODE satisfied by some class of solutions, almost always of the same order as the PDE itself. This is an approach we will pursue extensively, but again a great deal of structure is lost for ODEs of order greater than two where analysis on the phase plane has produced some extremely strong results. [21], [88] and [107] represent three major developments in the field, the latter two of which have proved resistant to higher-order generalization despite numerical evidence that something akin might hold, at least for the fourth order versions.

Of course, higher order equations will never fit such a strong theory as has been developed for second order ones since by their nature they don't imbue such rigid geometric restrictions. We refer to the book [90] for an account of solution features for higher order equations in a Boundary Value Problem setting.

An additional complication in this particular project is that the associated ODEs we study do not directly admit a variational formulation, rendering another well-developed tool set that otherwise is agnostic to the order the equation (see e.g. [85] or [29] for typical higher-order examples) of limited use. We do draw some connections to variational problems to indicate a direction in which future research might develop a rigorous approach, but given the seeming difficulty of this task we content ourselves with applying and adapting the existing tools that work, mostly asymptotic expansion, bifurcation theory, topological shooting and of course careful numerics. This work is essential to expand the limits of mathematics in directions where no obvious breakthrough that grants a whole new approach has occurred recently. We take more of a 'naturalist's perspective' of going out into the world, observing, recording and conjecturing, providing theorists with data to be picked apart and pieced together over the course of decades as we try and make sense of it all.

Higher order nonlinear models naturally arise in the study of phenomena

that evolve complicated spatio-temporal patterns. For instance, in the 1970s the *Kuramoto Sivashinksy* equation

$$u_t = -u_{xxxx} - u_{xx} - uu_x,$$

was proposed to understand wave propagation in reaction-diffusion systems in [122] based on a Ginzburg-Landau like approach, and in [154] to model the motion of a flame front. The mathematical literature written on the subject since then is vast as the equation exhibits a great variety of interesting phenomena depending on the precise setting of the problem, including but not limited to chaotic states [109], finite dimensional attractors [160], and an extensive bifurcation theory [113]. An exploration of the Cauchy Problem using some of the same techniques we use below can be found in [77].

Other examples come from Rayleigh-Bernard theory in the form of the *Swift Hohenburg* equation

$$u_t = \kappa u - \left(1 + \frac{\partial^2}{\partial x^2}\right)^2 u - u^3,$$

first appearing in the literature in 1977 [157], and the *Extended Fisher Kolomogorov* equation

$$u_t = -u_{xxxx} + u_{xx} + u - u^3, \tag{1.1.2}$$

proposed for the study of bistable systems in the late 1980s [40]. We refer to [146] for a thorough discussion of their properties and (diverse) applications.

Already from these relatively simple specimens of higher order equations, the stark difference from the second order theory is clear. Compare (1.1.2) with its second order counterpart, the Fisher-Kolmogorov equation (aka the Kolmogorov-Petrovskii-Piskunov equation):

$$u_t = u_{xx} + u - u^2, \tag{1.1.3}$$

which was devised in the 1930s [62] to model the spread of an advantageous genetic mutation through a population. It is famous as an early example of a reaction-diffusion model that admits *travelling wave* type solutions

$$u(x,t) = f(y), \quad y = x - ct, \tag{1.1.4}$$

which have become widespread in dissipative and dispersive PDE theory. However, with a slight modification of the nonlinearity so it matches that (1.1.2), it is quite straightforward to classify exhaustively all the stationary solutions into

constant solutions, monotone 'kinks' connecting the stationary states and 'single hump' periodic solutions. Its higher order cousin, however, can possess vastly many more types on solutions (at least in some parameter ranges), including families of non-monotone kinks, pulses (homoclinic connections of stationary solutions), multi-hump periodic solutions and even chaotic oscillatory patterns, see [146] Chapter 1. In a sense, this is both a feature and a bug of higher order models, widening their applicability at the cost of legibility. Of course, our job as mathematicians is to mitigate the drawbacks and leave only a powerful theory for understanding the world.

1.1.2. The History of the Cahn-Hilliard Equation: This equation and its generalizations provide the physical justification for our investigation. It has the form

$$u_t = -\Delta^2 u + \Delta\left(\phi(u)\right), \tag{1.1.5}$$

where $\phi(u)$ is a nonlinearity associated with a potential energy function $\Phi_h(u) = \int_0^u \phi$ called the *homogeneous free energy*, typically a quartic polynomial. The form of this term is not derived precisely from theoretical considerations. A variety of curves that have broadly the desired properties have been proposed, hence the equation is often referred to as 'phenomenological'; these properties essentially being that the homogeneous free energy has two local minima corresponding to the stable state of a pure phase. It was suggested as an attempt to describe the thermodynamic process of *spinodal decomposition*. At high enough temperatures, a molten alloy of two metals can exist in a single, mixed, thermodynamic phase. We take $u \in [0, 1]$ to be an 'order parameter' in the Ginzburg-Landau sense which essentially measures the concentration of one phase (and by extension the other according to $1 - u$). In the high temperature regime, u does not vary outside of random, local, minor fluctuations. However, as the temperature decreases, this mixed equilibrium becomes unstable and the dual fluid separates into regions consisting of only one or other of the constituents. This can happen in two ways, depending on which region of the phase diagram the system occupies following the temperature change.

The two curves labelled in Figure 1-1 represent transitions between the region of stability. The upper, 'coexistence' curve represents the limit of the stable region, which shows that the more even the proportions of the two components are, the higher the temperature must be for the fluid to be stable. In between the coexistence curve and the lower curve, known as the 'spinodal', which is determined by the locus of points where $\frac{\partial^2 G}{\partial u^2} = 0$, G is the *Gibbs Free Energy*,

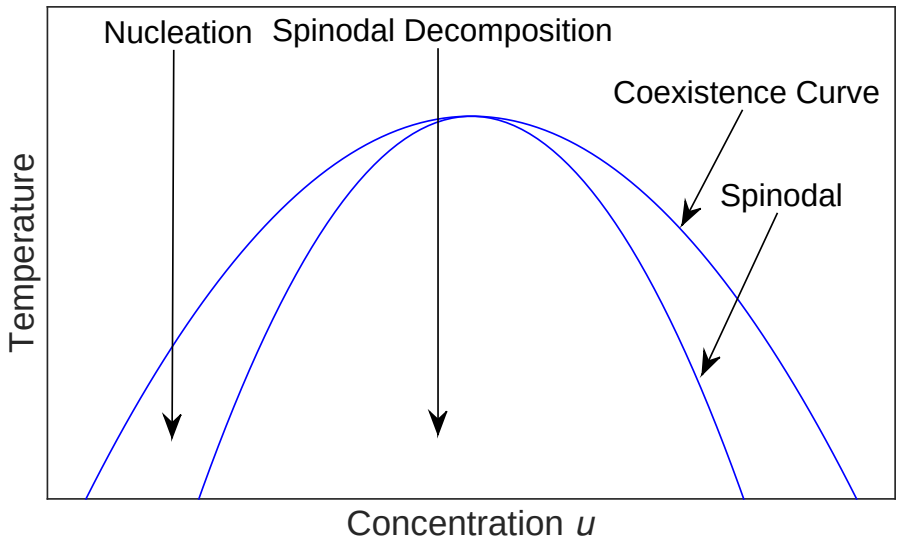

Figure 1-1: Phase Diagram of a Binary Alloy showing the Regions of Stability, Metastability and Instability.

the system is said to be metastable: it can remain in this state for some finite, possibly large time, but will eventually lapse into a more permanently stable one.

If the temperature drop is only sufficient that the mixture becomes metastable, represented by the left hand vertical arrow in Figure 1-1, then the decomposition happens by the process of nucleation: eventually, small regions with properties akin to the stable state emerge from the mixture at random as the particles flow about each other, and these grow in extent until the fluids are separated everywhere (N.B. the regions containing one or other of the component fluids need not be connected). This process can be quite slow as in order for the nuclei to form about which for the separate fluids to crystallize, a free energy barrier preventing them must be overcome.

The temperature change represented by the right hand vertical arrow leads to spinodal decomposition - in this case, there is no free energy barrier inhibiting the existence of homogeneous phases and so decomposition happens rapidly throughout the mixture, as opposed to just at potentially very few nucleation sites. When this occurs, the layers of separated fluid form characteristic quasi-periodic patterns; once again demonstrating the correspondence between pattern-forming phenomena and higher order equations. Interestingly, it can be shown that as the state of the system approaches the spinodal from above, the nucleation mechanism approaches that of spinodal decomposition continuously. See

[141], Chapter 2.3 for a more detailed account.

After some not very satisfactory attempts to ascribe an equation to this process, partial headway was made in the 1950s. Cahn and Hilliard chose to emphasize the diffusive aspect of the process over its hydrodynamics (though recently efforts have been made to incorporate these in addition as a coupling with the Navier-Stokes equations, see e.g.[16] and [2]). They began with the conservation law

$$u_t + \nabla \cdot \mathbf{j} = 0, \tag{1.1.6}$$

where $\mathbf{j}$ is the flux of the same component of the system of which u is the concentration. It arises from a basic consideration of continuity - any quantity u that changes in time over a bounded, arbitrary domain without being created or destroyed within it must be due to an equal quantity of u entering or leaving the domain. However, unlike in standard diffusion where the flux $\mathbf{j}$ is given by Fick's law $\mathbf{j} = -k\nabla u$ for a diffusivity k (usually constant although the case where k varies with u is also extensively addressed in the literature), it is necessary to account for the fact that the concentration varies non-uniformly by the nature of the process. This was the key to successfully capturing the behaviour, at least for small times, and also the cause of the appearance of a fourth order (Δ^2) term.

To derive an appropriate expression for $\mathbf{j}$, Cahn and Hilliard turned to energy considerations[1]. Their original treatment of free energies of nonuniform systems [31] was quite general, although focused on materials that exhibited certain crystalline symmetries. For the oil/water example mentioned earlier, and others, different techniques are required. They obtained an integral expression for the total free energy of the system by Taylor expanding the local free energy about that of a uniform system to second order, exploiting the symmetries to express it as the sum of two terms, then integrating over the entire domain. For the alloy system already discussed, this took the form

$$\Phi[u] = \int_\Omega f(u)\mathrm{d}x, \quad f(u) = \frac{1}{4}(u^2-1)^2 + \frac{\gamma}{2}|\nabla u|^2, \quad \Omega \subset \mathbb{R}^3. \tag{1.1.7}$$

In this case, the first term of $f(u)$ is the homogeneous free energy from above, having the form of a 'double-well' potential with each well (at $u = \pm 1$) corresponding to the stability of the pure phases, while the second is the Taylor correction term, the change in free energy due to the concentration gradient. γ is a parameter associated with gradient of the energy.

In [30], which addresses various aspects of how to derive an equation to de-

[1] An equivalent formulation by considering microforces was later achieved by Gurtin, see [97]

scribe spinodal decomposition, Cahn then went on to show that the mass flux $\mathbf{j}$ was proportional to the gradient of the chemical potential μ. The constant of proportionality is negative; here it can be absorbed in the non-dimensionalization process and so we ignore it. He demonstrated that this can be expressed as the first variation of $f(u)$, $\mu = \frac{\delta f}{\delta u}$, defined as

$$\int_\Omega \frac{\delta f}{\delta u} \mathrm{d}x = \frac{\mathrm{d}}{\mathrm{d}\epsilon} \int_\Omega f(u + \epsilon v) \mathrm{d}x \Big|_{\epsilon=0},$$

leading to the fourth order PDE that became the classical form of the phenomenological Cahn Hilliard equation:

$$u_t = -\gamma \Delta^2 u + \Delta(u^3 - u). \tag{1.1.8}$$

The model, however, fell out of favour, due in part to the difficulty of treating the nonlinearity, until it was resurrected in the 1970s by Novick-Cohen and Segel [137]. They treat a version including a cubic term in the potential Φ introducing an asymmetry, deriving its stationary states in one dimension (both periodic and not) and addressing some aspects of their stability in various limits. For further discussion of the physical, thermodynamic aspects of the equations, see chapter 4 of[37].

Since then there has been an explosion of interest in the model amongst the mathematical community. An investigation of well-posedness of (1.1.5) (again with a quartic homogeneous free energy) was conducted in [50] where standard existence, uniqueness and regularity results were obtained on bounded domains, although it is noteworthy that solutions that blow-up in finite time were shown to exist depending on the signs of the coefficients of the free energy term. Blow-up will be a major focus of this project and we shall discuss the issue in detail following our tour of neighbouring physical models. Indeed, the direct ancestor of this thesis was a deep study of this blow-up in the simplified *limit Cahn-Hilliard equation*

$$u_t = -\Delta^2 u - \Delta |u|^{p-1} u, \quad p > 1, \tag{1.1.9}$$

considered in [56], where the homogeneous free energy is condensed to only one term $\Phi_h(u) = \frac{1}{p+1}|u|^{p+1}$ to allow for a more detailed analysis of the precise asymptotic patterns that form. A loose justification for this follows from neglecting the non-leading terms in the nonlinearity as $u \to \infty$. A countable set of distinct radial blow-up patterns in detected and an asymptotic description is given in the critical cases $p = 3$ and $p = 2$ in one dimension, and some aspects of non-blowing

up solutions in the large time limit are considered.

Other variants and aspects of the Cahn-Hilliard model that have been scrutinized include well-posedness, asymptotic behaviour and existence of a finite dimensional attractor in cases where Φ_h is an arbitrary even order polynomial ([160] Chapter 4, [136]) or the logarithmic expression

$$\Phi_h = (1+u)\ln(1+u) + (1-u)\ln(1-u) \tag{1.1.10}$$

[39], which is in some sense a singular limit of the polynomial case, see [32] for an explanation and survey. In addition, formulations where the nonuniformity is introduced via a non-local operator have become popular, see [1]. We emphasize that this sample gives only a small flavour of some of the mathematical progress in this direction and encourage the interested reader to browse the references in the aforementioned to build a more complete picture.

1.1.3. Sixth Order Cahn-Hilliard Equations: The last five years have seen a number of generalizations of (1.1.5) leading to equations featuring quite novel sixth order operators. For instance, a model was derived in [152] for the 'epitaxial' growth of a crystal surface, where a substrate of some crystalline structure grows by deposition. In this case, the mechanism considered comprises the substrate interacting with a chemical vapour which reacts at a boundary layer between the two, resulting in growth governed by a flux normal to the surface. The features of the process include coarsening - the typical length scale of the crystal facets increases - in some sense akin to the appearance and growth of separate phases in spinodal decomposition. The details of the derivation are involved, but after some reductions we are left with a free energy

$$\Phi[u] = \int_\Omega \frac{1}{2}\left(\Delta h\right)^2 + \left(\frac{\alpha}{12}(h_x^4 + h_y^4) + \frac{\beta}{2}h_x^2 h_y^2 - \frac{1}{2}(h_x^2 + h_y^2)\right) \mathrm{d}x. \tag{1.1.11}$$

Here Ω is a 2D domain, h is the height of the surface, the rightmost three terms of the integrand are the bulk free energy with anisotropy coefficients α, β and the remaining term $\frac{1}{2}\left(\Delta h\right)^2$ is to account for the additional energy of edges and corners. This term is also what leads to the appearance of sixth derivatives. The evolution occurs according to the surface diffusion law

$$h_t = \sqrt{1+|\nabla h|^2}(M\Delta_s \mu - F\cdot \mathbf{n}), \tag{1.1.12}$$

where Δ_s is the Laplace-Beltrami operator, μ is the chemical potential $\frac{\delta\Phi}{\delta h}$, F is the flux of crystal material, M is a diffusion constant and $\mathbf{n}$ is the unit outward normal. After some more simplifications the resulting equation reads

$$h_t = \Delta^3 h + \Delta^2 h - \Delta\left[\beta(h_y^2 h_{xx} + h_x^2 h_{yy} + 4h_x h_y h_{xy}) + \alpha(h_x^2 h_{xx} + h_y^2 h_{yy})\right] + \frac{D}{2}|\nabla h|^2. \quad (1.1.13)$$

Of particular interest here is the last term, with coefficient $D \propto F$, which prevents the equation from being a gradient system. Nonetheless, global existence and uniqueness of weak solutions for this model are established in [118] supplementing the matched asymptotics and numerical simulations performed in the original paper [152].

It is worth mentioning the matched asymptotic analysis in that paper was principally performed on the *convective Cahn-Hilliard* equation

$$u_t = u_{xxxxxx} + \left(u - u^3\right)_{xxxx} + Duu_x \quad (1.1.14)$$

which is the one dimensional equivalent of (1.1.13) in the variable $u = h_x$. Weak solutions for this equation are discussed in [119]. The problem of a global attractor for this equation, established for the fourth order equivalent in [44], is addressed in [120].

The other major physical source for sixth-order Cahn-Hilliard equations comes from attempting to model the addition of 'surfactant' (a substance which lowers interfacial tensions between distinct, adjacent compounds, in this case a molecule which is part hydrophilic and part lypophilic) to oil/water mixtures. An unusual stable three phase structure can arise, consisting of separate oil-rich and water-rich phases and then a microemulsion in between them. The free energy describing this process was derived empirically by neutron scattering experiments, and in [95] was shown to have the form

$$\Phi[u] = \int_\Omega f_0(u) + \frac{1}{2}\kappa_1(u)|\nabla u|^2 + \frac{1}{2}\kappa_2(\Delta u)^2 \mathrm{d}x, \quad \Omega \subset \mathbb{R}^3. \quad (1.1.15)$$

Here, h_0 is a parameter measuring the deviation from the threefold coexistence and $f_0(u) = (u+1)^2(u^2+h_0)(u-1)^2$ is a triple-well potential with minima in the solely water phase, the solely oil phase and in the microemulsion that forms around the surfactant. The $(\Delta u)^2$ term arises from the nontrivial thickness of the

interfaces due to the presence of joint oil-water-surfactant mixtures along them. $\kappa_1(u) = g_0 + g_2u^2$, $g_2 > 0$ and $\kappa_2 > 0$ are coefficients of the gradient terms. This is then used in [143] to develop a sixth-order Cahn-Hilliard type equation:

$$u_t = M\kappa_2\Delta^3 u + M\Delta(f_{0,u}(u) - \frac{1}{2}\kappa_{1,u}|\nabla u|^2 - \kappa_1\Delta u) \tag{1.1.16}$$

where M is a mobility constant that arises from the derivation, following variational approach outlined by Cahn in [30]. The paper then goes on to explore global existence and uniqueness results, with existence for an IBVP problem in a bounded domain, continuous dependence of solutions on initial conditions and good boundary regularity being demonstrated.

The possibility of blow-up for (1.1.16) is discussed in [165] for more relaxed parameter regimes. There are a plethora of results for relatives of this model, for example optimal control problems in [132], [131], with singular diffusion like (1.1.10) in [153], [135], asymptotic behaviours in [134] and finite element simulations in [96] to mention just a few.

We conclude our discussion of Cahn-Hilliard equations by noting that for $m = 1$, (1.1.1) comes from considering a 'chemical potential' as the first variation of the simplified free energy

$$\Phi[u] = \int_{\mathbb{R}^N} \frac{1}{2}|\Delta u|^2 \pm \frac{1}{p+1}|u|^{p+1}\mathrm{d}x.$$

We are justified in considering a homogeneous free energy as a homogeneous polynomial (without the multiple well structure that informs the multiphase dynamics) since we are primarily interested in asymptotic behaviours.

For $m = 2$, (1.1.1) does not admit such a formulation and instead can be considered as a higher-order diffusion driven by a lower order free energy, with only first derivatives appearing.

1.2. Neighbouring Models and Related Phenomena

1.2.1. Porous Media and Thin Films: It is important to mention that the kinds of nonlinearity we focus on have appeared in other, widely studied contexts. On its own, the nonlinearity in (1.1.9) and (1.1.1) for $m = 1$ comprises the quasilinear *Porous Medium Equation* (PME):

$$u_t = \Delta|u|^{n-1}u, \quad n > 1. \tag{1.2.17}$$

We also draw attention to a fourth order generalization of it, the *Thin Film Equation* (TFE):

$$u_t = -\nabla \cdot (|u|^n \nabla \Delta u), \quad n > 0. \tag{1.2.18}$$

(The relation is more obvious when (1.2.17) is expressed in divergence form under the relabelling $n \to n-1$; we try and keep consistency with how they appear in most of the literature although they are presented in many different equivalent forms.) The former is a model for the behaviour of gas as it flows through a porous medium, where u is the density, while the latter for the motion of a viscous droplet spreading according to surface tension arising from the 'lubrication approximation' for the Navier-Stokes equation [138]. Here, u is the height of the droplet, typically $n = 3$ to fix that the droplet doesn't 'slip' at the interfaces, and the fourth order operator appears due to the assumption that the pressure at the surface is proportional to the curvature which, when small, is approximated by u_{xx}. Due to their quaslinearity, they represent examples of *degenerate* parabolic equations - the 'diffusivity' is a function of u that tends to zero as $u \to 0$ and sure enough, the behaviour in this limit is of special interest. We hope that our study of the 'unperturbed' cases will allow more progress on similar sixth order *quaslinear* equations. With the perturbation in effect, both exhibit compactly supported solutions that have moving interfaces at which u need not be differentiable, making the theory considerably harder to treat than their linear or even semilinear counterparts. However, some of these difficulties can still enter the semilinear theory when the nonlinear terms are non-lipschitz, see e.g. [68]. We avoid this difficulty by only considering $p > 1$.

The PME, famously and perhaps surprisingly, admits a non-trivial exact solution for $n > 1$:

$$u(x,t) = \max\left(t^{-\alpha}\left(m_0 - k|x|^2 t^{-2\beta}\right)^{1/(n-1)}, 0\right) \tag{1.2.19}$$

with constants taking the values

$$\alpha = \frac{N}{N(n-1)+2}, \quad \beta = \frac{\alpha}{N}, \quad k = \frac{\alpha(n-1)}{2Nn},$$

and $m_0 \in \mathbb{R}$ being uniquely determined by the (conserved) initial mass. It was discovered in the 1950s independently by Zeldovich and Kompaneets [169], Barenblatt [9] and later by Pattle [142] and is in some ways analogous to the Gauss Heat Kernel (1.3.38) that is fundamental to the linear theory. Indeed, the Heat Kernel can be recovered from (1.2.19) as a limit as $n \to 1$ just as one might

hope. Just like the heat kernel, the initial data corresponding to (1.2.19) is a Dirac Delta multiplied by the correct mass despite the PDE being fundamentally non-linear; in the literature this is referred to as a *source-type solution*. Using the comparison principle for second order equations it is useful for bounding the spread of the support of compactly supported solutions, and indeed for describing general large-time asymptotic patterns for the Cauchy problem serving as an attractor for wide classes of initial data; we refer to the comprehensive book of Vazquez [164] for details of these and more.

The situation is less ideal in the thin-film case and no exact fundamental solution is available except in the case $n = 1$, where it was shown in [155] to have the form

$$u(x,t) = t^{-1/5}\phi(xt^{-1/5}), \quad \text{with} \quad \phi(\xi) = (\xi_1^2 - \xi^2)^2/120, \quad \xi_1 = (225m_0/2)^{1/5}.$$

However it is still possible in general to express a radially symmetric, compactly supported one as the solution of the radial ODE

$$-\nabla \cdot (|f|^n \nabla \Delta f) + \frac{1-\alpha n}{4} y \cdot \nabla f + \alpha f = 0, \quad \alpha > 0 \tag{1.2.20}$$

This reduction is a consequence of a scaling invariance of (1.2.18) allowing for so called *self-similar solutions*. These will play a major role in our analysis of (1.1.1): see [13] for some early results in this direction in relation to the TFE. A thorough treatment of this powerful tool in PDE theory can be found in [10], containing a derivation from dimensional analysis and a plethora of examples of applications (the above ZKB solution being a prominent instance) and see e.g. [19] for details of the deep and beautiful Lie theory that underpins it. The reduction from $N + 1$ dimensional space-time to a N dimensional space that moves in time as if on rails makes it comparatively easier to describe solutions in the first place, and further the same mechanism that allows for this can be considered as a kind solution-'driver', frequently forcing the behaviour of solutions to the PDE for large periods of their evolution. Self-similar solutions emerge as 'intermediate asymptotic states', i.e. how the system behaves once the effect of the initial conditions has been 'forgotten' but before the large-time asymptotic behaviour fully manifests, or often make up part of the attractor outright. Self-similar behaviour of blow-up solutions is well known; in the next section we will get a taste of how ubiquitous it is in these kinds of equations.

The parameter α above is fixed to the value $\frac{N}{4+Nn}$ provided f has non-zero mass. This is of course necessary for non-trivial positive solutions, whose startling

existence was proved in [14]. For the $n = 0$ case non-negative solutions are impossible and the solution has oscillatory 'tails', see discussion in Section 1.3. However, note that we have written the non-linear terms in (1.2.17) and (1.2.18) with an absolute value function: $u^n \to |u|^{n-1}u$ or equivalent. This allows for solutions of changing signs. It is quite natural to generalize in this way when terms like these appear as lower-order perturbations in an equation that cannot be expected to admit non-negative solutions, hence this is the approach we adopt for our model (1.1.1). We do draw attention to the fact that for $m = 2$ the fourth-order non-linear term we consider in Chapter 5 is a different generalization of the PME which is far less well-studied; see [69] and [85] for some preliminary advances in this direction.

However, even in the pure PME and TFE, sign-changing solutions can be of considerable interest. For instance, there is strong numerical evidence of a *homoclininc* bifurcation point in n at $n_h \approx 1.76$ which marks a transition from solutions with *oscillatory* behaviour near the interfaces (infinite numbers of zeros) to pure-positive solutions, see [52] and [53]. This has yet to be explained analytically. Another intriguing open problem pertains to so-called *self-similar solutions of the second kind*: when the mass of the profile is zero the parameter α is free to vary and (1.2.20) becomes a non-linear eigenvalue problem. A proof of existence and categorization of the conjectured countable set of pairs (α_k, f_k) that solve it is has been so far elusive. The equivalent result for second kind self-similar solutions for the PME was given via reduction to an autonomous Dynamical System and subsequent phase plane analysis can be found in [107]; the first of this set is naturally the ZKB solution and the second is the famous 'dipole' solution [108] with odd symmetry. Some progress in the TFE problem using an n-branching homotopy approach is give in [51].

We mention these aspects in particular as they are germane to some of the themes of this thesis. Problems with a non-linear eigenvalue flavour compose the bulk of our results on blow-up in Chapters two and five. However, there are some aspects of degenerate equations that (mercifully) do not apply to us and remain deeply mysterious, especially from a rigorous perspective. For example, the correspondence between the Cauchy Problem (CP, where only initial data is prescribed and solutions are unconstrained in space except by the equation itself) and the Free Boundary Problem (FBP, where aspects of the solution are fixed on a boundary whose movement is also governed by an equation) is also addressed in [51]. While we seem to have a reasonable heuristic understanding on how solutions of the Cauchy Problem appear as 'maximally regular' limits of

the Free Boundary Problem, we rely heavily on numerical simulations and it is far from clear how this can be supplanted by more rigorous mathematics.

Of course, it would be wrong to suggest that there have not been some beautiful results in the field especially when including lower order nonlinear perturbations of (1.2.18), aside from those already mentioned we refer to [168], [15], [75], [124], [17], [115] and [5] as a base for more exploration. Again, it is worth highlighting the appearance of blow-up solutions in many of these settings.

Just as sixth order equations have just recently begun to appear in attempts to model processes with 'diffusion' according to rather complex free energies, resulting in Cahn-Hilliard equations like (1.1.13) and (1.1.16), they have arisen in a number of contexts where higher order correction terms have been necessary to properly capture the physics. In fact, the Thin Film theory is a conspicuous example of an area where this has occurred. Similar looking operators sixth order operators appeared in attempts to model the formation of Silicon Oxide during silicon wafer manufacture, [114], [57] and the motion of a fluid droplet supporting an elastic plate in [63]. Actually, there is no reason to stop at sixth order, and recently some properties of tenth(!) order TFEs appeared in [6] and [4].

In a pair of papers from 2006 [54] and [55] an extensive study of the CP and FBP for the equation

$$u_t = \nabla \cdot (|u|^n \nabla \Delta^2 u) - \Delta(|u|^{p-1}u) \tag{1.2.21}$$

was conducted. This model is a very close relative of (1.1.1) for the $m = 1$ case which appears in the limit $n \to 0$, and in many ways our problem can be seen as an 'intermediate' model between the quasilinear TFEs and the better understood Reaction Diffusion Equations we discuss in the next section in the context of blow-up, although possessing some interesting distinguishing qualities of their own (for one, they have more conserved quantities than either).

1.2.2. Blow-up and Reaction-Diffusion Theory: As we have already mentioned, finite-time blow-up of solutions is a major theme of this thesis, and appears in many physical model equations. This can be pathological, especially if we are attempting to model something that is inherently bounded, and then understanding this weakness in the ability of the equation to reflect reality can lead to better prototyping. Alternatively, some processes demand equations with solutions that can quickly grow many orders of magnitude, the obvious and principle example being combustion processes where some kind of ignition occurs. In this case understanding when, where and how blow-up occurs is crucial. Blow

up need not refer only to the magnitude of the solution; some equations where a solution derivative becomes infinite have applications. This scenario is referred to as rupturing. Our attention will be on solutions that start from bounded initial data and evolve classically for a period of time before L^∞ blow-up occurs, that is for some time T, solutions are well-defined for $0 < t < T$, while

$$\sup_{x\in\Omega} |u(x,t)| \to \infty \quad \text{as} \quad t \to T^-. \tag{1.2.22}$$

By fairly straightforward embedding theorems it can be shown that for semilinear equations such as ours blow-up in any derivative must imply L^∞ blow-up.

The canonical example of a differential equation with blow up is the very simple ODE:

$$u_t = u^2, \quad u(0) = c, \tag{1.2.23}$$

which has solution

$$u(t) = \frac{1}{\frac{1}{c} - t}. \tag{1.2.24}$$

The region of interest here is the limit as $t \to \frac{1}{c}$, where u quite clearly grows monotonically and without bound. This example is useful as it suggests the role nonlinearity plays in blow-up - the same qualitative behaviour occurs if the exponent is replaced by any $p > 1$ but abruptly vanishes when the equation becomes linear. The nonlinear term acts as a type of feedback, indeed a positive feedback loop is exactly what is required for a 'runaway' effect to take hold and singularities to form in finite (as opposed to the less interesting infinite) time. Nonlinearity will always be present in some way when blow-up is concerned, though it can be as a boundary condition rather in than in the equation itself, see for example [126] or [80]. This can occur in the context of external heat sources.

There is a straightforward necessary and sufficient condition for ODEs of the form

$$u_t = f(u), \quad u > 0 \implies f(u) > 0$$

to exhbit finite time blow up given positive initial data. Dividing through by the nonlinear term $f(u)$ and integrating from 0 to T, we find that $u(T) = \infty$ for $T < \infty$ iff $\int^\infty \frac{1}{f(v)} \mathrm{d}v < \infty$. This is known as *Osgood's Criterion*, and has a number of applications, its original derivation for proving uniqueness for ODEs absent a Lipschitz condition [139]. It is especially useful in the case of second order semilinear PDEs, where the comparison principle results in the criterion being a necessary condition for blow up.

A number of approaches for deriving sufficient conditions for blow-up, for PDEs of arbitrary kind and order, have been devised over the last hundred years, mostly involving the derivation of some differential inequality for a norm or norm-like quantity of the solution to the PDE. That quantity having finite time blow-up then implies the same for the solution of the PDE. A notable example of this approach is *Kaplan's Eigenfunction Method* ([112], Chapter 6), wherein the differential inequality applies to the projection of the solution onto the first eigenfunction of an appropriately chosen linear operator. This approach relies on the positivity of the eigenfunction as well as the boundedness of the domain, so does not find much use in this project. However, it is widely used, and approaches much in the same spirit can even be used for higher order equations on bounded domains (see e.g. [85], pp. 40 or [77]).

Of greater utility to us will be the concavity methods of Levine [125], which are expressed in a more abstract form and very well suited to higher order equations, a point explicitly emphasized in his seminal paper. His initial results were for equations of the form

$$Pu_t = -Au + \mathcal{F}(u), \tag{1.2.25}$$

where P and A are positive, symmetric linear operators on a Hilbert Space and $\mathcal{F}$ is any kind of nonlinearity with potential

$$\mathcal{G}(x) = \int_0^1 (\mathcal{F}(\rho x), x)\, \mathrm{d}\rho, \tag{1.2.26}$$

where $(\cdot, \cdot)$ denotes the Hilbert inner product, that satisfies

$$2(\alpha + 1)\mathcal{G}(x) \leq (x, \mathcal{F}(x))\,, \tag{1.2.27}$$

for some $\alpha > 0$. His results follow from demonstrating the concavity of a certain scalar function $F^{-\alpha}(t)$ of u and the initial condition u_0. Then if $F^{-\alpha}(0) > 0$ and $\left(F^{-\alpha}\right)'(0) < 0$, the concavity implies that there is a finite t at which the function becomes zero and so the solution must blow up in the appropriate norm. This very simple idea has been generalized extensively over the last years for parabolic and hyperbolic equations, see e.g. [18] or [127] for some recent examples. Of course, there have been many blow-up proofs devised for specific scenarios where some features of the equation suggest a certain line of attack, one example might be studying higher order equations via perturbation methods as in [65] amongst countless others. However, few are as general as Levine's method.

There are naturally more questions we can ask about blow-up than simply

whether it occurs: can we determine the blow up time T exactly, or at least achieve a reasonable estimate? How, if at all, does it depend on the initial data $u(x,0) = u_0(x)$? What is the asymptotic behaviour of the solution as $t \to T^-$? It is this last point that comprises the bulk of our results in this direction. The recent textbook [102] gives a thorough overview of questions of this nature and the methods for attaining them in the semilinear case, although focuses mostly on second order equations. A broad survery of blow-up phenomena 'in the wild' can be found in [87].

Other questions that demand consideration include: what form does the blow-up set,

$$B(u_0) = \{x \in \Omega : \exists \{x_n\} \to x,\ \{t_n\} \to T^- \text{ such that } |u(x_n, t_n)| \to \infty\}, \quad (1.2.28)$$

take? One point? Finitely many distinct points? A bounded region? The whole of $\mathbb{R}^N$? This case has been extensively addressed for second order semilinear equations, see e.g. [28], [166], where the maximum principle is instrumental. For higher order semilinear equations, see [129], whose methods we extend in Appendix C. The problem is discussed in detail for second order quasilinear equations of the form

$$u_t = \Delta\left(\phi(u)\right) + f(u) \quad (1.2.29)$$

in [151], where three possible regimes are identified - the LS-regime where (1.2.28) has measure zero, the S-regime where it has positive finite measure and the HS-regime where the measure is infinite - the solutions blows up 'everywhere at once'. Parameter ranges for which these result from bell-shaped initial data re identified.

Related to this question is whether it is possible to continue a solution in time past a singular point. This can occur in a number of ways. One is singularity formation and then immediate collapse, i.e. the singularity is valid initial data for a locally well-posed problem - this is referred to as *Leray's Scenario* and was originally proposed by Jean Leray as possible way to resolve the problem of blow-up in the 3D Navier Stokes equations, see [70] and [85] pp. 386. There, the scenario is shown to apply to the Nonlinear Dispersive Equation (NDE)

$$u_t = uu_{xxx} + 3u_x u_{xx}.$$

Alternatively, the blow-up interface can propagate with finite (or indeed zero) speed, leaving a 'burnt' region outside of which the evolution continues as normal. Both of these scenarios, and conditions on (1.2.29) that discriminate between

which, if any occur, are discussed in [88] and [86].

We now discuss some concrete results from the second-order semilinear theory that were amongst the earliest that spawned the intensive study of blow up, before going onto describe how these generalize to higher order. They are the *Frank-Kamenetskii* equation [84], with an exponential nonlinearity

$$u_t = u_{xx} + e^u, \tag{1.2.30}$$

and its cousin, the *Semilinear Heat* equation with power-law nonlinearity

$$u_t = \Delta u + u^p. \tag{1.2.31}$$

A rather complete understanding of these problems has been developed. (1.2.31) was famously studied by Fujita [66] in the 1950s. In his pioneering work he established the remarkable dichotomy: for the Cauchy problem in $\mathbb{R}^N$, blow-up occurs for any nonnegative initial data in the subcritical range $p < 1+\frac{2}{N}$, whereas for $p > 1 + \frac{2}{N}$, sufficiently small, in some rigorous sense, nonnegative initial data will lead to solutions that exist globally for all time. It was not until the 1970s that the critical case was settled, at least for low dimensions, it was shown in [100] and [117] that the critical behaviour mirrors the subcritical nonexistence result.

When generalizing (1.2.30) and (1.2.31) to higher order, we must bear in mind that the kernels of the higher-order heat equations are oscillatory (see (1.3.45); similar representations exist for all polyharmonic heat equations). As such, we must account for solutions that change sign in the power law case, either by replacing $u^p \to |u|^{p-1}u$ or $u^p \to |u|^p$. Both can by all means be used to study solutions of changing sign for the second order case as well.

For the non-monotone higher order RDE

$$u_t = -\left(-\Delta\right)^m u + |u|^p, \tag{1.2.32}$$

it is possible to generalize Fujita's result - the Cauchy problem with initial data $\int u_0 > 0$ always results in finite time blow-up for $p \leq 1 + \frac{2m}{N}$, which can be proved by a test function method. This is carried out for quite general quasilinear equations of similar form in [46]. However, again in the supercritical range $p > 1 + \frac{2m}{N}$, sufficiently small initial data can remain globally bounded [45]. See also [85] pp. 87 for more details of global solutions in the subcritical range. Moreover, the form of the nonlinearity, being always positive, allows for a rudimentary

comparison theorem for (1.2.32) using a 'majorized' integral kernel [78], giving estimates on the blow-up time from below. This seems quite rare amongst higher-order equations. The Fujita exponent concept is taken to its limits in a visionary paper by Shangbin Cui [36]. For a mth order semilinear system, solutions are shown to exist globally given sufficiently small initial data provided the $m-1$ lower-derivative terms each are bounded from above by power law terms with a sequence of powers decreasing with increasing derivative order. It is thought that this result is sharp for scalar equations, though it is known not to be for systems.

The perhaps more natural equation

$$u_t = -(-\Delta)^m u + |u|^{p-1}u, \tag{1.2.33}$$

has been extensively studied as the simplest possible entry to the domain of higher-order blow up. For $m = 1$ it is notable that blow-up is not self-similar, or rather the only non-zero solution of similarity equation

$$-(-\Delta)^m f + |f|^{p-1}f - \frac{1}{2m} y \cdot \nabla f - \frac{1}{p-1} f = 0 \tag{1.2.34}$$

is the constant function $f_* \left(\frac{1}{p-1}\right)^{\left(\frac{1}{p-1}\right)}$ [92]. To discern the 'approximately' self-similar blow-up patterns it is necessary to study the dynamics of the linearization of (1.2.33) around $(T-t)^{p-1} f_*$ on the centre manifold; this is extremely non-trivial and took some years to piece together, see [61], [20] and [79]. This is not the case for the second order quasilinear heat equation (1.2.29) which can exhibit non-trivial self-similar blow-up for $\phi(u) = u^m$, $m > 1$. It is also not the case for (1.2.33) for $m > 1$, it was shown in [24] that the number of solutions to (1.2.34) is bounded from below by $2\lfloor \frac{m}{2} \rfloor$ via μ-bifurcation (see Chapter 4). It is conjectured that that actual number is $m(m-1)$, though as so often with higher-order problems proof remains currently out of reach. For some discussion of the rich variety of non self-similar blow-up that can occur in (1.2.33), see [71], although it is expected that self-similarity is in some sense generic when it can occur.

Other interesting features of (1.2.33) include the possibility of non-unique solutions. For $m = 1$ this was demonstrated in the classic paper of Haraux and Weissler [99] by constructing certain self-similar solutions. The extension to higher order was done in [74], where similar results were shown to hold. Note that by non-uniqueness, we mean in the L^q topology, for certain $q > 1$, rather than in the classical sense, for more detail see discussion in Section2.4.1. It was also

for this equation with $m = 2$, $N = 1$ that blow-up was shown to be incomplete in Section [72], according to a Leray Scenario discussed in 2.4.5. This is in sharp contrast to $m = 1$, where according to [88] blow-up is always complete.

It is the Leray Scenario in particular than inspires consideration of evolution equations with non-classical initial data. Collapse of an initial singularity into a classical mode of evolution is integral and so understanding what kinds of singularities can generate such a solution is crucial. This motivates the final section of our literature survey.

1.2.3. Very Singular Solutions: In the early 1980s, Brezis and Friedman studied the Semilinear Heat Equation with Absorption:

$$u_t = \Delta u - |u|^{p-1}u. \tag{1.2.35}$$

They showed in [22] that for $p \geq 1 + \frac{2}{n}$, there is no solution with a measure for an initial condition. This rules out source-type solutions taking Dirac Delta type initial data, such as occur for the fundamental solution of the heat equation or (1.2.19) for the PME. However, for subcritical p, not only do such source type solutions exist, but there is another class of what came to be called *Very Singular Solutions* (VSS). The name is apt, since we have

$$\int_{\mathbb{R}^N} u(x,t)\eta(x)\mathrm{d}x \to \infty \quad \text{as} \quad t \to 0$$

for smooth, compactly supported η, and

$$\lim_{t\to 0} u(x,t) = 0 \quad \forall x \neq 0$$

if u is a VSS. Their existence was first established for (1.2.35) in [21], and have been shown to exist for numerous nonlinear dissipative and dispersive equations, see [145], [144], [59], [81]. Not only do they present an interesting phenomenon in the small-time limit, being self-similar they are also instrumental in understanding the large-time behaviour of solutions as we will establish.

The VSS terminology is usually associated with stable evolution equations although this seems to just be convention. Exactly the same initial structure can manifest in the subcritical range for the unstable equivalents like, e.g. (1.2.33).

1.3. Preliminary Results

We collect below a brief summary of some existing results we utilize during our investigation. They primarily concern the linear, triharmonic heat equation

$$u_t = \Delta^3 u \tag{1.3.36}$$

considered in $\mathbb{R}^N \times \mathbb{R}_+$. It is instructive to compare with the theory of the canonical second order heat equation (see e.g. [58] Chapter 2)

$$u_t = \Delta u, \tag{1.3.37}$$

for which solutions of the Cauchy problem can be represented as a spatial convolution against the *fundamental solution*

$$b(x,t) = \frac{1}{(4\pi t)^{N/2}} \exp\left(\frac{-|x|^2}{4t}\right), \tag{1.3.38}$$

which is the unique radial solution of (1.3.37) with Dirac delta initial data, in the sense that

$$\lim_{t\to 0} \int_{\mathbb{R}^N} b(x,t)\phi(x)\mathrm{d}x = \phi(0) \quad \forall \phi \in C_c^\infty\left(\mathbb{R}^N\right). \tag{1.3.39}$$

This can be derived either by Fourier Transform directly or by using the scale invariance of the equation to reduce the equation to the (radial) ODE

$$\Delta F(y) + \frac{1}{2} y \cdot \nabla F(y) + \frac{N}{2} F(y) = 0, \quad \int_{\mathbb{R}^N} F(y)\mathrm{d}y = 1 \tag{1.3.40}$$

with $b(x,t) = t^{-N/2}F(y)$, $y = xt^{-1/2}$. Many of the nice properties of the heat equation follow directly from the fact that $u(x,t) = b(t) * u_0$ for any reasonable kind of initial data u_0. In particular the positivity of the kernel means we have that $||b(t)||_{L^1} \equiv 1$, and so a simple application of Young's inequality for convolutions gives us that for initial data $u_{0,1}$, $u_{0,2}$ the corresponding solutions satisfy $||u_1(t) - u_2(t)||_{L^p} \leq ||u_{0,1} - u_{0,2}||_{L^p}$ $\forall t > 0$, $p \geq 1$. This reflects the well known fact that the Laplacian is the generator of a contracting semigroup and is intimately connected with the maximum principle for second order parabolic equations.

Furthermore, while equation (1.3.40) is not self-adjoint in L^2, we can multiply

through by $\rho(y) = \exp(|y|^2/4)$ to see that we now have the symmetric form

$$\rho \mathbf{B}_2 F := \nabla \cdot (\rho \nabla F) + \frac{N}{2} \rho F = 0. \tag{1.3.41}$$

This defines a self-adjoint operator acting on the weighted space $L^2_\rho(\mathbb{R}^N)$ with domain $H^2_\rho(\mathbb{R}^N)$, and the classical Hilbert-Schmidt theorem applies. The operator $\mathbf{B}_2$ has discrete real spectrum $\sigma(\mathbf{B}_2) = \{\lambda_\beta = -|\beta|/2,\ |\beta| = 0, 1, 2 \ldots\}$, with eigenfunctions comprising the (separable) Hermite polynomials in the sense that $\psi_\beta(y) = C_\beta \exp(-|y|^2/4) H_\beta(y)$, where C_β is an appropriate constant and $H_\beta(y)$ is the product of the suitable Hermite polynomial for each y_i, $i = 1 \ldots N$, where $y = (y_1, \ldots y_N)$, are components of the spatial variable.

Some of this structure is lost for heat equations of order greater than $2m$ for $m > 1$; although we can still derive a fundamental solution it doesn't have a closed form representation and is also of changing sign. For the specific case $m = 3$, we have that

$$b(x,t) = t^{-N/6} F(y), \quad y = x t^{-1/6}, \tag{1.3.42}$$

which follows from the scaling invariance of (1.3.36). The factor of $t^{-N/6}$ comes from the inherited conservation of mass. The rescaled kernel F is then the unique radial solution of the elliptic equation

$$\mathbf{B}F = \Delta^3 F + \frac{1}{6} y \cdot \nabla F(y) + \frac{N}{6} F(y) = 0 \text{ in } \mathbb{R}^N, \quad \int_{\mathbb{R}^N} F(y) \mathrm{d}y = 1. \tag{1.3.43}$$

Applying the Fourier Transform to the rescaled equation we find that

$$\mathcal{F}(F(\cdot))(\xi) = \exp(-|\xi|^6), \tag{1.3.44}$$

where ξ denotes the independent variable in the frequency domain. Then applying the inverse transform for radial functions we arrive at an integral formula for f,

$$F(y) = (2\pi)^{-N/2} \int_0^\infty \exp(-s^6)(s|y|)^{N/2} J_{(N-2)/2}(s|y|) \mathrm{d}s, \tag{1.3.45}$$

see [48] for details of the derivation. While this is still exponentially decaying, the tails are in fact oscillatory with infinitely many sign changes. However, it is

known to satisfy the pointwise estimate ([47]):

$$|F(y)| < D\hat{F}(y), \quad \hat{F}(y) = \omega_1 \exp(-a|y|^{6/5}) > 0, \quad \omega_1 = \left(\int \exp(-a|y|^{6/5}) \right)^{-1}, \tag{1.3.46}$$

with a a constant dependent on N and $D > 1$ a constant acting as an optimal 'order deficiency' for the semigroup. Roughly speaking this is a measure of how far apart nearby orbits can grow, see [45] for some discussion and [78] for the use of this estimate to construct a 'majorizing' integral equation for which a comparison principle with solutions of (1.3.36) and (1.2.32). It is not clear whether this (difficult) approach can apply to cases like (1.1.1), certainly we know of no way currently to account for the non-positivity of the nonlinear term. We emphasize that the oscillations of the kernel make it so that $||F||_{L^1} > 1$, and so $D > 1$ is the least constant such that $||u_1(t) - u_2(t)||_{L^p} \leq D||u_{0,1} - u_{0,2}||_{L^p}$, $p \geq 1$ holds for initial data $u_{0,1}$, $u_{0,2}$. This corresponds to the lack of a maximum principle for higher order equations.

1.3.1. The point spectrum of the non self-adjoint operator B: As we have seen, the major difference from the second-order case is that $\mathbf{B}$ ((1.3.43)) is not symmetric and does not admit a self-adjoint extension; the difference in order of the first two terms makes choosing a $\rho(y)$ that might allow us to collapse them together an impossible task. This complicates the theory considerably, but fortunately much of the essence carries through and in fact we end up again with a discrete real spectrum and complete sets of (bi)-orthogonal eigenfunctions. These results are presented in full in [45], with further details on the adjoint $\mathbf{B}^*$ in [67]. We refer to [93] for a full account of the spectral theory of non-self adjoint operators.

We consider $\mathbf{B}$ in the weighted space $L^2_\rho = L^2_\rho(\mathbb{R}^N)$ with the exponentially growing weight function

$$\rho(y) = \exp(a|y|^{6/5}) > 0 \quad \text{in} \quad \mathbb{R}^N, \tag{1.3.47}$$

and $a \in (0, 2d)$ is a sufficiently small constant. We ascribe to $\mathbf{B}$ the domain H^6_ρ being a weighted Hilbert space with the norm

$$\|v\|^2 = \int \rho(y) \textstyle\sum_{k=0}^6 |D^k v(y)|^2 \, dy,$$

induced by the corresponding inner product. Then we have the following lemma:

- $\mathbf{B} : H^6_\rho \to L^2_\rho$ is a bounded linear operator with the real spectrum

$$\sigma(\mathbf{B}) = \{\lambda_l = -l/6,\ l = 0, 1, 2, ...\}. \tag{1.3.48}$$

- The eigenvalues l_l have finite multiplicity with eigenfunctions

$$\psi_\beta(y) = \frac{(-1)^{|\beta|}}{\sqrt{\beta!}} D^\beta F(y), \quad \text{with any } |\beta| = l, \tag{1.3.49}$$

- The subset of eigenfunctions $\Phi = \{\psi_\beta,\ |\beta| = 0, 1, 2, ...\}$ is complete in L^2_ρ and in L^2.

This gives the centre and stable subspaces of $\mathbf{B}$, $E^c = \text{Span}\{\psi_0 = F\}$ and $E^s = \text{Span}\{\psi_\beta,\ |\beta| > 0\}$.

1.3.2. The polynomial eigenfunctions of the adjoint operator $\mathbf{B}^*$: We consider $\mathbf{B}^*$, the adjoint of $\mathbf{B}$ given by

$$\mathbf{B}^* = \Delta^3 - \frac{1}{6} y \cdot \nabla \tag{1.3.50}$$

in $L^2_{\rho^*}$ with the exponentially decaying weight function $\rho^*(y) = 1/\rho(y) \equiv e^{-a|y|^\alpha} > 0$.

- $\mathbf{B}^* : H^6_{\rho^*} \to L^2_{\rho^*}$ is a bounded linear operator with the same spectrum, (1.3.48).

- The eigenfunctions $\psi^*_\beta(y)$ with $|\beta| = l$ are l-the order polynomials

- $$\psi^*_\beta(y) = \frac{1}{\sqrt{\beta!}} \left[y^\beta + \textstyle\sum_{j=1}^{\lfloor |\beta|/6 \rfloor} \frac{1}{j!} (-\Delta)^{3j} y^\beta \right], \tag{1.3.51}$$

  and subset $\{\psi^*_\beta\}$ is complete in $L^2_{\rho^*}$.

With this definition of the adjoint eigenfunctions, the orthonormality condition

$$\langle \psi_\beta, \psi^*_\gamma \rangle = \delta_{\beta,\gamma} \tag{1.3.52}$$

holds. Here $\langle \cdot, \cdot \rangle$ denotes the standard (dual) L^2 inner product.

1.3.3. Compactness of the resolvent operator $(\mathbf{B} - \lambda \mathbf{I})^{-1}$: For any $\lambda \notin \sigma(\mathbf{B})$,

$$\mathbf{R}_\lambda := (\mathbf{B} - \lambda \mathbf{I})^{-1} : L^2_\rho \to L^2_\rho$$

is compact, and affords the explicit representation

$$\begin{aligned} \mathbf{R}_\lambda g(y) &= \int_{\mathbb{R}^{\mathbb{N}}} K(y,\eta) g(\eta) \mathrm{d}\eta, \\ K(y,\eta) &= \int_0^1 z^{\lambda-1}(1-z)^{-N/6} F\left[(y-\eta z^{1/6})(1-z)^{-1/6}\right] \mathrm{d}z, \end{aligned} \tag{1.3.53}$$

where F is the unique radial solution of (1.3.36).

1.4. Layout and Summary of Results

We briefly summarize here the original contributions made in this thesis. In Chapter 2 we conduct a detailed study of the similarity solutions of the unstable equation

$$u_t = \Delta^3 u - \Delta\left(|u|^{p-1}u\right), \quad p > 1.$$

We first concentrate on solutions that blow-up in finite time. We identify a critical exponent where the similarity solutions can have non-zero mass, and we construct an infinite set of them numerically for $N = 1$ and $N = 3$, where N is the spatial dimension. We supplement this with a matched asymptotic expansion for $N = 1$, as well as using the numerical scheme constructed in Chapter 3 to explore questions of stability. We construct a further countable set of solutions at a second critical exponent for which similarity solutions can admit non-zero first moment, and indicate a direction in which they might eventually be understood via bifurcation theory in a parameter corresponding to the rate of spatial decay of the profiles. Finally, we demonstrate a link between the non-variational elliptic equation that determines the similarity solutions and a problem that does admit a variational formulation.

We then turn to globally bounded self-similar solutions, first bounding the range for which self-similar solutions can exist from above in p, then demonstrating the existence of a continuous set of solutions in the p-critical case (which is always within this existence range) by two methods. The set is parameterized by mass, and by numerical construction we demonstrate that for $N = 1$ this parameterization is not monotone, a new feature not seen in the fourth order Cahn-Hilliard equation studied in [56]. We also construct the branch for $N = 3$. In both cases, we provide evidence that the solutions cannot exceed a certain mass that is smaller than the mass of the minimal blow-up profile, suggesting the nonexistence of a 'Leray scenario' that we discuss at the end of Chapter 2. Before that, we examine the dependence of solutions on p, with the bifurcation theory,

though the details of the argument are deferred to Chapter 4. We construct branches of solutions numerically for $N = 1$ and $N = 3$, the latter demonstrating a surprising global structure wherein the branches are not all connected to the bifurcation points.

In Chapter 3 we develop two related adaptive numerical schemes for simulating the evolution sixth order parabolic PDE that use moving meshes and time-transformations to resolve singularities. The Chapter begins with some history and mathematical background pertaining to adaptive techniques of this class, before the schemes are introduced. This work generalizes earlier schemes for second order [105] and fourth order [150] PDEs. The generalization is mostly straightforward with the exception of a different discretization of the time derivative of the solution that we propose, the enhanced stability properties of which are established. Truncation errors are calculated for both schemes and included in the relevant sections. We conclude the chapter with two examples from neighbouring areas of research to demonstrate the ability of the scheme to easily handle solutions with blow-up.

In Chapter 4 we consider the large time asymptotics of the equation

$$u_t = \Delta^3 u + \Delta\left(|u|^{p-1}u\right), \quad p > 1.$$

The bulk of this comprises a description, again, of self-similar solutions. We begin with some routine adaptations of already existing proofs to show that all solutions starting from bounded initial data can be uniformly bounded in the L^∞ norm for all time, over wide range of p. Then we develop three separate bifurcation arguments, with greater rigour than in previous work. First, we demonstrate the existence of the continuous mass-branch of solutions at the critical value of p and then a further countable set of p-branches that are analogous to those we consider in Chapter 2. We also construct another bifurcation argument in an artificial parameter that is linked to the variational connection in Chapter 2. We use the Lyapunov-Schmidt method to construct approximations to the solutions near the branch point in each case, then extend them globally (as far as possible) with numerics. From these, we conjecture the existence of finite sets of solutions below a certain value of p. We conclude with brief descriptions of first non-self-similar asymptotic patterns, then self-similar but 'non-physical' ones.

In Chapter 5 we condense some of the arguments in Chapters 2 and 4 and apply them to the much more difficult equation

$$u_t = \Delta^3 u \pm \Delta^2\left(|u|^{p-1}u\right), \quad p > 1.$$

We take both signs for brevity, the '+' sign corresponding to the unstable equation and the '-' sign to the stable one. We begin with blow-up solutions in the unstable case. First we consider the critical p for which self-similar solutions can have non-zero mass. We demonstrate the existence of a countable set of such solutions numerically, before sketching the beginnings of a matched asymptotic construction for the much more complicated structure revealed by the numerics. We then look at three further critical p values associated with conserved quantities, demonstrating a countable set of self-similar solutions at $p = 2$, proving non-existence of self-similar solutions $p = \frac{5}{3}$, and not being able to conclude either way at $p = \frac{3}{2}$ (all with $N = 1$). We exhibit some numerical solutions of the PDE at these p-values using the scheme introduced in Chapter 3 that suggest at the very least the self-similar blow-up is not generic. Finally, we reproduce the numerical aspects of the mass and p-bifurcation arguments of Chapter 4 for globally bounded self-similar solutions in both the stable and the unstable case.

Before we introduce the results, we note that unless stated otherwise, the numerical calculations used to generate the figures in this thesis were carried out with consistent tolerances and settings. In Matlab, we used the inbuilt ODE solver ode15s with Reltol and Abstol both set to 10^{-14}. The tolerance of Matlab's fsolve was also set to 10^{-14} where it was used. For the Matlab external software BVPsuite [116], we left the default tolerances of 10^{-10} unchanged. For the Fortran DAE solver DASPK [163], the tolerances were set to 10^{-5} and the order of the internal backwards differentiator was set to 5. The solver AUTO [42] was mostly used with constants NTST = 100, NCOL = 7 for following a branch and NTST = 20, NCOL = 4 for detecting a bifurcation point. In both cases we defaulted to EPSL = 10^{-7}, EPSU = 10^{-7} and EPSS = 10^{-5}. However, in some instances we had to adjust all of these settings mid-branch for the solver to converge, on a case by case basis.

Chapter 2

Cahn-Hilliard Equation with a Second Order Nonlinearity - Unstable Case

2.1. Preliminaries

We begin with the unstable sixth order Cahn Hilliard equation featuring second order derivatives of a power law nonlinearity:

$$u_t = \Delta^3 u - \Delta(|u|^{p-1}u) \quad \text{in} \quad \mathbb{R}^N \times \mathbb{R}_+, \tag{2.1.1}$$

supplemented with the initial condition

$$u(x,0) = u_0(x), \tag{2.1.2}$$

with $p > 1$. We usually assume that u_0 is smooth and with 'quick enough' decay as $|x| \to \infty$. In this chapter we begin by establishing some properties of the equation concerning existence, blow-up, and scaling invariance. This facilitates our main aim, which is to as much as possible describe and classify the possible asymptotic patterns and investigate which arise in the flow. These often manifest as self-similar solutions, and so we dedicate the remainder of the chapter to a detailed study of them. First we address the case of blow-up self-similar solutions, then self-similar solutions that remain globally bounded for all time, for which we adopt the terminology *spreading solutions*. The presence in (2.1.1) of both, and their interesting geometric properties, provide a perfect example of the merits of studying sixth order equations in this way.

2.2. General Properties of the Equation

2.2.1. Existence and Blow-up: For well-behaved initial data u_0, local in time existence and uniqueness of classical solutions or (2.1.2) is easy to see from the equivalent integral equation, also known as the 'variation of parameters' formulation ([64], Chapter 16):

$$u(x,t) = b(t) * u_0 - \int_0^t \Delta b(t-s) * \left(|u|^{p-1}u\right)(s)\mathrm{d}s, \tag{2.2.3}$$

where

$$b(x,t) = F(y), \quad y = xt^{-1/6},$$

with $F(y)$ the solution to (1.3.43). This is a contraction in the space of bounded, continuous functions in $\mathbb{R}^N \times [0,\delta]$, $\delta > 0$ with the sup norm provided that δ is sufficiently small, see e.g. [159]. Banach fixed point theorem thus gives a unique solution, and provided u is uniformly bounded it is possible to find a classical extension locally in time.

(2.1.1) is a gradient system in the space H^{-1}, defined on $\mathbb{R}^{\mathbb{N}}$ as the space of tempered distributions u such that

$$\left(1+|\xi|^2\right)^{-1/2}\hat{u}(\xi) \in L^2(\mathbb{R}^N),$$

where $\hat{u}$ denotes the Fourier Transform of u. We can identify the operator Δ^{-1} on the space of tempered distributions with the operator $\mathcal{F}^{-1}\left(\left(1+|\xi|^2\right)^{-1/2}\hat{u}(\xi)\right)$, where $\mathcal{F}^{-1}$ here represents the inverse Fourier Transform; we take this convention for the entirety of this thesis. This allows us to define the associated Lyapunov energy functional

$$E[u](t) = \frac{1}{2}||\Delta u||_2^2 - \frac{1}{p+1}||u||_{p+1}^{p+1}, \quad u \in H^2(\mathbb{R}^n) \cap L^{p+1}(\mathbb{R}^n), \tag{2.2.4}$$

which we can see is monotone decreasing in time as

$$\frac{\mathrm{d}}{\mathrm{d}t}E = \int_{\mathbb{R}^n} (\Delta u \Delta u_t - |u|^{p-1}uu_t)\mathrm{d}x = -\int_{\mathbb{R}^n} u_t(-\Delta)^{-1}u_t\,\mathrm{d}x = -||u_t||^2_{H^{-1}(\mathbb{R}^n)} \leq 0. \tag{2.2.5}$$

However, this gives us only a limited amount of control over the evolution of the solutions, as the difference in sign of the two components ensure that the functional is non-coercive (i.e. we can have $u \to \infty$ in $H^2(\mathbb{R}^N)$ and in $L^{p+1}(\mathbb{R}^N)$ but $E[u]$ remains finite). This allows for, though does not necessarily imply, solutions

to blow-up in finite time, and also means that despite the gradient system structure, we cannot necessarily conclude that the ω-limit set of flow comprises only the stationary solutions of the elliptic operator on the right hand side of (2.1.1): $\Delta^3 u - \Delta u^p = 0$. This is closely related to the biharmonic problem $\Delta^2 u - u^p = 0$ in $\mathbb{R}^N$, for which the solutions are well understood in the supercritical range $N > 5$, $p > \frac{N+4}{N-4}$ and described in [89]. However, it is hard to rule out nonstationary asymptotic behaviour, indeed this is known to happen for a class of semilinear heat equations, see for example [149].

Conclusive proof that some initial data for (2.1.2) leads to blow up can be seen by recasting (2.1.1) as the pseudoparabolic problem

$$(-\Delta)^{-1} u_t = \Delta^2 u - |u|^{p-1} u. \tag{2.2.6}$$

This allows us to use the concavity methods since we now have an equation of the form (1.2.25). The potential (1.2.26) has the form $G(u) = \frac{1}{p+1} \int_{\mathbb{R}^N} |u|^{p+1} \mathrm{d}x$ and can be easily shown to satisfy (1.2.27):

$$2(\alpha+1)G(u) \leq \left(|u|^{p-1}u, u\right) \iff \alpha \leq \frac{p-1}{2}.$$

This is clearly allowed for some $\alpha > 0$ since $p > 1$. So the result from [125] applies provided the following inequality for the initial condition is satisfied:

$$\frac{1}{2}||\Delta u_0||_{L^2}^2 - \frac{1}{p+1}||u_0||_{L^{p+1}}^{p+1} < 0. \tag{2.2.7}$$

This gives us the simple interpretation that for solutions with positive initial energy, the dissipative effect will likely cause the solution to vanish, whereas if the initial energy is negative, there will be a runaway effect as the energy becomes more and more so, leading to blow-up. Note that this does not necessarily rule out blow-up for all initial data with positive energy and we have not been able to exclude the possibility of this occurring for pathological u_0.

2.2.2. Scaling Invariance and Similarity Solutions: As we have seen in Chapter 1, one of the most powerful tools at our disposal is to look for similarity solutions to (2.1.1). The idea is that if the equations are invariant under a one-parameter family of scalings, then it is possible to reduce the number of independent variables by one (by considering groupings of the original variables) without losing any information. This often manifests in PDE theory as turning an equation in one time variable and N spatial variables into an ODE in

N pseudo-spatial variables that themselves scale with time. The nomenclature arises from the fact that there is a family of scalings for which these solutions maintain the same shape, which is effectively what invariance means in this context. Understanding these will go a long way towards giving a sense of what the PDE really does, informing our understanding of singularity formation and asymptotic patterns that tend to feature these kinds of solutions heavily.

We reiterate that the reason that these types of solutions emerge is their close relationship to the scaling properties of the underlying PDE. To find a one parameter family of transformations that leaves (2.1.1) invariant, we consider the scalings

$$x = \lambda_1 \bar{x}, \qquad t = \lambda_2 \bar{t}, \qquad u = \lambda_3 \bar{u},$$

with $\lambda_i > 0$. These give the rescaled equation

$$\frac{\lambda_3}{\lambda_2} \bar{u}_{\bar{t}} = \frac{\lambda_3}{\lambda_1^6} \bar{\Delta}^3 \bar{u} - \frac{\lambda_3^p}{\lambda_1^2} \bar{\Delta}(|\bar{u}|^{p-1}\bar{u}) \tag{2.2.8}$$

suggesting that for invariance, we require $\lambda_1 = \lambda_2^{\frac{1}{6}}$ and $\lambda_3 = \lambda_2^{-\frac{2}{3(p-1)}}$, and we have a one-parameter family of scalings; relabelling $\lambda_2 \to \lambda$,

$$t \to \lambda t, \quad x \to \lambda^{1/6} x, \quad u \to \lambda^{-2/3(p-1)} u. \tag{2.2.9}$$

Since λ is arbitrary, we can reduce (2.2.8) to a simpler PDE by allowing it to scale with time, i.e. set $\lambda = t$. To abuse notation, we then have

$$u(x,t) = t^{-2/(3(p-1))} \bar{u}(xt^{-\frac{1}{6}}, 1) = t^{-2/(3(p-1))} f(y), \quad y = xt^{-\frac{1}{6}}, \tag{2.2.10}$$

which we can substitute back into (2.1.1) to derive a sixth order, elliptic equation in f:

$$\Delta^3 f(y) - \Delta\left(|f(y)|^{p-1} f(y)\right) + \frac{1}{6} y \cdot \nabla f(y) + \frac{2}{3(p-1)} f(y) = 0. \tag{2.2.11}$$

Unfortunately, this equation is not the Euler-Lagrange equation for any energy functional, and so we are forced to proceed without the enormous power of variational theory to help us, though see Section 2.3.8 for a related variational problem.

To analyze convergence to, and stability of, self-similar solutions, we can keep the scalings above but reintroduce a time variable, τ. In doing so, we set $u(x,t) = t^{-2/(3(p-1))}\theta(y,\tau)$, and if we set $\tau = \ln t$, we recover a sixth order

parabolic PDE

$$\theta_\tau = \Delta^3\theta - \Delta\left(|\theta|^{p-1}\theta\right) + \frac{1}{6}y\cdot\nabla\theta + \frac{2}{3(p-1)}\theta, \tag{2.2.12}$$

which is the natural setting in which to investigate these questions. For cases in which solutions blow-up at time T, we can treat the problem more easily by stretching the blow-up time to infinity; in this case, by rescaling the time variable like $\tau = \ln(T-t)$, inducing the corresponding rescalings of solution and spatial domain

$$u(x,t) = (T-t)^{-2/(3(p-1))}\theta(y,\tau), \qquad y = x(T-t)^{-\frac{1}{6}},$$

for which we arrive at the semilinear PDE

$$\theta_\tau = \Delta^3\theta - \Delta\left(|\theta|^{p-1}\theta\right) - \frac{1}{6}y\cdot\nabla\theta - \frac{2}{3(p-1)}\theta. \tag{2.2.13}$$

For convenience, we combine (2.2.13) and (2.2.12) into one equation using the notation $\sigma = 1$ in the case where solutions blow up and $\sigma = -1,\ T = 0$ (or $T = 1$ if we want the initial condition θ_0 to agree with the non-rescaled u_0) for global solutions,

$$\theta_\tau = \mathbf{A_2}(\theta) = \Delta^3\theta - \Delta\left(|\theta|^{p-1}\theta\right) - \frac{\sigma}{6}y\cdot\nabla\theta - \frac{2\sigma}{3(p-1)}\theta. \tag{2.2.14}$$

Independent of τ stationary solutions $f(y)$ of

$$\mathbf{A_2}(f) = 0, \tag{2.2.15}$$

describe the exact self-similar profiles, and we expect that the rescaled flow will eventually converge to one of them for at least some initial conditions. Without the maximum principle or some other geometric argument (as it stands we have none) that imposes a predictable global structure, this can be done only by studying the linearized spectra around the steady states. We do this in Section 2.3.4.

To make headway in understanding the behaviour of f, we begin with cases where it is radially symmetric in y. To our knowledge, there have been no blow-up solutions of 'simple' semilinear equations such as ours that are both non-radial and self-similar. One or the other abound, for some examples of non-radial blow up see [23] or the recent high dimensional approach to the semilinear heat equation in [35]. Acknowledging that we have no way to prove or disprove the

existence of non-radial, self-similar solutions, we endow (2.2.15) with symmetric boundary conditions at the origin and a decay condition at infinity,

$$f'(0) = f'''(0) = f^{(\mathrm{v})}(0) = 0, \qquad f(y) \to 0 \quad as \quad y \to \infty. \tag{2.2.16}$$

2.2.3. Conservativeness and the Critical Exponent: If the decay at infinity is sufficiently rapid, (2.1.1) preserves the initial mass throughout the evolution, i.e.

$$\frac{\mathrm{d}}{\mathrm{d}t}\int_{\mathbb{R}^N} u(x,t)\mathrm{d}x = 0. \tag{2.2.17}$$

In parabolic evolution equations such as these, this condition is equivalent to being able to integrate up the elliptic part of the operator and consider an equation of one less order, as

$$\int_{\mathbb{R}^N} u_t(x,t)\mathrm{d}x = \int_{\mathbb{R}^N} \Delta^3 u(x,t) - \Delta\left(|u|^{p-1}u\right)(x,t)\mathrm{d}x = 0,$$

with the last equality following from the divergence theorem and the decay of u and its derivatives at infinity. To find out if this conservative property is preserved by the similarity rescaling, we look at an exact similarity solution u_S, and assuming $f \in L^1(\mathbb{R}^N)$, we find that

$$\int_{\mathbb{R}^N} u_S(x,t)\mathrm{d}x = [\sigma(T-t)]^{-2/(3(p-1))+N/6}\int_{\mathbb{R}^N} f(y)\mathrm{d}y.$$

This expression satisfies the condition (2.2.17) if and only if

$$p = p_0 = 1 + \frac{4}{N}. \tag{2.2.18}$$

This is the *Critical Exponent* for the problem and will be the focus of the first part of our investigation, although we will later treat some aspects of dependence of the solutions on p. Note that this coincides with the critical Fujita exponent for the equation (1.2.32) with $m = 2$, and with a change in the stability of the linearized equation about the trivial solution, see Section 4.2.3.

We can also draw the following useful conclusion:

Remark 2.1. *Any integrable similarity solutions for $p \neq p_0$ must have zero mass.*

2.2.4. Large-y Asymptotics of the Similarity Profiles: Understanding the behaviour of solutions to (2.2.15) in the limit $|y| \to \infty$ serves two purposes: it allows us to establish some existence results via a topological shooting procedure,

and also provides key information about the nature of the final time/initial profile in the original variables (for the blow-up and spreading cases respectively), both of which we will describe in the relevant sections below. Moreover, in the 'physically relevant' case where we demand that the self-similar profiles be bounded and integrable, the decay this imposes in the large $|y|$ limit allows us to work with a linearized equation for which the analysis is much more straightforward, making this a natural place to start.

We continue to assume that, at least for large $|y|$, the solutions have radial dependence only. Then the linearized equation for f small becomes

$$\begin{aligned}\mathbf{A_2}'(0)f = f^{(\mathrm{vi})} + \frac{3(N-1)}{y}f^{(\mathrm{v})} + \frac{3(N-1)(N-3)}{y^2}f^{(\mathrm{iv})} + \\ \frac{(N-1)(N-3)(N-8)}{y^3}f''' - \frac{3(N-1)(N-3)(N-5)}{y^4}f'' + \\ \frac{3(N-1)(N-3)(N-5)}{y^5}f' - \frac{\sigma}{6}yf' - \frac{2\sigma}{3(p-1)}f = 0. \quad (2.2.19)\end{aligned}$$

Working with the linearization is justified since zero is an equilibrium of the dynamical system. We apply the change of variables $z = y^{6/5}$ so we can write the equation as

$$f^{(\mathrm{vi})} - \frac{\sigma}{6}\left(\frac{5}{6}\right)^5 f' - \frac{2\sigma}{3(p-1)}\left(\frac{5}{6}\right)^6 z^{-1}f + \sum_{j=1}^{5} C_j z^{j-6} f^{(j)} = 0, \quad (2.2.20)$$

which allows us to apply theorem 2.1 from chapter 5 of [34]. Then the leading order exponential behaviour of an (at least) formal power series solution to the ode in z is the solution of

$$f^{(\mathrm{vi})} - \frac{\sigma}{6}\left(\frac{5}{6}\right)^5 f' = 0, \quad (2.2.21)$$

which is, up to a constant term,

$$f(z) = \sum_{j=1}^{5} C_j \exp(p_j z), \quad p_j = \beta \exp(i\pi(2j - \sigma + 1)/10). \quad (2.2.22)$$

We introduce $\beta = 5/6^{6/5}$ for brevity. Examining the number of coefficients p_j with negative real part is enough to establish the dimensionality of the (exponentially) stable bundle about the zero solution of (2.2.15): as $y \to \infty$ we have

- a three dimensional stable exponential bundle for the global case $\sigma = -1$;

- a two dimensional stable exponential bundle for the blow-up case $\sigma = 1$.

Note however that solving (2.2.21) fixes only five possible behaviours; for a linear sixth order equation such as (2.2.19) we should expect one more. We will establish the nature of this extra mode, but first we will derive a more accurate description of the linearized exponentially decaying solutions by including more terms in the series. This will be useful later in the investigation.

This is most easily achieved using the celebrated WKBJ method, developed in the early twentieth century to study the Schroedinger Equation, see [11], chapter 9 for some historical context and theory. The method is a perturbation technique and requires a small parameter multiplying the highest order term, since we are interested in large y we introduce one using the substitution $y = \frac{Y}{\theta}$, where θ is small. This has the effect of multiplying the radial $\Delta^3 f$ term by $\theta^6 \ll 1$, leaving the other two unchanged. We then make the WKBJ ansatz:

$$f(Y) \sim \exp\left[\frac{1}{\delta}\sum_{n=0}^{\infty}\delta^n g_n(Y)\right] \tag{2.2.23}$$

where δ is another small parameter (a gauge) that we will use to balance with θ to derive a consistent asymptotic expansion.

The expansion is too large to reproduce here, but the relevant balance in this case comes at $\theta = \delta^{5/6}$, resulting in a balance between the $f^{(\mathrm{vi})}$ and the $\frac{\sigma}{6}Yf'$ terms, giving, at $\mathcal{O}(\delta^{-1})$

$$g_0(Y) = \beta(\sigma)^{1/5}Y^{6/5}, \tag{2.2.24}$$

where $\beta = 5/6^{6/5}$. This means that the leading behaviour with 'controlling factor' is

$$f(y) \sim C\exp\left(\beta\sigma^{1/5}y^{6/5}\right) \quad \text{as} \quad y \to \infty, \tag{2.2.25}$$

which is consistent with what we found in (2.2.22).

Then at $\mathcal{O}(1)$ the equation reads

$$\frac{5}{6}\sigma Y g_1'(Y) + \frac{1}{2}N\sigma - 2\frac{\sigma}{3(p-1)} = 0$$

which has solution

$$g_1(Y) = -\frac{3}{5}\left(N - \frac{4}{3(p-1)}\right)\ln(Y).$$

Continuing in the same vein, the equation at $\mathcal{O}(\delta)$ can be solved to give $g_2(Y) \sim Y^{-6/5}$. Since this is decaying, it and all further terms play no significant role and

we are left with the family of behaviours

$$f(y) = \sum_{\mathrm{Re}(\sigma^{1/5})<0} C_\sigma y^{(-3/5)(N-4/(3(p-1)))} \exp(\beta\sigma^{1/5} y^{6/5})(1+o(1)) \quad \text{as} \quad y \to \infty. \tag{2.2.26}$$

The sum runs over those fifth roots of σ with negative real part, the constants C_σ arbitrary and allowed to differ for each of these values.

To pick up the remaining mode, it is helpful to rewrite (2.2.19) in the variable $y = 1/\zeta$ so we can look at the limit $\zeta \to 0$. The equation is then

$$\begin{aligned}\frac{\mathrm{d}^6}{\mathrm{d}\zeta^6} f - \frac{3(N-11)}{\zeta}\frac{\mathrm{d}^5}{\mathrm{d}\zeta^5} f + \frac{3(N^2-24N+123)}{\zeta^2}\frac{\mathrm{d}^4}{\mathrm{d}\zeta^4} f - \\ \frac{(N-9)(N^2-39N+188)}{\zeta^3}\frac{\mathrm{d}^3}{\mathrm{d}\zeta^3} f - \frac{9(N^3-23N^2+159N-337)}{\zeta^4}\frac{\mathrm{d}^2}{\mathrm{d}\zeta^2} f - \\ \frac{15(N-5)(N-7)(N-3)}{\zeta^5}\frac{\mathrm{d}}{\mathrm{d}\zeta} f + \frac{\sigma}{6\zeta^{11}}\frac{\mathrm{d}}{\mathrm{d}\zeta} f - \frac{2\sigma}{3(p-1)\zeta^{12}} f = 0.\end{aligned} \tag{2.2.27}$$

We expect the last two terms to be the largest since ζ is small (note the inverse powers of ζ are large enough that $\zeta = 0$ is an irregular singular point, precluding the use of classical Frobenius theory), and so to recover the balance we pose

$$f(t) = \zeta^\alpha g(t). \tag{2.2.28}$$

We then find at $\mathcal{O}(\zeta^{\alpha-12})$ that $\frac{\sigma}{6}\alpha g(\zeta) - \frac{2\sigma}{3(p-1)} g(\zeta) = 0$ giving us $\alpha = 4/(p-1)$. At $\mathcal{O}(\zeta^{\alpha-11})$ we get $\frac{\mathrm{d}}{\mathrm{d}\zeta} g = 0$ suggesting the leading order term of g is constant. Substituting $g(\zeta) = g_0 + g_1(\zeta)$, we find the balance must be between the terms at $\mathcal{O}(\zeta^{\alpha-11})$ and at $\mathcal{O}(\zeta^{\alpha-6})$, giving

$$\frac{-32p\,(p+1)\,(Np-N-2p-2)\,(Np-N-4p)\,(Np-N-6p+2)\,g_0}{(p-1)^6\,\zeta^6} + \frac{\sigma}{6}\frac{g_1'(\zeta)}{\zeta^{11}} = 0.$$

This enforces that $g_1(\zeta)$ has the form of a constant multiple of ζ^6. We thus pose an expansion

$$g(t) = \sum_{i=0}^{\infty} g_i \zeta^{6i}.$$

Then considering balances at $\mathcal{O}(\zeta^{\alpha-6n})$, tedious calculations substituting the ex-

pansion into (2.2.27) give the relation

$$\frac{g_{n+1}}{g_n} = \frac{8\zeta^6}{\sigma(p-1)^6(n+1)}\big(3n(p-1)+2\big)\big(3n(p-1)+p+1\big)\big(3n(p-1)+2p\big)$$
$$\big((N-6n)(p-1)-2p-2\big)\big((N-6n)(p-1)-4p\big)\big((N-6n)(p-1)-6p+2\big).$$

Clearly by the ratio test, the series is divergent. It does form an asymptotic approximation to g as $\zeta \to 0$ ([11], Chapter 3), and returning to the original y variable we find that

$$f(y) \sim Ay^{-4/(p-1)}\left(1+\mathcal{O}(y^{-6})\right), \tag{2.2.29}$$

completing our description of large y behaviours.

We have demonstrated in this section that if there exist any integrable solutions of (2.2.11), their asymptotic behaviours in this regime must be expressed by a combination of the modes described above. Much of the rest of this chapter will be dedicated to providing evidence that integrable solutions do exist, making use of this fact.

2.3. Blow-up Solutions

2.3.1. The Final-Time Profile and Implications: For the blow-up scenario $\sigma = 1$, the large-y asymptotics for the similarity profiles give us a description of the limit final time (radial) profile almost everywhere. We have

$$\lim_{t\to T^-} u(x,t) = \lim_{t\to T^-}(T-t)^{-2/(3(p-1)}f\left(\frac{x}{(T-t)^{1/6}}\right) =$$
$$x^{-4/(p-1)}\lim_{y\to\infty} y^{4/(p-1)}f(y),$$

then taking this limit we get the final time profile

$$u(x,T^-) = A|x|^{-4/(p-1)}, \quad |x| \neq 0. \tag{2.3.30}$$

It is striking that this is not integrable (nor indeed in any L^q space) if $A \neq 0$, and so one might expect that it cannot evolve from an initial profile of finite mass. For $p < p_0$, with p_0 as in (2.2.18), the singularity at the origin is the problem, whereas for $p \geq p_0$ the singularity is integrable but the decay at infinity is not sufficiently fast. However, the former scenario turns out to not present an obstruction to the finite mass case. Consider a self-similar solution u, integrate

and split over a ball at the origin of radius ε and its complement (we take y to be the radial coordinate):

$$\int_{\mathbb{R}^N} u(x,t) = \int_{B_\varepsilon(0)} u(x,t)\mathrm{d}x + \int_{\mathbb{R}^N\setminus B_\varepsilon(0)} u(x,t)\mathrm{d}x = (T-t)^{-2/3(p-1)+N/6}\,\omega_N\left[\int_0^{\varepsilon/(T-t)^{1/6}} y^{N-1}f(y)\mathrm{d}y + \int_{\varepsilon/(T-t)^{1/6}}^{\infty} y^{N-1}f(y)\mathrm{d}y\right],$$

where ω_N is the surface area of the unit ball in $\mathbb{R}^N$. Finite mass dictates the integrals inside the square brackets must converge $\forall\varepsilon>0$, $t<T$. Now choose ε and t such that $\varepsilon/(T-t)^{1/6}\gg 1$ where f behaves like $Ay^{-4/(p-1)}$. For the second integral to converge, we must have $y^{N-1-4/(p-1)} = o(y^{-1})$ which only occurs for $p<p_0$. Now in this case, we can evaluate the limit as $t\to T^-$ using l'Hôpital's rule since $(T-t)^{2/3(p-1)-N/6}\to 0$ and so do both $\int_0^{\varepsilon/(T-t)^{1/6}} y^{N-1}f(y)\mathrm{d}y$ and $\int_{\varepsilon/(T-t)^{1/6}}^{\infty} y^{N-1}f(y)\mathrm{d}y$, the former since $\int_{\mathbb{R}^N} f(y)\mathrm{d}y = 0$ (remark 2.1).

This gives us

$$\lim_{t\to T^-}\left(\int_{B_\varepsilon(0)} u(x,t)\mathrm{d}x + \int_{\mathbb{R}^N\setminus B_\varepsilon(0)} u(x,t)\mathrm{d}x\right) = \lim_{t\to T^-}\omega_N\left(\frac{\int_0^{\varepsilon/(T-t)^{1/6}} y^{N-1}f(y)\mathrm{d}y + \int_{\varepsilon/(T-t)^{1/6}}^{\infty} y^{N-1}f(y)\mathrm{d}y}{(T-t)^{2/3(p-1)-N/6}}\right) = \lim_{t\to T^-}\frac{\omega_N\varepsilon^N}{4/(p-1)-N}(T-t)^{-2/3(p-1)}\left[-f\left(\frac{\varepsilon}{(T-t)^{1/6}}\right)+f\left(\frac{\varepsilon}{(T-t)^{1/6}}\right)\right].$$

Now since $\lim_{t\to T^-}(T-t)^{-2/3(p-1)} f\left(\frac{\varepsilon}{(T-t)^{1/6}}\right) = A\varepsilon^{-4/(p-1)}$, this evaluates to

$$\lim_{t\to T^-}\left(\int_{B_\varepsilon(0)} u(x,t)\mathrm{d}x + \int_{\mathbb{R}^N\setminus B_\varepsilon(0)} u(x,t)\mathrm{d}x\right) = \frac{-A\omega_N\varepsilon^{N-4/(p-1)}}{4/(p-1)-N} + \frac{A\omega_N\varepsilon^{N-4/(p-1)}}{4/(p-1)-N} = 0, \quad (2.3.31)$$

splitting the mass between the singularity and the rest of the space. Since $p<p_0 \implies N<\frac{4}{p-1}$, letting $\varepsilon\to 0$ recovers from the second integral the infinite mass of (2.3.30) away from the origin but this is balanced by an 'equal and opposite' infinite mass accumulating there.

This does not preclude the existence of infinite mass self-similar solutions with $A\neq 0$ for $p>p_0$, and they may even attract solutions with finite mass initial data in some sense (e.g pointwise on compact subsets); observe that for the rescaled

flow (2.2.15) we have

$$\frac{\mathrm{d}}{\mathrm{d}\tau}\int_{\mathbb{R}^N}\theta \mathrm{d}y = \int_{\mathbb{R}^N}\left[\Delta^3\theta - \Delta\left(|\theta|^{p-1}\theta\right) - \frac{1}{6}y\cdot\nabla\theta - \frac{2}{3(p-1)}\theta\right]\mathrm{d}y.$$

Now employing the divergence theorem, the first two terms vanish and defining

$$M^\theta(\tau) = \int_{\mathbb{R}^N}\theta \mathrm{d}y, \quad c_p = \frac{N(p_0-p)}{6(p-1)}, \tag{2.3.32}$$

we find that

$$\frac{\mathrm{d}}{\mathrm{d}\tau}M^\theta = -c_pM^\theta \implies M^\theta = M_0^\theta\exp(-c_p\tau).$$

Thus the rescaled mass grows without bound as $\tau\to\infty \iff t\to T^-$ when $c_p<0 \iff p>p_0$. Such scenarios fall beyond the scope of this thesis. Now for $p=p_0$ the rescaled flow is also conservative and a solution whose initial mass is finite will remain that way, prohibiting non-zero values of A since (2.3.30) cannot occur. There may exist self-similar solutions with nontrivial A in this critical case, however, they will not play a role in the dynamics, and so we begin by studying with $p=p_0$, $A=0$.

2.3.2. The p_0 Critical Case in One Dimension: First and primarily, we focus on the case $N=1$. Not only does the radial restriction of (2.2.15) (c.f. (2.2.19)), taken for the remainder of this section with $\sigma=-1$, collapse to a much more manageable ODE, this is also the case where we have been able to to augment our analysis with numerical simulations of the PDE, see Chapter 3, and so merits the bulk of our attention.

Since for this critical case we have established that the coefficient A of algebraic decay (2.2.29) must be zero, the behaviour of solutions to (2.2.15) in the limit $y\to\infty$ is more constrained, being described by only the two-parameter family (2.2.25) with $\sigma=1$. That is, taking the linear combination of the two permissible modes of (2.2.26),

$$f(y)\sim C_0y^{-2/5}\exp(\beta e^{\frac{4\pi i}{5}}y^{6/5}) + C_1y^{-2/5}\exp(\beta e^{\frac{-4\pi i}{5}}y^{6/5}), \quad \beta = 5/6^{6/5}.$$

As f is real, this is more conveniently expressed as

$$f(y)\sim Cy^{-2/5}\exp(ay^{6/5})\cos(by^{6/5}+k), \tag{2.3.33}$$

where C, k are free parameters and

$$a = \beta\cos(\frac{4}{5}\pi),\ b = \beta\sin(\frac{4}{5}\pi). \tag{2.3.34}$$

Without loss of generality, we take $C > 0$.

Conspicuously, this bundle is oscillatory, a new phenomenon not present for blow up solutions of 4th order models studied in this manner (see [56], [72]). This comprehensively rules out both strictly non-negative and any possible monotone blow-up profiles $f(y)$, considerably complicating attempts at analysis and showing the now total departure from second-order theory.

Another advantage of the conservative case is that we can directly integrate (2.2.15), giving the ODE

$$f^{(\mathrm{v})} - (f^5)' - \frac{1}{6}yf = f^{(\mathrm{v})}(0) - 5f^4(0)f'(0) = -\frac{1}{6}A = 0,$$

the penultimate equality following from the consideration that the final term of the ODE on the left hand side is dominant as $y \to \infty$ when (2.2.29) is substituted in. This allows us to deduce that $f'(0) = 0 \implies f^{(\mathrm{v})}(0) = 0$ and the number of symmetry conditions at the origin that require fulfillment is reduced to two.

The asymptotic description (2.3.33) does not give us any information on how the solution behaves for small y, where the effects of the nonlinear term will strongly influence the solution, nor even for which pairs $[C, k]$ this behaviour might hold. However, it can be used to set up a 'boundary-value problem' for f, taking the form

$$\begin{aligned} &f^{(\mathrm{v})} - (f^5)' - \frac{1}{6}yf = 0, \quad f'(0) = f'''(0) = 0, \\ &f(y) \sim Cy^{-2/5}\exp(ay^{6/5})\cos(by^{6/5} + k) \text{ as } y \to \infty. \end{aligned} \tag{2.3.35}$$

That this is well-posed is established by calculating the number of restrictions the asymptotic behaviour (2.3.33) imposes on the problem; here it must be three to supplement the two symmetry conditions at $y = 0$ and this turns out to be the case, see Appendix A.

A standard approach to solving problems like (2.3.35) consists of *topological shooting*, especially for higher order equations, see [146]. In this case, we use C and k as parameters and shoot from the known large y behaviour to try and pick up the correct symmetry conditions (2.2.16) at the origin. This leads to a well-posed '2-2' shooting problem, as there must be at least as many parameters as conditions to fulfill for existence of solutions to be plausible. We favour this

approach over the more standard forward shooting, where $f(0)$, $f''(0)$ and $f^{(\mathrm{iv})}(0)$ furnish us with three parameters to try and 'catch' the correct asymptotic behaviour for large y since as the dimension of the trial space increases it becomes significantly harder to locate the desired points within it. Indeed, even the two shooting parameters for the backwards problem present a much greater challenge than the one parameter shooting problems tackled in [56], but it turns out that these equations possess some nice properties that make the approach tractable.

For context, we discuss some details about how this differs from the results in that paper about the shooting problem associated with p-critical self-similar blow-up solutions for (1.1.9). There, the problem took the form

$$\begin{aligned} &f''' + \big(f^3\big)' + \frac{1}{4} y f = 0, \quad f'(0) = 0, \\ &f(y) \sim C y^{-1/3} \exp(\bar{a} y^{4/3}) \text{ as } y \to \infty, \quad C > 0, \ \bar{a} = -3/4^{4/3}, \end{aligned}$$

with C as the single shooting parameter. It was shown that solutions to the ODE exist for all $y \in \mathbb{R}$ for any C, and the analytic dependence of solutions on C, and therefore also of the quantity $f'(0; C)$, was used to justify the existence of an at most countable discrete set of even solutions. The existence of a first, minimal profile was established via an adaptation of a three-step technique first used in second-order quasilinear blow-up problems ([151], Chapter 4) consisting of showing that

1. for $C \ll 1$, all solutions are strictly monotone decreasing,
2. for some $C_* > 0$ there exists a $y_* > 0$ such that $f(y_*)$ is a local maximum point,
3. then, by continuity, there exists a $C_1 \in [0, C_*)$ such that f is monotone decreasing for all $y > 0$ and $f'(0) = 0$.

For our problem, the shooting function f in fact blows up at some point $y_0 > -\infty$ for almost every $[C, k]$, as can be seen by examining the leading order terms $f^{(\mathrm{v})} = (f^5)'(1 + o(1))$ as f becomes large. It follows from the substitution $f(y) = \tilde{C} y^m h(y)$ and standard perturbation arguments that as $y \to y_0$,

$$f \sim f_0 := \kappa_0 (y - y_0)^{-1}, \quad \text{where } \kappa_0^4 = 4!. \tag{2.3.36}$$

Now the linearization about $f = f_0 + Y$ yields the ODE

$$Y^{(\mathrm{v})} = \left(\frac{5\kappa_0^4}{(y - y_0)^4} Y \right)',$$

with general solution

$$Y = \tilde{C}_1(y - y_0)^4 + \sum_{j=2}^{5} \tilde{C}_j (y - y_0)^{\rho_j},$$

with ρ_j such that $\rho_j(\rho_j - 1)(\rho_j - 2)(\rho_j - 3) = 5\kappa_0^4$ for $j = 2 \dots 5$. There are three roots, $\rho_j = 5$, $\frac{3}{2} \pm \frac{i}{2}\sqrt{39}$ with positive real part corresponding to stable behaviours of Y about f, and the remaining $\rho_j = -2$ unstable perturbation with negative real part. Hence, including the parameter $y_0(C, k)$, the dimension of the stable manifold about the singularities (2.3.36) is five and such behaviour is generic.

This is comparable to analysis done on the blow-up ODE associated with the fourth order (1.2.33) in [72] Chapter 2.4, which also demonstrates how simply this might be extended to the general p case. We expect that these arguments will generalize straightforwardly with an extra dimension appearing as we are not able to integrate the equation.

Returning to $p = 5$, we can show analytic dependence of solutions on the bundle parameters fairly easily (and do so below), as for odd powers the nonlinear term is an analytic function of f. However, this is less useful here than in the case when there is only one bundle parameter. Although zero sets of analytic functions (Analytic Varieties) must have Lebesgue measure zero, in two dimensions this imposes much less structure. Moreover, we seek the intersections of *two* Analytic Varieties defined by $f'(0; C, k) = 0$ and $f'''(0; C, k) = 0$, the theory of which quickly becomes difficult and without knowing the precise forms of the power series seems to us intractable. We claim with numerical evidence that $f'''(0; C, k) = 0$ defines two sub-manifolds of dimension one (π apart on the k-axis), see Figure 2-1. The same holds for $f'(0; C, k)$ and the numerical and asymptotic results in this chapter support that, like for (1.1.9), the admissible blow-up patterns form a discrete countable set.

Refined large y asymptotics and analytic dependence: The analytic dependence of the bundle (2.3.33) on the parameter k can be clarified by writing it in the form

$$f(y) \sim C y^{-2/5} \exp(a y^{6/5}) \sum_{n=0}^{\infty} \frac{-1^{\lfloor (n+1)/2) \rfloor}}{n!} k^n \cos\left(b y^{6/5} - (1 - (-1)^n)\frac{\pi}{4} \right). \tag{2.3.37}$$

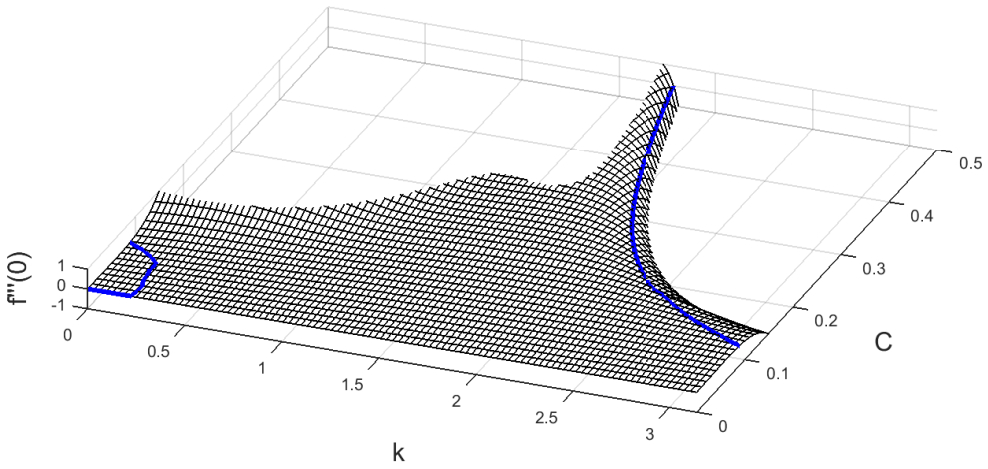

Figure 2-1: Zero Set of $f'''(0;C,k)$ for $0 \leq C \leq 0.5$, $0 \leq k \leq \pi$.

By introducing a family of functions $\phi_{0,n}$ such that $\phi_{0,n}^{(\mathrm{v})} - \frac{1}{6}y\phi_{0,n} = 0$ and each function has decay corresponding to a term in (2.3.37) with $C = 1$, $k = 1$ i.e.

$$\phi_{0,n} \sim y^{-2/5}\exp(ay^{6/5})\frac{-1^{\lfloor (n+1)/2)\rfloor}}{n!}\cos\left(by^{6/5} - (1-(-1)^n)\frac{\pi}{4}\right), \tag{2.3.38}$$

we can express the solution in terms of a formal power series

$$f(y;C,k) = \sum_{m=0}^{\infty}\sum_{n=0}^{\infty} C^{4m+1}k^n\phi_{m,n}(y). \tag{2.3.39}$$

The coefficient functions are then given by the relation

$$\phi_{m,n}^{(\mathrm{v})} - \frac{1}{6}y\phi_{m,n} = \sum_{\substack{0\leq i_l\leq m-1 \\ (\sum_{l=1}^{5} i_l = m-1)}} \sum_{\substack{0\leq j_l\leq n \\ (\sum_{l=1}^{5} j_l = n)}} (\phi_{i_1,j_1}\phi_{i_2,j_2}\phi_{i_3,j_3}\phi_{i_4,j_4}\phi_{i_5,j_5})', \tag{2.3.40}$$

with the condition $\phi_{m,n}(y) = o(\phi_{m-1,n}(y))$ as $y \to \infty$. Since the relation is linear, this determines the function exactly; of the two decaying modes permitted by the left hand side of (2.3.2), only one will have the correct phase determined (inductively) by the right hand side.

The following estimate:

$$|\phi_{m,n}(y)| < \frac{1}{n!}\left(\gamma_{m,n} + o(y^{-1})\right)y^{-(12m+2)/5}\exp\left((4m+1)ay^{6/5}\right), \tag{2.3.41}$$

with suitable constants $|\gamma_{m,n}| < 1$, can be derived inductively using the relation starting with the base cases (2.3.38). The largest term on the right hand side of

(2.3.2) will always be of the form $5\phi_{0,\cdot}^4.\phi'_{m-1,\cdot}(y)$ with any combination of second indices giving the $\frac{1}{n!}$. Now using the standard substitution $\phi_{m,\cdot} = h(y)\exp(S(y))$ in the left hand side and neglecting lower order terms, and some abuse of notation, we derive the relation

$$h(y)\left((S'(y))^5 - \frac{1}{6}y\right)\exp(S(y)) \sim 5\phi_{0,\cdot}^4.\phi'_{m-1,\cdot}(y) =$$
$$\frac{1}{n!}\left(\gamma_{m-1,n} + o(y^{-1})\right)y^{-(12(m-1)+2)/5}\exp(ay^{6/5})^4\exp((4(m-1)+1)ay^{6/5})$$
$$\implies S(y) = (4m+1)ay^{6/5}, \quad h(y) = \left(\gamma_{m,n} + o(y^{-1})\right)y^{-(12+2)/5}.$$

We have omitted some of the details concerning size of $\gamma_{m,n}$ and particularly the n dependence which quickly becomes unwieldy, but the size estimate is not affected by the oscillatory components and the specifics are not of particular interest of themselves. The importance of (2.3.41) itself is to establish uniform estimates on the coefficients of the homogeneous polynomials comprising each term of (2.3.39) for sufficiently large y. The form of the estimate clearly guarantees separate analyticity, at least for sufficiently large y, and in view of standard ODE theory on continuity and analyticity [34], we can guarantee analytic dependence of $f(y; C, k)$ on the shooting parameters wherever it exists.

Existence of a Minimal Self-Similar Blow-up Profile: In view of the difficulties discussed so far (total non-monotonicity and blow up), following the three-step procedure described above (that was used to prove existence of a minimal blow-up profile for (1.1.9)) precisely is not appropriate. However, some weaker properties can be established that will do most of the work in a manner at least approaching rigorous before we turn to numerics and asymptotics. We begin with the following lemma, which shows that despite non-monotonicity for all profiles even in the small C limit we can still recover at least some relations on the signs of f and its derivatives at the origin.

Lemma 2.2. *For C as in* (2.3.35) *sufficiently small and, wlog, k chosen such that $f(0) > 0$, $f'''(0) = 0$ imposes that $f'(0) < 0$. Moreover, this fixes $f''(0) > 0$ and $f^{(\mathrm{iv})}(0) < 0$.*

Proof. In the limit $C \to 0$, we use the rescaling $f = Cg$ in the ODE to arrive at the regularly perturbed problem

$$g^{(\mathrm{v})} - C^4(g^5)' - \frac{1}{6}yg = 0.$$

Then by standard ODE theory, the behaviour of g can be made arbitrarily close to the behaviour of g_0 defined by the unperturbed problem

$$g_0^{(\mathrm{v})} - \frac{1}{6} y g_0 = 0. \tag{2.3.42}$$

We will show that g_0 with the rescaled asymptotic behaviour $g_0 \sim y^{-2/5} \exp(a y^{6/5}) \cdot \cos(b y^{6/5} + k)$ cannot have a solution simultaneously satisfying the symmetry conditions $g_0'(0) = g_0'''(0) = 0$ for any value of k, and by fixing $g_0'''(0) = 0$ then automatically $g'(0) < 0$.

Multiplying (2.3.42) by g_0', g_0''' and $g_0^{(\mathrm{v})}$ in turn, and integrating over $[0, \infty)$, using the exponential decay at infinity, we derive the three useful identities

$$\begin{aligned}
-g_0^{(\mathrm{iv})}(0) g_0'(0) + g_0'''(0) g_0''(0) + \int_0^\infty (g_0'''(y))^2 + \frac{1}{12}(g_0(y))^2 dy = 0, \\
-g_0^{(\mathrm{iv})}(0) g_0'''(0) - \frac{1}{6} g_0'(0) g_0(0) - \int_0^\infty (g_0^{(\mathrm{iv})}(y))^2 + \frac{1}{4}(g_0'(y))^2 dy = 0, \\
-\frac{1}{6} g_0'''(0) g_0(0) + \frac{1}{3} g_0''(0) g_0'(0) + \int_0^\infty (g_0^{(\mathrm{v})}(y))^2 + \frac{5}{12}(g_0'''(y))^2 dy = 0.
\end{aligned}$$

Note that for nontrivial g_0 the integrands are all strictly positive. The second of these is the most principally useful; if $g_0'''(0) = 0$ then it gives $-\frac{1}{6} g_0'(0) g_0(0) < 0$. Since k has been chosen so that $g_0(0) > 0$ (that this is possible follows from linearity and invariance of (2.3.42) and, indeed, (2.3.35) under the transformation $f \to -f$), then we must have $g_0'(0) < 0$.

The remaining conditions now follow in the same way from the other identities, from the first we have $-g_0^{(\mathrm{iv})}(0) g_0'(0) < 0 \implies g_0^{(\mathrm{iv})}(0) < 0$ and from the third $\frac{1}{3} g_0''(0) g_0'(0) < 0 \implies g_0''(0) > 0$. □

The next step is to show that for C sufficiently large, solutions restricted to the manifold given by $f'''(0, C, k(C)) = 0$ can have $f'(0) > 0$, then by continuity the existence of at least one self similar profile will have been established. However, it seems a perturbative argument for large C cannot be readily applied in this case; while we expect solutions to become more oscillatory near the origin as C increases due to the balance between the first two terms of (2.3.35), it is hard to justify that this gives us the required sign change. The asymptotic construction in Section 2.3.3 provides in our opinion a more convincing account. First, we document the profiles we have found by computational methods.

2.3.3. Numerical Investigation of the Blow-up Profiles: To construct the profiles numerically, the shooting problem (2.3.35) with parameters C, k is first

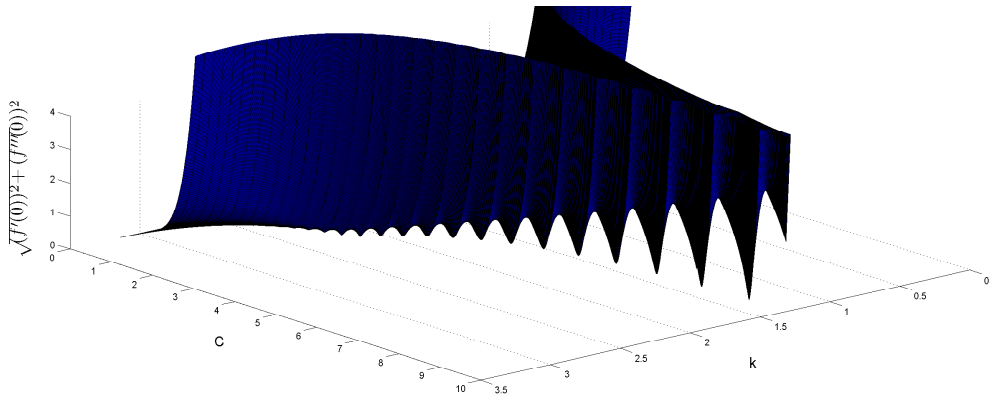

Figure 2-2: C, k dependence of normed odd derivatives of f at zero.

translated into an IVP. This is achieved by first locating a point L sufficiently far from zero that profiles are well described by (2.3.33); in practice we found that solving $CL^{-2/5}e^{aL^{6/5}} = 10^{-10}$ with Matlab's fsolve gave good results, the oscillatory part of the bundle discarded so that our shooting distance would be consistent. Then the initial conditions at L can be set to (2.3.33) and its first four derivatives, and the resulting problem solved with ODE15s routine (a stiff solver appropriate for dealing with quickly oscillating solutions).

All that remains is to search through C and k to ascertain which combinations result in the correct symmetry conditions $f'(0) = f'''(0) = 0$. Figure 2-2 shows the result of an exhaustive search for $0 \leq C \leq 10$, $0 \leq k \leq \pi$, with the quantity $S(C,k)^{1/2}$ plotted on the z-axis, defined as

$$S(C,k) \equiv (f'(0;C,k))^2 + (f'''(0,C,k))^2 = 0 \text{ iff } f'(0) = f'''(0) = 0. \qquad (2.3.43)$$

It is perhaps not clear from the diagram, but the surface does touch down at $C \approx 2.34..$, $k \approx 2.16$ giving the first even blow-up profile. However, it is clear that this is an extremely cumbersome technique; for not that large C most k values don't even result in a solution that exists until $y = 0$.

We could perhaps use the method discussed in the previous section of first locating a k for some C that gives $f'''(0) = 0$ and moving along the manifold given by $f'''(0, C, k(C)) = 0$ to find $f'(0)$, removing a dimension from our search. However, Matlab's fsolve struggles to find the correct $k(C)$ for even a reasonably good initial guess and the method proves unworkable.

However, we are able to perform a similar dimensional reduction thanks to some helpful properties of $(f^{(\mathrm{iv})} - f^5)'$. We first have the following simple lemma

showing that the sign of the solution remains the same near the point y_0 of blow up:

Lemma 2.3. *The ODE* (2.3.35) *does not admit solutions with oscillatory blow-up, so that if* $\limsup_{y\to y_0^+} |f(y)| = \infty$ *we cannot have both* $\limsup_{y\to y_0^+} f(y) = \infty$ *and* $\liminf_{y\to y_0^+} = -\infty$.

Proof. As in the local analysis performed in the previous section, we have that near y_0 the dominant balance of the ODE (2.3.35) is between the first two terms

$$f^{(\mathrm{v})} = (f^5)'(1 + o(1)),$$

which is easily integrated once, ignoring lower order terms, to give

$$f^{(\mathrm{iv})} = f^5 + \tilde{C}.$$

Now we assume that the blow-up is oscillatory. If we choose $y_1 < y_2$ both larger than y_0 to be the locations of a successive local maximum and minimum for f approaching the blow up point, we can multiply by f' and integrate again between them, giving

$$\int_{y_1}^{y2} f^{(\mathrm{iv})}(y)f'(y)\mathrm{d}y \sim \int_{y_1}^{y2} f^5(y)f'(y) + \tilde{C}f'(y)\mathrm{d}y \implies$$
$$-\frac{1}{2}\left[(f''(y))^2\right]_{y_1}^{y_2} \sim \frac{1}{6}\left[f^6(y)\right]_{y_1}^{y_2} + \tilde{C}\left[f(y)\right].$$

Provided that y_1 is sufficiently close to y_0, we will have $f^6(y_1) \gg f^6(y_2)$ and $|f''(y_1)| \gg |f''(y_2)|$. Thus, the leading order balance is given by

$$0 < \frac{1}{2}(f''(y_1))^2 \sim -\frac{1}{6}f^6(y_1) < 0,$$

providing a contradiction. □

In view of standard results on continuous dependence of solutions of ODEs with lipschitz nonlinearities on their initial conditions, it now seems plausible that if for some C there is a value k_1 such that $\lim_{y\to y_{0,k_1}} f(y) = +\infty$ and a value k_2 such that $\lim_{y\to y_{0,k_2}} f(y) = -\infty$, then between these two k values is a least one profile that exists for all y. To demonstrate this conclusively, we would need the stronger result that the blow up point $y_0(C,k) = \inf\{y \in \mathbb{R} \mid f(y;C,k)$ is a solution of (2.3.35) on $(y,\infty)\}$ is a continuous function of k for C fixed, which we have not been able to prove. Then, y_0 would

achieve its minima and maxima on the compact set $[k_1, k_2]$, in particular for the singularity of the profile to change sign with k it would have to occur that k would pass through a value such that $y_0(C, k) = -\infty$.

If the above does hold - and there is overwhelming numerical evidence that this is so - then due to the fact that $f(y; C, k) = -f(y; C, k+\pi)$ so if one of these blows up, then so must the other with opposite sign, we are always guaranteed at least two globally bounded profiles f for any value of C. That there are only these two requires a slightly more subtle argument, but seems probable given we have only two shooting parameters. As we keep C fixed, we have only one parameter to play with to pick up the one dimensional manifold of globally bounded (periodic) solutions of $(f^{(\mathrm{iv})} - f^5)' = 0$. Compare this with the more straightforward argument for a closely related problem in [74], Chapter 4.5.

To begin the procedure to locate the desired k value, we fix C and shoot with $k = 0$, $k = \pi$ and $k = \pi/2$, comparing the sign of the singularity of the latter against the two (different) former. In practice, the sign of the singularity can be established readily before f becomes very large; we've found that testing at even $|f| = 10$ has been sufficient. Certainly in terms of performance, smaller values are preferable. Then, the globally bounded solution will be in the interval $[0, \pi/2]$ or $[\pi/2, \pi]$ depending on which has solutions with opposite-signed singularities. This process is then repeated, constructing the globally bounded solutions as a 'separatrix' between orbits with positive and negative singularities. The procedure is illustrated in Figure 2-3. Note that this shows the beginning of an extra oscillatory bundle as $y \to -\infty$ for which all three terms of the ODE are the same size, defying a perturbative description. We may compare this with [72] Section 2, for which a similar behaviour was detected for the blow-up similarity ODE of (1.2.33). We expect this behaviour to be generic for globally bounded profiles, the exponentially decaying even solutions appearing only on a set of measure zero.

Having identified the unique (modulo π) value of k that results in a globally bounded profile, all that remains is to check the values of $f'(0)$ and $f'''(0)$ at the origin. Figure 2-4 shows both of these separately plotted against C for the globally bounded k value, which is shown plotted against C in Figure 2-6. For clarity, we also show $S(C, k)$ plotted against C with a logarithmic y-axis in Figure 2-5, demonstrating the intersections of $f'(0)$ and $f'''(0)$ really do occur at zero. For efficiency, we increased our stepsize with C and even then we find the zeros of $S(C, k)$ to within at least $\mathcal{O}(10^{-4})$.

We were only able to recover nine profiles by this method as for higher C values

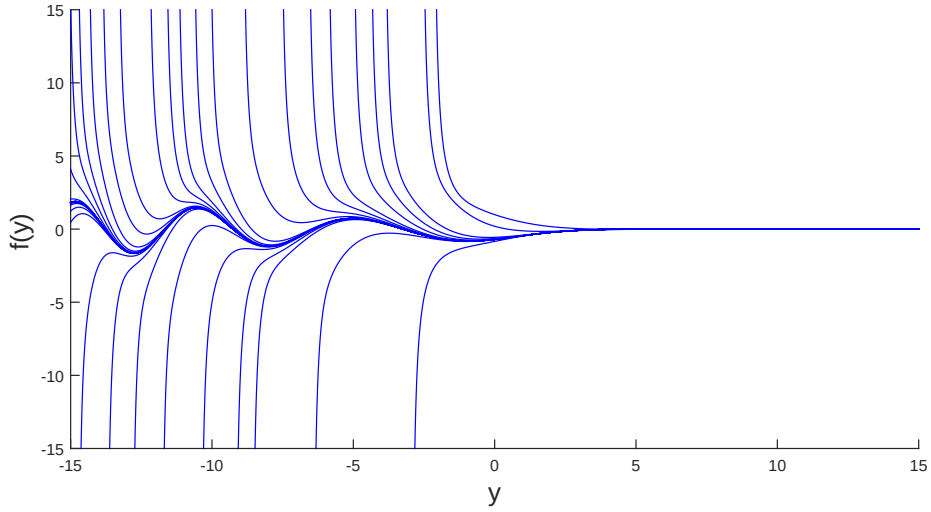

Figure 2-3: Constructing a globally bounded solution as a separatrix with $C = 1$.

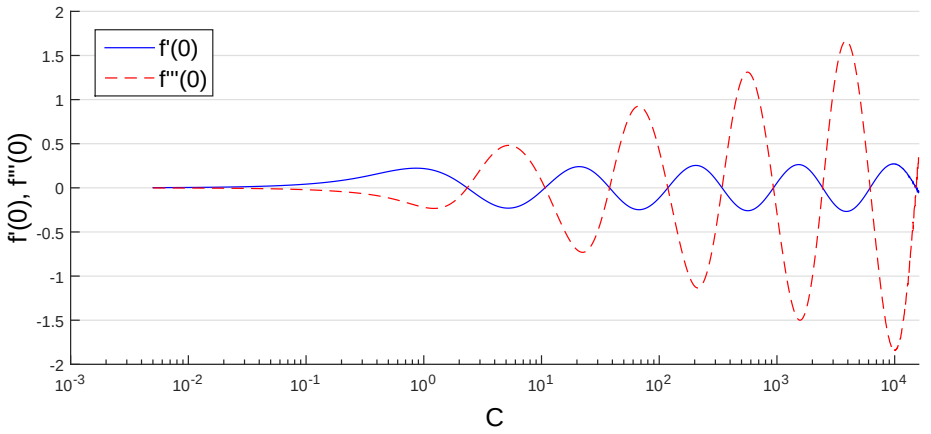

Figure 2-4: Dependence of odd derivatives at zero on C for unique globally bounded solutions of the ODE.

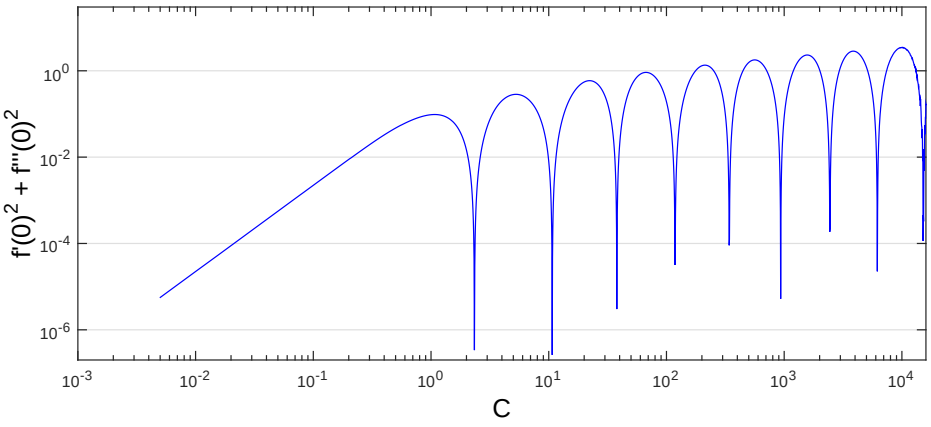

Figure 2-5: Dependence of normed odd derivatives at zero on C for unique globally bounded solutions of the ODE.

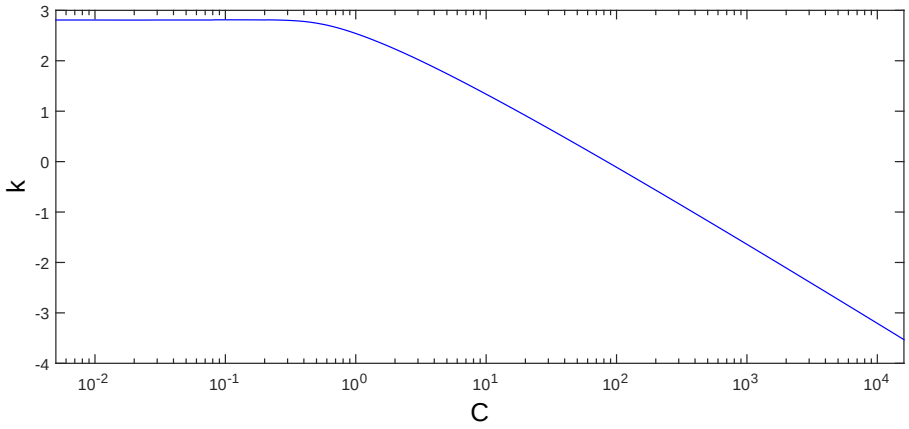

Figure 2-6: Relationship between C and k describing the unique globally bounded solutions of the ODE.

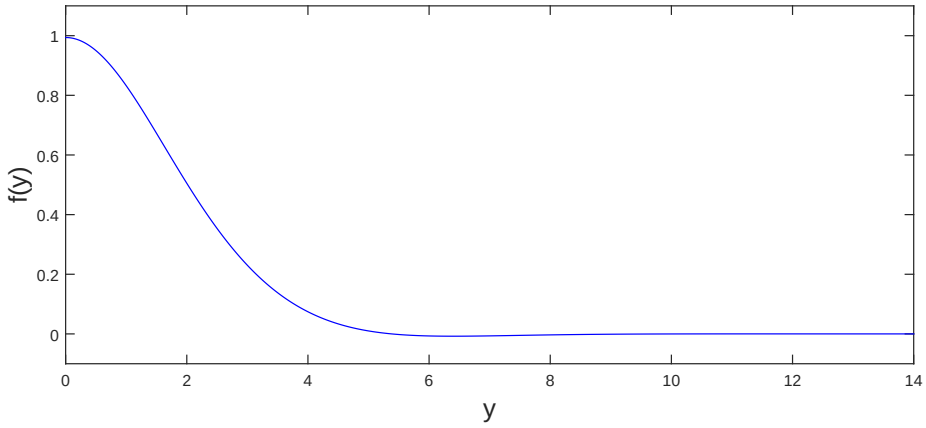

Figure 2-7: The first even blow-up profile.

than $C \approx 16,000$, as Matlab's double precision floating point calculations are only capable of dealing with representing numbers to roughly fifteen significant figures. Beyond this C value we require knowing k to greater precision to recover a profile that doesn't blow up before reaching the origin. In practice, we set the algorithm to stop when we have specified k to within 10^{-14}; this requires solving the ODE 50 times. We have been able to find further solutions using the Python arbitrary precision floating point 'MPF' library, see Figure 2-10 in the next section where we compare one such profile with the asymptotic estimate we derive, although the inbuilt solver based on Taylor expansions is too slow for it to be practical to use systematically. The profile from the figure was generated by using the MPF solver with $C = 1.5 \times 10^1 1$, for which it was necessary to calculated k to 45 digits. Of course, this profile was not quite even, but it was close enough to converge to an even profile when used as an initial guess in a BVP solver. Indeed the usual difficulties of controlling global error with an IVP solver, meant the profiles garnered from numerical shooting in both Matlab and Python accrued not insignificant global error even for not that large C. Therefore, the solutions corresponding to $S(C, k) = 0$, were used as initial guesses in the solver BVPSuite to achieve more accurate results, [116]. In addition to the symmetry conditions at the origin, the Dirichlet conditions $f(150) = f'(150) = f''(150)$ were imposed, with 150 chosen to be large enough to ensure that the exponentially decaying bundle would satisfy those conditions to double precision in the C range we examined.

Figure 2-7 shows the unimodal, fundamental profile the we expect to be evolutionarily stable and play the predominant role in the blow up dynamics of the

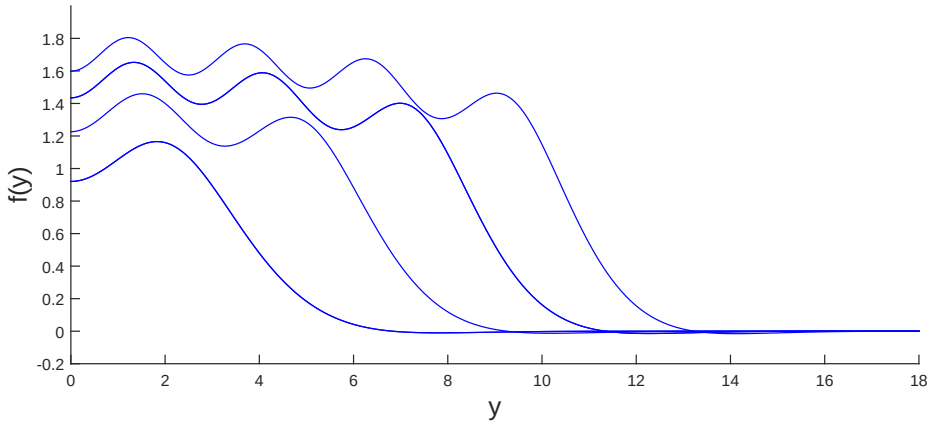

Figure 2-8: The first four even-numbered even blow-up profiles.

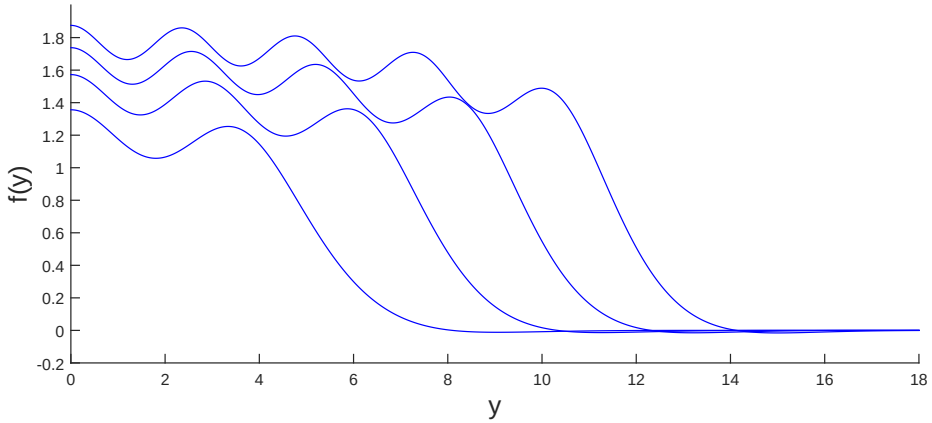

Figure 2-9: More odd-numbered even blow-up profiles.

problem. The other profiles we've found are split into those with $f''(0) > 0$ (figure 2-8) and those with $f''(0) < 0$ (figure 2-9) to avoid clutter.

Asymptotic Construction of a Countable Set of Similarity Profiles: Given the strong evidence for a countable set of solutions, we attempt to construct asymptotic approximations to understand their spatial structure and features in the limit of large C. In so doing we will gain some understanding of what it is about these equations that allow for a countable set of solutions. Our approach is in the spirit of analysis conducted on the blow up similarity equation of (1.1.9) in [56], Section 4, and here as there it turns out we can describe profiles in this limit in three separate but overlapping regions as is customary in matched asymptotics.

The first step is to recast (2.3.35) as a singular perturbation problem. If we

choose $a \in \mathbb{R}$ such that $a = f(0; C, k)$, then we can perform the rescaling

$$f(y) = ag(z), \qquad y = a^2 z,$$

and, assuming $a \to \infty$ as $C \to \infty$, this leads to the ODE

$$\varepsilon g^{(\mathrm{v})} - (g^5)' - \frac{1}{6} z g = 0 \tag{2.3.44}$$

where $\varepsilon = a^{-12} \ll 1$ for C large. With the three rescaled boundary conditions

$$g(0) = 1, \qquad g'(0) = g'''(0) = 0 \tag{2.3.45}$$

we can describe a two parameter family of solutions for small z which we can then match with the exponential bundle. Specifically, we will have

1. an outer region, where $0 \leq z < 15^{1/2}$ and $g = O(1)$,

2. a far-field region, where $z > 15^{1/2}$ and g is exponentially small and described by (2.3.33), and

3. an inner region, where $z = 15^{1/2} + O(\varepsilon^{1/5})$ and $g = O(\varepsilon^{1/20})$, which links together the other two behaviours.

We begin with the outer region. We can solve the unperturbed problem,

$$(g_0^5)' + \frac{1}{6} z g_0 = 0, \quad g(0) = 1, \tag{2.3.46}$$

to get

$$g_0(z) = \left(1 - \frac{z^2}{15}\right)^{1/4},$$

and then use this to expand around to approximate solutions to the full problem; in particular to recover the anticipated oscillatory behaviour in the outer region. The fact that a balance between the first two terms, $g^{(\mathrm{v})}$ and $-(g^5)'$ has oscillatory solutions is suggestive, and we can transform with the fast variable $z = \varepsilon^{1/4} Z$ to recover it:

$$\frac{\mathrm{d}^5}{\mathrm{d}Z^5} g - \frac{\mathrm{d}}{\mathrm{d}Z} g^5 - \frac{1}{6} \varepsilon^{1/4} z g = 0. \tag{2.3.47}$$

Then, expanding around the unperturbed solution, $g \sim g_0(z) + \theta g_1(Z)$, where

the gauge θ is a to-be-determined function of ε, the equation becomes

$$\varepsilon^{5/4}\frac{\mathrm{d}^5}{\mathrm{d}z^5}g_0+\theta\frac{\mathrm{d}^5}{\mathrm{d}Z^5}g_1-\varepsilon^{1/4}\frac{\mathrm{d}}{\mathrm{d}z}g_0^5-5\theta\frac{\mathrm{d}}{\mathrm{d}Z}g_0^4g_1-10\theta^2\frac{\mathrm{d}}{\mathrm{d}Z}g_0^3g_1^2 \\ -10\theta^3\frac{\mathrm{d}}{\mathrm{d}Z}g_0^2g_1^3-5\theta^4\frac{\mathrm{d}}{\mathrm{d}Z}g_0g_1^4-\theta^5\frac{\mathrm{d}}{\mathrm{d}Z}g_1^5-\frac{1}{6}\varepsilon^{1/4}zg_0-\frac{1}{6}\varepsilon^{1/4}\theta\ g_1=0.$$

At $O(\varepsilon^{1/4})$, we recover the unperturbed problem, and at $O(\theta)$ we have the equation

$$\frac{\mathrm{d}^5}{\mathrm{d}Z^5}g_1-5\frac{\mathrm{d}}{\mathrm{d}Z}g_0^4g_1=0. \tag{2.3.48}$$

We can solve this approximately if we assume $g_0^4(Z)=1-\frac{\varepsilon^{1/2}Z^2}{15}$ is close to 1, however this is only true for $z=O(\varepsilon^{1/4})$ and so we cannot hope to extend this solution anywhere near the inner and outer matching region. However, if we can transform (2.3.48) so that we need not make any approximations to solve it, then this issue would be resolved.

This can be achieved by introducing a new fast variable $t=F(Z)$, with F chosen so that (2.3.48) expressed in the t variable is an equation with constant frequency. Under this change of variables, (2.3.47) becomes

$$\frac{\mathrm{d}^5}{\mathrm{d}t^5}g+10\frac{F''(Z)}{(F'(Z))^2}\frac{\mathrm{d}^4}{\mathrm{d}t^4}g+10\frac{F'''(Z)}{(F'(Z))^3}\frac{\mathrm{d}^3}{\mathrm{d}t^3}g+15\frac{(F''(Z))^2}{(F'(Z))^4}\frac{\mathrm{d}^3}{\mathrm{d}t^3}g+5\frac{F^{(\mathrm{iv})}(Z)}{(F'(Z))^4}\frac{\mathrm{d}^2}{\mathrm{d}t^2}g \\ +10\frac{(F''(Z))(F'''(Z))}{(F'(Z))^5}\frac{\mathrm{d}^2}{\mathrm{d}t^2}g+\frac{F^{(\mathrm{v})}(Z)}{(F'(Z))^5}\frac{\mathrm{d}}{\mathrm{d}t}g-\frac{1}{(F'(Z))^4}\frac{\mathrm{d}}{\mathrm{d}t}(g^5)-\frac{1}{6}\frac{1}{(F'(Z))^5}\varepsilon^{1/4}zg=0, \tag{2.3.49}$$

and again, we posit the two term expansion $g\sim g_0(z)+\theta g_1(z,t)$, where this time the lower order term g_1 is a function of both z and t independently. Of course, z and t are not actually independent variables, however, this conceit of multiscale methods suits our purposes well here. The issue we face is not secularity per se, for which the multiscale approach was first devised (see [101]), but it will become clear how this will allow us to derive a linear ODE in t which describes the oscillatory behaviour in almost all of the outer region.

We must rewrite the operator

$$\frac{\mathrm{d}}{\mathrm{d}t}=\frac{\partial}{\partial t}+\frac{\varepsilon^{1/4}}{F'(Z)}\frac{\partial}{\partial z}. \tag{2.3.50}$$

The resulting expansion of (2.3.49) then has the form

$$\theta\frac{\partial^5}{\partial t^5}g_1(z,t)+\frac{5}{(F'(Z))}\varepsilon^{1/4}\theta\frac{\partial^5}{\partial t^4\partial z}g_1(z,t)+10\frac{F''(Z)}{(F'(Z)^3}\theta\frac{\partial^4}{\partial t^4}g_1(z,t)-$$
$$\frac{5}{(F'(Z))^4}\theta\frac{\partial}{\partial t}g_0^4(z)g_1(z,t)-\frac{1}{(F'(Z))^4}\varepsilon^{1/4}\frac{\partial}{\partial z}g_0^5(z)-\frac{5}{(F'(Z))^4}\varepsilon^{1/4}\theta\frac{\partial}{\partial z}g_0^4(z)g_1(z,t)-$$
$$\frac{1}{6}\frac{1}{(F'(z)^5}\varepsilon^{1/4}zg_0(z)-\frac{1}{6}\frac{1}{(F'(z)^5}\varepsilon^{1/4}\theta zg_1(z,t)+o(\varepsilon^{1/4}\theta)=0.$$

Note we have assumed here that both $\theta^2>\varepsilon^{1/4}$ and that $F''(Z)=\mathcal{O}(e^{1/4})$, and so on for all higher derivatives. Both assumptions are vindicated in the course of the procedure.

At the crucial $O(\theta)$ balance we get

$$\frac{\partial^5}{\partial t^5}g_1(z,t)=\frac{5}{(F'(Z))^4}\frac{\partial}{\partial t}g_0^4(z)g_1(z,t). \tag{2.3.51}$$

Now as z and t are independent, we are allowed to simply choose $F'(Z)$ such that it will cancel with the $g_0^4(z)$. This is allowable as g_0 has no t dependence and so we have circumvented the problem of having to approximate it. It is therefore straightforward to pick $F'(Z)=g_0=(1-\frac{\varepsilon^{1/2}Z^2}{15})^{1/4}$, giving us

$$t=\int_0^Z\left(1-\frac{\varepsilon^{1/2}u^2}{15}\right)^{1/4}\mathrm{d}u=\frac{z}{3\varepsilon^{1/4}}\left(2\left(1-\frac{z^2}{15}\right)^{1/4}+{}_2F_1\left(\frac{1}{2},\frac{3}{4};\frac{3}{2};\frac{z^2}{15}\right)\right),$$

where ${}_2F_1$ is the hypergeometric function. (2.3.51) then has general solution

$$g_1=A(z)-B(z)\cosh(5^{1/4}t)+C(z)\sinh(5^{1/4}t)-D(z)\cos(5^{1/4}t)+E(z)\sin(5^{1/4}t)$$

and, since t and z are independent, we can apply the initial conditions $g_1(z,0)=g_{1t}(z,0)=g_{1ttt}(z,0)=0$ to get

$$g_1=B(z)(1-\cosh(5^{1/4}t))+D(z)(1-\cos(5^{1/4}t)).$$

Now to get explicit expressions for $B(z)$ and $D(z)$ we can substitute this expression into the balance at $O(\varepsilon^{1/4}\theta)$, which gives

$$5\frac{\partial^5}{\partial t^4\partial z}g_1-\frac{z}{3(1-z^2/15)}\frac{\partial^4}{\partial t^4}g_1-5\frac{\partial}{\partial z}g_1+\frac{z}{2(1-z^2/15)}g_1=0,$$

and thus

$$\frac{B'(z)}{B(z)} = \frac{7}{120}\frac{z}{(1-z^2/15)},$$

with exactly the same expression for $D(z)$.

These are trivial to solve and we arrive, finally, at a two parameter family describing solutions to (2.3.44) in the outer region:

$$\begin{aligned} g &\sim g_0(z) + \theta \frac{1}{g_0^{7/4}(z)} \left(b(1-\cosh(5^{1/4}t)) + d(1-\cos(5^{1/4}t)) \right), \\ g_0(z) &= \left(1 - \frac{z^2}{15}\right)^{1/4}, \end{aligned} \tag{2.3.52}$$

where $b, d \in \mathbb{R}$ are parameters that will be determined during the matching procedure. We must note that the presence of g_0 on the bottom of the expression for g_1 means that as $z \to 15^{1/2}$, g_1 is unbounded. However, the rate of divergence is slow and this expression does turn out to be sufficient for a first-order match.

To enact this matching, we examine the solutions around the transition point $z = 15^{1/2}$. This is achieved using the rescalings

$$z = 15^{1/2} + \varepsilon^{1/5}\bar{z}, \qquad g = \varepsilon^{1/20}R,$$

and then solving the resulting equation

$$R^{(\mathrm{v})} - (R^5)' - \frac{1}{6}(15^{1/2} + \varepsilon^{1/5}\bar{z})R = 0, \tag{2.3.53}$$

in the limits $\bar{z} \to \infty$ and $\bar{z} \to -\infty$.

For first order matching, it suffices to solve the unperturbed equation,

$$R_0^{(\mathrm{v})} - (R_0^5)' - \frac{15^{1/2}}{6}R_0 = 0, \tag{2.3.54}$$

though since this is a regular perturbation problem it would be possible to bring the lower order term back in an expansion to examine further orders of matching.

In the $\bar{z} \to \infty$ limit, we can safely assume that the balance is between $R_0^{(\mathrm{v})}$ and $-\frac{15^{1/2}}{6}R_0$ as it proved to be in the WKBJ analysis of the full problem. Using a standard substitution, $R_0(\bar{z}) = \exp(S(\bar{z}))$, we get that solutions with exponential decay can be expressed as the two parameter family

$$R_0(\bar{z}) \sim A_0 \exp\left(\left(\frac{15^{1/2}}{6}\right)^{1/5}\cos(4\pi/5)\bar{z}\right)\cos\left(\frac{5}{6}\left(\frac{1}{6}\right)^{1/5}\sin(4\pi/5)\bar{z} + B_0\right). \tag{2.3.55}$$

The two parameters here, A_0 and B_0 are related to the C, k of (2.3.33).

In the $\bar{z} \to -\infty$ limit, we want to pick up slowly growing solutions to match with the slowly decaying first order g_0 behaviour. As such, we can deduce the dominant balance must be

$$(\tilde{R}_0^5)' \sim -\frac{15^{1/2}}{6}\tilde{R}_0,$$

which gives $\tilde{R}_0 \sim (-\frac{2}{15^{1/2}}\bar{z})^{1/4}$. This will match with the first term of the outer expansion; to pick up the equivalent to the oscillatory g_1 term (which contains to two parameters we hope to the C, k parameters in the far-field) in the inner region we can pose an expansion about $\tilde{R}_0$, $R_0 = \tilde{R}_0 + \tilde{R}_1$ with $\tilde{R}_1 \ll \tilde{R}_0$ as $\bar{z} \to -\infty$. Using this, we can easily derive that the leading order equation for $\tilde{R}_1$ is

$$\tilde{R}_1^{(\mathrm{v})} + \frac{10}{15^{1/2}}(\bar{z}\tilde{R}_1)' - \frac{15^{1/2}}{6}\tilde{R}_1 = 0. \tag{2.3.56}$$

Finding solutions to this equation, approximate or otherwise, is no easy task. However, being mindful of the fact that we want the solution in this limit to match with the outer behaviour (2.3.52), we can express the outer expansion in terms of the inner variables:

$$\begin{aligned} g(\bar{z}) = \varepsilon^{1/20}\left(\frac{2}{15^{1/2}}\right)^{1/4}(-\bar{z})^{1/4} + \theta\varepsilon^{-7/80}\left(\frac{2}{15^{1/2}}\right)^{-7/16}(-\bar{z})^{-7/16}\cdot \\ \left(b - b\cosh\left(\frac{5^{1/4}}{\varepsilon^{1/4}}t_0\right)\cosh\left(\frac{4}{5}\left(\frac{10}{15^{1/2}}\right)^{1/4}(-\bar{z})^{5/4}\right) + \right. \\ b\sinh\left(\frac{5^{1/4}}{\varepsilon^{1/4}}t_0\right)\sinh\left(\frac{4}{5}\left(\frac{10}{15^{1/2}}\right)^{1/4}(-\bar{z})^{5/4}\right) + \\ d - d\cos\left(\frac{5^{1/4}}{\varepsilon^{1/4}}t_0\right)\cos\left(\frac{4}{5}\left(\frac{10}{15^{1/2}}\right)^{1/4}(-\bar{z})^{5/4}\right) - \\ \left. d\sin\left(\frac{5^{1/4}}{\varepsilon^{1/4}}t_0\right)\sin\left(\frac{4}{5}\left(\frac{10}{15^{1/2}}\right)^{1/4}(-\bar{z})^{5/4}\right)\right). \end{aligned} \tag{2.3.57}$$

The first order term is obtained by writing t in terms of $\bar{z}$,

$$t = \frac{1}{\varepsilon^{1/4}}\int_0^{15^{1/2}+\varepsilon^{1/5}\bar{z}}\left(1-\frac{v^2}{15}\right)^{1/4}\mathrm{d}v = \frac{1}{\varepsilon^{1/4}}t_0 + \frac{1}{\varepsilon^{1/4}}\int_{15^{1/2}}^{15^{1/2}+\varepsilon^{1/5}\bar{z}}\left(1-\frac{v^2}{15}\right)^{1/4}\mathrm{d}v,$$

with the constant $t_0 = \int_0^{15^{1/2}}\left(1-\frac{v^2}{15}\right)^{1/4}\mathrm{d}v$. Then under a change of variable

$w := 15^{1/2} - v$, we get

$$t = \frac{1}{\varepsilon^{1/4}} t_0 - \frac{1}{\varepsilon^{1/4}} \int_0^{-\varepsilon^{1/5}\bar{z}} \left(\frac{2}{15^{1/2}} w - \frac{1}{15} w^2 \right)^{1/4} \mathrm{d}w.$$

Rewriting the integrand as $\left(\frac{2}{15^{1/2}} w\right)^{1/4} \left(1 - \frac{1}{2 \cdot 15^{1/2}} w^2\right)^{1/4}$, we can see that to leading order,

$$t \approx \frac{1}{\varepsilon^{1/4}} t_0 - \frac{4}{5} \left(\frac{2}{15^{1/2}} \right)^{1/4} (-\bar{z})^{5/4}$$

giving us (2.3.57) as claimed.

To find a match, then, it is prudent to 'peel off' part of the first order expression: we seek a solution of the form

$$\tilde{R}_1(\bar{z}) = \left(\frac{2}{15^{1/2}} \right)^{-7/16} (-\bar{z})^{-7/16} F(\psi(\bar{z})).$$

Substituting this into (2.3.56), the leading order balance is

$$\frac{1}{\bar{z}} (\psi')^4 F^{(\mathrm{v})}(\psi) + \frac{10}{15^{1/2}} F'(\psi) = 0 \tag{2.3.58}$$

and since ψ is arbitrary, we can choose it so that $\frac{1}{\bar{z}}(\psi')^4 = -\frac{10}{15^{1/2}}$, which gives that $\psi(z) = \frac{4}{5} \left(\frac{2}{15^{1/2}}\right)^{1/4} (-\bar{z})^{5/4}$. (2.3.58) now reads

$$F^{(\mathrm{v})}(\psi) - F'(\psi) = 0,$$

which has general solution

$$\begin{aligned} F(\psi) =& a_1 + a_2 \cosh(\psi) + a_3 \sinh(\psi) + a_4 \cos(\psi) + a_5 \sin(\psi), \\ \psi(\bar{z}) =& \frac{4}{5} \left(\frac{2}{15^{1/2}} \right)^{1/4} (-\bar{z})^{5/4}, \end{aligned} \tag{2.3.59}$$

with the parameters a_i being real numbers. It is now possible to match (2.3.59) with (2.3.57), yielding the matching criteria

$$\begin{aligned} \theta = \varepsilon^{11/80}, \quad a_1 = b + d, \\ a_2 = -b \cosh\left(\frac{5^{1/4}}{\varepsilon^{1/4}} t_0 \right), \quad a_3 = b \sinh\left(\frac{5^{1/4}}{\varepsilon^{1/4}} t_0 \right), \\ a_4 = -d \cos\left(\frac{5^{1/4}}{\varepsilon^{1/4}} t_0 \right), \quad a_5 = -d \sin\left(\frac{5^{1/4}}{\varepsilon^{1/4}} t_0 \right). \end{aligned}$$

Now, we can see from (2.3.57) that the coefficients of the cosh term grow ex-

ponentially quickly as $\varepsilon \to 0$, and so these cannot be involved in the matching. Thus, we can fix $b = 0$, $a_2 = a_3 = 0$, $a_1 = d$. In addition, $a_4^2 + a_5^2 = 1$.

It remains to determine a_1, a_4 and a_5 in terms of A_0 and B_0 from (2.3.55). In [56], Chapter 4, an easier version of this was carried out by exploiting the fact that (2.3.54) is autonomous. Thus translating the axis by $\bar{z} - \bar{z}_0$, we do not change the nature of the behaviours as $\bar{z} \to \pm\infty$, only their coefficients. If we can introduce $\bar{z}_0$ into both sides, then we can substitute for it to solve the problem.

(2.3.55) transforms easily under translation, giving us

$$R_0(\bar{z}; \hat{A}_0, \hat{B}_0) = R_0(\bar{z} - \bar{z}_0; A_0, B_0), \text{ with}$$
$$\hat{A}_0 = A_0 \exp\left(-\left(\frac{15^{1/2}}{6}\right)^{1/5} \cos(4\pi/5)\bar{z}_0\right) \text{ and } \hat{B}_0 = B_0 - \left(\frac{5}{6^{6/5}}\right)\sin(4\pi/5)\bar{z}_0.$$

We have reduced the expression for the behaviour of R_0 in the $\bar{z} \to -\infty$ limit to

$$R_0 \sim \left(-\frac{2}{15^{1/2}}\bar{z}\right)^{1/4} + \left(-\frac{2}{15^{1/2}}\bar{z}\right)^{-7/16} \left(a_1 + a_4\cos(\psi(\bar{z})) + a_5\sin(\psi(\bar{z}))\right).$$

Now, replacing $\bar{z} \to \bar{z} - \bar{z}_0$, we can see the correction from the first term is of lower order $\mathcal{O}((-\bar{z})^{-3/4})$ than the second term, and so a_1 is not affected by the translation. Further, the a_4 and a_5 will change to reflect the shift by $\bar{z}_0$, but we have not been able to derive a useful expression for the form they take. Without this, we cannot conclude this argument. We do remark that once this correspondence is determined, a numerical simulation of the inner equation (2.3.54) will still be required to absolutely determine the values that these constants can take.

We conclude with a simple but effective argument using the formation of humps in the outer region as C increases. Since each new bump of a solution must be generated at the left hand edge of the inner region, this process must correspond with a_4, a_5 changing sign. This gives a very rough estimate for values of ε_j, and hence $||f_j||_{L^\infty}$, associated with admissible profiles:

$$\left(\frac{5^{1/4}t_0}{\varepsilon_j^{1/4}}\right) \sim \pi j \implies \varepsilon_j \sim \left(\frac{5t_0^4}{\pi^4}\right) j^{-4} \implies f_j(0) \sim \left(\frac{5t_0^4}{\pi^4}\right)^{-1/12} j^{1/3},$$

for $j \ll 1$.

In figure 2-10, we plot the outer approximation of the profile with $||f_{27}||_{L^\infty}$ calculated in this way alongside a profile calculated by the high precision numerics. We observe a very close agreement not only in absolute size, but also general

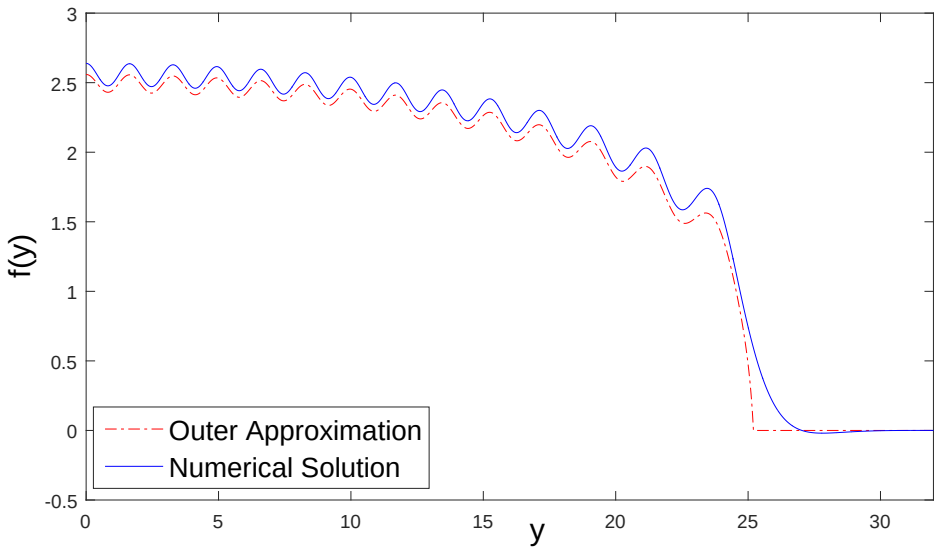

Figure 2-10: Comparison of the asymptotic two-term approximation with a numerically derived profile.

shape. That this is true for $f(0)$ not even that large is extremely promising.

We note finally that we can in principle derive an approximate value of d through careful numerical simulation of (2.3.54) via backwards shooting with initial conditions determined by (2.3.55) with given values of A_0 and B_0. However, we anticipate that the solutions with sufficiently large interval of existence will demonstrate nonlinear oscillatory behaviour that requires advanced algorithms to solve. We refer to a similar, easier problem tackled in [56], Section 4.4 for which techniques described in [110] were necessary for good resolution. Time constratints have prohibited us from adapting this to the current scenario; for the purposes of this demonstration a value of d has been chosen to make the close alignment in qualitative behaviour visually obvious.

2.3.4. Asymptotic Stability of Blow-up Profiles: Ultimately we want to understand which of the countable set of blow-up profiles we've constructed might describe of the blow-up behaviour for a given u_0 that satisfies the blow-up criterion (2.2.7). This is an extremely challenging problem for even semilinear PDEs, so we try and establish a simpler result. We analyze their asymptotic stability in the $\tau \to \infty$ limit of (2.2.13) via trying to describe the spectra of the linearizations

around each profile f_j. In the $N = 1, p = 5$ case, the equation takes the form

$$\theta_\tau = \mathbf{A_2}(\theta) = \theta_{yyyyyy} - \frac{1}{6}(y\theta)_y - (\theta^5)_{yy},$$
$$\theta(y,0) = \theta_0(y).$$

Those equilibria with a nontrivial stable subspace (i.e. one associated with eigenvalues with negative real part) are expected to constitute the ω-limit sets $\omega(\theta_0)$ for non-trivial classes of appropriate θ_0, and by extension blow-up patterns manifesting for equivalent classes of u_0 in the non-rescaled variables.

The linearization around the trivial solution $f \equiv 0$ is closely related to the adjoint operator $\mathbf{B}^*$ from (1.3.50) associated with the triharmonic equation, with spectrum $\sigma(\mathbf{B}^*) = \{-\frac{k}{6},\ k = 0, 1, 2, ...\}$, see [67]. We have

$$\mathbf{A_2}'(0) = \frac{\mathrm{d}^6}{\mathrm{d}y^6} - \frac{1}{6}y\frac{\mathrm{d}}{\mathrm{d}y} - \frac{1}{6}\mathbf{I} = \mathbf{B}^* - \frac{1}{6}\mathbf{I},$$

and as a straightforward consequence, $\sigma(\mathbf{A_2}'(0)) = \{-\frac{k+1}{6},\ k = 0, 1, 2, ...\}$. This implies any sufficiently small solution $\theta(y, \tau)$ satisfies the inequality

$$|\theta(y,\tau)| \leq A\mathrm{e}^{-\tau/6}$$

uniformly in $\mathbb{R}$ for some $A > 0$, giving that u is bounded near the blow-up time T, providing a contradiction to the blow-up hypothesis. We can thus conclude that $0 \notin \omega(\theta_0)$ provided the associated u_0 leads to blow-up.

It is far less easy to draw such concrete conclusions about the spectra of the linearized operators about the nontrivial stationary solutions f_j:

$$\mathbf{A_2}'(f_j) = \mathbf{B}^* - \frac{1}{6}\mathbf{I} - 5\frac{\mathrm{d}^2}{\mathrm{d}y^2}(f_j^4\mathbf{I}) \tag{2.3.60}$$

although it is possible to show that the they will be discrete by using the theory of compact perturbations of integral operators. The most promising line of attack would seem to be using numerical simulations of the PDE (2.2.13) to measure the rates of convergence in the L_∞ norm. The principle difficulty in this is utilizing a numerical scheme that can be assured to be reliable, coupled with needing to know the value of the blow-up time T to perform the correct rescaling which in turn requires good simulations of the original PDE (2.1.1). The scheme we use will be discussed in Chapter 3.

In Figure 2-11 we show the convergence to the self-similar profile shown in

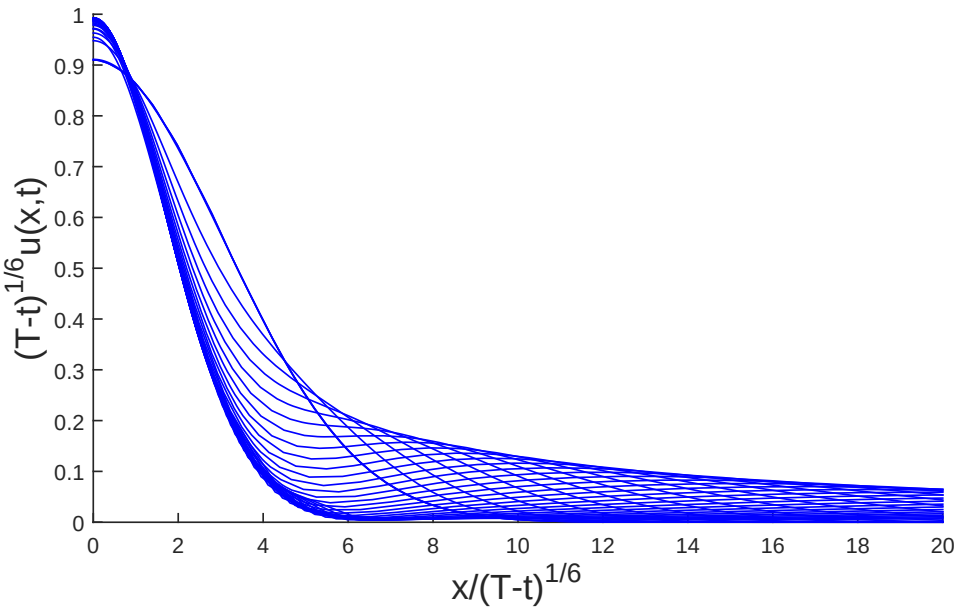

Figure 2-11: Convergence to the first self-similar profile from bell shaped initial data.

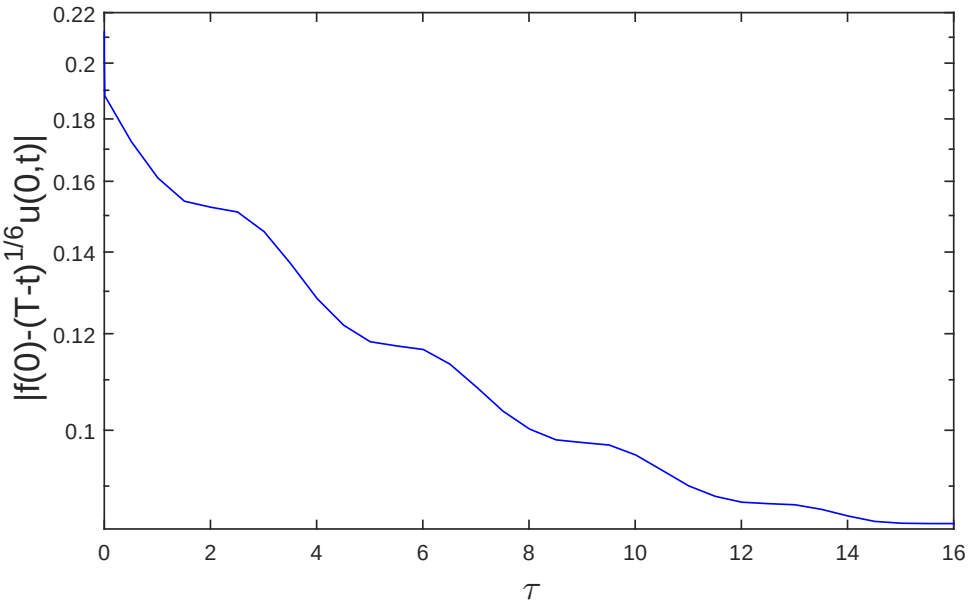

Figure 2-12: Rate of convergence away from mass defect.

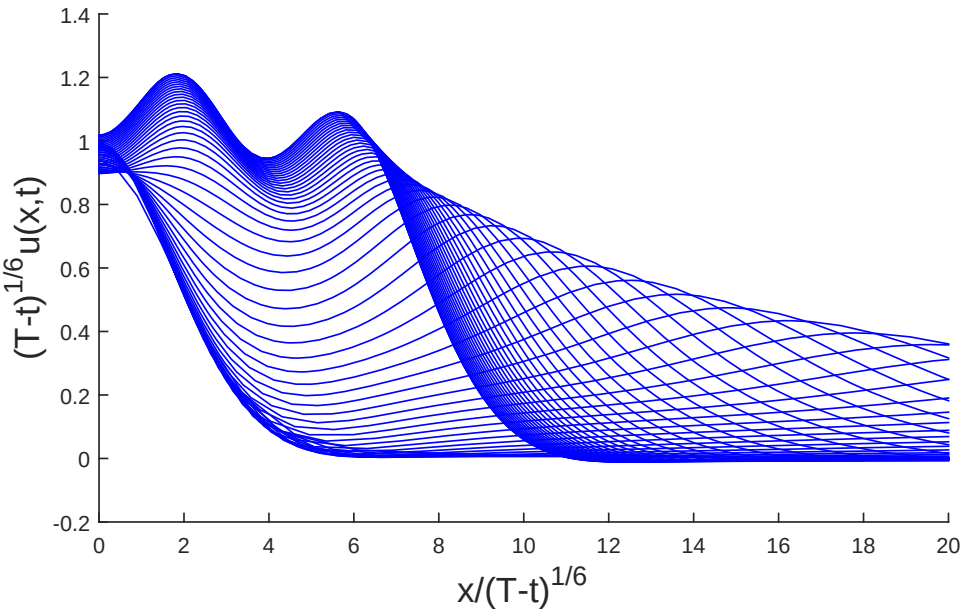

Figure 2-13: Instability of the fourth self-similar profile.

Figure 2-7 from bell shaped initial data in the rescaled variables. In this case we have taken $u_0 = 2\exp(-x^2/4)$. This has mass greater than the eventual blow-up profile and so, as in the fourth order case [56], this extra mass is 'left behind', i.e. goes off to infinity in y as $t \to T$. Thus the convergence rate in the *sup* norm is best measured at the origin where the singularity develops, as this is the only place the measurement will not be skewed by the mass defect. This is presented in Figure 2-12. Note the convergence is not at a uniform rate, a feature not clearly present in the fourth order case.

We also exhibit an example of the instability of the other self-similar profiles. In Figure 2-13 the flow generated by taking the fourth self-similar blow-up profile shown in Figure 2-8 as an inital condition, in the rescaled coordinates. The divergence occurs slowly at first before converging rapidly, again to the first self-similar profile. Identical experiments on the first few self-similar profiles suggest that, as expected, only the first is stable and in fact attracts a wide class of even initial data that results in blow-up.

We have included two further figures demonstrating the robustness of our numerical scheme by how easily it deals with the instability. In Figure 2-14 we see the mesh points change direction to follow the features of the profile as the structure develops, and in Figure 2-15 we see how the time transformation smoothly handles a rapid change in the rate of blow up as we transfer from a

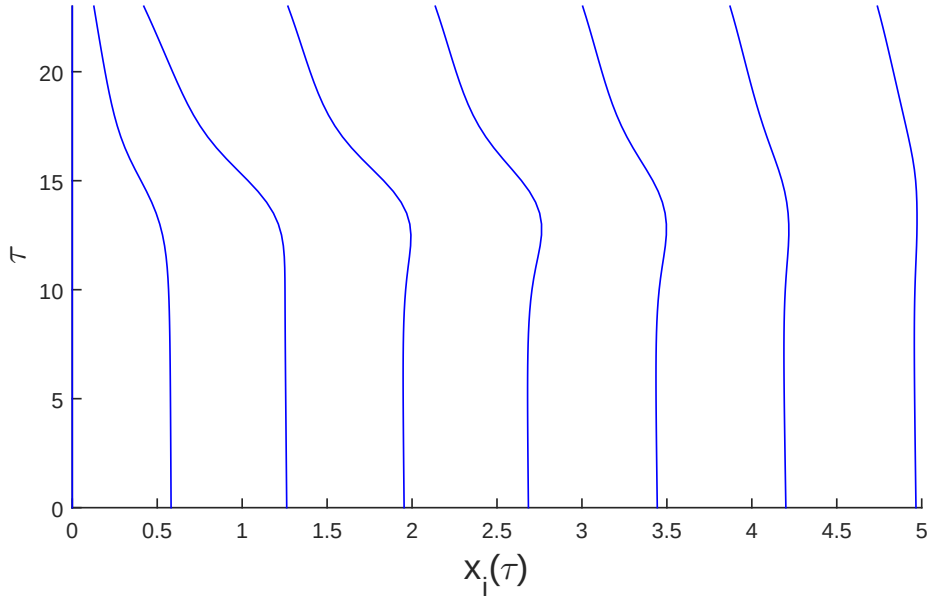

Figure 2-14: Mesh movement as instability develops.

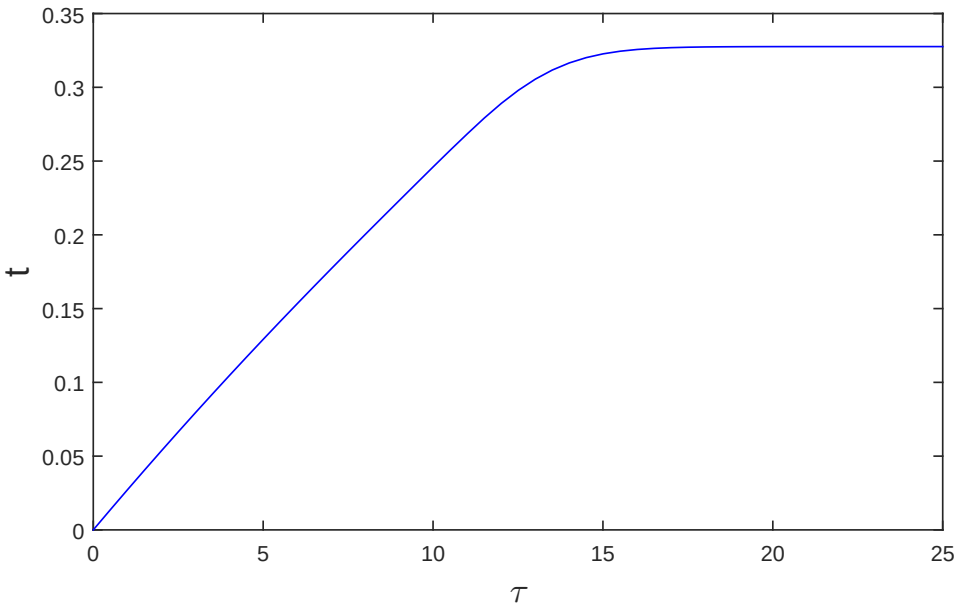

Figure 2-15: Time transformation as instability develops.

solutions dominated by the fourth self-similar profile to the first.

2.3.5. The p_1 Critical Case in One Dimension: The case of general p is more complicated than for the conservative case as without conservation the ODE ((2.2.15)) remains truly sixth-order and comprising four terms. However, (2.1.1) does possess a second conserved quantity, admitting a second critical exponent for which a reduction in order for the ODE is possible, though its form is not quite as convenient. For simplicity, we again begin considering only $N = 1$. The conserved quantity other than mass is the first moment, which we can see by multiplying by x in the PDE ((2.1.1)) and integrating by parts. We have

$$\begin{aligned}\frac{\mathrm{d}}{\mathrm{d}t}\int_{\mathbb{R}} xu\mathrm{d}x = \frac{\mathrm{d}}{\mathrm{d}t}\int_{\mathbb{R}} x\left(u_{xxxx} - |u|^{p-1}u\right)_{xx}\mathrm{d}x = \\ -\frac{\mathrm{d}}{\mathrm{d}t}\int_{\mathbb{R}}\left(u_{xxxx} - |u|^{p-1}u\right)_{x}\mathrm{d}x = 0 \\ \implies \frac{\mathrm{d}}{\mathrm{d}t}\left[(T-t)^{-2/3(p-1)+1/3}\int_{\mathbb{R}} yf(y)\mathrm{d}y\right] = 0.\end{aligned}$$

Thus, $p = 3$ defines the exponent for which a non-trivial centre of mass is conserved. The same procedure in $\mathbb{R}^N$ leads to the second critical exponent $p_1 = 1 + 4/(N+1)$ in the sequence of critical exponents we introduce in Proposition 2.9. By the same token as Remark 2.1, we can see that

$$\text{for any } p \neq p_1, \quad yf \in L^1 \implies \int yf = 0.$$

Now, multiplying the ODE (2.2.15) in $\mathbb{R}$ with y and integrating once, we derive the fifth order ODE

$$yf^{(\mathrm{v})} - f^{(\mathrm{iv})} - y(f^3)' + f^3 - \frac{1}{6}y^2 f = -f^{(\mathrm{iv})}(0) + f^3(0) = -\frac{1}{6}A, \tag{2.3.61}$$

where the constant $A \in \mathbb{R}$ determines the rate of algebraic decay at infinity. Recall that from ((2.2.29)) with $p = 3$ the asymptotic algebraic behaviour is

$$f(y) = Ay^{-2}(1 + o(1)) \quad \text{as } y \to \infty. \tag{2.3.62}$$

This ensures integrability of the (bounded) similarity profiles for any A.

Note that unlike for the equation from (2.3.35), the presence of y multiplying the fifth order term in (2.3.61) means that $f^{(\mathrm{v})}(0; C, k, A)$ is truly independent of the other parameters, and we are left with a '3-3' shooting problem that must

include non-trivial values of A.

This problem is simply too difficult to solve directly; while it plausible that the 'separatrix' property we exploit for the p_0 case persists, even if it does it will be a two-dimensional manifold of complicated form. Instead, our approach is to solve a simpler problem, then continue these solutions in the A parameter (for sufficiently large y that the exponential contributions are negligible) until the branch we construct passes through a solution to the full problem.

More precisely, we solve (2.3.61) with the boundary conditions

$$f'(0) = f'''(0) = 0, \quad f(y) \sim Ay^{-2} \text{ as } y \to \infty, \tag{2.3.63}$$

on the domain $y \in [0, 60]$, the right boundary chosen so that the algebraic contribution $f'''(60)$ is within the numerical tolerances but sufficiently large that the exponential contribution (2.2.26)

$$f(y) = Cy^{-1/5} \exp(ay^{6/5}) \cos(by^{6/5} + k)(1 + o(1)) \text{ as } y \to \infty \tag{2.3.64}$$

is of $\mathcal{O}(C \cdot 10^{-29})$. a, b are as in (2.3.34). We do not expect this to effect the accuracy of simply differentiating $f(y) = Ay^{-2}$ three times and applying at the boundary for the values we consider. Then, we solve the boundary value problem (2.3.61), (2.3.63) using the BVPsuite solver, and use its pathfollowing routines [116] to perform continuation in A until we find a solution satisfying $f^{(\mathrm{v})}(0) = 0$.

To generate initial profiles for the solver, our simplified problem amounts to '3-2' shooting and by relatively quick trial and error we can find profiles close to satisfying the reduced symmetry conditions at the origin. We emphasize that even for this simplified problem, however, deducing a general pattern for the behaviour of the profiles based on the bundle parameters is far from straightforward. Fortunately, the BVPsuite solver will converge to a correct nearby profile for not-that-good initial guesses (e.g. with $f'(0),\ f'''(0) = \mathcal{O}(10^{-1})$). Because we have not been able to systematize our approach to any greater extent than this, there is perhaps some concern that we have missed solution branches. However, the emergence of the same pattern as the p_0 critical case, describing the beginning of a countable set of solutions indexed by the number of 'non-trivial' local minima and maxima (humps) near the origin provides some reassurance.

The branches of positive dominant solutions are presented in figure 2-16. Note that rather than taking our dependent bifurcation variable as $f^{(\mathrm{v})}(0)$, we instead use the easier-to-measure mass. We know that the admissible solutions must have zero mass by remark 2.1, but that this is equivalent to the condition on the

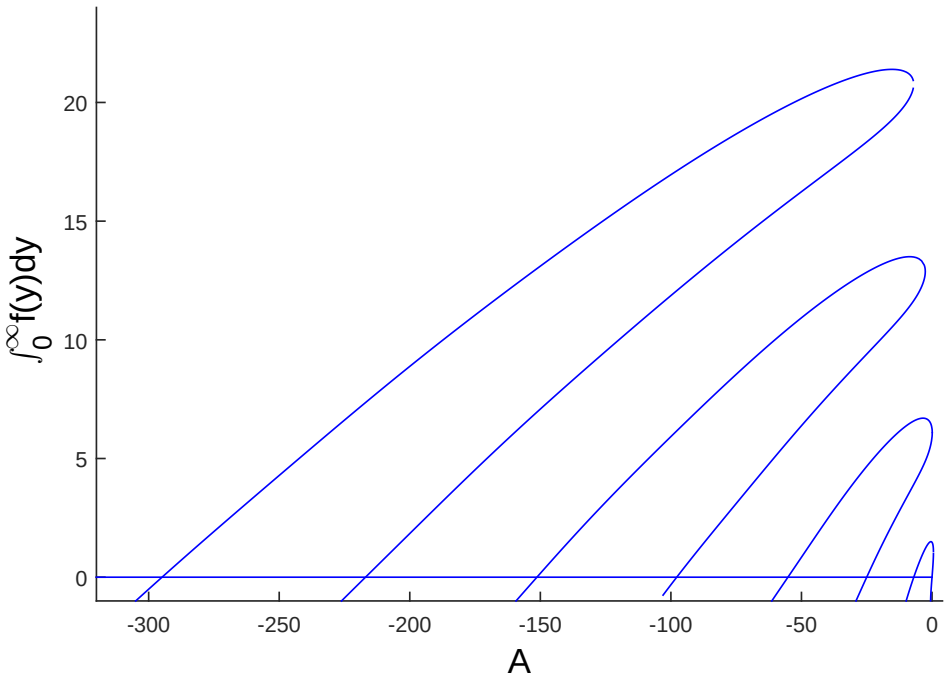

Figure 2-16: Continuation in A of solutions to the reduced BVP. The intersection with the line of zero mass corresponds to the solutions of the full problem.

derivative is a consequence of the following simple lemma, which will also prove useful later on:

Lemma 2.4. *For $N = 1$, $p \neq p_0$, integrable solutions of (2.2.15) satisfy the following property:*

$$f'(0) = 0 \implies \left(f^{(\mathrm{v})}(0) = 0 \iff \int_0^\infty f(y)\mathrm{d}y = 0 \right). \tag{2.3.65}$$

Proof. From the equation we have

$$\frac{2}{3(p-1)} \int_0^\infty f(y)\mathrm{d}y = \int_0^\infty f^{(\mathrm{vi})}(y) - \left(|f|^{p-1}f\right)'' - \frac{1}{6}yf'(y)\mathrm{d}y \implies$$
$$c_p \int_0^\infty f(y)\mathrm{d}y = -f^{(\mathrm{v})}(0) + p|f|^{p-1}f'(0),$$

with c_p as in (2.3.32). Thus (2.3.65) follows when $c_p \neq 0$, i.e. $p \neq p_0$. □

Thus, it is clear that the intersections of the branches in Figure 2-16 with the zero-mass line provide an exhaustive list of solutions, providing we have identified all the branches. These solutions are presented in figure 2.3.5.

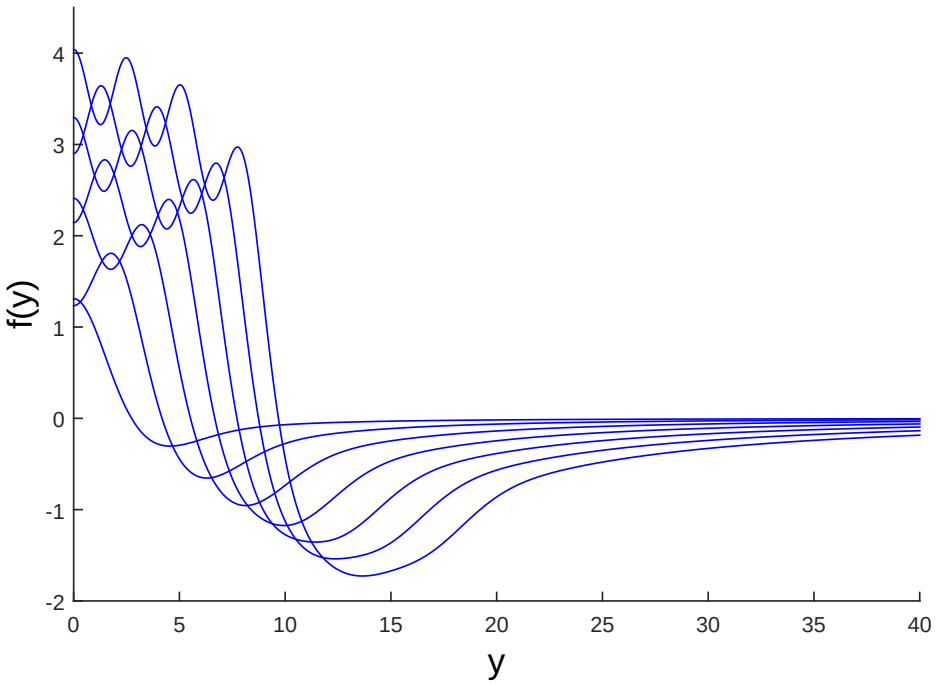

Figure 2-17: The first seven even blow-up profiles for $p = 3$.

A few aspects of this approach bear further comment; first we note that the bifurcation diagram has rotational symmetry of order 2 about the origin, and so the branches of negative-dominant solutions follow the same pattern. Thus, there is a (weak) topological equivalence between the first positive-dominant and negative-dominant solutions (the branch passes through the trivial solution), and thereafter between every consecutive pair of solutions. The branches appear at a sequence of saddle-node bifurcations that occur for apparently decreasing values of A (and vice versa for positive-dominant solutions). As far as we have been able to determine, there are no further links between the branches as we follow them as $A \to -\infty$, and so these branches are distinct. A full bifurcation theory for these solutions will require a thorough understanding of the Volterra-type integral equation of the second kind

$$g(y) = -5g(0) - \frac{1}{2}g''(0)y^2 + \frac{1}{720}y^4 + \int_0^y \left[\frac{6}{y} - \frac{1}{6}\frac{(y-t)^4t^2}{y}\right] g(t) + A^2(y-t)^3(2y-3t)g^3(t)\mathrm{d}t,$$

derived by the performing the scaling $f = Ag$ then integrating (2.3.61) five times,

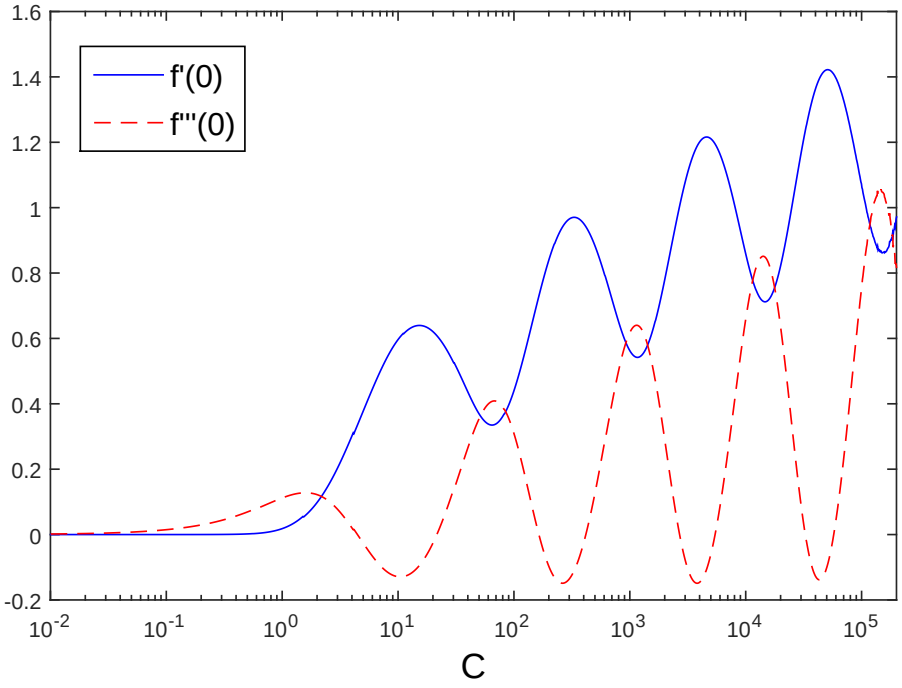

Figure 2-18: Odd derivatives of non-singular profiles at the origin resulting from shooting in C and k for $A = 0$.

using where necessary the identity

$$\int_0^y \int_0^t \Psi(s)\mathrm{d}s\mathrm{d}t = \int_0^y \Psi(s) \int_s^y \mathrm{d}t\mathrm{d}s = \int_0^y (y-t)\Psi(t)\mathrm{d}t,$$

which follows from Fubini's Theorem. However, this seems difficult even linearizing around $g = 0$, let alone the more interesting cases where g is a nontrivial solution of (2.3.61) not admitting a closed form, so we leave this as an avenue for future research.

We conclude this section with some numerical evidence that there exist no even (or indeed odd) similarity profiles with pure exponential decay, using the same 'separatrix' procedure as Section 2.3.3; Figure 2-18 demonstrates that no profiles with pure exponential decay that exist for all $\mathbb{R}$ can satisfy even $f'(0) = f'''(0) = 0$.

2.3.6. General p in One Dimension: Existence and multiplicity results for general p remain hard since it is not possible to integrate up. Instead we once again rely on evidence from the numerical simulation of the PDE. Starting from initial data $u_0 = 2\exp(-x^2/4)$ we solve as far into the singularity as possible and

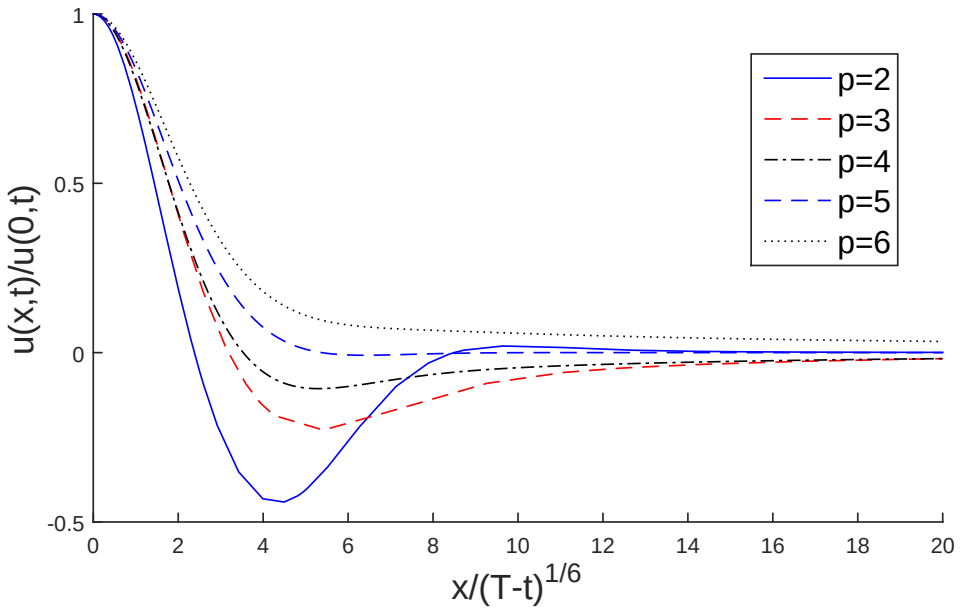

Figure 2-19: Self-similar blow up profiles for a sample of $p > 1$.

observe convergence to a stationary profile in the rescaled coordinates (2.2.9) for a wide sample of $p > 1$. These are presented in Figure 2-19, with the u-scaling normalized to account for inaccuracies in the measurement of T, which can have a large effect on the rescaled profiles very near the blow-up time.

Note that for all profiles here except $p = 2$, the 'correctly' scaled versions generate convergent solutions when used as initial data in the boundary value problem solver BVPsuite for equation (2.2.15). Moreover, the results of this agree closely with the solutions taken directly from the full PDE simulation. For $p = 2$ despite clear convergence of the profiles to the solution pictured, the BVPsuite algorithm fails to converge over any mesh we have tried. The source of this irregularity is not clear to us at the current time.

2.3.7. The p_0 Critical Case in Three Dimensions: There is one more case in which (2.2.15) becomes relatively easy to treat, though not without its own complications; for $N = 3$, all but the first two terms of the radial Δ^3 disappear and we are left with

$$f^{(\mathrm{vi})}(y)+\frac{6}{y}f^{(\mathrm{v})}(y)-\left(|f|^{p-1}f\right)''(y)-\frac{2}{y}\left(|f|^{p-1}f\right)'(y)-\frac{1}{6}yf'(y)-\frac{2}{3(p-1)}f(y)=0. \tag{2.3.66}$$

In this instance, the critical p (2.2.18) is $p_0 = \frac{7}{3}$.

Like for $N = 1$, we are able to integrate once to obtain a fifth order ODE. However, since we are treating y as a radial coordinate we must first multiply by $y^{N-1} = y^2$ thus, assuming that f and its derivatives exist at zero, we get

$$y^2 f^{(\mathrm{v})}(y) + 4y f^{(\mathrm{iv})}(y) - 4f'''(y) - \frac{7}{3} y^2 f^{4/3} f'(y) - \frac{1}{6} y^3 f(y) = -\frac{1}{6} A, \quad (2.3.67)$$

where as ever A is the coefficient of the algebraically decaying large-y bundle (2.2.29), here having the form

$$f(y) = A y^{-3}(1 + o(1)).$$

Since by section 2.3.1 we know the finite mass solutions we are interested in must have $A = 0$, and so we get that $A = 0 \iff f'''(0)$ by simply looking at the $y \to 0$ limit. This is unlike the $N = 1$ case where it was the fifth derivative symmetry condition which was equivalent to no algebraic decay.

The assumption that f and its derivatives exist at 0, where the coefficients of the second and fourth terms of (2.3.66) become singular, is in fact a strong one. Looking at the form of the equation, we can see that this in fact requires

$$\lim_{y \to 0} \left| \frac{6 f^{(\mathrm{v})}(y) - \frac{14}{3} f^{4/3} f'(y)}{y} \right| < \infty. \quad (2.3.68)$$

This can only happen when the numerator itself tends to zero, and so for bounded solutions with $f(0) \neq 0$, we find that $f'(0) = 0 \iff f^{(\mathrm{v})}(0) = 0$.

Thus we need only find a profile with

- f is bounded on $[0, \infty]$,
- $f'(0) = 0$, and
- no algebraic decay as $y \to \infty$

to ensure radial symmetry. This leads to a slightly more subtle shooting problem, using the two parameters from the exponential bundle (2.2.26) now having the form

$$f(y) = C y^{-6/5} \exp(a y^{6/5}) \cos(b y^{6/5} + k)(1 + o(1)) \text{ as } y \to \infty,$$

with a, b as in (2.3.34). So, the full problem with the integrated form of the ODE

(2.3.67), is

$$f^{(\mathrm{v})}(y) + \frac{4}{y} f^{(\mathrm{iv})}(y) - \frac{4}{y^2} f'''(y) - \frac{7}{3} f^{4/3} f'(y) - \frac{1}{6} y f(y) = 0,$$
$$|f(0)| < \infty, \quad f'(0) = 0, \quad f \sim C y^{-6/5} \exp(a y^{6/5}) \cos(b y^{6/5} + k) \text{ as } y \to \infty. \tag{2.3.69}$$

Once again, our procedure for finding these profiles numerically entails a 'divide and conquer' approach, attempting to construct bounded profiles for each C in small increments as a separatrix, testing the sign of the singularity of a profile with k value halfway between two k values known to have singularities of opposite sign. We have not been able to prove that the value of k converged to by this method for this more complicated problem is unique modulo π, however we do again have very strong numerical evidence.

Here even finding k to within 10^{-14} will almost certainly not be sufficient to give a profile with $|f(0)| < \infty$ due to the very strong singularity at the origin in the equation and (2.3.68); it is with probability zero that we can pick up the correct balance to make this finite. However, as we get closer to the k value that will give a profile bounded on $[0, \infty]$, it does hold that y_0, the location of the singularity, tends to zero monotonically. In fact, the profiles seem 'well behaved' very close to the origin before becoming singular in an increasingly small interval. Hence, to find candidates for even profiles, we test $f'(10^{-4})$, which we have found empirically to be comfortably outside the singular boundary layer. Then, the bounded profile will have $f'(0)$ very close to this value, the dependence of which on C is shows in Figure 2-20.

Again, we can use BVPsuite to recover better approximations. We take as initial guesses to profiles corresponding to the four zeros of $f'(10^{-4})$, which we are able to find before our shooting method breaks down on the interval $[10^{-4}, 150]$, and copy the value of $f(10^{-4})$ at zero. The solver converges quite rapidly and the solutions are shown in Figure 2-21. It is observed again that we have a sequence of profiles indexed by the number of (non-trivial) local minima and maxima near the origin.

2.3.8. Connection to a Variational Problem: Questions on solution existence and multiplicity for higher order equations are often best answered when a variational formulation of the problem is available, i.e. when solutions to a differential equation are equivalent to stationary points of an associated functional. Then various techniques have been developed to understand the geometric and topological properties these functionals induce on the function space, among them

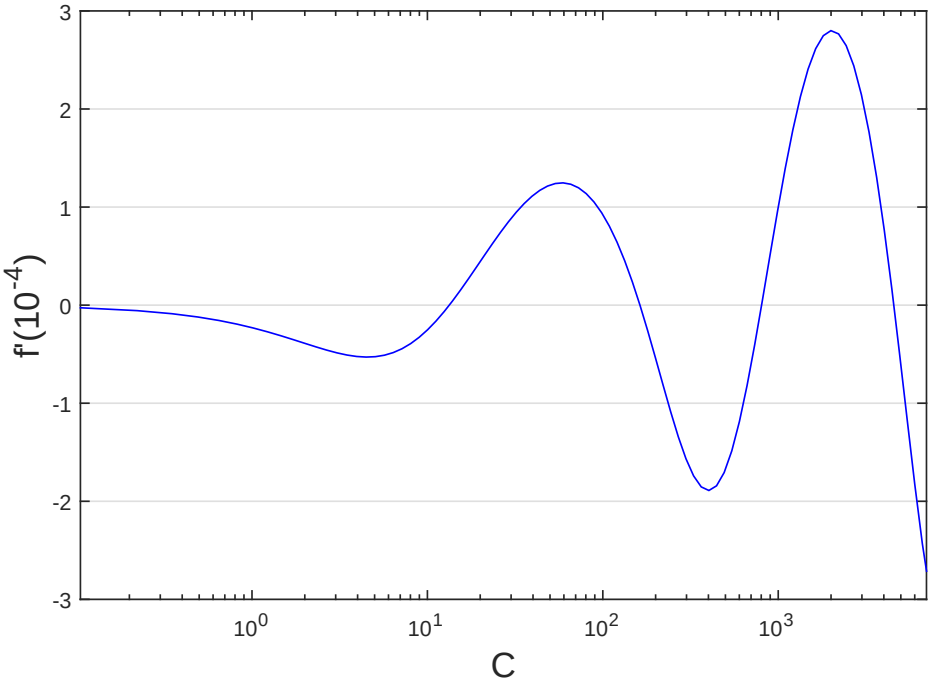

Figure 2-20: $f'(0)$ against C for the 3D radial blow-up equation.

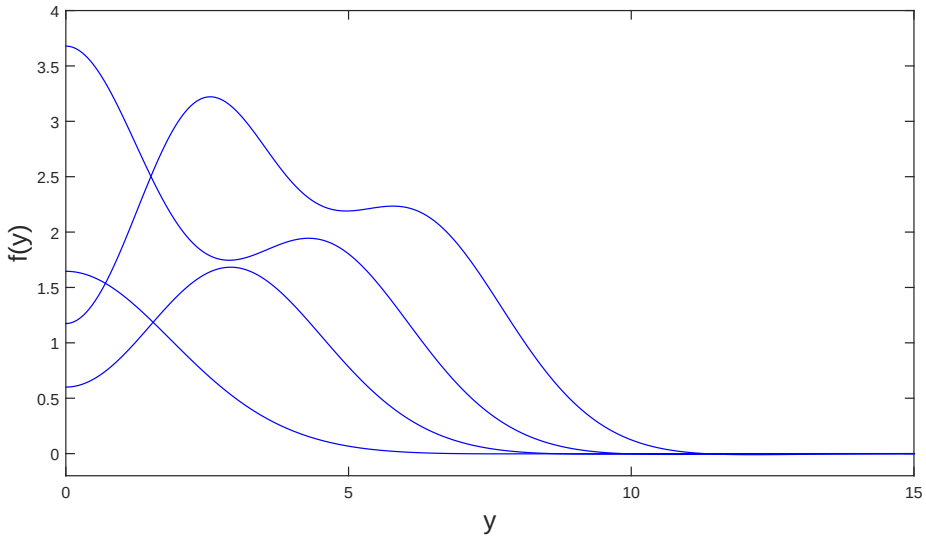

Figure 2-21: $f'(0)$ against C for the 3D radial blow-up equation.

the theories of Morse, Smale, Palais, Krasnoselskii, Ambrosetti-Rabinowitz and Ljusternik-Schnirelman to name but a few (overviews of which can be found in [121], [12] or, more recently [156]).

This is not possible for an equation of the form (2.2.15); the non-autonomous term presents an insurmountable barrier in any functional space. This is not always the case; for the Semilinear Heat Equation (1.2.31) it was shown in [167] that global self-similar solutions have a variational interpretation in certain weighted spaces (essentially the weight function allows the non-autonomous term to be combined with the higher derivative, which is not possible for equations of order greater than two). Additionally, some higher order quasilinear equations possess scaling groups at critical exponent values such that their similarity equations do not feature a non-autonomous term at all and so a functional formulation exists, see [161].

However, there has been some success studying blow up similarity solutions of (1.2.33) via a so-called μ-bifurcation approach, where the coefficient of the non-autonomous term is replaced by a parameter μ which can be varied as convenient to try and pick up solution branches and follow them to the desired value. In [24], multiple self-similar solutions are detected by following solutions in μ from both non-zero bifurcation points, where solutions branches emanate from a non-trivial constant solution, and from the variational $\mu = 0$ case. Then, the number of branches that persist to $\mu = 1/6$ (in the sixth order case) gives an idea of the number of self-similar solutions.

For us, the bifurcation theory does not apply as there is no non-trivial stationary solution and the linearization of $\mathbf{B}^*$ (1.3.50) about zero does not have the correct spectral properties (although we return to this in a different context in Chapter 4). However, it is still possible to see what can be said about the $\mu = 0$ case, and then whether any of the solutions can be continued in μ sufficiently far as to generate self-similar profiles. The results we have uncovered in this direction are only rather preliminary, and the complete answers, especially to the second part, will require major research efforts to describe satisfactorily. However, we believe that they are of sufficient interest to include.

Subsituting $1/6 \to \mu$ in the non-autonomous term, (2.2.15) becomes

$$\Delta^3 f - \Delta\left(|f|^{p-1} f\right) - \mu y \cdot \nabla f - \frac{2}{3(p-1)} f = 0. \tag{2.3.70}$$

Then, for $\mu = 0$, we can multiply through by $(-\Delta)^{-1}$, giving

$$-\Delta^2 f + |f|^{p-1} f - \frac{2}{3(p-1)}(-\Delta)^{-1} f = 0.$$

This allows us to define the functional

$$\mathcal{F}_p(f) \equiv \frac{1}{2}\int_{\mathbb{R}^N} |\Delta f|^2 - \frac{1}{p+1}\int_{\mathbb{R}^N} |f|^{p+1} - \frac{1}{3(p-1)}\int_{\mathbb{R}^N} |(-\Delta)^{-1/2} f|^2. \quad (2.3.71)$$

The correct functional setting for this over $\mathbb{R}^{\mathbb{N}}$ is subtle and to avoid unnecessary detail we refer to [140] where a similar function for a fourth order Cahn-Hilliard equation is analyzed in depth. We do note that a WKBJ analysis of (2.3.70) in a similar vein (although in fact easier) than before gives that solutions with $\lim_{y\to\infty} f(y) = 0$ in the radial geometry have a three parameter family of exponentially decaying solutions

$$f(y) = y^{-(N-1)/2}\left(C_1 \exp(-\kappa y) + C_2 \exp\left(-\frac{\kappa}{2}y\right)\cos\left(\frac{\sqrt{3}\kappa}{2}y + k_2\right)\right)(1 + o(1)),$$

as $y \to \infty$. Here $\kappa = \left(\frac{2}{3(p-1)}\right)^{1/6}$. In principle, this might be used for determining solutions numerically via backward shooting, as above. However, this is unappealing as not only are there three shooting parameters, but the coefficient of exponential decay for the C_2 term is quite small, requiring a large 'shooting range' and meaning parameters must be determined to high precision to ensure existence of the profile as far as $y = 0$; we do not pursue it here.

(2.3.71) is an even functional and it can be verified that it satisfies the conditions for the Ljusternik-Schnirelman theory (in particular, Clark's variant, [33]) to apply. Considering the functional subset

$$\mathcal{R}_0 \equiv \left\{ v \in W^{2,2}(\mathbb{R}^N) \cap H^{-1}(\mathbb{R}^N) \;\middle|\; \frac{1}{2}\int_{\mathbb{R}^N} |\Delta v|^2 - \frac{1}{3(p-1)}\int_{\mathbb{R}^N} |(-\Delta)^{-1/2} v|^2 = 1 \right\},$$

it can be shown by mimicking the argument of [140], Chapter, 4 that $\mathcal{R}_0$ contains a sphere of arbitrary bounded dimension, and so its Category ([12] Chapter 6) must be infinite. This is connected with the problem being posed on all of $\mathbb{R}^N$. Thus considering the functional

$$\Phi_p(f) = \frac{1}{p+1}\int_{\mathbb{R}^N} |f|^{p+1}, \quad f \in \mathcal{R}_0,$$

we construct an infinite set of 'eigenfunctions' of the problem $\Delta^3 v - \frac{2}{3(p-1)} v =$

$\lambda_\beta \Delta\left(|v|^{p-1}v\right)$ using the customary min-max procedure where critical values of the functional are determined as infima over maximal families of sets of category β., see e.g. [85], pp. 18. In some ways this is a nonlinear analogy to the Rayleigh quotient in classical potential theory. The λ_β are Lagrange multipliers that can be scaled out to retrieve solutions of the original equation.

Despite being a powerful tool for proving abstract existence and multiplicity results, the Ljusternik-Schnirelman theory tells us nothing about the features of the solutions we unearth, for instance there is nothing to stop them even being non-radial. We do not know whether or not this occurs. Worse, even if we could describe solution patterns, the problem we really want to solve is determining which solutions lie on μ-branches that cross through the relevant value $\mu = 1/6$. It may well be that in trying to find more satisfactory proofs of the original problem, we have begun to explore an alternate method that is even more difficult to work with!

We provide partial answers to these two questions numerically, and in some sense backwards, by using BVPsuite's pathfollowing routine to start from the $\mu = 1/6$ similarity profiles we discovered by shooting and then extending them into the $\mu < 1/6$ region in the hope of finding branches that cross the origin. We focus on the case $N = 1$ and supplement (2.3.70) with boundary conditions $f'(0) = f'''(0) = f^{(v)}(0) = 0$, $f(300) = f'(300) = f''(300) = 0$, 300 chosen so as to account for the slower y-decay as $\mu \to 0$.

In Figures 2-22, 2-23 we see the μ-branches starting from the first four similarity solutions. As the complexity of the similarity profile increases, the path of the μ-branch does so rapidly, becoming non-monotone on the third branch and extremely so by the fourth. Details of this branch near $\mu = 0$ are shown in Figure 2-24 so its structure is more evident. Not shown in the diagram is that after the branches cross the origin once, some of them can return for further crossings although this has been too time-consuming to explore fully. It may be that all solutions for $\mu = 0$ lie on a branch connected to a similarity solution, but with some branches passing through more than one, although this is pure speculation. This is definitely an area for further research.

Figures 2-25- 2-28 show the similarity solutions superimposed with solutions on the μ -branches the first time they cross zero. Clearly the solutions to the variational problem have a less regular structure and if there is a pattern to the connections it is not obvious. In order to make this rigorous to any extent, we will have to fully understand the spectra of the linearized operators along the branch. If we make the change of variables $y = (6\mu)^{-1/6}z$ in (2.3.70), then we

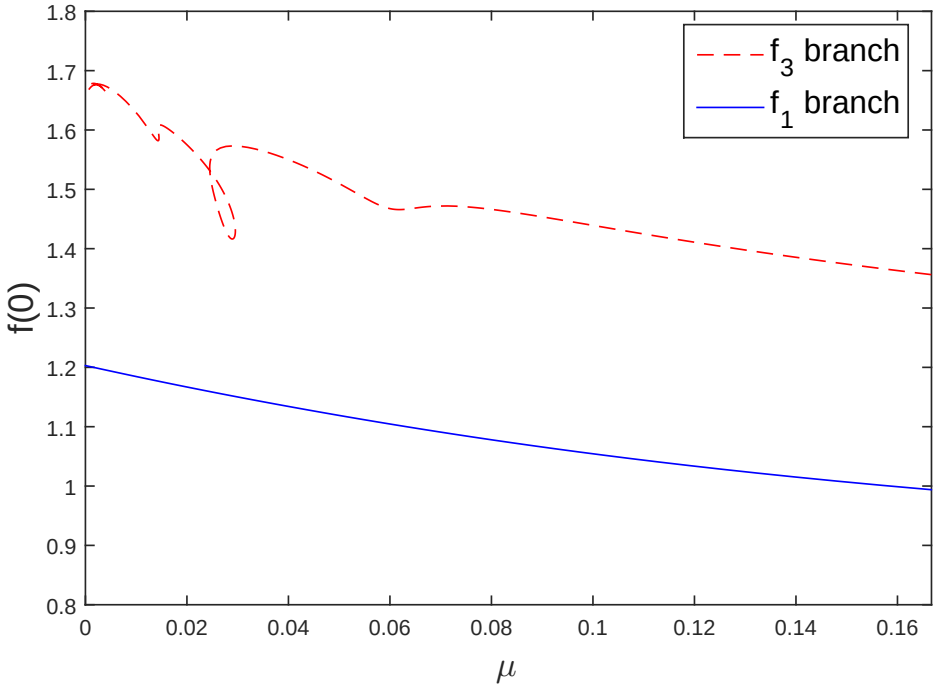

Figure 2-22: Continuation in μ from the 1st and 3rd blow up profiles.

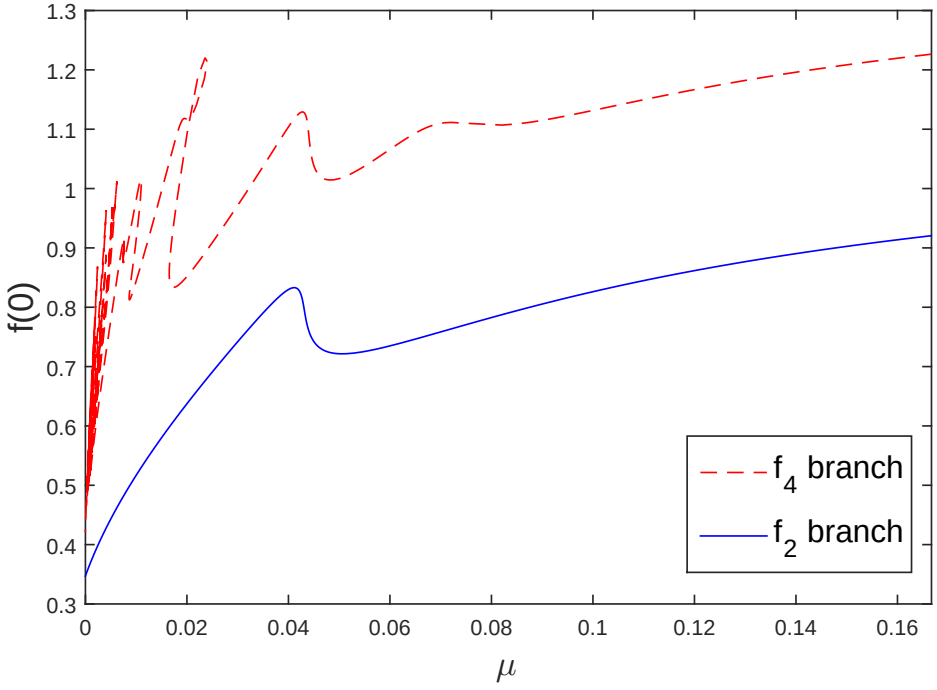

Figure 2-23: Continuation in μ from the 2nd and 4th blow up profiles.

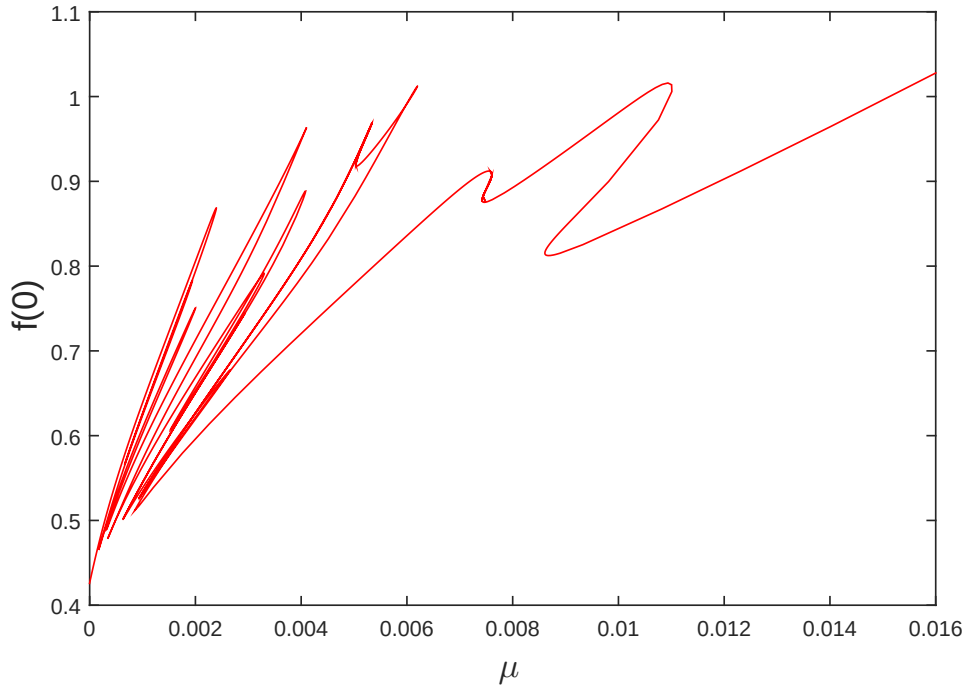

Figure 2-24: Detail of the 4th branch near $\mu = 0$.

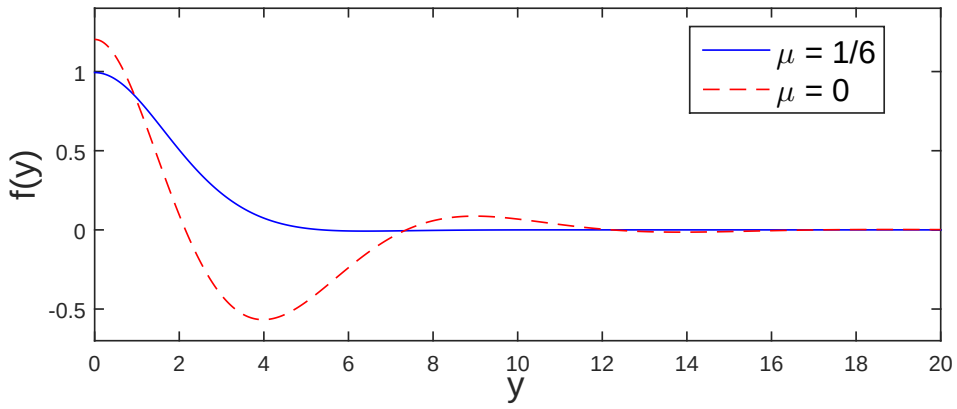

Figure 2-25: Comparison of profiles on the first branch for $\mu = 1/6$ and $\mu = 0$.

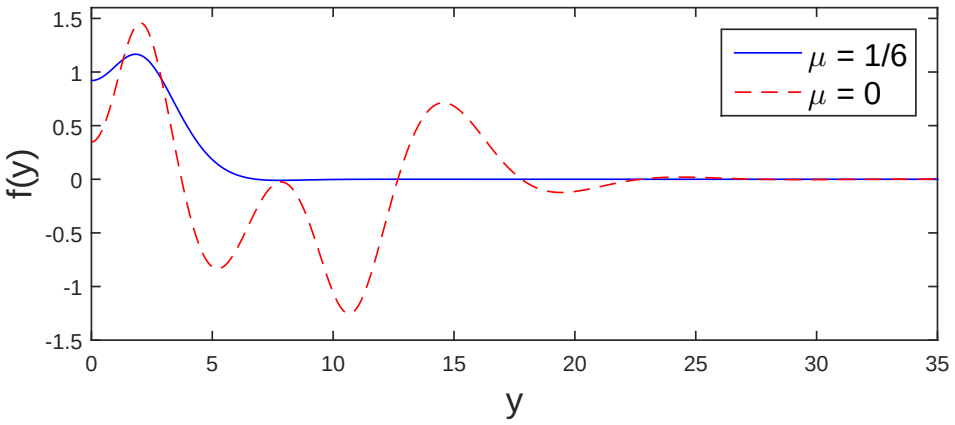

Figure 2-26: Comparison of profiles on the second branch for $\mu = 1/6$ and $\mu = 0$.

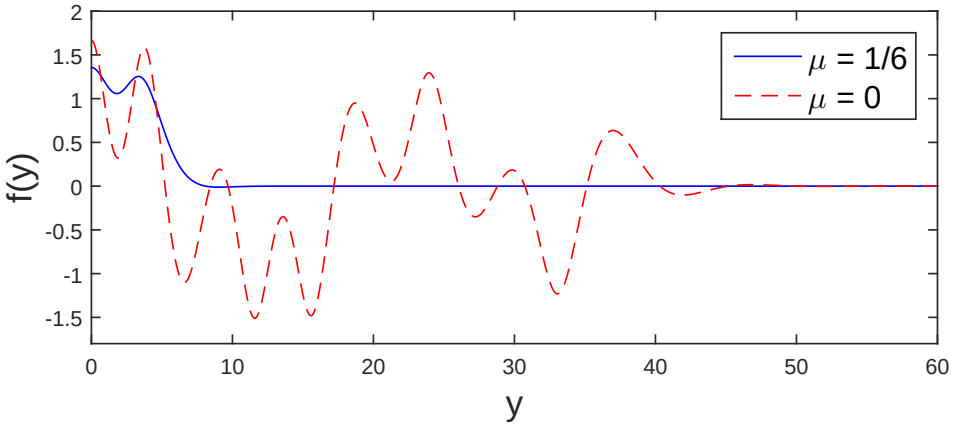

Figure 2-27: Comparison of profiles on the third branch for $\mu = 1/6$ and $\mu = 0$.

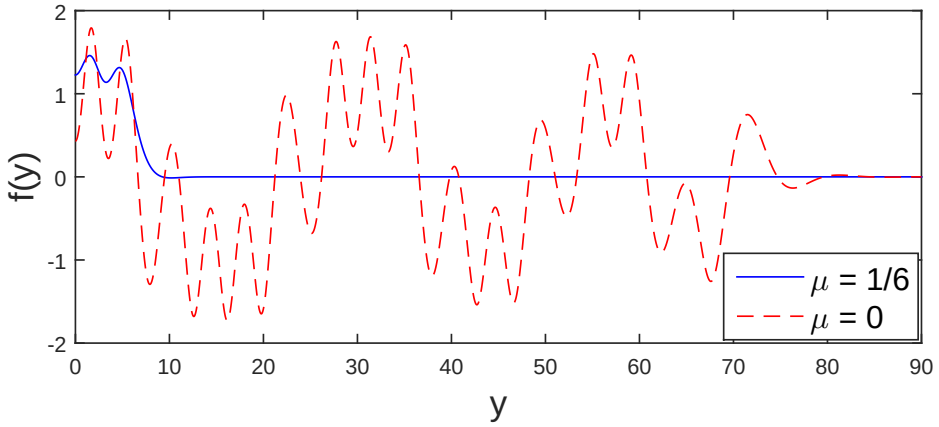

Figure 2-28: Comparison of profiles on the fourth branch for $\mu = 1/6$ and $\mu = 0$.

can write it in the form of the implicit function problem

$$G(f,\mu) \equiv \mathbf{B}^* f - \frac{1}{9\mu(p-1)} f - \frac{1}{(6\mu)^{2/3}} \Delta\left(|f|^{p-1} f\right) = 0.$$

Then for there to be a unique solution $f(y;\mu)$ in a neighbourhood of a point (f_0, μ_0), implicit function theorem demands that the linearization about f_0, $G_f(f_0, \mu_0)$ be invertible. Thus, a necessary condition for a saddle-node bifurcation, where the branches double back on themselves, is

$$0 \in \sigma\left(\mathbf{B}^* - \frac{1}{9\mu_0(p-1)}\mathbf{I} - \frac{p}{(6\mu_0)^{2/3}} \Delta\left(|f_0|^{p-1}\mathbf{I}\right)\right). \tag{2.3.72}$$

Given the evident difficulty of this eigenvalue problem (f_0 must be solved for) on top of the intricate configuration of saddle-node bifurcations we observe from the numerics (particularly Figure 2-24), it may be that the only way to approach these problems is numerically.

2.4. Spreading Solutions

2.4.1. Self-Similar Existence Ranges and Non-Uniqueness: Aside from having interest as potential large t asymptotic attractors for solutions that exist globally in time, self-similar solutions of (2.1.1), that is solutions of (2.2.15) taken for the remainder of this section with $\sigma = 1$, are involved in some interesting phenomena that can occur in 'unstable' equations of this type. We adopt the terminology *spreading solutions* in analogy with Thin Film Equations, as the self-similar profiles become wider and shorter in space during the evolution, in direct contrast to the growing, concentrating blow-up profiles.

One of these phenomena is the possibility of non-uniqueness, first discovered for the Semilinear Heat Equation (1.2.31) in the works of Weissler et al from the 1980s (see e.g. [99]) precisely by construction of self-similar solutions; the result then follows from how the associated scaling group behaves in certain limits. The extension to higher order equations of the type (1.2.33) was done in [74], and from there the generalization to equations of the unstable verstion of (1.1.1) is fairly straightforward, although we do think that the persistence of non-uniqueness to conservative equations with right-hand sides with full divergence form bears some remark.

This non-uniqueness naturally cannot apply in a classical sense; rather it concerns solutions evolving from some kind of initial singularity *in the equivalence*

class of 0 in some L^q space, a somewhat weaker property. Specifically, if solutions to (2.1.1) are considered in the space $C\left([0,T];L^q(\mathbb{R}^N)\right)$ defined via the semigroup representation (2.2.3), then for a self-similar solution $u(x,t) = t^{-2/3(p-1)}f(y)$, $y = xt^{-1/6}$ (2.2.10) we can consider the limit

$$\lim_{t\to 0^+}\left(\int_{\mathbb{R}^N}|u(x,t)|^q\,\mathrm{d}x\right)^{1/q} = \lim_{t\to 0^+}\left(t^{-2/3(p-1)+N/6q}\left(\int_{\mathbb{R}^N}|f(y)|^q\,\mathrm{d}y\right)^{1/q}\right), \tag{2.4.73}$$

provided the L^q norm of the similarity profile is finite. This leads to the following proposition.

Proposition 2.5. *Let $q > 1$, $p > 1 + \frac{4q}{N}$. Then if there exists a self-similar profile f with coefficient of algebraic decay $A = 0$ (2.2.29) it describes a non-zero global-in-time solution of* (2.1.1) *with initial condition* 0 *in $L^q(\mathbb{R}^N)$.*

This is a trivial consequence of the condition that the exponent of t in the right hand side of (2.4.73) be greater that zero. The condition $A = 0$ is necessary otherwise the similarity profiles will not in fact be in L^q, see comments in Section 2.3.1. The necessity of $q > 1$ forces $p > p_0$ and so the solutions we require must have pure exponential decay from the bundle (2.2.26). We construct such solutions numerically in Section 2.4.4.

Obviously, this gives us at least three solutions of the PDE with the same intial condition (the others being $-f$ and the trivial solution). To our knowledge, it is still open whether this result can be extended to other initial data even for second order equations, marking a significant gap in our understanding of these problems.

Before we move on to constructing solutions, we remark that it can be shown the p-range for which self-similar solutions that are global in time exist is bounded from above, the proof of which can be adapted from a similar result from [74].

Theorem 2.6. *Let $p \geq p_S$, where p_S is the critical sobolev exponent for the imbedding $H^2 \hookrightarrow L^{p+1}$*

$$p_S = \begin{cases} \frac{N+4}{N-4}, & N \geq 5, \\ \infty, & N = 1,2,3,4. \end{cases} \tag{2.4.74}$$

Then there exist no non-trivial solutions to (2.2.15).

Proof. Recall the Lyapunov function $E[u](t)$ defined in (2.2.4) was shown to be monotone decreasing (for nontrivial u) by (2.2.5). Assuming u exists for all $t > 0$

and is self-similar, and taking $t \to 1+t$ so that $u_0(x) \equiv f(y)$, we have by (2.2.10) that the Lyapunov satisfies the identity

$$E[u](t) = (1+t)^{\kappa} E[u](0), \quad \kappa = \frac{(N-4)(p-p_S)}{6(p-1)}.$$

Now for $p \geq p_S$, $\kappa \geq 0$, and so for this to not violate the monotonic decrease of $E[u](t)$ we must have $E[u](t) < 0$ for all $t \geq 0$. However, by (2.2.7), we know that any solution of (2.1.1) with $E[u](0) < 0$ must blow up in finite time, contradicting the assumption that f is a global-in-time self similar solution. □

It is interesting that despite the extra divergence operators compared with (1.2.33), this behaviour is still determined according to the Sobolev imbeddings of the pure power-law nonlinearity.

2.4.2. The p_0 Critical Case in One Dimension: As in the case of blow-up in Section 2.3.2, we begin with the analysis of global self-similar solutions in the simplest case $N = 1$, $p = p_0 = 5$:

$$u(x,t) = t^{-1/6} f(y), \quad y = x/t^{1/6},$$

where f satisfies the ODE obtained from (2.2.15), with $\sigma = 1$. By integration and using that the constant of algebraic decay $A = 0$ for finite-mass solutions, we derive the ODE and left boundary conditions

$$f^{(\mathrm{v})} + \frac{1}{6} y f - (f^5)' = 0, \quad f'(0) = f'''(0) = 0. \tag{2.4.75}$$

Recall that unlike the blow-up case (2.3.35), the ODE ((2.4.75)) admits a three-dimensional exponential bundle as $y \to \infty$ (2.2.26), here having the form

$$f(y) = y^{-2/5} \left(C_1 \exp(-y^{6/5}) + C_2 \exp(\tilde{a} y^{6/5}) \cos(\tilde{b} y^{6/5} + k) \right),$$

where $\tilde{a} = (5/6^{6/5}) \cos(3\pi/5)$, $\tilde{b} = (5/6^{6/5}) \sin(3\pi/5)$ and -1 are the fifth roots of -1 with real part less than zero, $\tilde{a}$ and $\tilde{b}$ distinguished from (2.3.34). This means, in view of requiring only two (independent) symmetry conditions be fulfilled, that we have a '3-2' shooting problem which can in principle admit a continuous family of solutions, as in the critical case for global similarity solutions of (1.1.9) ([56], chapter 6). However, proving this definitively is much more difficult for a number of reasons.

Firstly, we must derive an expression for the slowly growing large-y behaviour.

Making the ansatz $f(y) \sim \frac{y^{1/2}}{15^{1/4}} + g(y)$ as $y \to \infty$, we find that at leading order, the linearized ode becomes

$$g^{(\mathrm{v})} - \frac{1}{3}y^2 g'(y) - \frac{1}{2}yg(y) = 0,$$

whose exact solutions are expressed in terms of linear combinations of generalized hypergeometric functions. This should come as no surprise, the analysis of Section 2.3.2 holds at leading order for (2.4.75) also, and we expect that almost all initial data will result in blow-up of f at some point $y_0 < \infty$. This will be mirrored by finite convergence radii of the aforementioned hypergeometric functions. However, we can recover an asymptotic approximation using the substitution

$$g(y) = y^{-5/2} h(y^{3/2}).$$

Then, the dominant balance has the form

$$\left(\frac{3}{2}\right)^5 h^{(\mathrm{v})} - \frac{1}{2}h' = 0.$$

Solving this is simple and we find that as $y \to \infty$, f can have the asymptotic behaviour

$$f \sim \frac{y^{1/2}}{15^{1/4}} + y^{-5/2}\left(\alpha_1 + \alpha_2 \cos\left(\frac{2}{3^{5/4}}y^{3/2}\right) + \alpha_3 \sin\left(\frac{2}{3^{5/4}}y^{3/2}\right) + \alpha_4 \cosh\left(\frac{2}{3^{5/4}}y^{3/2}\right) + \alpha_5 \sinh\left(\frac{2}{3^{5/4}}y^{3/2}\right)\right),$$

with the $\alpha_i \in \mathbb{R}$. Since the cosh and sinh terms diverge more quickly than the multiplicative factor of $y^{-5/2}$, this provides the existence of a three dimensional stable manifold around the slowly growing solutions parameterized by α_1, α_2 and α_3.

Now, for any fixed $f(0) \equiv a_1$, we have to address the interplay between the remaining two parameters $f''(0) \equiv a_2$, $f^{(\mathrm{iv})}(0) \equiv a_3$ and we will see that this can be fairly abstruse. We begin by noting that:

Remark 2.7. *For fixed a_1, a_2, any sufficiently large $a_3 \gg 1$ will have $\lim_{y\to y_0} f(y) = \infty$ for $y_0 < \infty$ and for sufficiently small $a_3 \ll -1$ then $\lim_{y\to y_0} f(y) = -\infty$.*

By continuity we can thus hope to deduce the existence of at least one globally existent profile for all a_1, a_2, see comments in Section 2.3.3.

However, in general there will not be only one such profile, although we can

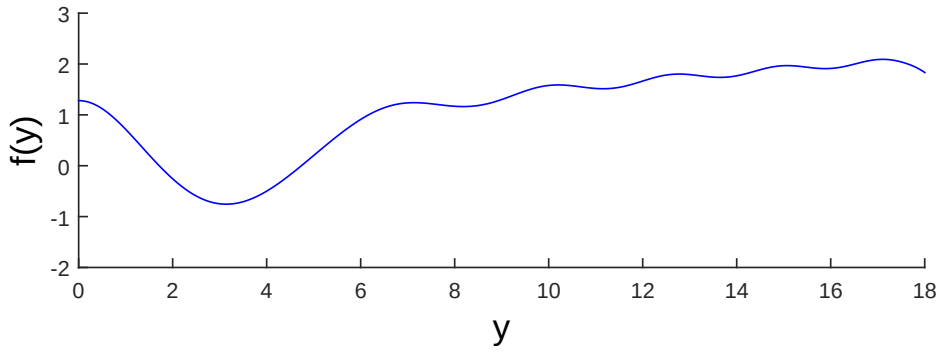

Figure 2-29: Globally existent solutions with $f(0) = 1.28$, $f''(0) = -1.33$.

guarantee by Remark 2.7 that there will be an odd number. Otherwise, the sign of the singularities would have to change an even number of times across each globally existent profile, leading to a contradiction.

We now proceed by presenting some illustrative evidence from our numerical investigations. Our approach was to first fix a_1 and a_2, then pick two initial values $a_{3,1} \gg 1$ and $a_{3,2} \ll -1$ such that both result in profiles with 'extremal' singular behaviour, in the sense that incrementing them or decrementing them respectively will not result in their singularities changing sign. Then we advance as in the blow-up case, testing the sign of the singularity of the profile resulting with $a_3 = \frac{1}{2}(a_{3,1} + a_{3,2})$, and recursing the process between the new profile and the previous one with opposite-signed singularity. This will always converge to a globally existent profile as the result of each step will always have opposite singularity-sign to only one of the previous profiles.

Once we have one globally bounded profile, unfortunately there seems no more elegant way of finding any others than meticulously testing values of a_3 either side of the established one and then launching our recursive procedure described in the last paragraph between any two we find with changing singularity signs. We have found stepping a_3 up and down 0.04 in increments of 10^{-5} has been effective, if time consuming, for values of $a_1 \approx 1$. Much smaller range or larger increment can result in missed solutions.

Figures 2-29-2-34 show the result of this approach applied with $a_1 = 1.28$ and various values of a_2, with each globally existent profile shown. The values of a_2 are clustered on either side of a critical value that will give a profile with the correct exponential decay. Observe how as we approach the critical value the number of globally existent profiles increases from 1 to 3 to 5 and then decreases in kind once it has crossed, and also how the 'sign-dominance' changes in the

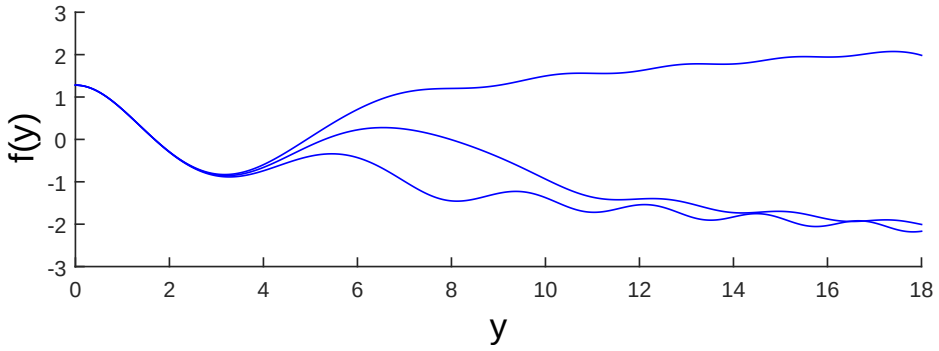

Figure 2-30: Globally existent solutions with $f(0) = 1.28$, $f''(0) = -1.35$.

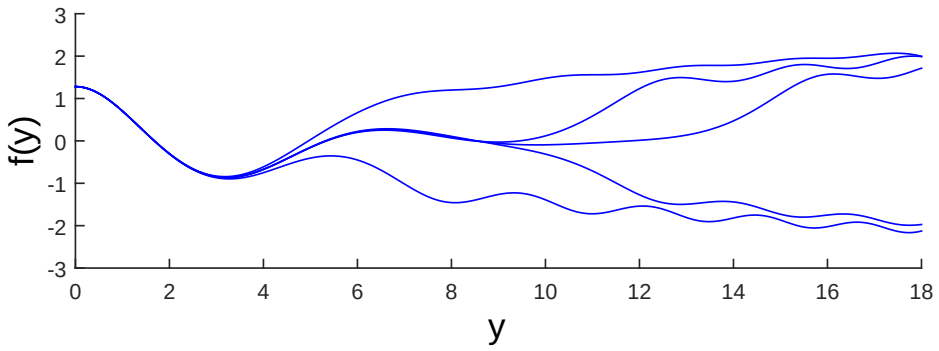

Figure 2-31: Globally existent solutions with $f(0) = 1.28$, $f''(0) = -1.35425$.

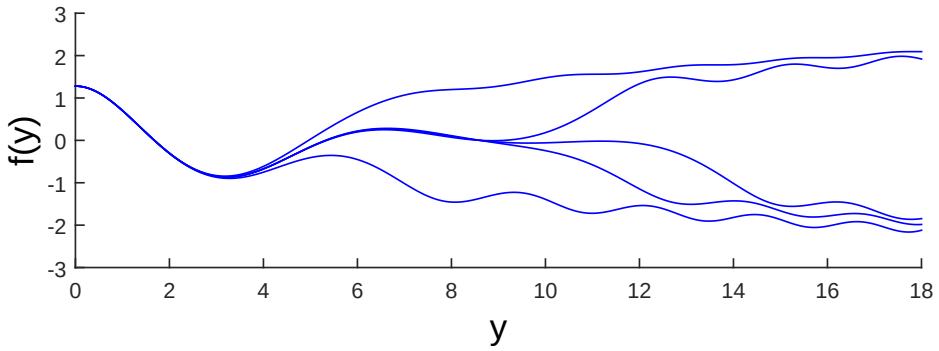

Figure 2-32: Globally existent solutions with $f(0) = 1.28$, $f''(0) = -1.3545$.

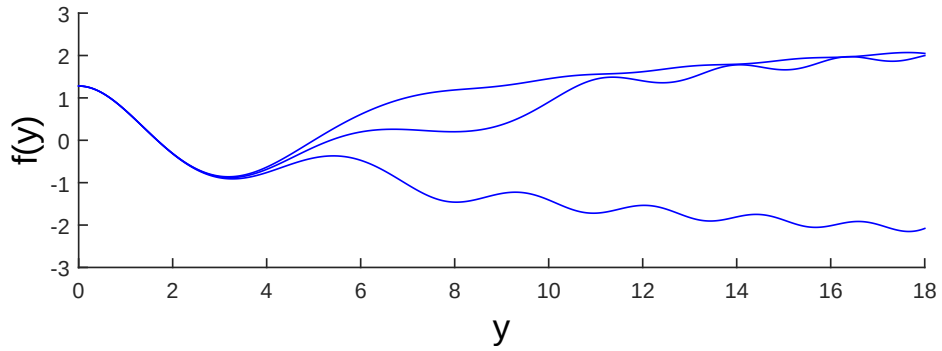

Figure 2-33: Globally existent solutions with $f(0) = 1.28$, $f''(0) = -1.36$.

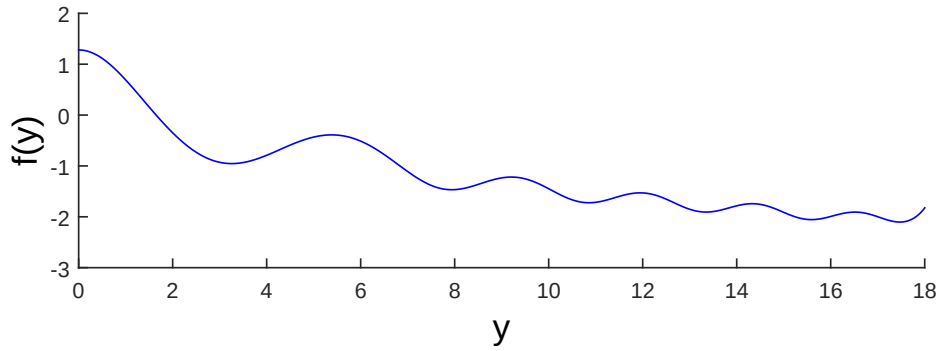

Figure 2-34: Globally existent solutions with $f(0) = 1.28$, $f''(0) = -1.38$.

sense that the asymptotic signs of the innermost profiles flips. For $a_2 > a_2^{crit}$, then we have

- The innermost profile is asymptotically positive if there are 1 or 5 values of a_3 corresponding to globally existent profiles, and
- The innermost profile is asymptotically negative if there are 3 values of a_3 corresponding to globally existent profiles,

and *vice versa* for $a_2 < a_2^{crit}$. This pattern has proved robust for all the values of a_1 and a_2 we have tested, and this property can then be used in the obvious way to write an algorithm that converges to values of a_2 and a_3 that give an exponentially decaying solution of (2.4.75). We call the routine that generates the values of a_3 corresponding to globally existent solutions for $a_2^+ \gg 1$ and $a_2^- \ll 1$, then descend by bisecting the interval $[a_2^+, a_2^-]$, testing the asymptotic sign of the innermost of these profiles and picking each new value of a_2 appropriately. Note that the profile converged to for a given a_1 might not necessarily be unique, as we will see in the next section.

Despite having observed this behaviour consistently we have not been able to convert it into a proof. The asymptotic matching that would be required to determine how parameters at the origin translate into parameters in the large y regime does not seem accessible and we have not found any geometric arguments that apply to equations of this form. However, we feel confident on the strength of this evidence and the numerical construction in Section2.4.3 that we can pose the following:

Conjecture 2.8. *The ODE* (2.4.75) *has an unbounded continuous family of exponentially decaying solutions.*

We have also investigated the possibility of an asymptotic description of the profiles for large a_1. However, unlike for the blow-up case this does not seem tractable. Under the scalings $f = \alpha g$, $y = \beta z$ the 'correct' balance for the outer region near the origin fixes $\beta = \alpha^{-1}$; any other balance leads to divergent behaviour. Then the perturbation problem becomes

$$g^{(\mathrm{v})} - \left(g^5\right)' + \frac{1}{6}\varepsilon z g = 0, \quad \varepsilon = \alpha^{-6} \ll 1.$$

The unperturbed problem has no exact solution and we have not found a clever way of extracting a usable approximation, so we leave by remarking that we expect integrable profiles f to exhibit oscillatory behaviour for some period that

lengthens with a_1, governed by the operator $f^{(\mathrm{v})} - (f^5)' = 0$, before entering the exponentially decaying regime.

2.4.3. Mass Bifurcation at the Critical Exponent: We can provide more evidence for the veracity of Conjecture 2.8 via bifurcation argument, in fact proving existence of a continuous branch of solutions that are sufficiently small. This branch can then be continued numerically to provide more insight into the structure of these solutions, and does in fact reveal an unbounded family with the kind of spatial structure suggested by our brief perturbation argument.

We defer details of the bifurcation argument to Chapter 4, for both this and for the following p-bifurcation, as the differing sign of the nonlinear term does not have a significant effect on the mechanics. See Section 4.2.1, in which we establish the existence and local stability of a branch of solutions bifurcating from the trivial solution via the Lyapunov-Schmidt method. The branch is parameterized by the mass $m_0 = \int_{\mathbb{R}^N} f(y)\mathrm{d}y$.

However, the differences in the global structure of the branch as it develops are stark. Here, the branch is non-monotone in m_0 and, for $N = 1$, also in the bifurcation parameter $f(0)$, a new phenomenon not observed for the fourth order Cahn-Hilliard equation [56]. We show the bifurcation diagram for $N = 1$ in Figure 2-35. We zoom in on the region where the doubling back (via a pair of saddle-node bifurcations) occurs in Figure 2-37 for clarity. Interestingly, this allows for up to three separate profiles with the same value of $f(0)$, distinguished only by their mass m_0 or equivalently their second derivative at the origin. Figure 2-38 demonstrates this visually for $f(0) = 1.3$. This has significant implications for any further attempts to develop the shooting type arguments begun in the last section; the interplay between the shooting parameters $f(0)$, $f''(0)$ and $f^{(\mathrm{iv})}(0)$ is clearly intricate and solutions can't be studied by considering their effects separately.

Another feature obvious from the diagram is that the mass a globally bounded self-similar solution can have is bounded from above. This has ramifications for the possibility of extending solutions past the blow-up time (Section 2.4.5) as well as interest in its own right. The profile with maximum allowable mass is shown in Figure 2-36. It is not clear whether initial data with mass greater than $m_0 \approx 1.043\ldots$ but with positive initial energy (2.2.7) so as to avoid finite-time blow up might converge to this profile in a suitable norm. The stability argument in Section 4.2.1 for small m_0 also holds here but unlike in that case the spectrum

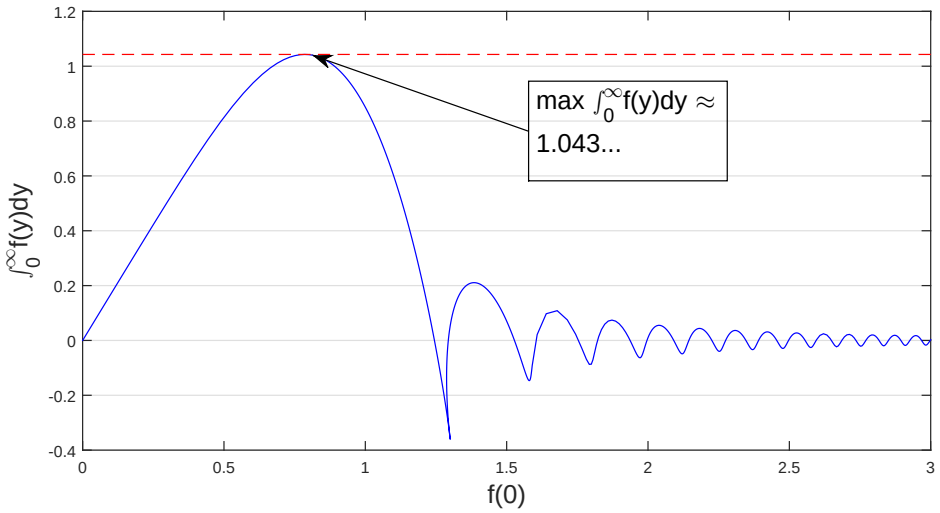

Figure 2-35: The mass bifurcation diagram in the critical case, $N = 1$.

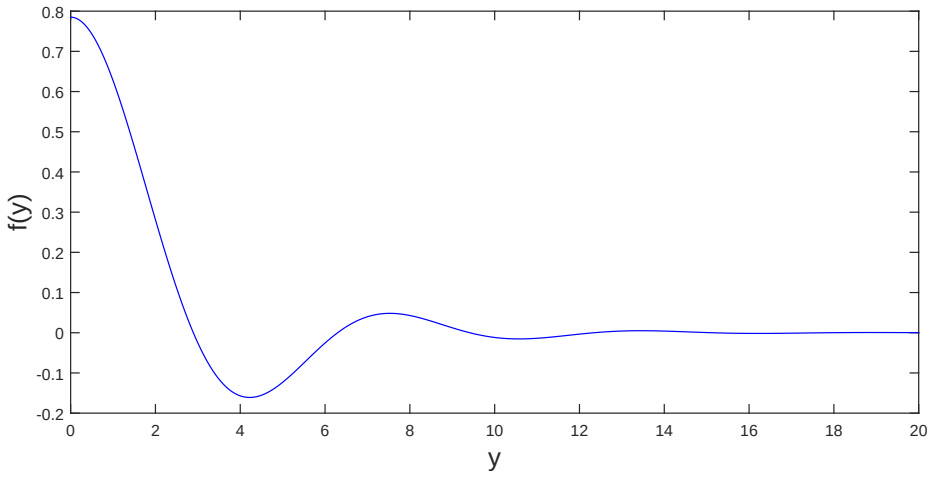

Figure 2-36: The profile with largest possible mass $m_0 \approx 1.043\ldots$.

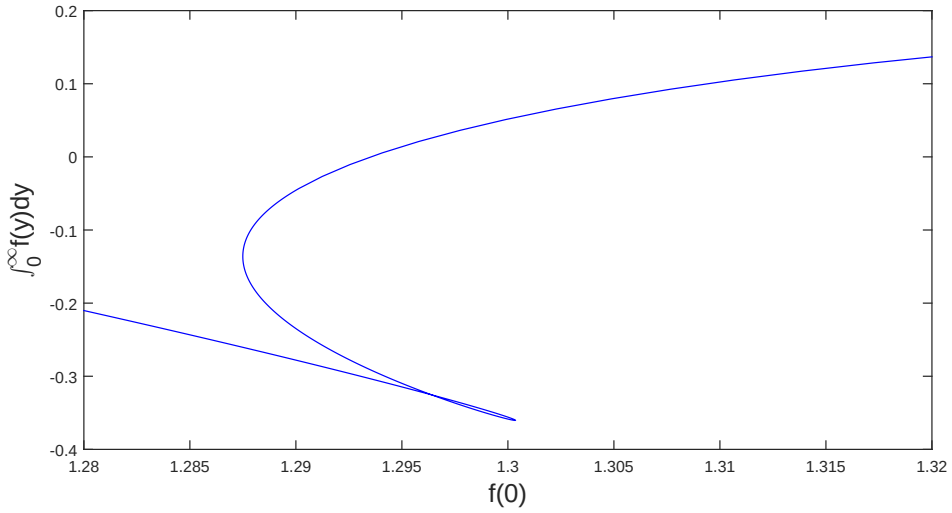

Figure 2-37: Close-up of the region where the bifurcation diagram doubles back on itself.

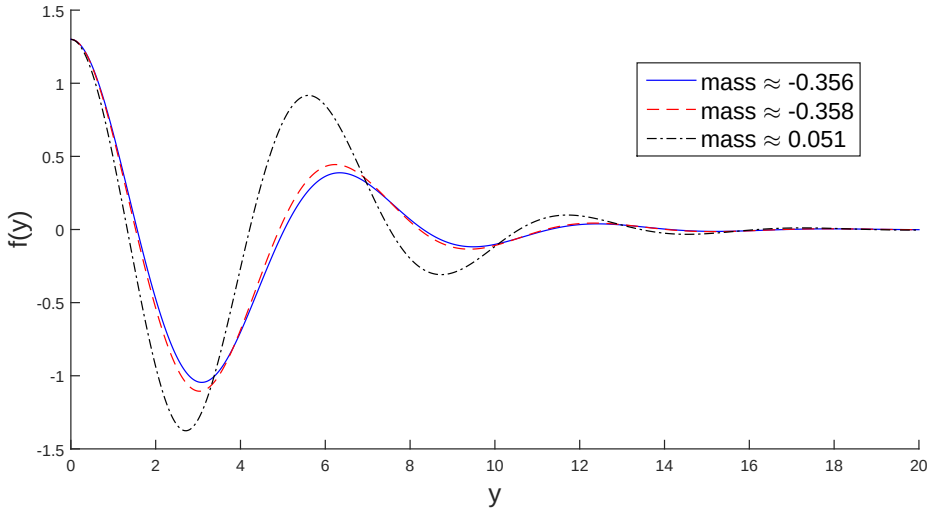

Figure 2-38: Three distinct profiles with $f(0) = 1.3$.

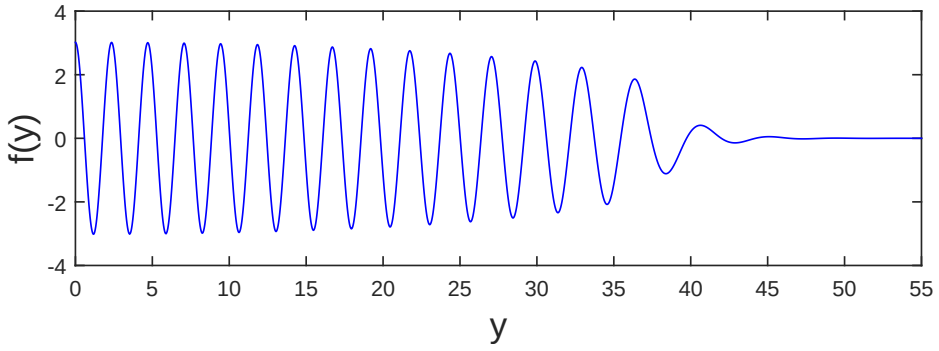

Figure 2-39: A global similarity profile with $f(0) = 3$.

of the linearization about f for small (f, m_0) is given by

$$\sigma\left(\mathbf{A}_2'(f)\right) \approx \left\{-\frac{l}{6} - |m_0|^{4/N} p_0 \langle \Delta\left(|F|^{4/N}\psi_l\right), \psi_l^* \rangle,\ l = 1, 2 \ldots\right\},$$

refer to (4.2.29). The signs here suggest that at some finite m_0 the spectrum will cross the imaginary axis and so solutions on this branch will become unstable, possibly for m_0 very small. It may be fruitful in future research to test extensive sets of initial data with the Numerical Schemes of Chapter 3 to develop an empirical understanding of how solutions deveolp and their stability.

We note that the mass bifurcation diagram suggests oscillatory decay of m_0 as $f(0) \to \infty$. This suggests that for an $m_0 \neq 0$, there will be an at most finite set of profiles with that mass. It is also consistent with the structure we propose above, with an 'outer region' becoming more oscillatory as $f(0)$ increases. We demonstrate this is Figure 2-39, even for $f(0) = 3$ there is a large range of y for which the solution is nearly indistinguishable from that of $f^{(\mathrm{v})} - (f^5)' = 0$ before the third term begins to balance and we see the transition to the exponentially decaying tail.

We also feature the $N = 3$ case, which has some small but important differences. The ODE takes the form

$$f^{(\mathrm{v})}(y) + \frac{4}{y} f^{(\mathrm{iv})}(y) - \frac{4}{y^2} f'''(y) - \frac{7}{3} f^{4/3} f'(y) + \frac{1}{6} y f(y) = 0,$$

supplemented with the boundary conditions $f'(0) = f'''(0) = 0$, see (2.3.67). Now, the mass-bifurcation diagram in Figure 2-40 has no saddle-node bifurcations and is monotone in $f(0)$, somewhat more traditionally. However, while the maximum possible value of m_0 is still bounded, its is not attained until the

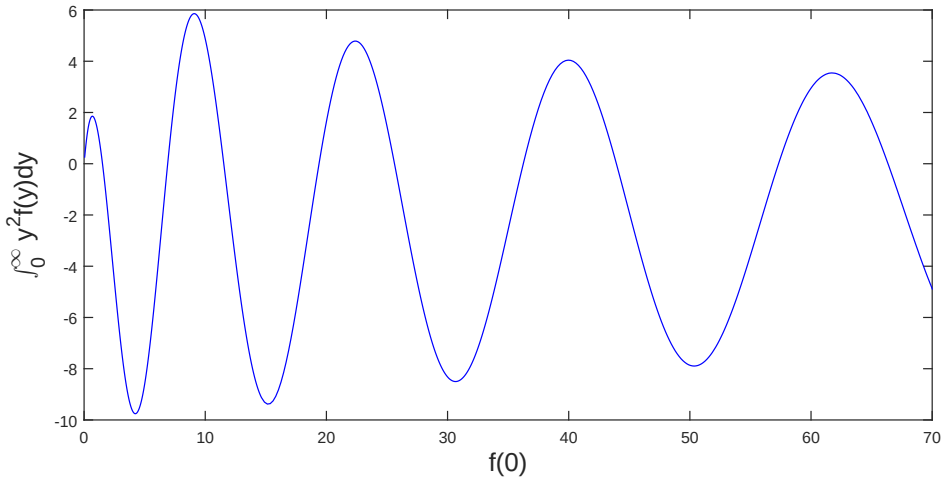

Figure 2-40: The Mass bifurcation diagram for $N = 3$

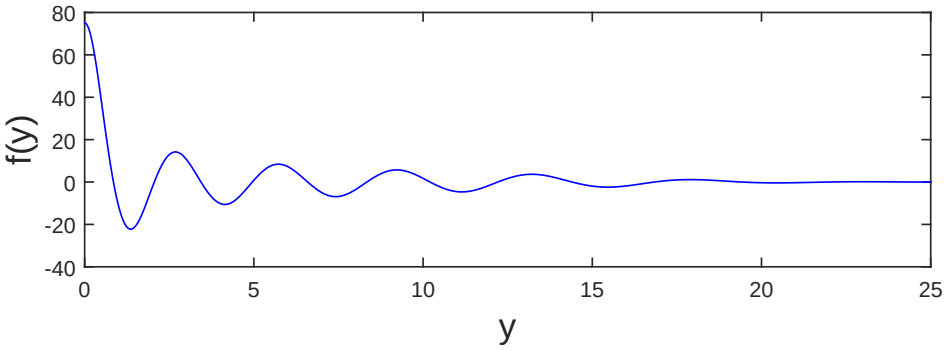

Figure 2-41: Example of a profile on the critical branch for $N = 3$

second 'oscillation', suggesting an even more complicated underlying structure. It seems very unlikely this profile will be stable. Here, too, we include a profile with relatively large $f(0)$ in Figure 2-41 so that we might better understand how solutions behave in this limit. The oscillatory character is still present, however a different behaviour seems to take over near the origin.

BVPsuite's [116] pathfollowing routine was used to make every diagram in this section.

2.4.4. Solutions for General p: Again, the best way we have of understanding the general structure of solutions for all $p > 1$ comes from the bifurcation theory heavily supplemented with numerics. Again, we defer exposition of the theory to Chapter 4, Section 4.2.4 and make the following statements whose proofs can be found there, before demonstrating the outcome of our numerical experiments.

Proposition 2.9. *Let $l \geq 0$ be such that $-l/6$ is an eigenvalue of $\mathbf{B}$ with odd multiplicity. Then*

$$p_l = 1 + \frac{4}{N+l} \tag{2.4.76}$$

are bifucation points for (2.2.15) *from the trivial solution.*

Proposition 2.10. *Near the bifurcation points, solutions can be approximated by the eigenfunctions ψ_l of the operator $\mathbf{B}$, (see Section 1.3.1):*

$$f(y) = \left(\frac{(N+l)^2}{24\kappa_l}(p_l - p)\right)^{1/(p-1)} (\psi_l(y) + o(1)),$$

with $\kappa_l = \langle \psi_l^{p_l}, \Delta\psi_l^* \rangle$.

See Proposition 4.5 and the ensuing discussion. Aside from being a useful result in its own right, this also gives us starting points for our numerical experiments. Note that the sign of the κ_l here, at least for $N = 1$, suggests that the bifurcations are pitchfork bifurcations occuring to the right of the p_l. However, as we shall see, this is by no means a guarantee on the global properties of the branches.

For $N = 1$, we found it slightly more stable to use the condition that profiles must have mass zero for $p \neq p_0$ rather than imposing $f^{(\mathrm{v})}(0) = 0$. These are equivalent by Lemma 2.4. Therefore, we solved the system

$$g'(y) = f(y),\ f^{(\mathrm{v})}(y) - \left(|f|^{p-1}f\right)'(y) + \frac{1}{6}yf(y) + \left(\frac{2}{3(p-1)} - \frac{1}{6}\right)g(y) = 0,$$

with the boundary conditions

$$g(0) = g(\infty) = 0, \quad f'(0) = f'''(0) = f(\infty) = f'(\infty) = 0,$$

or suitable numerical approximations. The conditions on g are how we impose the zero mass conditions . We were not able to use BVPsuite's path-following routine since it calculates Jacobians symbolically, resulting in a singular problem for the p stepping since $\frac{\mathrm{d}}{\mathrm{d}p}\left(|f|^{p-1}f\right)'(y) \approx p|f(y)|^{p-1}\ln(f(y))$, which has singularities where $f = 0$. Recall that we expect the solutions to change sign infinitely often due to the oscillatory tails.

However, a simple natural parameter continuation suffices to make figure 2-42. We found it more natural to start from the solutions corresponding to zeros of the mass branch in figure 2-35 and follow the branches (all of which existed) to either side in p. Observe how the branches going to the left join up with the

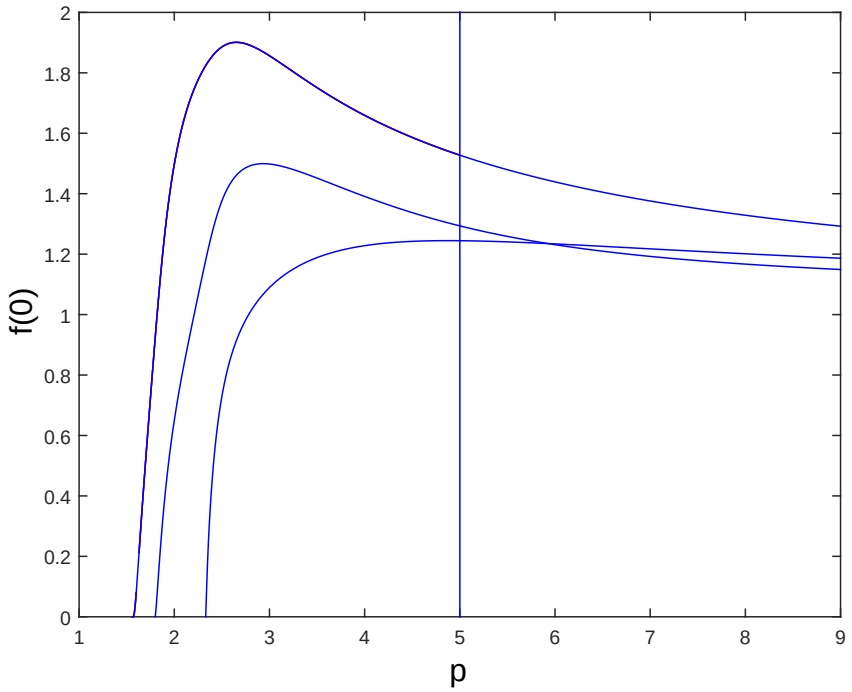

Figure 2-42: The p-bifurcation diagram for $N = 1$.

predicted bifurcation points, and how the branches are all monotone in p. The pattern establishes itself quickly, and it seems we have countable sets of solutions for any $p > 1$ just as in [56], Chapter 6 and [74].

Things are much more interesting for $N = 3$. We found natural parameter continuation with BVPsuite ineffective and so used the specialized bifurcation software AUTO [42], whose sophisticated pseudo-arclength algorithms were able to make more progress, although not without some difficulty; it proved quite sensitive over a number of parameters including number of mesh points, number of collocation points, tolerance, step size etc. AUTO only works for first order, autonomous systems of ODEs and then only those scaled to be posed on $[0, 1]$. We initially tried the coordinate transformation $y = \frac{1}{1+t}$ to map the whole half-line into the unit interval, however this proved extremely unstable as all the features

of the profile occurred in a very small interval. Instead, we solved the system

$$\begin{aligned}
f_1' =& 100 f_2, \\
f_2' =& 100 f_3, \\
f_3' =& 100 f_4, \\
f_4' =& 100 f_5, \\
f_5' =& 100 f_6, \\
f_6' =& -100\bigg(\frac{6}{f_7} f_6 + \frac{1}{6} f_7 f_2 + \frac{2}{3(p-1)} f_1 + p|f_1|^{p-1} f_3 + \\
& p(p-1)|f_1|^{p-3} f_1 f_2^2 + \frac{2}{f_7} p|f_1|^{p-1} f_2\bigg), \\
f_7' =& 100,
\end{aligned}$$

with boundary conditions $f_2(0) = f_4(0) = f_6(0) = f_1(1) = f_2(1) = f_3(1) = 0$. Then to recover the desired solutions to (2.2.15), we simply take f_1 with the scaling $y \to 100y$.

The results are presented in Figure 2-43. The most striking aspect of this diagram is that the p-branches around the critical mass branch at $p = 7/3$ are not in general connected to the branches coming from the bifurcation points (2.4.76). Once again, every zero mass solution seen in Figure 2-40 can be continued in p to the left and right, but only the first of these connects to a bifurcation point, in this case at p_2. The remaining bifurcation points seem to have homoclinic connections to one another, although we only managed to find one such pair. The other branches around the mass branch connect pairwise with each other for some $p < 7/3$ completely separate from the bifurcation theory applied so successfully for $N = 1$ (and indeed $N = 3$ for the stable PDE, see Figure 4-7). There is a clear gap suggesting nonexistence of self-similar solutions in roughly the interval $1.6 < p < 1.8$. We remark that we have found no such evidence that the branches do anything but continue as $p \to \infty$ to the right of p_0, although we have not managed to follow them much beyond $p \approx 4$.

In many ways this is the most interesting and surprising result we present, and it signifies how much is still mysterious about these seemingly rather innocuous equations.

2.4.5. Continuation after the blow-up time and Leray's Scenario: We end the Chapter on a speculative note. These questions are some way off being solved although we feel they are amongst the most interesting open problems in

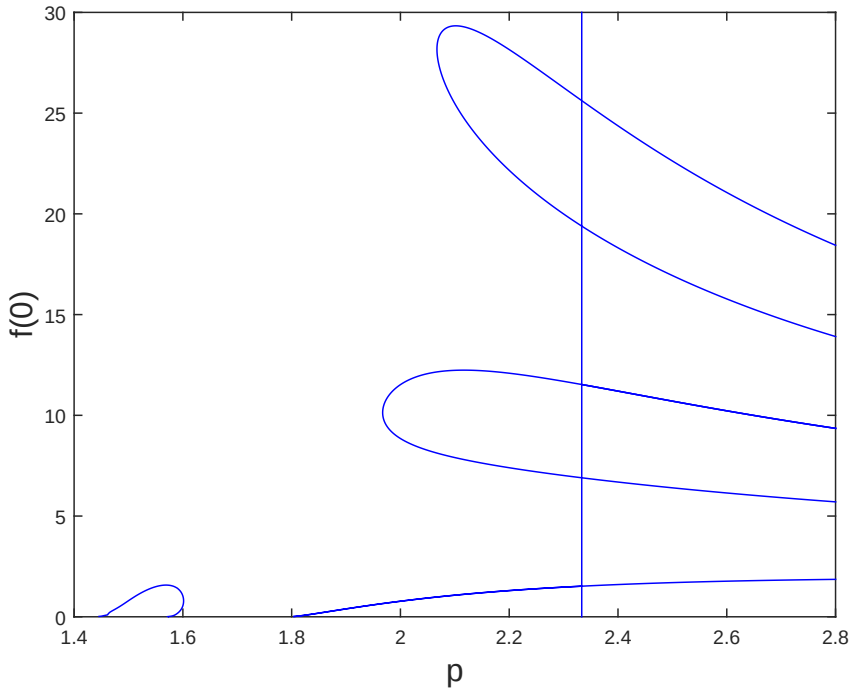

Figure 2-43: The p-bifurcation diagram for $N = 3$

the area, if only due to the total lack of a unified approach.

In [72], the surprising fact was demonstrated that (1.2.33), with $m = 2$, permitted self-similar blow up that could be *extended past the blow-up time*. That is to say, the singularity formed in the blow-up limit can act as inital data for a globally bounded self-similar solution, so that self-similar pairs $f_{BU}(y)$ (with blow-up time T) and $f_{GL}(y)$ can exist such that

$$\lim_{t-T^-}(T-t)^{-1/(p-1)}f_{BU}(y) = \lim_{t-T^+}(t-T)^{-1/(p-1)}f_{GL}(y), \quad y = \frac{x}{|T-t|^{1/4}}.$$

This is known as Leray's Scenario; it was first proposed by Leray in the 1930s as part of his seminal work on the *Navier-Stokes* equations central to fluid mechanics. Leray sought to justify the physicality of the equations in the famously as yet undecided eventuality that their solutions can blow up in finite time, an event whose physical meaning is suspect. He proposed that if singularities in the velocity field did form, they might instantaneously generate globally bounded solutions thereafter by the mechanism above. It was shown in the 90s that if blow-up does occur for the Navier-Stokes equations, it cannot be self-similar, so Leray's precise scenario turns out not to be applicable in its original context.

The question is not confined to the self-similar case. For second order equa-

tions the concepts of extended semigroups are well established, and proper minimal extensions arrived at via approximation and comparison principal arguments are more or less understood. For details of this, and a lovely result completely classifying the conditions for which solutions of the generalized Quasilinear Heat Equation

$$u_t = \Delta\left(\Phi(u)\right) + f(u),$$

can and cannot admit an extension, see [88] [86]. The main results come from a Sturmian intersection argument with special classes of travelling-wave solutions.

It turns out that the second order semilinear heat equation (1.2.31) does not admit a proper extension: all blow-up is total, i.e. the only extension past the blow-up time is infinite everywhere. This makes it all the more surprising that its fourth order cousin seems to.

Unlike (1.2.33), (2.1.1) is conservative, and we expect this to be an important factor in whether extensions can exist.

We discuss two cases beginning with $p = p_0$, for which non-zero mass solutions can occur and the rescaled flow (2.2.14) also preserves mass. We run immediately into problems: for $N = 1$, the mass of the minimal blow-up profile in Figure 2-7 can be calculated numerically to be $\approx 2.13\ldots$. However, the largest mass permitted by spreading self-similar solution belonging to the branch bifurcating from zero is $\approx 1.04\ldots$, see Figure 2-35. Likewise for $N = 3$, the minimal blow-up profile has mass $\approx 14.9\ldots$, whereas none of the global profiles have mass greater than ≈ 5.86, see Figures 2-21 and 2-40 respectively. This likely rules out a 'pure' Leray Scenario, since unlike when the evolution is not self-similar throughout, no mass defects can occur at the blow-up time; it will all go into forming a distribution like $m_0\delta$, a dirac delta distribution. This cannot generate a self-similar globally bounded solution. However, not enough is known, at least by the author, about how singular initial data might develop in general to rule out some kind of non-self-similar solutions arising. It is certainly not possible to apply (2.2.7) to a distribution. More research is needed.

We also examine the case $p = 3$, $N = 1$ as a first look at the subcritical p range. Here, we might feel on more promising ground since all blow-up and globally bounded self-similar profiles must have the same mass: zero. However, The coefficient of algebraic decay A in (2.2.29) now plays an important role, since the final time profile of a blow-up solution with $A \neq 0$ will be $u(x, T^-) = Ax^{-2}$, $x \neq 0$. Thus, a candidate self-similar continuation must originate from such a profile and must have matching A value.

Now, establishing existence of globally bounded solutions of (2.1.1) is a fairly

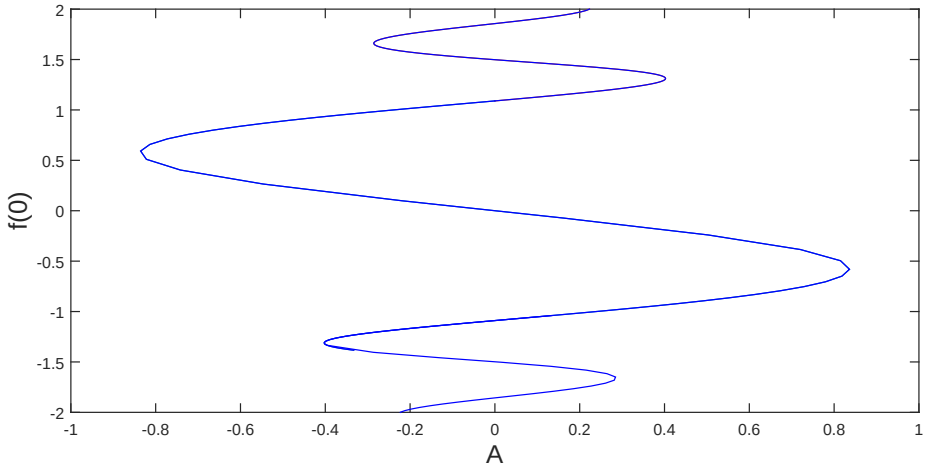

Figure 2-44: A-branch of spreading solutions for $N = 1$, $p = 3$.

standard exercise in operator theory (see [36], but it will almost by necessity rely on a smallness condition for the initial data. For small A this might be possible, however the minimal blow-up profile has $A \approx -6.99\ldots$, see Figure 2-16. In Figure 2-44 we show the result of continuing the solutions seen in Figure 2-42 in A (in fact, we conjecture that the discrete set of solutions seen there all lie on the same A-branch). The largest A value we find has $|A| \approx 0.8$, roughly an order of magnitude away from being a candidate for a Leray extension.

We acknowledge these results are extremely preliminary and a far more thorough investigation is required before jumping to conclusions, however we believe this makes a Leray Scenario for (2.1.1) unlikely. A perhaps more promising line of inquiry might lie in approximating the equations, for example, we can analytically truncate the nonlinear term

$$u_t = \Delta^3 u - \Delta\left(\frac{|u|^{p-1}u}{1+\varepsilon|u|^{p-1}u}\right), \tag{2.4.77}$$

for which solutions are globally bounded if $\varepsilon > 0$ and from which we can recover the original equation in the limit $\varepsilon \to 0$. However, establishing how the solutions behave in that limit without the order-preserving properties that accompany second order PDEs represents one of the bigger challenges in the field.

Chapter 3

Numerical Simulation of the PDEs

3.1. Motivation and Background

Accurate numerics for the evolution of solutions of (2.1.1) (and sixth order PDE in general) are crucial to understanding various key aspects of the flow; as we note in Chapter 1 the array of analytical tools that fuel our understanding of second-order problems have as yet few equivalents at higher order, and the construction of such machinery will be the work of many years. For example, with no comparison principle available, estimates of the blow-up time for an initial profile u_0 are hard to come by and so being able to measure it with good precision is helpful. We can also observe properties of solutions as they develop, that are non-obvious from the equations themselves. This allows us to answer questions about the rates and manner of convergence to self-similar profiles (if this occurs), or the large-time behaviour of solutions that don't blow up, which are particularly pertinent to the stability of solutions. The numerics, then, will supplement the asymptotic analysis of the previous section. While perhaps less satisfying than deducing results from a more rigorous, formal approach, it is certainly better to provide some kind of answer than none at all, and sometimes observational evidence gathered from the simulation can provide the insight that leads to a proof.

There are two particular difficulties particularly associated with the equations we study here that must be addressed to ensure that our simulations are meaningful. Problems with blow-up, where solutions vary rapidly over many orders of magnitude, are notoriously difficult to handle with most schemes; in discretizing solutions with important features over small and large scales simultaneously it is all too easy to lose critical information, compoundingly, at each step. Secondly, there is a degree of instability introduced by having the flow depend on a sixth derivative, which in itself significantly magnifies the scale variation of the solution

even when blow-up does not occur. It is clear that our scheme must be designed to mitigate these considerations as far as possible.

The approach we adopt extends 'adaptive' techniques used to successfully solve similar types of equations of second and fourth order, featuring both spatial adaptation and, in cases where blow-up occurs, temporal adaptation as the singularity develops. Spatial adaptation entails one, or a combination of, three main paradigms: *h-adaptivity*, in which mesh points upon which the solution are evaluated are added in regions where higher resolution is required, *p-adaptivity*, in which the order of the scheme is locally increased in those areas, and *r-adaptivity*, in which the number of mesh points are fixed but they are free to move, and clustered dynamically around the important features of the solution as they develop [158]. The last of these is particularly well suited to the problem at hand as the mesh points can be set to move according to the same symmetries that drive the emergence of self-similarity in the PDE, allowing us to track any convergence to an appropriately rescaled solution in a natural way. The obvious potential disadvantage of this compared to the h-adaptive technique, namely that the resolution can suffer in the 'flat' regions, is not significant enough to offset the superior performance and elegance of the 'moving mesh' method. The general procedure is thoroughly addressed in the literature, with a broad overview given in [106], and a more specific discussion in relation to problems with symmetries and the potential to develop singularities in [27], which also includes details on the time transformation we will employ for solutions with blow up. For the sake of completeness, we will describe some of the theory before detailing the precise schemes involved in the application to problems of sixth order, and our problem in the specific.

As is typical for parabolic problems posed in both space and time, the underlying algorithm for everything we discuss below follows a *method of lines* approach, wherein the PDE is discretized in space and the resulting system is integrated in time with an ODE or DAE solver. For our purposes we mostly use the FORTRAN solver DASSL [147] or its successor DASPK [163], designed to solve implicit systems of index 1 DAEs via backwards differentiation and Newton's method, or Krylov subspaces in the case of the latter.

For the duration of this chapter we deal exclusively with the one spatial dimension case. There are ways to extend these results to higher dimensions, but they lie outside the scope of this project. As such, we will use N to refer to the number of mesh points of the discretization and not the spatial dimension. Here we reiterate that all PDE simulations in this thesis are conducted with the

settings abstol = reltol = 10^{-5} and with the order of the backwards differentiation routine set to five.

3.1.1. Moving Mesh Methods: There are a wide variety of techniques that fall under the moving mesh umbrella and of course the choice of which combination to use depends on the problem at hand. At the most fundamental level the algorithm by which the mesh is driven can fall into one of two broad classes. In the first of these, *rezoning*, the solution $u_i^j = u(x_i^j, t^j)$ at time t^j on a mesh $x_i^j,\ i = 1, \ldots, N$ is first interpolated onto a new mesh x_i^{j+1}; only then does the solver steps forward to time t^{j+1} and attempt to calculate the new u_i^{j+1}. In contrast to the intermittency of this approach, techniques from the *quasi-Lagrange* class model the mesh points as moving continuously in time. This necessitates recasting the physical time derivatives as total derivatives along mesh trajectories and subtracting a convective term to account for this change, so that

$$u_t(x(t), t) = \frac{\mathrm{D}}{\mathrm{D}t} u(x(t), t) - \frac{\partial}{\partial x} u(x(t), t)\dot{x}(t), \tag{3.1.1}$$

and then the right hand side of this is discretized appropriately. There are trade offs between the two methods; the quasi-Lagrange allows for a discretized mesh equation to be coupled with the physical system and solved simultaneously, which is ideal in situations where the solution can develop very rapidly. The mesh is then forced to move in accordance with these rapidly changing features by the solver, avoiding problems that can occur in rezoning when a fixed mesh at time t_n might become inappropriate before the next re-interpolation time is reached and so introduce a source of inaccuracy. It is also simpler in some regards to deal with a single, self-contained system of equations, and the linearization process results in far sparser matrices (often banded, or approximately so) than the dense matrices necessary for the interpolation during the rezoning process. However, the coupling between mesh and physical equations can often be extremely nonlinear and far more trouble to solve. The introduction of the transport term in (3.1.1) also requires careful handling in the discretization, as we will describe later. Furthermore, by avoiding coupling it is not necessary to use an equation to move the mesh, and options such as directly minimizing some relevant quantities become available, although for less straightforward problems this is rarely practicable. For the cases considered here, it is possible to choose a mesh equation with the same symmetry properties as the underlying PDE, and in addition to the rapid blow-up that can occur this leads us to prefer a simultaneous, quasi-Lagrange approach despite the associated difficulties.

To understand how the location of the mesh points can be controlled, we introduce the notion of a *computational domain*. For a PDE posed in some physical domain $\Omega_P \subset \mathbb{R}$, the corresponding computational domain is Ω_C, typically the unit interval $[0, 1]$, so that for *computational coordinate* ξ we have $\int_{\Omega_C} \mathrm{d}\xi = 1$. The physical coordinates can then be described as the image of a continuous map $x = x(\xi, t)$ from the computational to the physical domain, and a fixed, uniform mesh in Ω_C maps to a not-necessarily uniform mesh that can be repositioned with time in Ω_P. This description easily allows us to express the properties of the physical mesh in terms of the transformation between the coordinate regimes.

In one dimension, this is approached via the principle of *equidistribution*. For a physical domain $\Omega_P = [a, b]$, we pick a monitor function $M : [a, b] \times \mathbb{R}_+ \to \mathbb{R}$ and prescribe that the mapping $x : [0, 1] \times \mathbb{R}_+ \to [a, b]$ satisfies the relation

$$\int_a^{x(\xi,t)} M(s, t)\mathrm{d}s = \xi \int_a^b M(s, t)\mathrm{d}s, \quad \xi \in \Omega_C = [0, 1]. \tag{3.1.2}$$

Then, the image of the uniform mesh $0 = \xi_0 < \ldots \xi_N = 1$ is $a = x_0(t) < \ldots < x_N(t) = b$, where $x_i(t) = x(i\Delta\xi, t)$, and is said to be equidistributed with respect to M. The t dependence is included to emphasize that, as the solution to the PDE evolves in time, the mesh will be required to do so in kind; in fact in our case we will see that M should be a particular function of the solution u and not x directly.

Provided that M is strictly positive, the equidistributed mesh is uniquely determined. This construction means that the integral of M is the same over any subinterval of the physical mesh, whence a major source of the interest in it: the monitor function is often chosen to be the local error term for a given approximation, and it can then be proved that the equistributed mesh this generates minimizes the total error. In general, it is not possible to directly evaluate the integrals in (3.1.2), although iterative algorithms such as de Boor's [38] can generate convergent approximations to an equidistributed mesh.

The map $x(\xi, t)$ can also be formulated as the solution to a BVP by differentiating (3.1.2) twice with respect to ξ, giving

$$\frac{\mathrm{d}}{\mathrm{d}\xi}\left(M(x, t)\frac{\mathrm{d}x}{\mathrm{d}\xi}\right) = 0, \quad x(0) = a,\ x(1) = b. \tag{3.1.3}$$

This can then be solved in conjunction with the system of ODEs that come from the discretized PDE, although the resulting system of DAEs (the time independence of (3.1.3) means their discretization will entail a purely algebraic contri-

bution) can be extremely stiff, and problematic even for sophisticated solvers. A resolution comes from considering, loosely speaking, (3.1.3) as the 'stationary' aspect of a PDE that also explicitly involves the mesh speed x_t (there are a number of more satisfactory formulations, e.g. by considering a gradient flow for the functional associated with the equivalent equation to (3.1.3) for the inverse coordinate transform $\xi(x,t)$, see [106] Chapter 2.3, or alternatively by differentiating (3.1.3) with respect to time [104]). This has the additional benefit of regularizing the problem, and the cost of no longer having a precisely equidistributed mesh turns out to be low.

There are an array of moving mesh PDEs (MMPDEs), derived and analysed in detail in [104]. We focus on MMPDE6:

$$-\epsilon x_{t\xi\xi} = (M x_\xi)_\xi, \tag{3.1.4}$$

as it behaves in a convenient way under scaling, and numerical experiments conducted in [103] suggest that when discretized it converges very quickly under Newton iteration. It can be shown that the mesh points in this scheme never cross, a fact which follows from the positivity of M. The ϵ multiplying the left hand side is a small constant related to the 'relaxation time', i.e. how long it takes the mesh to converge to an equidistributed pattern. The smallness usually ensures this time is brief, however this is not always the case as a singularity is approached. We typically take $\epsilon = 10^{-3}$.

Since we are particularly interested in solutions with extreme spatial variation, this will often also manifest in the monitor function M, which can lead to problems solving (3.1.4). In [43] it was shown that this can be ameliorated by an appropriate smoothing procedure applied directly to the monitor function, generalized in [103] to the form

$$\tilde{M}_i = \sqrt{\sum_{k=i-\rho}^{i+\rho} (M_k)^2 \left(\frac{\gamma}{1+\gamma}\right)^{|k-i|} \Big/ \sum_{k=i-\rho}^{i+\rho} \left(\frac{\gamma}{1+\gamma}\right)^{|k-i|}}, \tag{3.1.5}$$

where M_i is the value of the monitor function at the point $x_i = x(i\xi, t)$, γ is a positive constant called the 'smoothing parameter' (higher values of γ result in the physical grid points having more inertia), and ρ is the 'smoothing index', which refers to the extent over which the smoothing kernel is applied. At the boundaries, the smoothing is only taken over the two outermost grid points and with equal weight (i.e. independent of γ) by necessity. In the same way, for $\rho > 1$, at points with too few mesh points to the left or right for (3.1.5) to apply, the

smoothing is conducted over the largest possible symmetric pencils in the obvious way. There is a trade off between the additional smoothness afforded by higher ρ values and the higher computational cost this incurs, which can be significant. All of our simulations are conducted with $\rho = 1$.

3.1.2. Scale Invariant Mesh Adaptivity: Equations like (2.1.1) lend themselves particularly well to moving mesh methods as the scaling invariance discussed in Section 2.2.2 play such a dominant role in the features that emerge during the flow, in particular we expect exactly self-similar solutions to make up a large part of the set of asymptotic behaviours in various limits. As such, we would like to choose a monitor function that ensures mesh points move according to the x-scaling in (2.2.9) as the solution tends towards self-similarity; this will ensure the shapes of the solution are correctly resolved (in fact, this method is equally effective for *approximately* self-similar solutions, which occur for the semilinear heat equation (1.2.31). It is not necessary to know the transformation that the solutions obey, merely the scaling invariance of the equation, see the discussion in [27]).

This is achieved, naturally, through fixing a choice of monitor function M such that (3.1.4) is invariant under the same set of scalings as the underlying PDE. For (2.1.1), these are given in (2.2.9). If we take M as a function of u alone, this imposes the functional relation

$$M(\lambda^{-2/3(p-1)}u) = \lambda^{-1}M(u), \tag{3.1.6}$$

which is satisfied by $M(u) = u^{3(p-1)/2}$. However, in practice a monitor function of this form will draw every mesh point into the blow-up core as the singularity is approached, leading to the computation halting early. Moreover, the absence of a maximum principle allows for sign-changing solutions and so pure power-law relations like (3.1.6) can have non-positive range for some values of p. Sign changing solutions are expected to be generic for (2.1.1); for $p < p_0$ even solutions must have zero mass, see Remark 2.1, and for $p = p_0$ the solutions change sign infinitely often thanks to (2.3.33).

A simple, often effective remedy is to consider the corrected monitor function

$$M(u) = u^{3(p-1)/2} + \alpha \int_a^b u^{3(p-1)/2} \mathrm{d}x, \tag{3.1.7}$$

where α is a problem-dependent positive parameter. This possesses the same scale invariance and the integral term prevents too large a mesh concentration

away from areas where the solution is small, as well as ensuring monitor non-negativity in most common scenarios for appropriate α.

When we couple the quasi-Lagrange corrected (2.1.1) (see (3.1.1), noting the extra term has the same scale factor: $\lambda^{-(2/3(p-1))-1/6}u_x\lambda^{1/6-1}x_t = \lambda^{-(2/3(p-1))-1}u_x x_t$) with (3.1.4), M as in (3.1.7), the resulting augmented system of ODEs will inherit the scale invariance of the PDEs even after discretization. This follows from the simple observations that the actions of rescaling and discretization commute. Thus, our system will have the form

$$A(\mathbf{X},\mathbf{U})\dot{u}_i + B(\mathbf{X},\mathbf{U})\dot{x}_i = F(\mathbf{X},\mathbf{U}), \quad \dot{x}_i = G(\mathbf{X},\mathbf{U}), \tag{3.1.8}$$

with $\mathbf{X} = (x_1,\ldots,x_N)$ and $\mathbf{U} = (u_1,\ldots,u_N)$. The forms of A, B, F and G will in general be very complicated and it is not necessary to write them explicitly to implement the scheme, though we believe it is helpful to see the abstract equation written in this form. The schemes we discuss below will define them implicitly, after taking into account the following final modification.

3.1.3. Time Transformation: The rapid change in the size of the solution as the blow up time is approached not only leads to extreme stiffness but make it hard to resolve the qualitative properties of the solution that manifest as the final time profile is approached, for example, in the critical case $p = 5$ an exactly self-similar profile with height $||u||_\infty = 1$ at time $t = 0$ will blow up at time $T = 1$ according to the scale factor $(T-t)^{1/6}$, and so the solution will not reach $||u||_\infty = 10$ until time $t = 1 - 10^{-6}$. To observe the profiles with the large infinity norm that approach the blow-up profile, we will clearly need a scheme that can time step adaptively, and respond rapidly enough to catch the near-blow-up behaviour that is of particular interest. Again, we can exploit the underlying symmetry of the PDE which naturally suggests a time rescaling for the equations that is suitable for our purposes.

We proceed by introducing a computational time variable $\tau = \tau(t)$. So that the stepsize $\tau_{n+1} - \tau_n$ changes in the desired way, we couple it with u via a 'Sundman transformation' (see [25] for a derivation and analysis of the method)

$$\frac{\mathrm{d}t}{\mathrm{d}\tau} = g(u), \tag{3.1.9}$$

where we must have that $g \to \infty$ as $u \to \infty$ in an appropriate manner; this will force the stepsize in τ to become small enough as blow up is approached. The form of g is chosen by requiring, quite naturally, that it be invariant under the

same symmetry as (3.1.8), and so using (3.1.9) we find that we must set

$$\lambda g(u) = g(\lambda^{-2/3(p-1)}u). \tag{3.1.10}$$

Now g can be chosen of simple form $g = \max_x \left(u^{3(p-1)/2}\right)$, for only the largest value of u need be retained for the proper scaling to emerge as the singularity develops. Note that this is simply the maximum of the reciprocal of the uncorrected monitor function in practice we want the scalings in space and time to have the same nature so that the invariance is maintained, and indeed taking

$$g = \left(1/\max_x(M(u))\right), \tag{3.1.11}$$

is more effective in practice. Of course, this correction still observes (3.1.10).

The system to be solved is finally fully realized as

$$A(\mathbf{X},\mathbf{U})u_{i,\tau} + B(\mathbf{X},\mathbf{U})x_{i,\tau} = g(\mathbf{U})F(\mathbf{X},\mathbf{U}),\ x_{i,\tau} = g(\mathbf{U})G(\mathbf{X},\mathbf{U}),\ \frac{\mathrm{d}t}{\mathrm{d}\tau} = g(\mathbf{U}), \tag{3.1.12}$$

which possesses many advantages over the more straightforward fixed mesh; in particular it will admit *discrete self-similar solutions* and so accurately capture the shape of any self-similar patterns that emerge, and the local truncation of the time integrator will be independent of scale, which is of course ideal for solutions with large variation [25]. We reiterate that the expressions involved in writing the scheme in the form (3.1.12) will be too cumbersome to deal with explicitly and its value is purely instructional.

We now give details of the schemes we employ for the spatial discretization which are more or less straightforward generalizations of the 'moving collocation' approach developed in [105] and [150] to deal sixth order differential operators, although some additional complications arise from this extension that require special attention. For simplicity, we henceforth denote all time parameters by the symbol t with the understanding they may represent the rescaled τ, unless we wish to draw specific attention to the time scaling.

3.2. The Schemes

3.2.1. Collocation Scheme: Moving mesh methods can be applied to any reasonable discretization of the physical problem. For the purposes of this investigation, it is important to choose a scheme that can easily handle sixth derivatives on a non-uniform mesh, as well as enforce the conservation of mass that is is a

key aspect of these equations.

Collocation has many advantages: providing a high order of convergence, affording us continuous representation of solutions, handling boundary conditions easily and being relatively straightforward to modify to enforce conservation of mass. In addition, Movcol4 [150], the cousin of this method written for fourth-order PDEs, has been successfully deployed to simulate solutions to the conservative fourth order limit Cahn-Hilliard equation (1.1.9) in [56] and the non-conservative fourth order reaction-diffusion equation (1.2.33) in [24] with great success, both of which are closely related models to (2.1.1) with similar features and difficulties. However, it entails keeping track of not just the solution, but five of its derivatives at each mesh point, which can lead to some problems especially at initialization, see Section 3.2.3 below.

These problems can be avoided by writing the physical sixth order equation as a system of three second order equations with $[u_1, u_2, u_3] = [u, u_{xx}, u_{xxxx}]$, however to account for the mesh speed we would have to include terms like $(u_{1,xxx} - u_{2,x})x'(t)$ which, due to truncation errors, will not be identically zero and can be severely destabilizing, refer to the discussion in [150] Chapter 6. As such, we proceed with discretizing (2.1.1) directly.

First, we address the approximation to the mesh equation (3.1.4). High accuracy is less important as an approximately equidistributed mesh is 'good enough' for our purposes; errors in the mesh point location do not affect the values of the solution there. As such, a standard central difference approach suffices, and we fix that the mesh $x_0(t) < \ldots < x_N(t)$ moves according to

$$x'_{i-1}(t) - 2x'_i(t) + x'_{i+1}(t) = -\frac{g}{\epsilon}\left(M_{i+1/2}(x_{i+1}(t) - x_i(t)) - M_{i-1/2}(x_i(t) - x_{i-1}(t))\right), \tag{3.2.13}$$

where $x'_i(t)$ is the speed at which the point x_i, $i = 2 \ldots N-1$ is moving either in the computational time if the solution blows up, or in regular time otherwise. g is the approximate value of the Sundman transformation (3.1.11) in the former case or identically one in the latter, and $M_{i+1/2}$, $M_{i-1/2}$ are average values of the (smoothed, (3.1.5)) monitor function (3.1.7) over the cells $[x_i, x_{i+1}]$ and $[x_{i-1}, x_i]$ respectively. The boundaries are held in place by imposing Neumann-type conditions $x'_0 = x'_N = 0$.

We discretize the physical PDE over the physical mesh by representing the solutions by eleventh-order piecewise polynomials, where u and its first five spatial derivatives are known at each mesh point. Then in the interval $[x_i(t), x_{i+1}(t)]$, u has the representation:

$$
\begin{aligned}
u(x,t) \approx V_i(x,t) := u_i(t)\phi_{0,0}(s) + \\
u_{x,i}(t)h_i(t)\phi_{0,1}(s) + \\
u_{xx,i}(t)h_i^2(t)\phi_{0,2}(s) + \\
u_{xxx,i}(t)h_i^3(t)\phi_{0,3}(s) + \\
u_{xxxx,i}(t)h_i^4(t)\phi_{0,4}(s) + \\
u_{xxxxx,i}(t)h_i^5(t)\phi_{0,5}(s) + \\
u_{i+1}(t)\phi_{1,0}(s) + \\
u_{x,i+1}(t)h_i(t)\phi_{1,1}(s) + \\
u_{xx,i+1}(t)h_i^2(t)\phi_{1,2}(s) + \\
u_{xxx,i+1}(t)h_i^3(t)\phi_{1,3}(s) + \\
u_{xxxx,i+1}(t)h_i^4(t)\phi_{1,4}(s) + \\
u_{xxxxx,i+1}(t)h_i^5(t)\phi_{1,5}(s) \quad (3.2.14)
\end{aligned}
$$

where $u_{\cdot,i}(t)$ and $u_{\cdot,i+1}(t)$ represent the (known) value of u or a derivative at mesh point $x_i(t)$ and $x_{i+1}(t)$ respectively, $h_i(t) := x_{i+1}(t) - x_i(t)$ is the width of the interval, and $s := (x - x_i(t))/h_i(t)$ is the appropriate local coordinate. $V_i(x,t)$ is the ith component of the (at least) C^5 approximating function $V(x,t)$.

The shape functions $\phi_{i,j}(s)$ are eleventh order Hermite polynomials, uniquely determined by fixing $p(s) = \sum_{k=0}^{11} a_k s^k$ and its derivatives (with respect to x, accounting for the extra factors of $h_i(t)$ appearing in the expression) equal to the corresponding $u_{\cdot,i}$ for $s = 0$ and $u_{\cdot,i+1}(t)$ for $s = 1$, then refactoring accordingly. They have the explicit forms

$$
\begin{aligned}
\phi_{0,0}(s) &= (252s^5 + 126s^4 + 56s^3 + 21s^2 + 6s + 1)(s-1)^6, \\
\phi_{1,0}(s) &= -s^6(252s^5 - 1386s^4 + 3080s^3 - 3465s^2 + 1980s - 462), \\
\phi_{0,1}(s) &= s(126s^4 + 56s^3 + 21s^2 + 6s + 1)(s-1)^6, \\
\phi_{1,1}(s) &= s^6(s-1)(126s^4 - 560s^3 + 945s^2 - 720s + 210), \\
\phi_{0,2}(s) &= \frac{1}{2}s^2(56s^3 + 21s^2 + 6s + 1)(s-1)^6, \\
\phi_{1,2}(s) &= -\frac{1}{2}s^6(56s^3 - 189s^2 + 216s - 84)(s-1)^2, \\
\phi_{0,3}(s) &= \frac{1}{6}s^3(21s^2 + 6s + 1)(s-1)^6, \\
\phi_{1,3}(s) &= \frac{1}{6}s^6(21s^2 - 48s + 28)(s-1)^3, \\
\phi_{0,4}(s) &= \frac{1}{24}s^4(6s + 1)(s-1)^6, \\
\phi_{1,4}(s) &= -\frac{1}{24}s^6(6s - 7)(s-1)^4, \\
\phi_{0,5}(s) &= \frac{1}{120}s^5(s-1)^6, \\
\phi_{1,5}(s) &= \frac{1}{120}s^6(s-1)^5.
\end{aligned}
\tag{3.2.15}
$$

We can then differentiate the continuous approximation (3.2.14) and evaluate at any point $x \in [x_i(t), x_{i+1}(t)]$ according to the formulae:

$$
\begin{aligned}
u_x(x,t) \approx \frac{\partial}{\partial x}V_i(x,t) = (u_i(t)\phi'_{0,0}(s) + u_{x,i}(t)h_i(t)\phi'_{0,1}(s) + \\
u_{xx,i}(t)h_i^2(t)\phi'_{0,2}(s) + \\
u_{xxx,i}(t)h_i^3(t)\phi'_{0,3}(s) + \\
u_{xxxx,i}(t)h_i^4(t)\phi'_{0,4}(s) + \\
u_{xxxxx,i}(t)h_i^5(t)\phi'_{0,5}(s) + \\
u_{i+1}(t)\phi'_{1,0}(s) + \\
u_{x,i+1}(t)h_i(t)\phi'_{1,1}(s) + \\
u_{xx,i+1}(t)h_i^2(t)\phi'_{1,2}(s) + \\
u_{xxx,i+1}(t)h_i^3(t)\phi'_{1,3}(s) + \\
u_{xxxx,i+1}(t)h_i^4(t)\phi'_{1,4}(s) + \\
u_{xxxxx,i+1}(t)h_i^5(t)\phi'_{1,5}(s))/h_i(t),
\end{aligned}
\tag{3.2.16}
$$

and so on for each extra x derivative of the solution (in particular affording us an approximate value of u_{xxxxxx} anywhere the solution is defined). The t derivatives are slightly less straightforward as we must be careful how our discretization accounts for the Quasi-Lagrange correction term (3.1.1). The approximation we take differs from the choice taken in [105] and [150] as it has better stability properties, which becomes more important the higher order the scheme.

To see this, consider the Taylor expansion in s about x_i of $u(x_i + sh_i, t)$. We have

$$u(x_i + sh_i, t) = \sum_{n=0}^{\infty} \frac{1}{n!} \frac{\partial^n}{\partial x^n} u(x_i, t) s^n h_i^n \implies$$
$$\frac{\mathrm{D}}{\mathrm{D}t} u(x_i + sh_i, t) - u_x(x_i + sh_i, t)(x_i' + sh_i') = \sum_{n=0}^{\infty} \frac{1}{n!} \frac{\partial^n}{\partial x^n} u_t(x_i, t) s^n h_i^n. \quad (3.2.17)$$

Hence if we take our piecewise Hermite approximation of u_t to be

$$\begin{aligned} u_t(x,t) \approx \frac{\partial}{\partial t} V_i(x,t) = {} & u_i'(t)\phi_{0,0}(s) + \\ & u_{x,i}'(t) h_i(t) \phi_{0,1}(s) + \\ & u_{xx,i}'(t) h_i^2(t) \phi_{0,2}(s) + \\ & u_{xxx,i}'(t) h_i^3(t) \phi_{0,3}(s) + \\ & u_{xxxx,i}'(t) h_i^4(t) \phi_{0,4}(s) + \\ & u_{xxxxx,i}'(t) h_i^5(t) \phi_{0,5}(s) + \\ & u_{i+1}'(t) \phi_{1,0}(s) + \\ & u_{x,i+1}'(t) h_i(t) \phi_{1,1}(s) + \\ & u_{xx,i+1}'(t) h_i^2(t) \phi_{1,2}(s) + \\ & u_{xxx,i+1}'(t) h_i^3(t) \phi_{1,3}(s) + \\ & u_{xxxx,i+1}'(t) h_i^4(t) \phi_{1,4}(s) + \\ & u_{xxxxx,i+1}'(t) h_i^5(t) \phi_{1,5}(s) - \\ & \frac{\partial}{\partial x} V_i(x,t)(x_i'(t) + sh_i'(t)), \end{aligned} \quad (3.2.18)$$

then the residual $|u_t(x_i + sh_i, t) - \frac{\partial}{\partial t} V_i(x,t)|$ in each cell is given by, using the notation $u_{lx,i} = \frac{\partial^l}{\partial x^l} u_i$,

$$\left(\frac{3!}{12!} u_{12x}(x_i, t) s^5 (2s-1)(s-1)^5 (x_i'(t) + sh_i'(t)) \right) h_i^{11} + \mathcal{O}(h_i^{12}). \quad (3.2.19)$$

This can be destabilizing either in the left or right half of the cell depending on the sign of $(x_i'(t) + sh_i'(t))$, however, the highest order operators in our equations (see e.g. (3.2.23) for this scheme) will have a stabilizing effect at much lower order than $\mathcal{O}(h_i^{11})$ and problems will not manifest unless $(x_i'(t) + sh_i'(t))$ is very large. See [128] for more discussion of stability in moving mesh schemes.

We can now use our discretizations to derive the equations to feed into DASPK. With the mesh points, time transformation, u and five derivatives, we have $7N + 1$ unknowns and so we require the same number of equations. The equations for the mesh points (3.2.13) and boundary conditions account for N of those and the time transformation requires no discretization, so we need to find a further $6N$ from the physical PDE.

The first scheme we introduce is a more-or-less standard Gauss point collocation. Using (2.1.1) as an example, we enforce

$$\frac{\partial}{\partial t}V_i(x,t) - g\left(\frac{\partial^6}{\partial x^6}V_i(x,t) + \frac{\partial^2}{\partial x^2}(|V_i|^{p-1}V_i(x,t))\right) = 0$$

in each cell, where again g is set to (3.1.11) for blow-up problems or unity otherwise, at the points $s = \rho_l$, $l = 1, \ldots, 6$ in each interval. These are given by the roots of the polynomial

$$P_6(x) \equiv (\sqrt{13}\left(1 - 42x + 420x^2 - 1680x^3 + 3150x^4 - 2772x^5 + 924x^6\right), \tag{3.2.20}$$

the sixth in the series of orthogonal polynomials given by $\int_0^1 P_l(x)P_m(x)\mathrm{d}x = \delta_{lm}$, $P_0(x) = 1$ (compare with the Legendre polynomials on the interval $[-1, 1]$). $P_6(x)$ is the first in the series whose roots are not solvable by radicals, but they can easily by calculated numerically, see e.g. [94], to give

$$\begin{aligned}\rho_1 = 0.033765242898424,\ \rho_2 = 0.1693953067668679,\ \rho_3 = 0.3806904069584033,\\ \rho_4 = 0.6193095930415716,\ \rho_5 = 0.8306046932332015,\ \rho_6 = 0.9662347571015317.\end{aligned} \tag{3.2.21}$$

It is clear how this can be generalized to other equations approximated by V and its derivatives.

This Gauss-Hermite interpolation is attractive for its simplicity and the high order of convergence it engenders. For a fixed time t, it can be shown by the Taylor expansion (3.2.17) that the local truncation error is $\mathcal{O}(h_i^{12})$, from which

follows the global estimate

$$|u(x) - V(x)| = \mathcal{O}(h^{12}), \quad h = \max_i h_i, \tag{3.2.22}$$

see e.g. [8].

In fact, the form of the truncation error in each subinterval is

$$|u(x_i + sh_i) - V(x_i + sh_i)| = \frac{1}{12!}s^6(s-1)^6|u_{12x,i}|h_i^{12} + \frac{1}{12!}s^6(s-1)(21s^4 - 91s^3 + 154s^2 - 119s + 36)|u_{13x,i}|h_i^{13},$$

and since at each mesh point we have either $s = 0$ or $s = 1$ our approximation is even higher order there, a phenomenon known as superconvergence. Moreover, the choice of the Gauss points can be motivated by the following characterization: on each interval $[x_i(t), x_{i+1}(t)]$, the truncation error of the sixth derivative term is given by

$$|u_{6x}(x_i + sh_i) - \frac{\partial^6}{\partial x^6}V(x_i + sh_i)| = \frac{6!}{12!}P_6(s)|u_{12x,i}|h_i^6 + \frac{6!}{13!}(1716s^7 - 9702s^5 + 14700s^4 - 8820s^3 + 2352s^2 - 245s + 6)|u_{13x,i}|h_i^7, \tag{3.2.23}$$

with $P_6(s)$ as in (3.2.20). Hence the approximate equation we solve also has better truncation terms if and only if the collocation is carried out at (3.2.21).

We now have $6(N-1)$ equations over the interiors of the $N-1$ intervals $[x_{i-1}(t), x_i(t)]$ which can be completed with three boundary conditions on the left of the interval ($x_0(t) \equiv 0$): typically for us we will impose even symmetry of solutions with $u_x = u_{xxx} = u_{xxxxx} = 0$. The remaining three boundary conditions are imposed at $x_N(t)$, typically fixed and large. Given our focus on solutions of (2.1.1) with exponential decay, these are often Dirichlet type conditions $u = u_x = u_{xx} = 0$, and we expect this to be sufficiently close to simulating the Cauchy problem provided x_N is large enough.

We need to bear in mind, though, that the conservation property of (2.1.1) is crucial to determining its behaviour. A classical Gauss point scheme like 3.2.1 will not conserve mass of solutions in general, although just as in [150] we note that there are circumstances where it will. Below and for the remainder of the chapter F will represent an 'integrated up' differential operator in divergence form appearing on the right hand side of an evolution equation $u_t = F_x$. This should

not be confused with the F in (3.1.12), which we use to refer to a discretization of a term that is not differentiated.

Proposition 3.1. *The Gauss Point Scheme conserves mass for equations of the form*

$$u_t = (F(x, u, u_x, u_{xx}, u_{xxx}, u_{xxxx}, u_{xxxxx}))_x$$

in the sense that

$$\frac{\mathrm{d}}{\mathrm{d}t}\int_a^b u\mathrm{d}x = F(b) - F(a), \tag{3.2.24}$$

when

$$g(x, u, \dots u_{5x}) = \gamma_1 u + \gamma_2 u_x + \gamma_3 u_{xx} + \gamma_4 u_{xxx} + \gamma_5 u_{xxxx} + \gamma_6 u_{xxxxx} \tag{3.2.25}$$

is a linear function of u and its spatial derivatives only.

Proof.

$$\frac{\mathrm{d}}{\mathrm{d}t}\int_a^b V\mathrm{d}x = \int_a^b \gamma_1 V_x + \gamma_2 V_{xx} + \gamma_3 V_{xxx} + \gamma_4 V_{xxxx} + \gamma_5 V_{xxxxx} + \gamma_6 V_{xxxxxx}\mathrm{d}x =$$
$$\sum_{i=0}^{N-1}\sum_{j=1}^{6}\gamma_j\left(\sum_{k=0}^{5}(h_i)^{k-j}\left(u_{kx,i}\int_0^1 \frac{\mathrm{d}^j}{\mathrm{d}s^j}\phi_{0,k}(s)\mathrm{d}s + u_{kx,i+1}\int_0^1 \frac{\mathrm{d}^j}{\mathrm{d}s^j}\phi_{1,k}(s)\mathrm{d}s\right)\right) =$$
$$\sum_{i=0}^{N-1}\sum_{j=1}^{6}\gamma_j\left(u_{(j-1)x,i+1} - u_{(j-1)x,i}\right) =$$
$$\sum_{j=1}^{6}\gamma_j\left(u_{(j-1)x,N} - u_{(j-1)x,0}\right) = F(b) - F(a).$$

The third line follows from the well known identity for Hermite polynomials that $\frac{\mathrm{d}^p}{\mathrm{d}x^p}\phi_{l,m}(x_j) = 1$ for $l = j$ and $m = p$ and zero otherwise. This proof is a direct extension of that in [150] and we expect the same to hold for any Movcol$2m$ involving Gauss-Hermite interpolation with $(4m-1)$th order polynomials over $2m$ Gauss points. □

3.2.2. Conservative Collocation Scheme: We notice that, writing (2.1.1) in divergence form,

$$u_t = \left(u_{xxxxx} - \left(|u|^{p-1}\right)_x\right)_x, \tag{3.2.26}$$

the right hand side clearly suggests that (3.2.24) will hold, however it is not of the form (3.2.25) and so we cannot expect 3.2.1 to inherit this property. As such, we are forced to modify our approach slightly. Luckily, it is possible to extend the

conservative collocation schemes of [105] and [150] in a natural way to produce a scheme that does.

Here is a convenient point to introduce notation that will simplify our presentation as well as clarify how this scheme applies to more general equations. The two Movcol papers present their results for equations of the form

$$G(t, x, u, u_t, u_x, \ldots) = (F(t, x, u, u_t, u_x \ldots))_x \tag{3.2.27}$$

and since this method extends theirs it is hopefully clear how our results might be similarly applicable. With maximum generality, G and F can be functions of up to five spatial derivatives of u (we do not consider mixed derivatives although it seems in principle they could be included). We adopt this convention here, for example for (2.1.1) we have $u_t = G$, $u_{xxxxx} - (|u|^{p-1})_x = F$. Of course, our conclusions will be true for arbitrary G and F providing they are regular enough. We denote by G^π and F^π the approximations to G and F derived replacing u and its derivatives by the Hermite interpolant V ((3.2.14)) and its derivatives ((3.2.16), (3.2.16) etc.).

The method is referred to as a 'cell-averaged collocation scheme' since the scheme is derived from imposing the conservation property directly in subdivisions of each cell. Specifically, we set

$$\int_{x_i+\tilde{\rho}_l}^{x_i+\tilde{\rho}_{l+1}} G^\pi \mathrm{d}x = F^\pi|_{x_i+\tilde{\rho}_{l+1}} - F^\pi|_{x_i+\tilde{\rho}_l}, \tag{3.2.28}$$

where $\tilde{\rho}_l$ are points in $[0, 1]$ such that $0 = \tilde{\rho}_1 < \ldots < \tilde{\rho}_q = 1$ for some q. To minimize the eventual residual term, these should be taken (fixing $q = 7$) to be the *Lobatto points*:

$$\tilde{\rho}_1 = 0,\ \tilde{\rho}_2 = \frac{1}{2} - \frac{1}{66}\sqrt{495 + 66\sqrt{15}},\ \tilde{\rho}_3 = \frac{1}{2} - \frac{1}{66}\sqrt{495 - 66\sqrt{15}}, \tag{3.2.29}$$

$$\tilde{\rho}_4 = \frac{1}{2},\ \tilde{\rho}_5 = \frac{1}{2} + \frac{1}{66}\sqrt{495 - 66\sqrt{15}},\ \tilde{\rho}_6 = \frac{1}{2} + \frac{1}{66}\sqrt{495 + 66\sqrt{15}}, \tag{3.2.30}$$

$$\tilde{\rho}_7 = 1, \tag{3.2.31}$$

found by fixing the evaluation points 0 and 1 then taking the other five as the roots of the derivative of (3.2.20).

Now we solve approximately the system given by (3.2.28) with $l = 1, \ldots 6$. To do this, we begin by taking the Lagrange interpolant of G^π through the Gauss points on each interval. It is well known that the integral of the polynomial approximant of G^π at the Gauss points has no extra error above that of the

integral of the initial Hermite approximation. The interpolant has the form

$$\tilde{G}_i^\pi = \sum_{j=1}^{6} G_{i,j}^\pi Q_j,$$

where $G_{i,j}^\pi := G^\pi(x_i + h_i\rho_j, t) := G^\pi(x_{i,j}, t)$ and $Q_j(x) = \prod_{\substack{k=1 \\ k\neq j}}^{6} \frac{x - x_{ik}}{x_{ij} - x_{ik}}$. Then we can integrate the approximation exactly over each interval $[x_i, x_{i+1}]$ to give the system

$$\left\{ R_{l,m} \tilde{G}_m^\pi \right\}_i = \left\{ S_{l,m} F_m^\pi \right\}_i / h_i, \tag{3.2.32}$$

where $h_i = x_{i+1} - x_i$ appears during the integration, $G_m^\pi = G^\pi(x_{i,m})$ and likewise for F_m^π,

$$R_{l,m} = \int_{\tilde{\rho}_l}^{\tilde{\rho}_{l+1}} Q_m \mathrm{d}s, \quad l, m = 1, \ldots, 6$$

and

$$S_{l,m} = \begin{cases} 1 \text{ if } l = m, \\ -1 \text{ if } m = l + 1, \\ 0 \text{ otherwise,} \end{cases}$$

with $l = 1, \ldots, 6$, $k = 1, \ldots, 7$. Finally, we can solve the system (3.2.32) by inverting R, giving a system of six equations for each cell:

$$h_i \left\{ G_m^\pi \right\}_i = \left\{ (R^{-1} S)_{l,m} F_m^\pi \right\}_i.$$

The matrix quantity $R^{-1}S$ must be evaluated numerically; we used Maple's solve function with fifteen decimal places of accuracy.

It is clear by construction that since (3.2.28) holds, we can take a telescoping sum over each cell and then over the whole mesh in kind to demonstrate the conservation laws

$$\int_{x_i}^{x_{i+1}} G_i^\pi \mathrm{d}x = F^\pi(x_i + 1) - F^\pi(x_i), \quad \int_a^b G^\pi \mathrm{d}x = F^\pi(b) - F^\pi(a),$$

and so the underlying mass conservation of the equations will be upheld by the discretization.

As in [150], we can use [8], Theorem 5.147 to write an expression for the local truncation error of the scheme in the form $G = F_x$. The theorem gives us that

$$|F_x - \tilde{F}_x^\pi| = h_i^7 \frac{F^{(\mathrm{viii})}}{8!} \prod_{j=1}^{7} (s - \tilde{\rho}_j) + \mathcal{O}(h_i^8).$$

Then the truncation error for G has two sources - the first from the Hermite approximation evaluated at the Gauss points, then the second from taking the interpolating polynomial through them. The first of these will, in general, be neglible - recall from (3.2.19) that if $G = u_t$ then the error is $\mathcal{O}(h_i^{11})$. The Langrage interpolating polynomial has the well known error

$$|G^\pi - \tilde{G}^\pi| = h_i^6 \frac{G^{(\mathrm{vi})}}{6!} \prod_{j=1}^{6} (s - \rho_j),$$

and so the residual can be approximated by

$$|\tilde{G}^\pi - F_x^\pi| = |(\tilde{G}^\pi - G) - (F_x^\pi - F_x)| = \left| h_i^7 \frac{F^{(\mathrm{viii})}}{8!} \prod_{j=1}^{7} (s - \tilde{\rho}_j) + h_i^6 \frac{F^{(\mathrm{vii})}}{6!} \prod_{j=1}^{6} (s - \rho_j) \right| + \mathcal{O}(h_i^8).$$

Thus, the scheme is at worst $\max_i \mathcal{O}(h_i^6)$ with superconvergence at the Gauss points.

3.2.3. Initialization and Implementation: The implementation follows the template of previous Movcols with the subroutines changed accordingly to fit the schemes dervied above. Our implementation is written in Fortran 90. The routines will be made available at github.com/BenedictBoyle/Movcol6 upon the conclusion of this project. The one notable structural change we've made is motivated by performance; due to the number of calculations involved in determining V (3.2.14) and its derivatives for each step, we can save time by evaluating the shape functions (3.2.15) and their appropriate derivatives at the Gauss and Lobatto points in advance in the main routine, reducing the number of operations involved considerably.

Calculating the monitor functions often involve integrals of the function and its derivatives (e.g. (3.1.7)); since the schemes require knowing these values at the Gauss points anyway it is simple to implement this with Gauss-Legendre quadrature, which is comfortably accurate enough within the context of the mesh equation. We also include a routine to output the solution at the Gauss points for the purposes of plotting. This is the natural choice, especially in the context of the conservative scheme where the error is minimized at them.

There are two considerations involved in assembling suitable initial conditions to input into the scheme, which is the only remaining detail to resolve. Firstly, it is often the case that unless the initial conditions are posed on a mesh that is

already equidistributed, or close to it, the system will be too stiff and the solver will not start. Thus, an equidistributed mesh must be determined. Secondly, not just the initial profile, but five of its derivatives will need to be known on this mesh for the scheme to start. This is not so much of a problem for initial conditions that can be expressed explicitly as a function which can be differentiated directly, but in general it will be necessary to approximate values of derivatives of an arbitrary function on a non-uniform mesh.

For Movcol and Movcol4, these were overcome simultaneously by solving a dummy problem with largely the same machinery as is used for the full problem. For any initial function $u_0(x)$, provided it can be continuously represented, the problem

$$u_t = u_0 \quad \text{in} \quad [a,b] \times [0,1] \quad u(x,0) = 0, \tag{3.2.33}$$

will generate $u_0(x)$ and an appropriate number of derivatives posed on mesh equidistributed according to the choice of monitor function when solved with either Gauss-point collocation scheme described in Appendix B, as can easily be seen by integrating with respect to time.

Often this also works with our case. By solving (3.2.33) with the Gauss point scheme described in Section 3.2.1 we can determine an equidistributed mesh and the correct values of the first five derivatives on it starting with just a continuous representation of u_0. When initial data consisting of discrete values from e.g. an ODE solver is desired, this can be provided using a simple spline or piecewise-cubic interpolation routine as appropriate. However, the instability from the truncation of u_t discussed in that section can lead to problems given the absence of an elliptic regularizing term on the right hand side. The higher derivatives in particular can become wildly inaccurate by $t = 1$. Often the procedure will still work and the contributions from the higher derivatives are sufficiently small due to the high powers of h_i in (3.2.14) that this presents no barrier to the simulation, but not always.

To get around this, we can run the Movcol2 or Movcol4 initializer code which have better stability properties. This will give us the collection x_i, $u_0(x_i)$, $u_{0,x}(x_i)$, and in the latter case also $u_{0,xx}(x_i)$, $u_{0,xxx}(x_i)$ with the x_i equidistributed. Then the higher derivatives can be recovered by a numerical differentiation scheme to a sufficient degree of accuracy that the PDE simulation routine will start. For completeness, we include brief descriptions of the lower order Movcols in Appendix B.

3.3. Examples

3.3.1. Reaction-Diffusion Equation: Aside from the application to Cahn-Hilliard equations considered elsewhere in this thesis, the schemes we've derived are much more widely applicable. We present here two models demonstrating some of their features.

The first is the sixth-order *Reaction-Diffusion Equation*, that is (1.2.33) with $m = 3$:

$$u_t = u_{xxxxxxx} + |u|^{p-1}u, \quad u \in \mathbb{R} \times \mathbb{R}_+, \tag{3.3.34}$$

whose blow-up similarity solutions are considered in [24]. In that paper, it is shown how these solutions can be located via a μ-bifurcation similar to the procedure outlined in Section 2.3.8, although quite different in its details. For this example we focus on the case $p = 2$, the qualitative properties of the solutions not differing significantly in p.

The two solutions bifurcating from the constant solution $f_* = \left(\frac{1}{p-1}\right)^{\left(\frac{1}{p-1}\right)}$, where f signifies a solution of the corresponding similarity equation in the vein of e.g. (2.2.15), are presented in Figure 3-1. We denote them by f_s and f_u following the terminology used in [24] for self-similar solutions of the fourth order equivalent of (3.3.34). The subscripts are suggestive that we expect the former to be a stable (in fact attractive for bell-shaped initial data) with the latter unstable just as in the fourth order case, and we shall demonstrate this to be the case as a test of the non-conservative scheme described in Section 3.2.1.

For these simulations we posed the problem for $x \in [0, 100]$ with $u_x(0) = u_{xxx}(0) = u_{xxxxx}(0) = 0$ and $u_{xxx}(100) = u_{xxxx}(100) = u_{xxxxx}(100) = 0$, the latter since we expect the solutions to exhibit algebraic (slow) decay, see [24], Section 2. We want to avoid fixing lower order derivatives to zero as this may not accurately approximate an infinite domain with no boundary conditions. Simulations were conducted with mesh size $N = 100$ and monitor function

$$M_c = |u|, \quad M = M_c + \alpha \int_0^{100} M_c \mathrm{d}x,$$

with parameter $\alpha \in \mathbb{R}_+$, compare with adjusted monitor function (3.1.7). Typically we took $\alpha = 1$, though unlike for the next example the rather gentler scaling groups driving the singularity development here meant that the problem was not particularly sensitive to its value.

First we exhibit the attractivity of f_u, beginning with initial data $u_0 = 2\exp(-x^2)$. Figure 3-2 shows the flow under the similarity scalings, with T

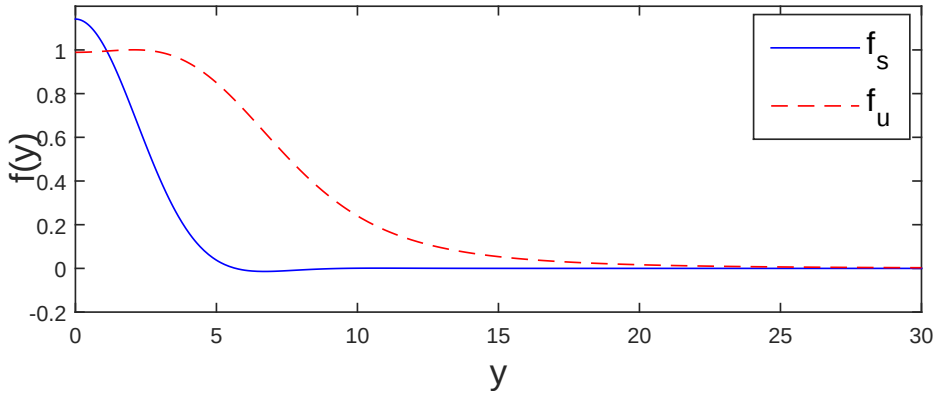

Figure 3-1: Two solutions of the similarity equation for (3.3.34).

extrapolated from the relation in Figure 3-3 demonstrating the time rescaling under the transformation (3.1.9). The figure clearly demonstrates the exponential (in τ) convergence to f_s and experiments have shown similar convergence for a wide class of data.

Indeed, in demonstrating the instability of f_u we find once again that in the limit $t \to T^-$ the asymptotic behaviour is described by f_s, suggesting its generic stability for even initial data. Figure 3-4 shows the behaviour of u with initial data f_u, again in rescaled variables. Imperfections in the initialization procedure mean the *de facto* initial data is slightly perturbed, hence the solution diverges from it with time, at first slowly then converging to f_s again with exponential rate. In both of these phenomena the broad strokes are identical to those revealed by the numerical calculations performed on the fourth order equivalent of (3.3.34) in [24], Chapter 7.

3.3.2. Thin Film Equation: Finally we present results from a quasilinear equation exhibiting more exotic phenomena than the equations considered in the rest of this thesis. We draw a direct analogy with the final example of [150] to demonstrate in some ways the limitations of the scheme as applied to higher-order equations.

The equation we consider is the sixth order *Long-Wave Unstable Thin Film Equation*, having the form

$$u_t = \left(uu_{xxxxx} - 6u^5u_x\right)_x, \quad u \in \mathbb{R} \times \mathbb{R}_+. \tag{3.3.35}$$

The fourth order equivalent, $u_t = -\left(uu_{xxx} + 4u^3u_x\right)_x$, is studied in depth in [168], and was chosen as a test for Movcol4 as it exhibits finite time blow-up coupled

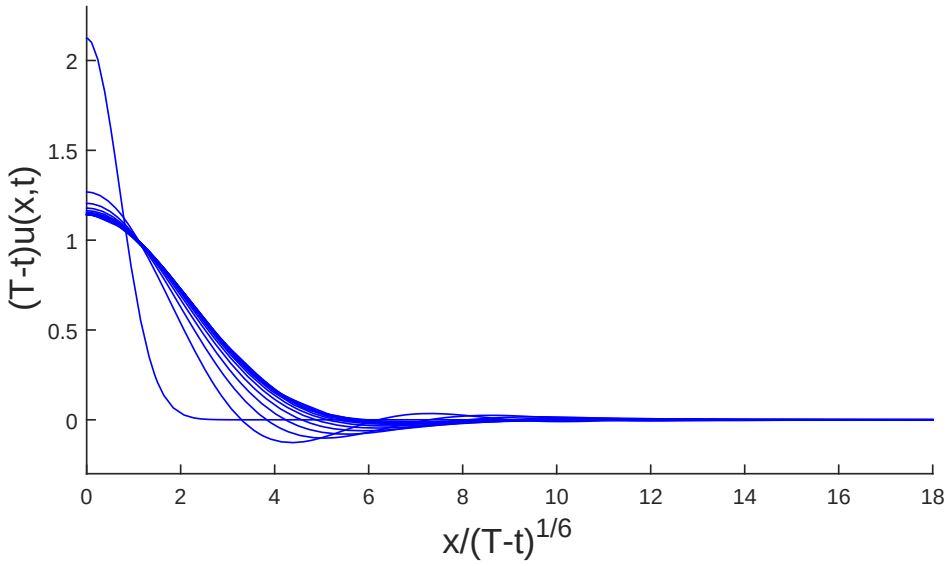

Figure 3-2: Convergence of bell-shaped initial data to f_s.

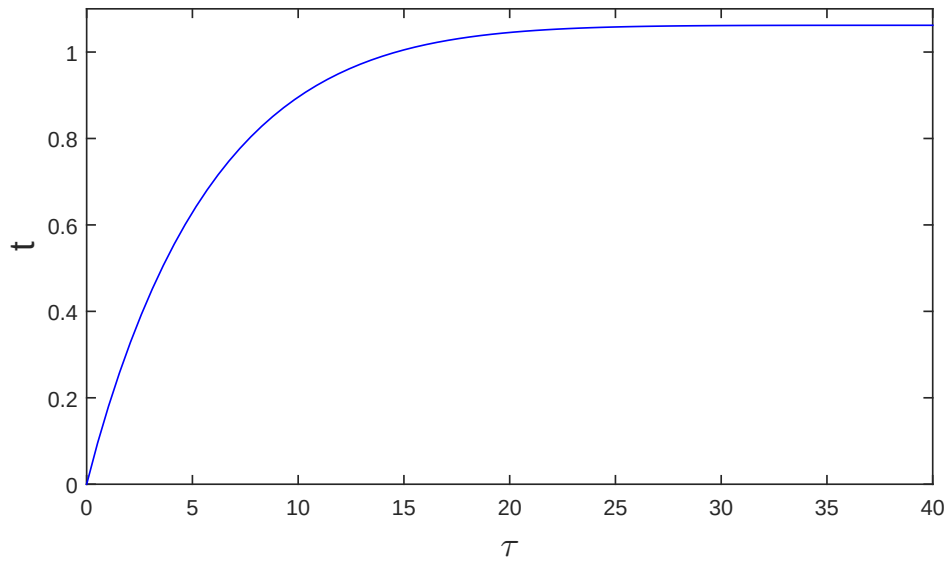

Figure 3-3: Time rescaling for Figure 3-2.

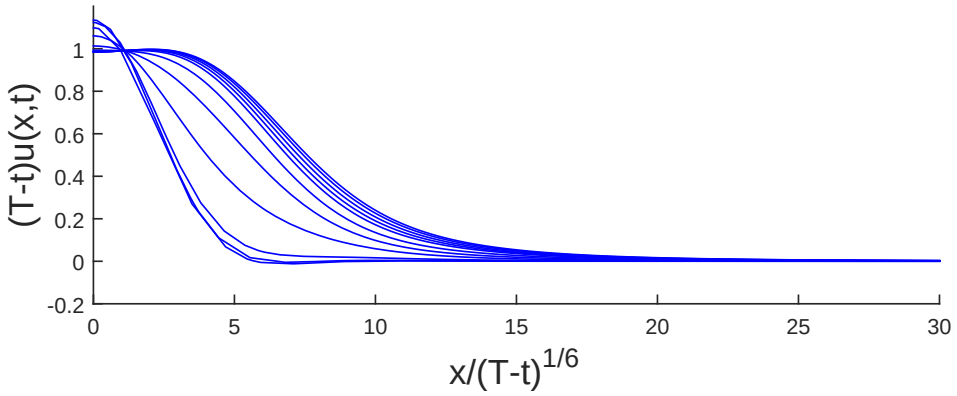

Figure 3-4: Instability of f_u and eventual convergence to f_s

with 'rupturing' of positive solutions, at least for large enough mass. This is a consequence of the fact that the self-similar blow-up solutions are compactly supported with only certain permissible masses. Since the equation is conservative, if the initial data has mass greater than the mass of the blow-up profile then extra mass must split off from the singularity-region (possibly synchronous with the blow-up time), at which point that solution is supported on (at least) two disjoint regions; this is what is meant by rupturing.

This scenario is much the same for (3.3.35) (for further details for blow-up in sixth order thin film equations, particularly this 'mass critical' case, see [54]), and so again it seems a good candidate to test our scheme. Here we use the conservative collocation scheme (3.2.2) since mass conservation is an important feature. To ensure we are in the blow-up plus rupturing regime, we pose the problem for $x \in [0, 10]$ with Neumann boundary conditions $u_x(0) = u_{xxx}(0) = u_{xxxxx}(0) = u_x(10) = u_{xxx}(10) = u_{xxxxx}(10) = 0$ and initial condition $u_0 = \frac{6}{\sqrt{2\pi}} \exp(-x^2/2)$. Then, we pick the monitor function

$$M_c = u^7 + |x^2 u_{xx}|^7, \quad M = M_c + \alpha \int_0^{10} M_c \mathrm{d}x,$$

suggested by the scaling symmetries of (3.3.35), with the second term aiming to concentrate some mesh points in the region of high curvature where the rupturing will occur, as in [150]. The monitor function is corrected in the same vein as (3.1.7), with some parameter $\alpha \in \mathbb{R}_+$.

Difficulties arise from the apparent necessity in this scheme to trade between the value of α and the number of mesh points N. Smaller α makes for a more responsive monitor function in regions of small M_c, which is preferable for resolving

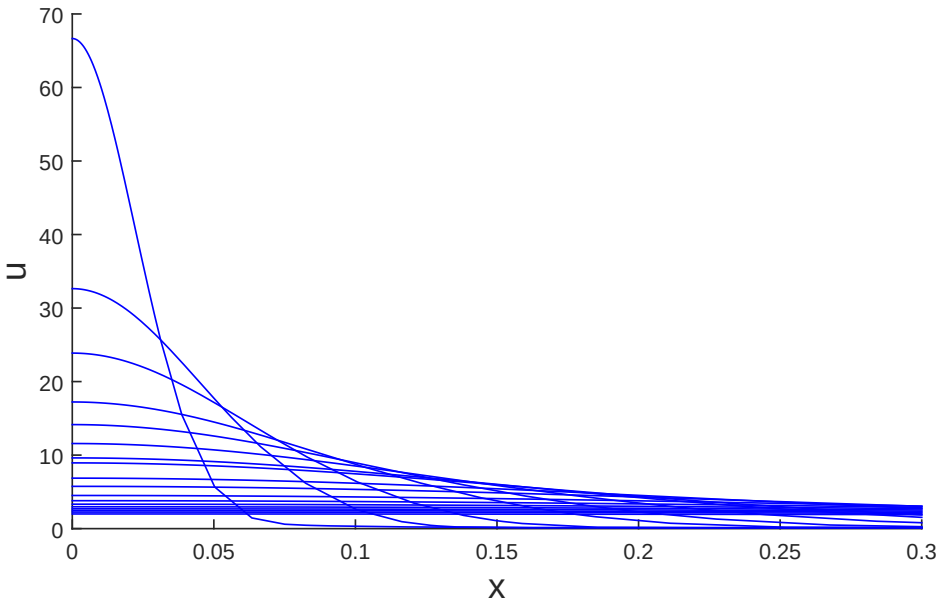

Figure 3-5: A blowing-up solutions of (3.3.35).

the rupturing point. However, the resulting system becomes too stiff for DASPK to solve if N is large (i,e. the mesh is dense), and so attempts to increase the resolution at the rupture point can only be realized by lowering the resolutions everywhere! For instance, if we set $\alpha = 0.1$ then the solver will not run with N much larger that 16. In practice, we've found the small α small N regime less satisfactory than with larger values than both, a drawback not apparent for the scheme for fourth order equations in [150]. It seems that stiffness is the enemy here.

It is possible in future this might be alleviated by specialized solvers or perhaps a different choice of MMPDE than (3.1.4), however even with the above caveats we have achieved somewhat respectable results with the parameters $\alpha = 0.8$, $N = 46$. The solution is presented in Figures 3-5 and 3-6, the former showing the formation of the singularity and the latter the approach towards the sundering of the blow-up solution from the remaining droplet. The movement of the mesh points under (3.2.13) is shown in Figure 3-7; compare with [150], Section 7, Figure 8 where a smaller value of α results in better clustering of mesh points around the eventual rupture and concomitantly a smoother representation of the profile there than in Figure 3-6. Nonetheless, we still seem to be capturing the qualitative behaviour well in our case.

We conclude with Figure 3-8 showing the real time plotted against the com-

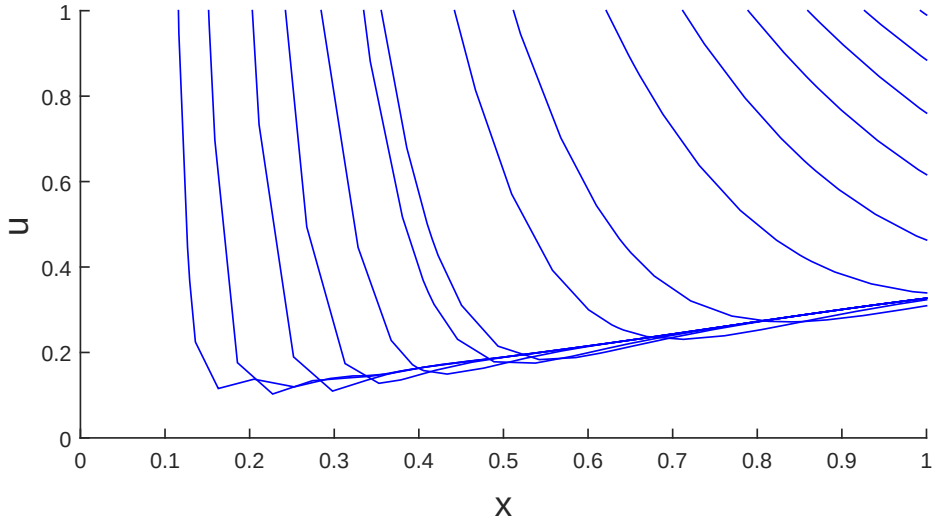

Figure 3-6: Evolution towards the rupturing point.

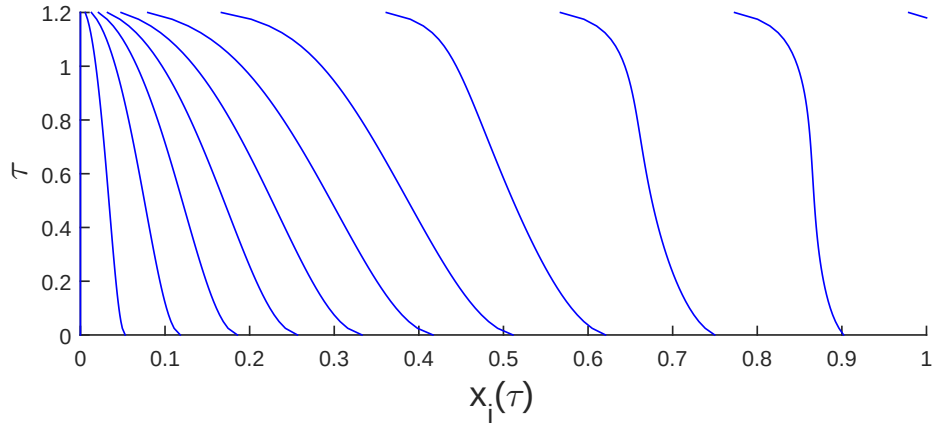

Figure 3-7: Movement of the mesh points towards the singularity.

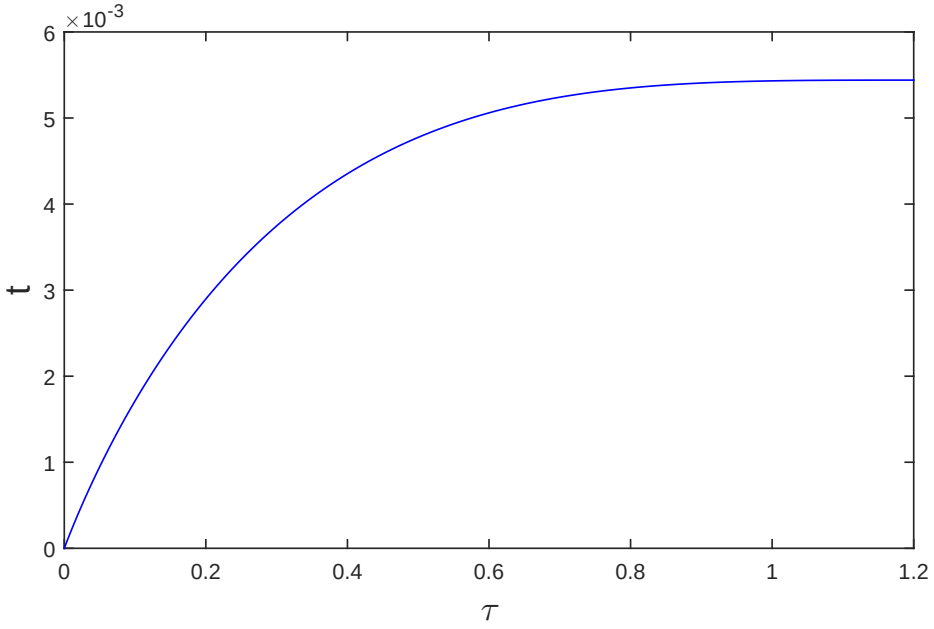

Figure 3-8: Time rescaling of the evolution.

putational time, again demonstrating the power of this method and its ability to take sufficiently-small steps as the blow-up time is approached.

Chapter 4

Cahn-Hilliard Equation with a Second Order Nonlinearity - Stable Case

4.1. Preliminaries

We now turn our focus to the equation

$$u_t = \Delta^3 u + \Delta\left(|u|^{p-1}u\right), \tag{4.1.1}$$

which is the stable equivalent of (2.1.1). Both operators on the right hand side (the triharmonic heat equation and the signed porous medium equation) lead to well posed problems when taken separately. Together they form a coercive, monotone operator and so in some ways this equation is less interesting than the unstable case considered in Chapter 2 as we do not expect any solutions with finite time blow-up and, as it turns out, the 'non-uniqueness' phenomena for the spreading solutions (see Section 2.4.1) does not occur. However, the interplay between the high order of the operators and the conserved quantities this confers makes for some novel and surprising features, as we shall demonstrate.

We once more are considering asymptotic behaviour of the Cauchy problem in $\mathbb{R}^N$ and we complete the model with a bounded, integrable initial condition

$$u(x,0) = u_0(x) \in L^\infty\left(\mathbb{R}^N\right) \cap L^1\left(\mathbb{R}^N\right). \tag{4.1.2}$$

However, note that our main results pertain to self-similar *Very Singular Solutions*, for which a typical functional setting for the initial data is not available. As it turns out, these will be a big factor amongst the possible large-time asymptotic patterns, along with the more traditional *Source Type* solutions whose initial

condition, however, is still not in L^1, so we do not dwell on these questions. For the most part we assume u_0 is smooth and with decay as $|x| \to \infty$, which we can achieve by a suitable positive time translation.

In the absence of blow up, our main goal will be to say as much as we can about the possible asymptotic patterns that form as $t \to \infty$. This problem's ancestor was the study of the Semilinear Heat Equation with absorption

$$u_t = \Delta u - u^p. \tag{4.1.3}$$

Besides the history of this equation in conjunction with 'Very Singular Solutions', its large time behaviour is also well understood: its asymptotic 'eigenfunctions' were categorized in [76]. This investigation was rather complete, beginning with a description of radial self-similar solutions of (4.1.3), which admit only algebraic decay for large values of the similarity variable in the supercritical case $p \geq 1 + \frac{2}{N}$ (notably, this is proved by considering properties of the *PDE* and not directly from the similarity ODE itself, as well as the coefficient of decay uniquely determining each profile) and a unique minimal solution with exponential decay for $p \in (1, 1 + \frac{2}{N})$ separating compactly supported and algebraically decaying ones. Then in the supercritical case, the basin of attraction for each of the infinitely many self-similar solutions was characterized according to the large-$|x|$ decay rates of the initial data, and for initial data with 'too-fast' decay it was shown that the appropriate large-t asymptotic behaviour is given by 'approximately' self-similar solutions of the linear heat equation. The subcritical case is slightly more involved, and the basins of attraction for self-similar solutions are determined by whether for a given pair of upper and lower solutions there is only one self-similar solution in between. If so, the naturally initial data 'bounded' in an appropriate sense between this pair is naturally attracted to the self-similar behaviour. Moreover, the minimal profile with exponential decay is shown to be stable from below, although without precluding existence of at least one more exponentially decaying solution stability from above cannot be settled. Finally, the critical case is shown to give rise to asymptotic behaviour described by logarithmic perturbations of the Gauss Heat Kernel provided the decay of the initial profile is fast enough.

Many similar results for the Quasilinear Heat Equation with absorption

$$u_t = \Delta u^m - u^p, \quad m > 1 \tag{4.1.4}$$

were later derived in a number of papers by some of the same authors, see [49],

[123] and references therein, though of course with the introduction of quasilinearity leads to more complexity in the range of behaviours, notably 'heat localization' (compactly supported solutions) become a possibility.

Much of this analysis relies heavily on comparison principles and so higher-order generalizations of (4.1.3) are of course going to be far more difficult to resolve, though some results do generalize. In particular, the $2m$th order case

$$u_t = -(-\Delta)^m u - |u|^{p-1} u \tag{4.1.5}$$

is considered in [81], where the signed nonlinearity $|u|^{p-1} u$ is as ever used to account for the loss of a maximum principle for $m > 1$, since non-negative initial data is not expected to generate solutions that remain non-negative. Here it is established that the number of self-similar solutions (VSS) with exponential decay is given by the Morse index of an associated linearized operator, in particular there are arbitrarily many as $p \to 1^+$ that bifurcate from the zero solution having asymptotic form of rescaled eigenfunctions of the linear $2m$th order heat equation. It also seems that only one solution, bifurcating from the critical value $p = 1 + \frac{2m}{N}$, is 'generically' stable (we will define the term below), and for $m = 1$ this is the minimal exponentially decaying solution in the subcritical range described above.

It is still open whether there are exponentially decaying self-similar solutions in the range $p \in (1 + \frac{2m}{N}, 1 + \frac{4m}{N})$ for $m > 1$, though this seems unlikely, as the non-existence result for $m = 1$ follows from the maximum principle for the PDE for which no analogue exists. However, some simple aspects of self-similar solutions with algebraic decay in the supercritical range are discussed.

These solutions, however, are not particularly 'physical', lying neither in L^1 nor L^2_ρ, and we expect similar results to hold in our case where we have modified only the nonlinear term, so we will pay them only cursory attention in Section 4.2.7 below. Hence, in general, we impose that

$$u_0 \text{ has exponential decay as } |x| \to \infty. \tag{4.1.6}$$

We take the opportunity to fill in the analysis of the spreading solutions from chapter 2 since the rigorous aspects are identical, although significant differences in global behaviour occur in the numerical analysis. We will compare and contrast as we go. We will also note that this can serve as a basis for understanding the more mysterious solutions to the sixth order stable Thin-Film Equation

$$u_t = \nabla \cdot \left(|u|^n \nabla \Delta^2 u \right) + \Delta \left(|u|^{p-1} u \right), \tag{4.1.7}$$

using the same bifurcation methods as employed for the fourth order case in [51].

Once more, the critical exponent

$$p = p_0 = 1 + \frac{4}{N}, \tag{4.1.8}$$

will play a key role; like in the pure power law case it marks a transition in stability for the trivial solution, see Section 4.2.3. Also, as in chapter two, gives rise to a continuous mass-branch of solutions due to the introduction of conserved quantities in (4.1.1) via the Laplacian acting on the nonlinearity. These *source-type* solutions appearing only at the critical exponent, supplementing the existence of subcritical *very singular solutions*, are a large departure from the reaction-absorption theory.

We first address some basic PDE estimates.

4.1.1. Global existence of Classical solutions: Global existence of weak solutions to (4.1.1) is straightforward and follows from the existence of a Lyapunov function [98]. Specifically, in this instance we multiply (4.1.1) through by $(\Delta^{-1})\, u_t$ in L^2 and integrate to arrive at the equality

$$|| \left(\Delta^{-1/2}\right) u_t(t)||^2_{L^2} + \frac{\mathrm{d}}{\mathrm{d}t}\left[\frac{1}{2}||\Delta u(t)||^2_{L^2} + \frac{1}{p+1}||u(t)||^{p+1}_{L^{p+1}}\right] = 0. \tag{4.1.9}$$

Then the leftmost term is non-negative and so the expression enclosed in square brackets can easily be seen to be non-negative and non-increasing. From here the bounds

$$||\Delta u(t)||^2_{L^2} \leq C, \quad ||u(t)||^{p+1}_{L^{p+1}} \leq C, \tag{4.1.10}$$

are enough to establish existence of a weak solution $u \in C\left((0,\infty); H^2 \cap L^{p+1}\right)$ via a Galerkin method and uniqueness for the Cauchy problem is a relatively straightforward consequence of both terms on the right hand side having the same sign. The standard reference here is [130]. Provided we can prove the existence of an L^∞ bound, higher regularity will follow from standard parabolic theory; we set about this task below. Here and for the remainder of this Chapter we use C to represent arbitrary finite constants, not necessarily the same from one appearance to the next.

This relies on the integral form of (4.1.1):

$$u(x,t) = b(t) * u_0 + \int_0^t \Delta b(t-s) * |u|^{p-1}u(s)\mathrm{d}s. \tag{4.1.11}$$

As in Chapter 2, we have used

$$b(x,t) = F(y), \quad y = xt^{-1/6},$$

with $F(y)$ the solution to (1.3.43).

A simple application of Young's inequality for convolutions gives

$$|u(x,t)| \leq \sup_x |u_0| \int_{\mathbb{R}^N} |b(t)| \mathrm{d}x + \int_0^t ||\Delta b(t-s)||_{L^{p+1}} ||u(s)||_{L^{p+1}}^p \mathrm{d}s,$$

and then from (4.1.10) and the scaling properties of the fundamental solution we arrive at

$$|u(x,t)| \leq \sup_x |u_0| \, ||F||_{L^1} + C||\Delta F||_{L^{p+1}} \int_0^t (t-s)^{-((N+2)p+2)/6(p+1)} \, \mathrm{d}s,$$

which provides a finite bound on $[0,T]$ when the integral converges, i.e. $p < \frac{N}{N-4}$, or any $p > 1$ for $N < 4$.

This can be improved by estimating $|u|^{p-1}u(x,t) \leq |u|^{p-1}(x,t)U(t)$, with $U(t) = \sup_x u(x,t)$. Then again applying Young's inequality gives

$$|u(x,t)| \leq \sup_x |u_0| \int_{\mathbb{R}^N} |b(t)| \mathrm{d}x + \int_0^t ||\Delta b(t-s)||_{L^{(p+1)/2}} ||u(s)||_{L^{p+1}}^{p-1} U(s) \mathrm{d}s,$$

and by (4.1.10) and scaling this yields

$$|u(x,t)| \leq \sup_x |u_0| \, ||F||_{L^1} + C||\Delta F||_{L^{(p+1)/2}} \int_0^t (t-s)^{-((N+2)(p+1)+2N)/6(p+1)} \, U(s) \mathrm{d}s.$$

The Gronwall-Bellman inequality can be applied to $U(t)$, giving

$$U(t) \leq \sup_x |u_0| \, ||F||_{L^1} \exp\left(C||\Delta F||_{L^{(p+1)/2}} \cdot \int_0^t (t-s)^{-((N+2)(p+1)+2N)/6(p+1)} \, \mathrm{d}s \right), \quad (4.1.12)$$

the right hand side of which is finite on $[0,T]$ when the integral converges, i.e. $p < p_S = \frac{N+4}{N-4}$, or any $p > 1$ for $N < 4$.

This shows that $U(t)$ has at most exponential growth as $t \to \infty$ in the strictly subcritical Sobolev range, however, we can improve this considerably and in fact derive uniform L^∞ bounds for $p < p_S$. The technique employs a scaling method

based on similar arguments in [81], Chapter 2 and [7], Chapter 4.

We start with the assumption that there exist sequences $t_k \to \infty$, $C_k \to \infty$ and $x_k \in \mathbb{R}^N$ such that

$$\sup_{\mathbb{R}^N \times (0,t_k)} u(x,t_k) := u(x_k,t_k) = C_k \tag{4.1.13}$$

and seek a contradiction. The scaling aspect is introduced via the change of variables

$$u(x_k + x, t_k + t) = C_k v_k(y,s), \quad x = a_k y,\ t = a_k^6 s \tag{4.1.14}$$

with $\{a_k\} \to 0_+$ a sequence determined under the consideration that the inequalities (4.1.10) are satisfied for the v_k in the limit. These take the form

$$||\Delta u||_{L^2}^2 = C_k^2 a_k^{N-4} ||\Delta v||_{L^2}^2, \quad ||u||_{L^{p+1}}^{p+1} = C_k^{p+1} a_k^N ||v_k||_{L^{p+1}}^{p+1},$$

prompting us to take $a_k = C_k^{-(p+1)/N}$ so the second bound is always satisfied; the first bound also holds as $\{a_k\} \to 0_+$ provided $p \le p_S$.

Now the v_k satisfy the perturbed equation

$$(v_k)_s = \Delta^3 v + \delta_k \Delta \left(|v|^{p-1} v \right), \quad v_{0,k} = C_k^{-1} u(x,t_k) \tag{4.1.15}$$

with $\delta_k = C_k^{p-1-4(p-1)/N} \to 0$ as $k \to \infty$ provided $p < p_S$. Note that the v_k are defined for $s \in \left(-\frac{t_k}{a_k^6}, \infty \right)$ thanks to (4.1.14).

This allows us to consider $\tilde{v}_k(s) := v_k(s - s_0)$ for $s_0 \gg 1$. By (4.1.12) and (4.1.14), we have that $|\tilde{v}_k(s)| \le 1$ for $s \in (0, s_0]$. Indeed, $\sup_y \tilde{v}(y, s_0) = 1$ by assumption. But now the $\tilde{v}_k$ are a uniformly bounded family of solutions of the uniformly parabolic equation with smooth coefficients (4.1.15), hence uniform boundedness of the derivatives is guaranteed by the classical parabolic regularity theory.

Thus applying Arzela-Ascoli theorem, we find that $\lim_{k\to\infty} \tilde{v}_k = \tilde{v}$ is a bounded weak solution, hence a classical solution, of the triharmonic equation (1.3.36) with initial data $\tilde{v}_0$ satisfying $|\tilde{v}_0| < 1$, $||\Delta \tilde{v}_0||_{L^2}^2 \le C$, $||\tilde{v}_0||_{L^{p+1}}^{p+1} \le C$.

We can now derive the contradiction by showing that $\tilde{v}$ becomes small for large s_0. Using Hölder's inequality on the integral representation for $\tilde{v}$ we get

$$|\tilde{v}(s_0)| = \left| \int_{\mathbb{R}^N} b(y - z, s_0) \tilde{v}_0(z) \mathrm{d}z \right| = s_0^{-N/6} \left| \int_{\mathbb{R}^N} F\left(\frac{y-z}{s_0^{1/6}} \right) \tilde{v}_0(z) \mathrm{d}z \right| \le$$
$$s_0^{-N/6} s_0^{-Np/6(p+1)} ||F||_{L^{(p+1)/p}} ||\tilde{v}_0||_{L^{p+1}} \le C s_0^{-N/6(p+1)} ||F||_{L^{(p+1)/p}} \ll 1,$$

when $s_0 \gg 1$. But then this implies $\sup_y |\tilde{v}_k(y, s_0)| \ll 1$ for $k \gg 1$, whereas we have assumed that $\sup_y |\tilde{v}_k(y, s_0)| = \sup_y |v_k(y, 0)| = 1$. Thus, for $p < p_S$, there can be no sequences $t_k \to \infty$, $C_k \to \infty$ and $x_k \in \mathbb{R}^N$ such that (4.1.13) holds and the solution remains uniformly bounded for all time.

4.2. Similarity Solutions

4.2.1. Source-Type Solutions in the Critical Case: Before we proceed we remind ourselves of the scaling invariance of equation (4.1.1) as we will use it heavily in the sequel. Recall that scalings are preserved by the group of transformations

$$x \to \lambda^{1/6} x, \quad t \to \lambda t, \quad u \to \lambda^{-2/3(p-1)} u, \ \lambda > 0. \tag{4.2.16}$$

Therefore, on passing to the rescaled variables

$$u(x,t) = t^{-2/3(p-1)} f(y), \quad y = x t^{-1/6}, \tag{4.2.17}$$

we can look for solutions to (4.1.1) that are solutions of the elliptic equation

$$\Delta^3 f + \Delta \left(|f|^{p-1} f \right) + \frac{1}{6} y \cdot \nabla f + \frac{2}{3(p-1)} f = 0, \tag{4.2.18}$$

should they exist.

Once more, we find that the conservative nature of (4.1.1) manifests itself particularly starkly at the critical exponent (4.1.8). Like in the unstable case, we have using (4.2.17) that

$$\frac{\mathrm{d}}{\mathrm{d}t} \int_{\mathbb{R}^N} u(x,t) \mathrm{d}x = \frac{\mathrm{d}}{\mathrm{d}t} \left(t^{-2/3(p-1)+N/6} \int_{\mathbb{R}^N} f(y) \mathrm{d}y \right) = 0, \tag{4.2.19}$$

implying solutions with non-trivial mass can occur only at the critical exponent. We also have a characterization in terms of the initial singularity formation in the distributional sense as $t \to 0$ in the non-rescaled variables. For any test function $\phi(x) \in C_c^\infty$,

$$\lim_{t \to 0^+} \int_{\mathbb{R}^N} u(x,t) \phi(x) \mathrm{d}x = \lim_{t \to 0^+} \left(t^{-2/3(p-1)+N/6} \int_{\mathbb{R}^N} f(y) \phi(y t^{1/6}) \mathrm{d}y \right). \tag{4.2.20}$$

Then for $p = p_0$, the limit exists and is equal to $M\delta_0$, where $M = \int f(y) \mathrm{d}y$ is the mass of the profile and δ_0 is Dirac's delta. This justifies the 'source type' terminology, and also the sense in which solutions in the subcritical range $p \in$

$(1, p_0)$ are referred to as 'very' singular, since there clearly the exponent of t outside the integral is negative and the expression blows up in the limit. Thus, no notion of $u(x, 0)$ as a measure can be considered.

Significantly, we are able to integrate (4.2.18) up to get a fifth order ODE. In one dimension it has the form

$$f^{(\mathrm{v})}(y) + \left(f^5\right)'(y) + \frac{1}{6} y f(y) = 0, \quad f'(0) = f'''(0) = 0. \tag{4.2.21}$$

The constant of integration is set to zero by implicitly imposing that f has exponential decay, which turns out here to be enough to guarantee that we also have $f^{(\mathrm{v})}(0) = 0$. We again focus only on even radial solutions - numerical evidence suggests that no other forms of solutions with appropriate decay exist.

The large-y asymptotics are identical to the unstable case as the respective linearizations about zero bear no trace of the nonlinear term. As such we do not repeat the calculations here and refer the reader to Section 2.2.4. Recall that we have a three parameter family of behaviours with exponential decay,

$$f(y) = y^{(-3/5)(N-4/3(p-1))} \left(C_1 \exp(\beta y^{6/5}) + C_2 \exp(a y^{6/5}) \cos(b y^{6/5} + k)\right) \tag{4.2.22}$$

Since we have three free parameters to catch only two conditions fixed by the symmetry consideration, we have necessary (though not sufficient) grounds to conjecture a continuous set of solutions in this critical case.

We saw in Chapter 2 the difficulties of establishing existence results via shooting for fifth order equations even when conditions are in some sense favourable to us with regards to constructing bounded solutions as separatrices (Section 2.4.2). Here, too, the solutions of the ODE blow up with probability one, however in this instance the dominant balance as $|f| \to \infty$ has the form $f^{(\mathrm{iv})} = -f^5(1 + o(1))$ and the blow-up is oscillatory. This can be demonstrated using the change of variables $f(y) = (y - y_0)^{-1}\phi(s)$, where y_0 is the blow-up point and $s = \ln(y - y_0)$. The leading order ode then becomes

$$\phi^{(\mathrm{v})}(s) - 15\phi^{(\mathrm{iv})}(s) + 85\phi'''(s) - 225\phi''(s) + 274\phi'(s) - 120\phi(s) + 5\phi^4(s)\phi'(s) - 5\phi^5(s) = 0,$$

for which the existence of a periodic orbit can be demonstrated numerically, see [73]. This technique is also commonly used to study oscillatory behaviour near interfaces in degenerate equations like (4.1.7). Since any profile that develops a singularity will tend to both positive and negative infinity as the blow-up point is

approached, we will not be able to construct separatrices from information about the sign of the profile near the singularity.

However, the bifurcation approach is effective even if limited in scope. Consider the critical equation

$$\mathbf{A}_{2s}(f) := \Delta^3 f + \frac{1}{6} y \cdot \nabla f + \frac{N}{6} f = -\Delta \left(|f|^{p-1} f \right), \quad \int f = m_0 > 0 \tag{4.2.23}$$

where m_0 is the mass of the initial profile $\left| \int u_0 \right|$. Then setting $f = m_0 v$ and writing the integral operator $\mathbf{C} = \mathbf{B} - \mathbf{I}$, $\mathbf{B}$ as in (1.3.43), we arrive at the integral equation

$$v = \mathbf{D}(v) = -\mathbf{C}^{-1} v - m_0^{4/N} \mathbf{C}^{-1} \Delta \left(|v|^{4/N} v \right). \tag{4.2.24}$$

This is in some ways quite non-standard; in particular since we are on an unbounded domain, namely the whole of $\mathbb{R}^N$, compactness is a delicate issue and, since $\Delta : L^2_\rho \to L^2_\rho$ is not a continuous operator the nonlinear term does not admit simple interpretation as a Nemytskii operator. We can sidestep these issues by applying Deimling's formulation of the bifurcation theory for integral operators discussed in [41], Chapter 28. We state Theorem 28.1 (pp. 381) here for reference.

Theorem 4.1. *Let X be a real Banach space, $K \in L(X)$, $\Omega \subset \mathbb{R} \times X$ a neighbourhood of $(\lambda_0, 0)$, $G : \Omega \to X$ continuous and $G(\lambda, 0) = 0$. Suppose also that*

i $\mathbf{I} - \lambda_0 K$ *is Fredholm of index zero and λ_0 is an isolated characteristic value of K of odd algebraic multiplicity.*

ii $|G(\lambda, x) - G(\lambda, \tilde{x})| \leq \phi(r)|x - \tilde{x}|$ *if* (λ, x), $(\lambda, \tilde{x}) \in \Omega$, $|\lambda - \lambda_0| \leq \delta$ *and* x, $\tilde{x} \in \bar{B}_r(0)$, *for some $\delta > 0$ and some $\phi : \mathbb{R}^+ \to \mathbb{R}^+$ such that $\phi(r) \to 0$ as $r \to 0$.*

Then $(\lambda_0, 0)$ is a bifurcation point for $F(\lambda, x) = x - \lambda K x + G(\lambda, x) = 0$.

Here $L(X)$ denotes the space of linear operators from X into itself. (4.2.24) is clearly of the correct form to apply the theorem with $\lambda = m_0$, $x = v$, and $X = L^2_\rho$. We set $K = -\mathbf{C}^{-1}$ and $G(m_0, v) = m_0^{4/N} \mathbf{C}^{-1} \Delta \left(|v|^{4/N} v \right)$.

It requires a bit of work to show that part ii applies to our $G(m_0, v)$. That is the contents of the following lemma, which we prove for general $p > 1$ as it will useful later.

Lemma 4.2. *For v, $\tilde{v}$ in L^2_ρ, and $||v||_{L^2_\rho}$, $||\tilde{v}||_{L^2_\rho} < r$ for $r > 0$ we have*

$$|| - \mathbf{C}^{-1} \Delta \left(|v|^{p-1} v - |\tilde{v}|^{p-1} \tilde{v} \right) ||^2_{L^2_\rho} \leq \phi(r) ||v - \tilde{v}||^2_{L^2_\rho}$$

for a function $\phi \to 0$ *as* $r \to 0$.

Proof. According to (1.3.53), we can write $|| - \mathbf{C}^{-1}\Delta\left(v^{p-1}v - \tilde{v}^{p-1}\tilde{v}\right)||^2_{L^2_\rho}$ in the form

$$-\int_{\mathbb{R}^N} \rho(y) \left(\int_{\mathbb{R}^N} K(y,\eta)\Delta\left(|v|^{p-1}v(\eta) - |\tilde{v}|^{p-1}\tilde{v}(\eta)\right) \mathrm{d}\eta \right)^2 \mathrm{d}y. \tag{4.2.25}$$

First, we note that by Hadamard's lemma we have the identity

$$|v|^{p-1}v(\eta) - |\tilde{v}|^{p-1}\tilde{v}(\eta) = (v(\eta) - \tilde{v}(\eta))p \int_0^1 |sv(\eta) + (1-s)\tilde{v}(\eta)|^{p-1} \mathrm{d}s.$$

Now, we can integrate (4.2.25) by parts to move the Laplacian onto the kernel K, and then apply Schwarz's inequality to bound the expression from above by

$$\int_{\mathbb{R}^N} \rho(y) \left[\int_{\mathbb{R}^N} \rho(\eta)^{-1} \tilde{K}(y,\eta)^2 p^2 \left(\int_0^1 |sv(\eta) + (1-s)\tilde{v}(\eta)|^{p-1} \mathrm{d}s \right)^2 \mathrm{d}\eta \cdot \right.$$
$$\left. \int_{\mathbb{R}^N} \rho(\eta) \left(v(\eta) - \tilde{v}(\eta)\right)^2 \mathrm{d}\eta \right] \mathrm{d}y,$$

with $\tilde{K}(y,\eta) = \int_0^1 z^{1/3}(1-z)^{-(N+2)/6} \Delta F\left[(y - \eta z^{1/6})(1-z)^{-1/6}\right] \mathrm{d}z$ being the result of applying Δ_η to $K(y,\eta)$ and inheriting its exponential decay for large y, η. For sharp estimates on ΔF, recalling that F is the fundamental solution of (1.3.36) see e.g. [36]. Hence, rearranging we arrive at the bound

$$\int_{\mathbb{R}^N} \rho(\eta) \left(v(\eta) - \tilde{v}(\eta)\right)^2 \mathrm{d}\eta \cdot$$
$$\left(\int_{\mathbb{R}^N} \int_{\mathbb{R}^N} \rho(y)\rho(\eta)^{-1} \tilde{K}(y,\eta)^2 p^2 \left(\int_0^1 |sv(\eta) + (1-s)\tilde{v}(\eta)|^{p-1} \mathrm{d}s \right)^2 \mathrm{d}\eta \mathrm{d}y \right).$$

The result then follows if the second line of this expression satisfies the vanishing condition required of $\phi(r)$ as $r \to 0$ for all $p > 1$. Since $\rho(y)\tilde{K}(y,\eta)^2$ is sufficiently quickly decaying in y, some manipulations (applying Jensen's inequality for the interior integral in s and bringing the weight $\rho(\eta)^{-1}$ inside it) reveal that this requires the inequality

$$\int_{\mathbb{R}^n} \rho(\eta)^{-1} |w(\eta)|^{(p-1)/2} \mathrm{d}\eta \leq C \int_{\mathbb{R}^n} \rho(\eta) |w(\eta)|^2 \mathrm{d}\eta$$

to hold, i.e. there must be a continuous imbedding $L^2_\rho \subset L^{(p-1)/2}_{\rho^*}$. We believe this must be the case due the behaviour at infinity imposed by the increasing

weight function for the former space, however we have not been able to show this rigorously. □

With the above qualification, this demonstrates that $G(m_0, v)$ satisfies condition ii of Theorem 4.1, and so it remains to establish that $\mathbf{I} + \mathbf{C}^{-1}$ is Fredholm of index one, and that the linearization $\mathbf{D}'(0) = -\mathbf{C}^{-1}$ has eigenvalue 1 of odd multiplicity, so that condition i holds. These follow from the properties of $\mathbf{B}$, the former from the eigendecomposition (Section 1.3.1) and resolvent compactness (Section 1.3.3). The latter we can calculate this directly from the known spectral properties of $\mathbf{B}$, (1.3.48), giving $\sigma(\mathbf{D}'(0)) = \{1, \frac{6}{7}, \frac{6}{8}, \ldots\}$ and the first eigenvalue 1 always has multiplicity 1, so branching occurs from $m_0 = 0, f = 0$.

We can now use the Lyapunov-Schmidt Theory [162] to obtain a description of the branch near the bifurcation point. For small values of m_0 the solution takes the form $f = \psi_0 + w$, $w \in \{\psi_0\}^{\perp}$, $\psi_0 = F$, with F as in (1.3.43). The coefficient of F is fixed by the mass scaling of v. On subsitution back into (4.2.24) we obtain $w = \mathcal{O}(m_0^{4/N})$, so for $m_0 \ll 1$, w is small in L^2_ρ. Passing back to the original variables, we find that there is a continuous branch of solutions leaving the bifurcation point, and for sufficiently small m_0 they have the approximate form

$$f(y) = m_0 F(y) + \mathcal{O}(m_0^{p_0}). \tag{4.2.26}$$

We plot these branches parameterized by the value at the origin $f(0)$, for $N = 1$ in Figure 4-1 and for $N = 3$, where the equation also takes on a more simple form

$$f^{(\mathrm{v})}(y) + \frac{4}{y} f^{(\mathrm{iv})}(y) - \frac{4}{y^2} f'''(y) + \left(f^{7/3}\right)'(y) + \frac{1}{6} y f(y) = 0, \quad f'(0) = f'''(0) = 0. \tag{4.2.27}$$

in figure 4-2. Samples of solutions from these branches are included in Figures 4-3 and 4-4 respectively.

The figures clearly suggest that, unlike in Chapter 2 when the mass of any globally bounded self-similar profile was bounded from above, any initial mass profile can develop into a self-similar one without the necessity for mass discrepancies. This is not that surprising given the differences in stability of the underlying PDE.

We can use the approximation (4.2.26) to establish some notion of the stability of these solutions. To do this we examine the linearization of (4.2.23),

$$\mathbf{A}'_{2s}(f) = \mathbf{B} + p_0 \Delta\left(|f|^{4/N}\mathbf{I}\right) \approx \mathbf{B} + |m_0|^{4/N} p_0 \Delta\left(|F|^{4/N}\mathbf{I}\right) \tag{4.2.28}$$

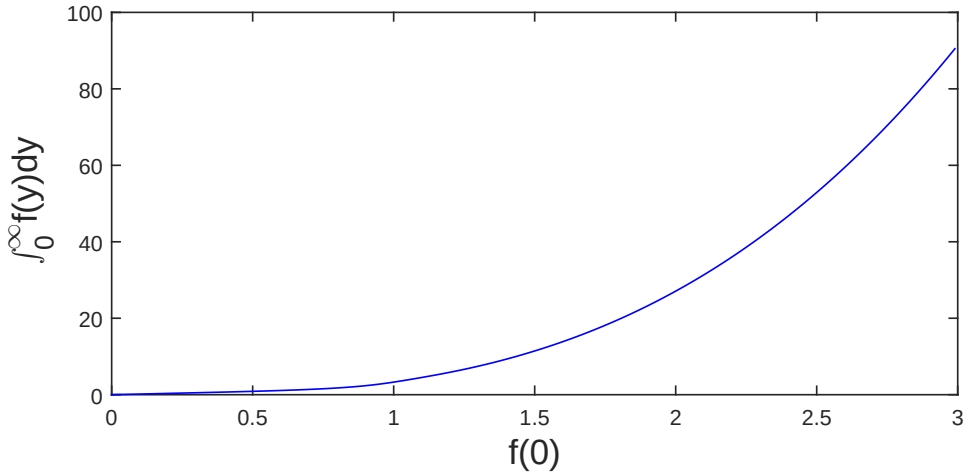

Figure 4-1: Continuous Family of Solutions parameterized by $f(0)$ for $N = 1$.

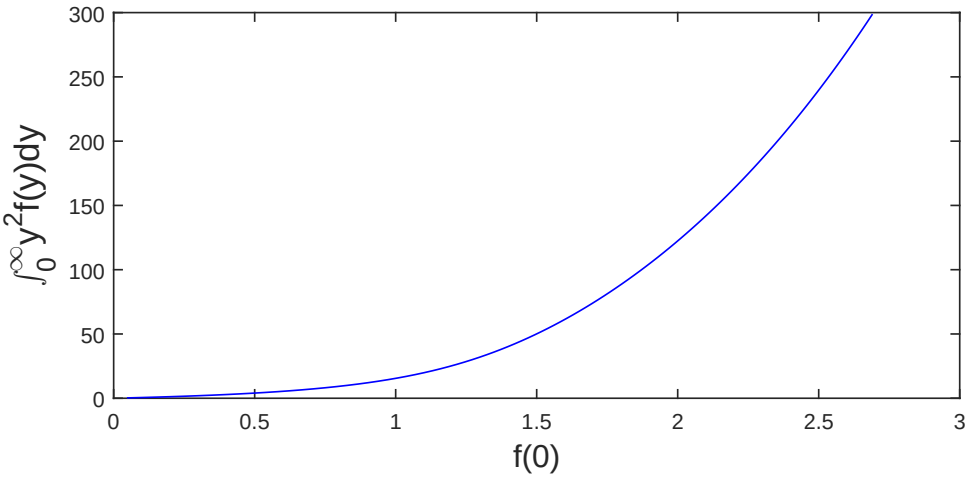

Figure 4-2: Continuous Family of Solutions parameterized by $f(0)$ for $N = 3$.

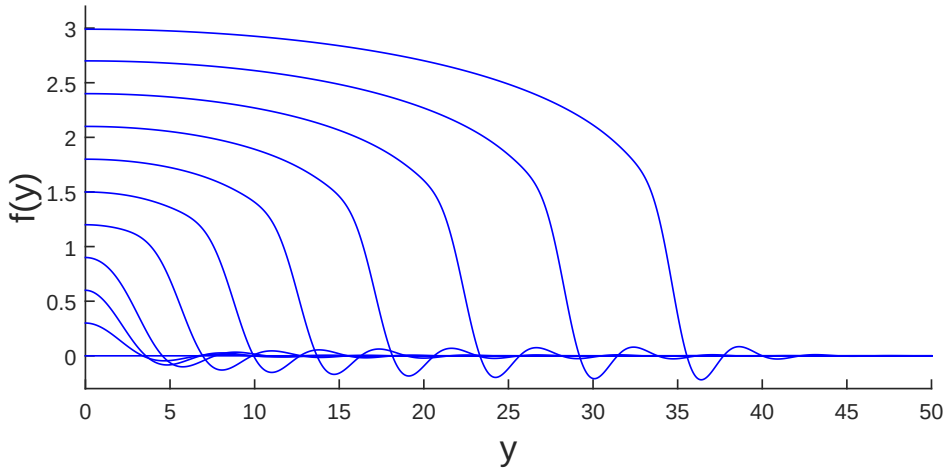

Figure 4-3: Solutions from the vertical branch from p_0 for $N = 1$.

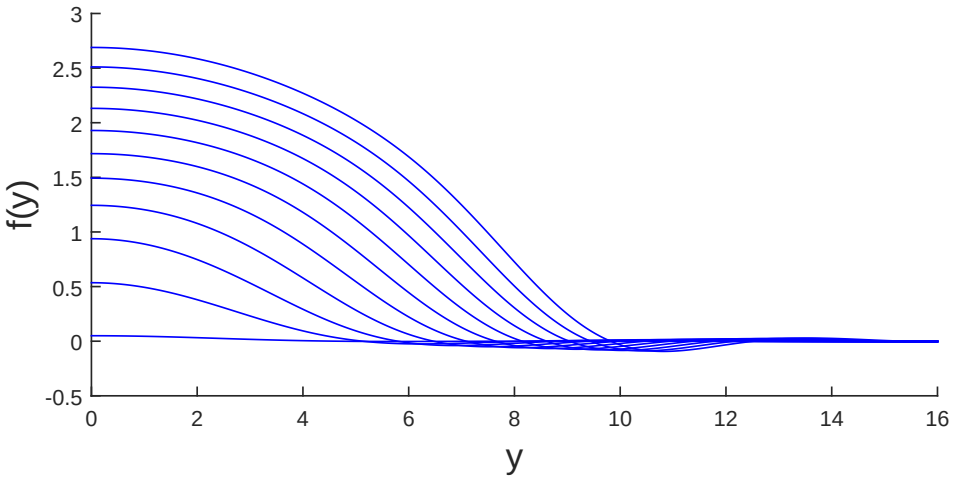

Figure 4-4: Solutions from the vertical branch from p_0 for $N = 3$.

with the last approximation holding for small $|m_0|$. As is a theme for this project, information about solutions and their linearized spectra far from bifurcation points, where expansions cease to hold and fully nonlinear patterns dominate, is hard to acquire or even estimate with classical methods. For large m_0 the only methods we know of are numerical and come from careful simulations of the PDE. However, in some instances there are estimates we can make, and for small m_0 we have that the operator on the right hand side in (4.2.28) is a lower-order perturbation of $\mathbf{B}$, so the linearization inherits compactness and its discrete spectrum is a perturbation of the spectrum of $\mathbf{B}$, see [56], Proposition 4.7. Thus inserting the approximation (4.2.26) we arrive at a rough estimate of the spectrum,

$$\sigma\left(\mathbf{A}'_{2s}(f)\right) \approx \left\{ -\frac{l}{6} + |m_0|^{4/N} p_0 \langle \Delta\left(|F|^{4/N}\psi_l\right), \psi_l^* \rangle,\ l = 1, 2 \dots \right\}, \qquad (4.2.29)$$

at least in the case where the eigenvalues are simple (i.e. in the radial or one-dimensional geometry). Note that a perturbation by ψ_0 is not included as it has non-zero mass and so is prohibited by the conservative property of the flow.

Clearly for m_0 sufficiently small the point spectrum of the perturbation is strictly negative and so is exponentially stable - it can be expected to attract various classes of initial data of small enough mass. Moving away from that regime, a very rough apprehension can be gained by noting that $|F|^{4/N} \geq 0$, $\langle \psi_l, \psi_l^* \rangle = 1 > 0$ and the Laplacian is a negative operator. Therefore, we might hope for the perturbations to also be 'negative dominant' (although a rigorous proof of this does not seem possible), and for stability to in fact increase with m_0, though of course even then the expansion we use will not necessarily be valid. However, the seeming monotone shape of the branches leads some support to this.

4.2.2. Existence of Very Singular Solutions in the Subcritical Range: In cataloguing the class of fully non-linear self-similar solutions, it is important to know for which parameter ranges they might exist. Pohozaev's results from the 1960s on existence and nonexistence of solutions for simple semilinear elliptic equations with power-law nonlinearities in certain parameter ranges [148] are still rightly celebrated today and their extensions are still fruitful areas of research. We can provide a straightforward 'energy' proof that existence of self-similar solutions is bounded from above in p:

Proposition 4.3. *No integrable, non-trivial self-similar solutions of equation* (4.1.1) *exist in the range* $p \geq p_E = 1 + \frac{8}{N}$.

Proof. Multiplying (4.2.18) through by f and integrating over $\mathbb{R}^N$ we arrive at the identity

$$-\int_{\mathbb{R}^N}(\nabla\Delta f)^2\,\mathrm{d}x - p\int_{\mathbb{R}^N}|f|^{p-1}(\nabla f)^2\,\mathrm{d}x + \left(\frac{2}{3(p-1)}-\frac{N}{12}\right)\int_{\mathbb{R}^N} f^2\mathrm{d}x = 0. \tag{4.2.30}$$

All of the integrals are definite and so for $\left(\frac{2}{3(p-1)}-\frac{N}{12}\right)\leq 0 \iff p\geq 1+\frac{8}{N}$ they are all of the same sign, and must each be zero. □

This bound is unlikely to be sharp (later we will construct what seems an exhaustive set that remain outside of the supercritical range $p > 1+\frac{4}{N}$) and below we sketch out a possible improvement, although some of the details remain unsettled. We also speculate that the monotonicity of the non-rescaled PDE might be exploitable to prove the conjectured sharp existence bound for the ODE, though we do not pursue that direction here.

To find an improved bound on the existence range we can instead multiply (4.2.18) by $(-\Delta)^{-1}f$. We claim there exists a $g:\mathbb{R}^N\to\mathbb{R}$ such that

$$-\Delta g = f \text{ in } \mathbb{R}^N, \quad g(y)\to 0 \text{ as } y\to\infty, \tag{4.2.31}$$

provided one of

1. $N\geq 3$,
2. $N=2$, $\int_{\mathbb{R}^2} f(y)\mathrm{d}y = 0$, or
3. $N=1$, $\int_{\mathbb{R}} f(y)\mathrm{d}y = \int_{\mathbb{R}} yf(y)\mathrm{d}y = 0$

holds. This follows from straightforward properties of the Newton Kernel

$$g(y) = \int_{\mathbb{R}^n} N(y-\eta)f(\eta)\mathrm{d}\eta, \quad N(y) = \begin{cases} C_N|y|^{2-N} \text{ if } N\neq 2, \\ C_2\log|y| \text{ otherwise,}\end{cases}$$

for known constants C_N, and decay estimates for $f(y)$.

Now, multiplying (4.2.18) through by g and formally integrating by parts, we get

$$-\int_{\mathbb{R}^N}(\Delta f)^2 - \int_{\mathbb{R}^N}|f|^{p+1} - \frac{1}{6}\int_{\mathbb{R}^N} yg\cdot\nabla\Delta g - \frac{2}{3(p-1)}\int_{\mathbb{R}^N} g\Delta g. \tag{4.2.32}$$

The first two terms have been integrated by parts in the natural way, and the last one corresponds to $\frac{2}{3(p-1)}||f||^2_{H^{-1}}$. The third term we can integrate by parts

three times, working on $B_R(0)$ for large R to keep track of the boundary data

$$\int_{B_R} yg \cdot \nabla \Delta g = \int_{\partial B_R} yg \Delta g \cdot \mathbf{n} - N \int_{B_R} g \Delta g - \int_{B_R} (y \cdot \nabla g) \Delta g = \int_{\partial B_R} yg \Delta g \cdot \mathbf{n} - N \int_{\partial B_R} g \nabla g \cdot \mathbf{n} + N \int_{B_R} (\nabla g)^2 - \int_{\partial B_R} (y \cdot \nabla g) \nabla g \cdot \mathbf{n} + \int_{B_R} \nabla (y \cdot \nabla g) \cdot \nabla g. \quad (4.2.33)$$

Turning to the Einstein summation convention, we can write

$$\nabla (y \cdot \nabla g) \cdot \nabla g = \frac{\partial}{\partial y_j} \left(y_i \frac{\partial g}{\partial y_i} \right) \frac{\partial g}{\partial y_j} = \frac{\partial g}{\partial y_j} \frac{\partial g}{\partial y_j} + y_i \frac{\partial^2 g}{\partial y_i \partial y_j} \frac{\partial g}{\partial y_j} = (\nabla g)^2 + y \cdot \nabla^2 g \nabla g, \quad (4.2.34)$$

where $\nabla^2 g$ is the Hessian matrix of second partial derivatives and $\nabla^2 g \nabla g$ is the usual product of a matrix and a vector. The second term of the last expression can be integrated by parts a final time to give

$$\int_{B_R} y \cdot \nabla^2 g \nabla g = \int_{\partial B_R} g \nabla^2 g y \cdot \mathbf{n} - \int_{B_R} g \nabla \cdot \left(\nabla^2 g y \right). \quad (4.2.35)$$

We have played a bit fast and loose with matrix transposition in the last integrand for notational convenience, facilitated by the symmetry of the Hessian. Again, we can represent this final integrand more easily as

$$g \nabla \cdot \left(\nabla^2 g y \right) = g \frac{\partial}{\partial y_j} \left(y_i \frac{\partial^2 g}{\partial y_i \partial y_j} \right) = g \frac{\partial^2 g}{\partial y_j \partial y_j} + g y_i \frac{\partial^3}{\partial y_i \partial y_j \partial y_j} = g \Delta g + yg \cdot \nabla \Delta g. \quad (4.2.36)$$

Putting this all together gives

$$\int_{B_R} yg \cdot \nabla \Delta g = \int_{\partial B_R} yg \Delta g \cdot \mathbf{n} - \int_{\partial B_R} (y \cdot \nabla g) \nabla g \cdot \mathbf{n} - N \int_{\partial B_R} g \nabla g \cdot \mathbf{n} + \int_{\partial B_R} g \nabla^2 g y \cdot \mathbf{n} + (N+2) \int_{B_R} (\nabla g)^2 - \int_{B_R} yg \cdot \nabla \Delta g, \quad (4.2.37)$$

or, providing the boundary integrals disappear as $R \to \infty$,

$$\int_{B_R} yg \cdot \nabla \Delta g = \frac{N+2}{2} \int_{B_R} (\nabla g)^2. \quad (4.2.38)$$

Hence, we arrive at the improved energy identity

$$-\int_{\mathbb{R}^N}(\Delta f)^2-\int_{\mathbb{R}^N}|f|^{p+1}-\left(\frac{N+2}{12}-\frac{2}{3(p-1)}\right)\int_{\mathbb{R}^N}\left((-\Delta)^{-1/2}f\right)^2=0, \tag{4.2.39}$$

which implies that a nontrivial solution must have $\frac{N+2}{12}-\frac{2}{3(p-1)}<0 \implies p<p_{IE}=1+\frac{8}{N+2}$. To complete the proof, we need to ensure that existence of g with appropriate decay is enough to guarantee existence of the last integral in (4.2.39), i.e. that $\int_{\mathbb{R}^N}\left(1+|\xi|^2\right)^{-1/2}\hat{f}^2\mathrm{d}\xi<\infty$, where $\hat{f}$ is the Fourier Transform of f. However, we have not been able to correctly treat the nonlinear term of (4.2.18) in this context and so we relinquish this to speculation for the time being.

4.2.3. Stability of the zero solution: To study the asymptotic stability of solutions to equation (4.2.18), we look at (4.1.1) under the extended set of scalings

$$u(x,t)=(1+t)^{-2/3(p-1)}\theta(y,\tau),\quad y=x(1+t)^{-1/6},\tau=\ln(1+t) \tag{4.2.40}$$

Where the translation $1+t$ ensures τ is non-negative and there is no initial singularity. We are interested here only in behaviour as $\tau\to\infty$. Now the flow can be expressed in the rescaled variables in terms of the operator (1.3.43) as the autonomous equation

$$\theta_\tau=\mathbf{A}_{S,2}\theta=\left(\mathbf{B}+c_p\mathbf{I}\right)\theta+\Delta\left(|\theta|^{p-1}\theta\right), \tag{4.2.41}$$

where

$$c_p=\frac{2}{3(p-1)}-\frac{N}{6}=\frac{N}{6(p-1)}\left(p_0-p\right)$$

and p_0 is the critical exponent (4.1.8). This form makes it easy to demonstrate that this critical exponent also characterizes the change in stability of the zero solution. Indeed, since the linearization of (4.2.41) about zero has no contribution at all from the nonlinear term, the spectral information comes solely from the operator $(\mathbf{B}+c_p\mathbf{I})$, and we have that

$$\sigma\left(\mathbf{B}+c_p\mathbf{I}\right)=\left\{c_p-\frac{l}{6},\ l=0,1,2,\ldots\right\}. \tag{4.2.42}$$

Then by the principle of linearized stability [133], zero is asymptotically stable if $c_p-\frac{l}{6}<0 \iff p>p_0$ but is not for $p\in(1,p_0)$, where it possesses a non-trivial unstable manifold.

This allows us to conclude the following, see [81], Chapter 5 for a similar

description. Given a family $\{\theta_k,\ k = 0, 1, 2, \ldots\}$ of solutions of the dynamical system (4.2.18), we define a *generically stable* one as follows:

Definition 4.4. *Let W^u and W^s denote the unstable and stable manifolds an equilibrium point. Then a stationary solution (equilibrium) θ_k of* (4.2.41) *is generically stable if*

1. $W^u(\theta_k) = \emptyset$.
2. $W^u(\theta_j) \neq \emptyset$ *for* $j \neq k$.
3. $\forall \theta(0) \notin (\cup_j W^s(\theta_j)) \cup W^s(0),\ \theta(\tau) \to \theta_k$ *as* $\tau \to \infty$.

This definition encapsulates the idea of a non-trivial stationary solution of the dynamical system that attracts at least 'most' randomly chosen initial data. Clearly this cannot happen in the supercritical range where the zero solution has a stable manifold with codimension 0, in which case we expect the asymptotic behaviour in the rescaled coordinates to tend preferentially to it, which manifests in the non-rescaled coordinates as the dominance as $t \to \infty$ of behaviour related to the linear equation (1.3.36). This can be seen by scaling (4.1.1) with the transformation group associated with the symmetries of (1.3.36):

$$u(x,t) = (1+t)^{-N/6}\varphi(y,\tau), \quad y = x(1+t)^{-1/6}, \quad \tau = \ln(1+t),$$

to give the equation

$$\varphi_\tau = \mathbf{B}\varphi - \mathrm{e}^{\gamma\tau}\Delta\left(|\varphi|^{p-1}\varphi\right),$$

with $\gamma = \frac{N}{6}(p_0 - p)$. For $p > p_0$ the perturbation decays exponentially with τ and so for sufficiently small initial data with $m_0 = \int u_0 > 0$ we can deduce the equation exhibits the asymptotic behaviour

$$u(x,t) = m_0 t^{-N/6}\left(F\left(xt^{-1/6}\right) + o(1)\right) \text{ as } t \to \infty.$$

This result is entirely typical for semilinear equations in the supercritical range and so we do not dwell on the details, see [45] for how it might be made rigorous. Note that this argument does not depend on the sign or indeed the form of the nonlinear term and so the same supercritical asymptotics will manifest for the equations considered in Chapters 2 and 5.

While there remains the narrow possibility that we can have non-trivial self-similar solutions for $p_0 < p < p_{IE}$ for $N > 2$, we can emphasize that even if it exists it will not play a large role in the dynamics.

4.2.4. Self-similar solutions via p-bifurcation: In the subcritical case, we can gain a much clearer picture since we can detect solutions branching off from the trivial solution with p. Like with the mass branch for critical $p = p_0$, the argument here will also apply to the unstable equation (2.1.1) with only minor alterations, so we make it only once. However, the small differences in the local behaviour near the bifurcation points lead to markedly different patterns in the large. In the unstable case for any $p > 1$ we can find a countable set of solutions for any $p > 1$, whereas here we can find evidence of only a finite number. First, we address the local p-bifurcation argument.

Proposition 4.5. *Let $l \geq 0$ be such that $-l/6$ is an eigenvalue of $\mathbf{B}$ with odd multiplicity. Then*

$$p_l = 1 + \frac{4}{N+l} \tag{4.2.43}$$

are bifucation points for (4.2.18) *from the trivial solution.*

Proof. Consider again the operator $\mathbf{C} = \mathbf{B} - \mathbf{I}$. Then by the known spectral properties of $\mathbf{B}$ and the compactness of the resolvent, $\mathbf{C}^{-1} : L^2_\rho \to L^2_\rho$ is a compact operator with spectrum $\sigma(\mathbf{B}_1^{-1}) = \frac{-1}{1+l/6}$, $l \in \mathbb{N}$, and has the explicit representation (1.3.53)

This allows us to rewrite the equation (4.2.18) as the integral equation

$$f = \mathbf{D_p} f = -(1 + c_p)\mathbf{C}^{-1} f - \mathbf{C}^{-1}\Delta\left(|f|^{p-1} f\right), \tag{4.2.44}$$

Where $\mathbf{D_p} : L^2_\rho \to L^2_\rho$. Now apply Theorem 4.1. By Lemma 4.2 we have once again that part ii holds. That $\mathbf{I} + (1 + c_p)\mathbf{C}^{-1}$ is Fredholm follows from the properties of $\mathbf{B}$ (Sections 1.3.1 and 1.3.3), thus for part i to hold it is necessary for the linearization of $\mathbf{D}$ about zero has eigenvalue 1 with odd multiplicity. $\mathbf{D_p}'(0)$ has the form $-(1 + c_p)\mathbf{C}^{-1}$, and so simple operations on the known spectrum of $\mathbf{B}$ provide that $\sigma\left(\mathbf{C}^{-1}\right) = \{\frac{-6}{6+l},\ l = 0, 1, 2, \ldots\}$ and

$$\sigma\left(\mathbf{D_p}'(0)\right) = \left\{ \frac{N(p_0 - p) + 6(p-1)}{(p-1)(6+l)},\ l = 0, 1, 2, \ldots \right\}$$

and so clearly bifurcation can only occur when p is as in(4.2.43), provided $-l/6$ has odd multiplicity. □

In one dimension and the radial geometry, the eigenspaces for each operator are one dimensional and so we are assured bifurcation always occurs in these scenarios. In general, the eigenspace is N-dimensional for $l = 1$ and $N(N+1)/2$ dimensional for $l = 2$ and so on, and the parity can be even. In these instances

difficult analysis involving the topological degree of $\mathbf{C}^{-1}\Delta\left(|f|^{p-1}f\right)$ on the unit sphere of the eigenspace is required.

The Lyapunov-Schmidt method [162] allows us to describe solutions near the known bifurcation points. From here we assume one-dimensional eigenspaces to simplify the analysis.

Denoting E_0 as the space spanned by ψ_l the lone eigenvector of $\ker\left(\mathbf{D_p}'(0)\right)$, $P_0 : L^2_\rho \to E_0$ the projection onto it and E_1 the invariant subspace spanned by $\psi_j, j \neq l$ so that $L^2_\rho = E_0 + E_1$, we can decompose the solution likewise into the sum $f = f_0 + f_1$, $P_0 f = f_0$, $(\mathbf{I} - P_0)f = f_1$. Clearly, $f_0 = C_l\psi_l$ and $f_1 = \sum_{j\neq l} C_j\psi_j$ for some constants C_i depending on $\varepsilon = p - p_l$. Now, applying P_0 to (4.2.44) we get the bifurcation equation

$$C_l \frac{(N+l)^2\varepsilon}{4(6+l)} = \left\langle \mathbf{C}^{-1}\Delta\left(|f|^{p-1}f\right), \psi_l^* \right\rangle + \mathcal{O}(\varepsilon^2).$$

Now we proceed by writing

$$\left\langle \mathbf{C}^{-1}\Delta\left(|f|^{p-1}f\right), \psi_l^* \right\rangle = \left\langle \Delta\left(|f|^{p-1}f\right), (\mathbf{C}^*)^{-1}\psi_l^* \right\rangle = \\ - \frac{6+l}{6}\left\langle |\psi_l|^{p-1}\psi_l, \Delta\psi_l^* \right\rangle + o(C_l^p),$$

where we have used $(\mathbf{C}^{-1})^* = (\mathbf{C}^*)^{-1}$. Hence we derive a simple expression for

$$|C_l|^{p-1} = -\left(\frac{(N+l)^2}{24\kappa_l}(p - p_l)(1 + o(1))\right),$$

where, for p sufficiently close to p_l,

$$\kappa_l = \left\langle \psi_l^{p_l}, \Delta\psi_l^* \right\rangle. \tag{4.2.45}$$

We therefore require the right hand side to be non-negative, so it is the sign of κ_l that will determine the sign of $p - p_l$ and therefore in which direction the branches will bifurcate. We know of no way in the literature to obtain reasonable estimates for expressions like (4.2.45), or even to be reasonably certain of their sign, and so we are forced to verify this numerically. Our tests for the first four even spectral pairings in 1D give

- $\left\langle \psi_2^{7/3}, \Delta\psi_2^* \right\rangle \approx -0.00152137$,
- $\left\langle \psi_4^{9/5}, \Delta\psi_4^* \right\rangle \approx -0.00453657$,
- $\left\langle \psi_6^{11/7}, \Delta\psi_6^* \right\rangle \approx -0.00605437$,

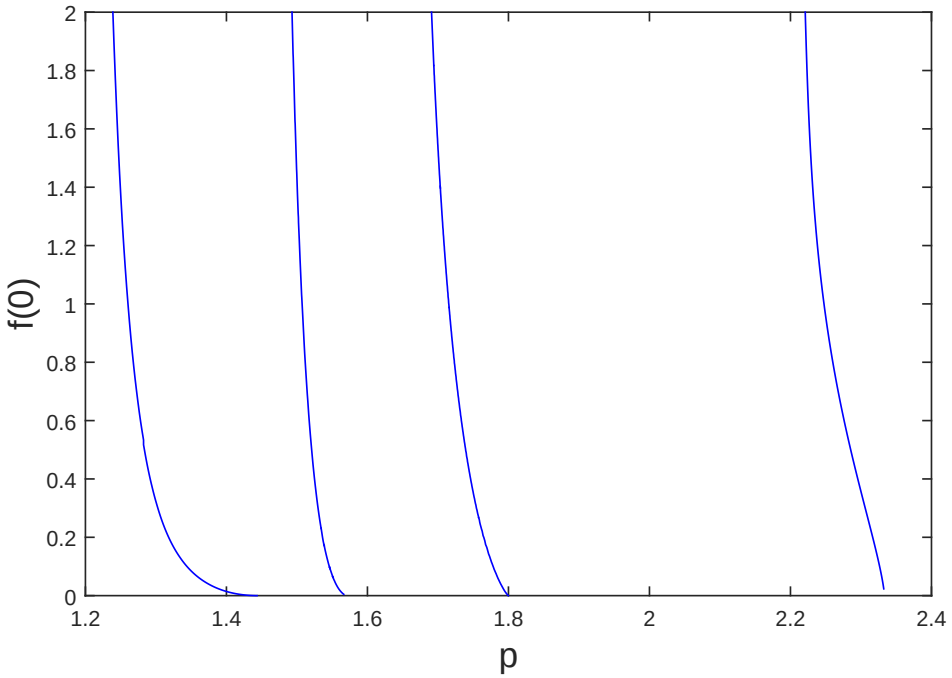

Figure 4-5: Branches of (even) solutions coming originating from p_l.

- $\left\langle \psi_8^{13/9}, \Delta\psi_8^* \right\rangle \approx -0.00662957,$

and this gives strong evidence that $p - p_l > 0$, i.e. that the branches grow to the left of the critical points, as p decreases towards $p \to 1^-$. Explicitly, we have a countable family of pitchfork bifurcations (With the positive and negative branches mirror images of each other) that accumulate towards $p \to 1^-$. The odd eigenfunctions give rise to analogous branches of odd self-similar solutions, with a vertical branch emanating from $p = 3$ in 1D etc.

The bifurcation diagram was constructed numerically and is presented in 4-5. The most striking feature is how rapidly the solutions grow above a certain point, and it is not clear immediately from the diagram whether the branches persist indefinitely to the left. This also made them very difficult to follow with even the BVPsuite solver, and to get get even as far as we did required a certain amount of brute force. For each step in p, we took as an initial guess the Lagrange interpolant through the past three solutions, and our forward stepping routine was, in a rudimentary way, adaptive, albeit only by trying successively smaller steps upon each failure of the solver to converge. We remark that it is not clear there is a better way and there seemed to be no regularity with which point a solutions would 'catch', sometimes making comparatively large steps on steep

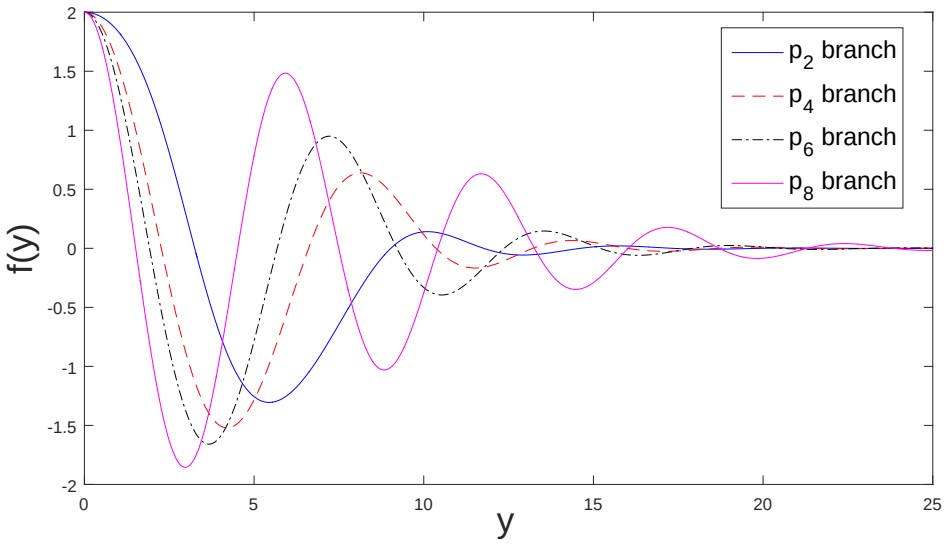

Figure 4-6: Profiles from the p-branches in Figure 4-5 with $f(0) = 2$

gradients and barely incrementing on shallow ones. Even with this, we were forced to use the regularization

$$|f|^{p-1} \to (f^2 + \varepsilon^2)^{(p-1)/2}, \ \varepsilon \approx 10^{-3}$$

and turn the tolerances abstol and reltol down to roughly 10^{-4}. Sample profiles from each branch are shown in 4-6. We have chosen profiles with $f(0) = 2$ so we are reasonably far into the 'fully nonlinear' regime.

Despite the rapid growth of the branches we conjecture they remain monotone and approach $p = 1^+$. They cannot become singular for any other p since that would require existence of an 'asymptotic bifurcation point' of (4.2.44) (see again [41], Chapter 28), which does not occur. The rapid growth of the branches is supported by looking the the leading order balance of (4.2.18) as $p \to 1^+$, given by (in one dimension)

$$\left(|f|^{p-1} f\right)'' + \frac{2}{3(p-1)} f \approx 0.$$

Scaling $f = C\bar{f}$, to get an idea of the scale of the solutions, we find that $C \approx \left(\frac{3}{2}(p-1)\right)^{-1/(p-1)}$, roughly demonstrating the magnitude of the growth.

The qualitative behaviour is much the same for $N = 3$, the p-bifurcation diagram is shown in Figure 4-7. The specialized path-following and bifurcation software suite AUTO [42] was used to create it. Even with this it was non-trivial

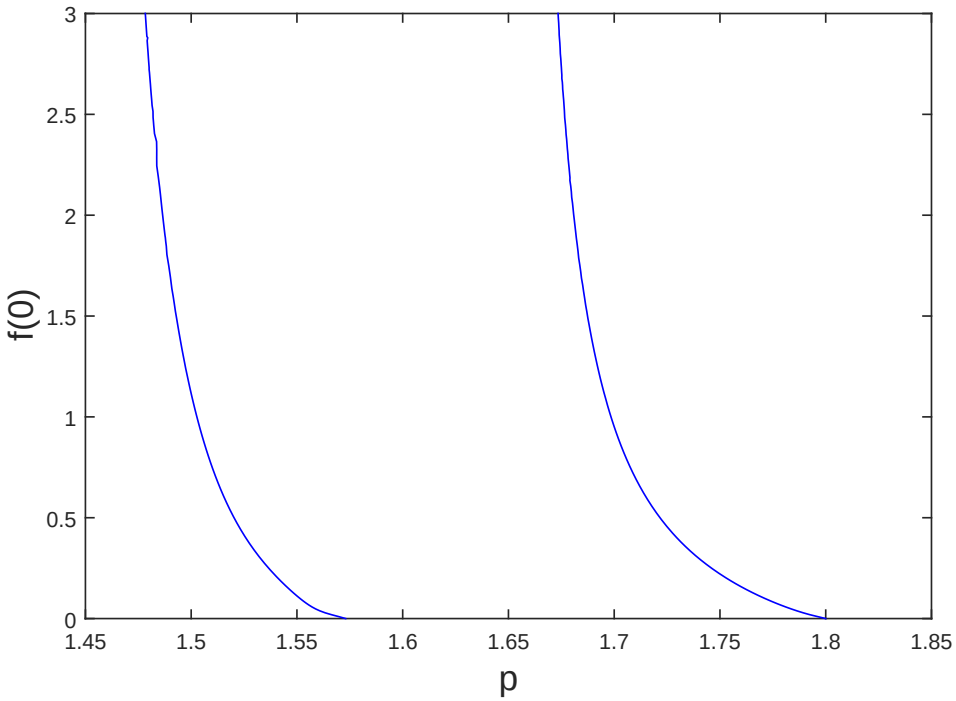

Figure 4-7: Branches of (even) solutions coming originating from p_l for $N = 3$.

to follow the branches and a certain amount of tinkering with parameters was required; what worked in some regions was ineffective in others.

4.2.5. Self-Similar Solutions via μ-bifurcation: We present an alternative branching method for locating solutions to (4.2.18) which can give additional insight into the problem, although the parameter space is large and our inability to ascertain global properties of branches leave us once again only able to adopt a numerical path-following approach. These branches prove easier to pick up with AUTO than the p-branches although we were still not able to follow them and BVPsuite's in-built path following routine was also somewhat effective although requiring good initial guesses.

This method was also used to supplement the investigation of the profiles in the pure-power law case in [81], and was the main tool that allowed the understanding of the multiplicity of blow-up solutions for the unstable version in [24], see comments in Section 2.3.8.

Our strategy is to replace the coefficient of the non-autonomous term by a

parameter μ. We introduce the operator

$$\mathbf{B}_\mu = \Delta^3 + \mu y \cdot \nabla + \frac{2}{3(p-1)}\mathbf{I}. \tag{4.2.46}$$

Then naturally solutions to (4.2.18) correspond to solutions of the equation

$$\mathbf{B}_\mu f + \Delta\left(|f|^{p-1}f\right) = 0 \quad \text{in} \quad \mathbb{R}^N. \tag{4.2.47}$$

for $\mu = 1/6$, where we impose that f has exponential decay. We will show that there are values of μ, dependent on p, where small solutions branch off from zero. Then if a branch crosses the critical μ-value we will have established the existence of an admissible self-similar profile.

Spectral information about $\mathbf{B}_\mu$ in L^2_ρ can be recovered from $\mathbf{B}$ using the scaling $z = (6\mu)^{1/6}y$, so that

$$\mathbf{B}_\mu = 6\mu\mathbf{B} + \left(-\mu N + \frac{2}{3(p-1)}\right)\mathbf{I} \implies \sigma(\mathbf{B}_\mu) = \left\{-\mu(N+l) + \frac{2}{3(p-1)}\right\}. \tag{4.2.48}$$

This suggests, the following proposition. Once again we use the theory as presented in [41] to establish the existence of bifurcation points μ_l rigorously.

Proposition 4.6. *If the l^{th} eigenvalue of $\mathbf{B}$, $\lambda_l = -l/6$, has odd multiplicity, then*

$$\mu_l = \frac{2}{3(N+l)(p-1)} \tag{4.2.49}$$

is a bifurcation point for (4.2.47).

Proof. Writing (4.2.47) as an integral equation in the z variable we find that

$$f = \mathbf{D}_\mu f = c_\mu \mathbf{C}^{-1} f - (6\mu)^{-2/3}\mathbf{C}^{-1}\Delta\left(|f|^{p-1}f\right), \quad \mathbf{C} = \mathbf{B} - \mathbf{I},$$

with $c_\mu = \frac{N}{6} - \frac{1}{9\mu(p-1)} - 1$. By Lemma 4.2 we have bifurcation when $1 \in \sigma\left(\mathbf{D}_\mu{}'(0)\right)$ with odd multiplicity.

Now,

$$\sigma\left(\mathbf{D}_\mu{}'(0)\right) = \sigma\left(c_\mu\mathbf{C}^{-1}\right) = \left\{\frac{3\mu(p-1)(N-6)-2}{3\mu(p-1)(6+l)},\ l = 0, 2, 1, \dots\right\}$$

and clearly the bifurcation criterion holds for the μ values (4.2.49), with the same caveats on multiplicity as Proposition 4.5. □

Another application of the Lyapunov-Schmidt procedure allows us to describe

local behaviour of the branches and solutions near the bifurcation points. Setting $\mu = \mu_l + \varepsilon$, we use the decomposition $f = C_l\psi_l + \sum_{j\neq l} C_j\psi_j$ and take the inner product with ψ_l^* to obtain

$$C_l\frac{(N+l)^2(p-1)\varepsilon}{4} = \left[\left(\frac{(N+l)(p-1)}{4}\right)^{2/3} - \frac{(N+l)^{5/3}(p-1)^{5/3}\varepsilon}{4^{2/3}}\right]\left\langle |f|^{p-1}f, \Delta\psi_l^*\right\rangle + \mathcal{O}(\varepsilon^2).$$

The second term in brackets on the right hand side only ends up manifesting at higher order when we solve for C_l, which gives us

$$C_l \approx \left(\left(\frac{p-1}{4}\right)^{1/3}(N+l)^{4/3}\frac{\sigma}{\kappa_l}(\mu-\mu_l)\right)^{1/(p-1)}, \quad \kappa_l = \left\langle |\psi_l|^{p-1}\psi_l, \Delta\psi_l^*\right\rangle.$$

The symbol σ can take the values 1 or -1 depending on the sign of $\mu - \mu_l$; the quantity in the brackets must be positive and so the sign of κ_l affects the direction of the bifurcation branch as before. Here $p > 1$ is not fixed and so estimating this sign *a priori* is even harder, though it can be calculated from the known values of the spectral pairs.

In the y variable, then, the solutions near a μ_l-bifurcation point have the form

$$f(y) = C_l\psi_l(6\mu_l y) + o(|\mu - \mu_l|).$$

Figure 4-8 shows the result of using BVPsuite's pathfollowing routine on the μ_2 branch starting from the approximation near $\mu_z > \frac{1}{6}$ to just past the critical $\mu = \frac{1}{6}$ value. Observe it crosses the critical value in agreement with the p_2 branch in Figure 4-5 at that value, and in fact the profiles generated by these two methods are identical. However, BVPsuite's solver struggled to progress much further than this.

We were able to find more structure with AUTO although this was still not foolproof. Figure 4-9 shows a typical example for $p = 89/60$, although we failed to resolve some branches to the left of the critical value at all. Those we did find (there are two, one very small to the right of the other just about visible in the diagram) formed homoclinic connections of the trivial solution, or closed loops. We suspect those we failed to find join with the large branches to the right of the critical value, which kept the same near vertical shape as far as we followed them ($f(0) \approx 50$). We do see the μ_6 branch cross the critical value generating a self-similar solution.

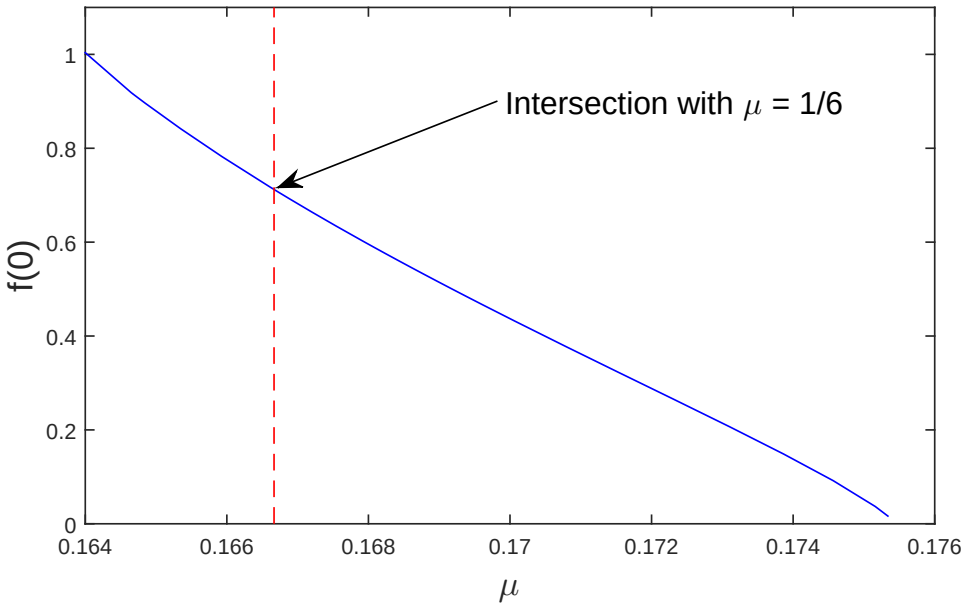

Figure 4-8: Branch of solutions coming from μ_2 for $p = 34/15$.

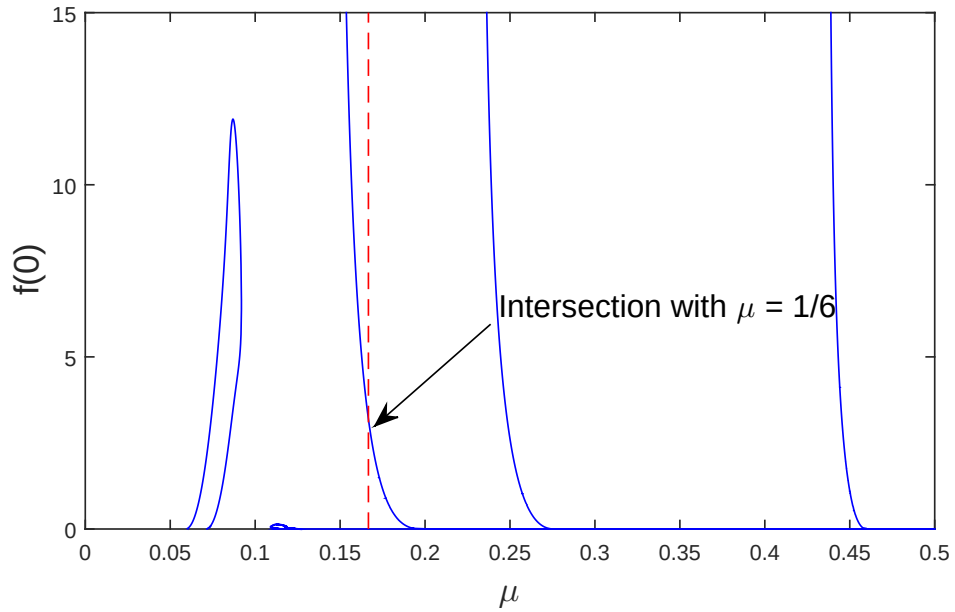

Figure 4-9: Branch of solutions coming from μ_2 for $p = 89/60$.

The p and μ bifurcation diagrams prompt the following conjecture:

Conjecture 4.7. *For* $1 < p < p_0$ *and* $p \neq 1 + \frac{4}{N}$, $p \neq 1 + \frac{4}{N+1}$ *there are* $\max\left\{l \,\middle|\, p < 1 + \frac{4}{N+2+l}\right\}$ *self-similar solutions of* (4.1.1).

The difference from [81] arises since the two conserved quantities of (4.1.1) generate two vertical branches of solutions, and the monotone decreasing (in p) behaviour of the branches that can give discrete families of solutions doesn't manifest until the second critical p value.

4.2.6. Aymptotic Behaviours on the centre manifold: We now briefly address another class of large t behaviour of (2.1.1) with exponential decay in the spatial domain. This is largely well known, see [82], and so we include it only as an overview for the sake of completeness. We once again focus on the simple eigenvalues case of the one dimensional or radial geometry.

In addition to being bifurcation points, the points (4.2.43) also mark p values where the operator $\mathbf{B}$ possesses a non-trivial centre subspace. We can pick up prospective centre manifold behaviour in the rescaled equation (4.2.41) by posing

$$\theta(y,\tau) = \alpha_l(\tau)\psi_l + \omega(\tau), \quad \omega(\tau) \in (E^c)^{\perp} = o(\alpha_l(\tau)),$$

where E^c denotes the centre subspace spanned by ψ_l. Using this expression in (4.2.41) and projecting onto E^c, we find that

$$\dot{\alpha}_l(\tau) = \kappa_l |\alpha|^{p_l - 1}\alpha(\tau)\left(1 + o(1)\right),$$

with κ_l as in (4.2.45). The right-hand side must be negative else it is well known that solutions of this ODE all blow up in finite time making this behaviour unstable. The values of κ_l we calculated above support this, and thus we do not expect this behaviour to occur in the unstable PDE studied in Chapter 2, as the sign of the nonlinearity is different.

We can easily calculate that

$$\alpha_l(\tau) = \pm A_l \tau^{-(N+l)/4}, \quad A_l = \left(\frac{N+l}{4}|\kappa_l|\right)^{-(N+l)/4},$$

giving us that in the non-rescaled variables we have the asymptotic centre manifold patterns

$$u(x,t) = \left(\frac{N+l}{4}|\kappa_l|\right)^{-(N+l)/4} t^{-(N+l)/6} \ln(t)^{-(N+l)/4}\left(\psi_l\left(xt^{-1/6}\right) + o(1)\right)$$

as $t \to \infty$. This log-corrected asymptotic behaviour is fairly common for parabolic PDE in certain regimes, see e.g. [111].

Moreover, for $p > p_l$ there exists a l-dimensional stable manifold on which solutions can evolve. The same process as above taking ψ_l as an eigenvector on the stable subspace of $\mathbf{B}+c_p\mathbf{I}$ yields the slightly more complicated Bernoulli-type differential equation for α_l:

$$\dot{\alpha}_l(\tau) = \left(-\frac{l}{6} + c_p\right)\alpha)l(\tau) + \kappa_l|\alpha|^{p_l-1}\alpha(\tau)\left(1+o(1)\right).$$

Nonetheless, this can be solved by standard methods to give

$$\alpha_l(\tau) = \pm\tilde{A}_l \exp\left(\frac{-(N+l)(p-p_l)}{6(p-1)}\tau\right)\left(1+o(1)\right).$$

$\tilde{A}_l$ is some constant. In the rescaled variables this translates to the asymptotic behaviour, as $\tau \to \infty$:

$$\theta(y,\tau) = \pm\tilde{A}_l \exp\left(\frac{-(N+l)(p-p_l)}{6(p-1)}\tau\right)\left(\psi_l(y)+o(1)\right).$$

This is permissible for any l such that $p > p_l$ and which, if any, of these behaviours manifest will depend on the initial data. For a more rigorous account than we've sketched out here, refer to [45].

We believe that this completes the description of all possible asymptotic behaviours of (4.1.1) when the initial data is exponentially decaying; it is certainly hard to see from where else others might arise. However, in the supercritical range, if we remove the restriction that the solution need be integrable, we encounter another wide class of asymptotic behaviours we shall briefly address.

4.2.7. Algebraically decaying profiles in the supercritical range: For any $p > 1$, possible self-similar solutions of (4.1.1) with the algebraic decay (2.2.29)

$$f(y) \sim Ay^{-4/(p-1)}, \tag{4.2.50}$$

as $y \to \infty$ in the rescaled coordinates cannot be in L^2_ρ and so will not appear in the dynamics for the class of initial data we have considered until now. However, we can adapt a result from [81], Chapter 8 to show that if they exist they can attract solutions satisfying a (quite strong) property.

We denote by $u_S(x,t) = (1+t)^{-2/3(p-1)}f(x(1+t)^{1/6})$ a self-similar solution of (4.1.1) with decay (4.2.50). Then,

Proposition 4.8. *If* $u(x,t) = (1+t)^{-2/3(p-1)}V(x(1+t)^{1/6},t)$ *is a solution of* (4.1.1) *such that* $||u-u_S||_{H^3} < \infty$ *for all* $t > 0$*, then* $p > 1+\frac{8}{N} \implies ||V-f||_{L^2} \to 0$ *as* $t \to \infty$*.*

Proof. We can derive an L^2 bound for the difference $w = u - u_S$ by multiplying it with its equation and integrating over $\mathbb{R}^N$, yielding

$$\frac{1}{2}\frac{\mathrm{d}}{\mathrm{d}t}||w||_{L^2}^2 = -\int_{\mathbb{R}^n} (\nabla\Delta w)^2 \,\mathrm{d}x + \left\langle \Delta\left(|u|^{p-1}u - |u_S|^{p-1}u_S\right), u - u_S \right\rangle \leq 0.$$

That the second term in the middle expression is non-positive can be shown by integrating by parts once and applying Hadamard's lemma $|u|^{p-1}u - |u_S|^{p-1}u_S = (u-u_S)p\int_0^1 |su+(1-s)u_S|^{p-1}\,\mathrm{d}s$. Hence by assumption w is uniformly bounded in L^2 and, by scaling, $||w||_{L^2}^2 = ||u-u_S||_{L^2}^2 = (1+t)^{-4/3(p-1)+N/6}||V-f||_{L^2}^2 \leq C$ for all time. However, for $p > 1+\frac{8}{N}$, $(1+t)^{-4/3(p-1)+N/6} \to \infty$ as $t \to \infty$ and so the proposition must hold. □

This gives only a flavour of these kind of convergence results and we suspect hypotheses on p and u might be weakened by working carefully with the integral equation (4.1.11). We leave this for future work.

Perhaps not surprisingly, a very wide class of self-similar solutions with non-trivial A as in (4.2.50) exist. Unlike for the unstable PDE, solutions exist globally even for large initial data and so even for large A we have been able to construct self-similar profiles numerically. Indeed, even imposing different values of A as $y \to \pm\infty$ has not been an impediment. Were shooting arguments possible, we could justify these apparently continuous branches simply by having more parameters available to describe the $y \to \infty$ behaviour than are required to shoot for any solutions decaying correctly as $y \to \infty$. It seems in some way this structure remains.

We round off this section with an example of such a profile for $N = 1$, $p = 7$ shown in Figure 4-10.

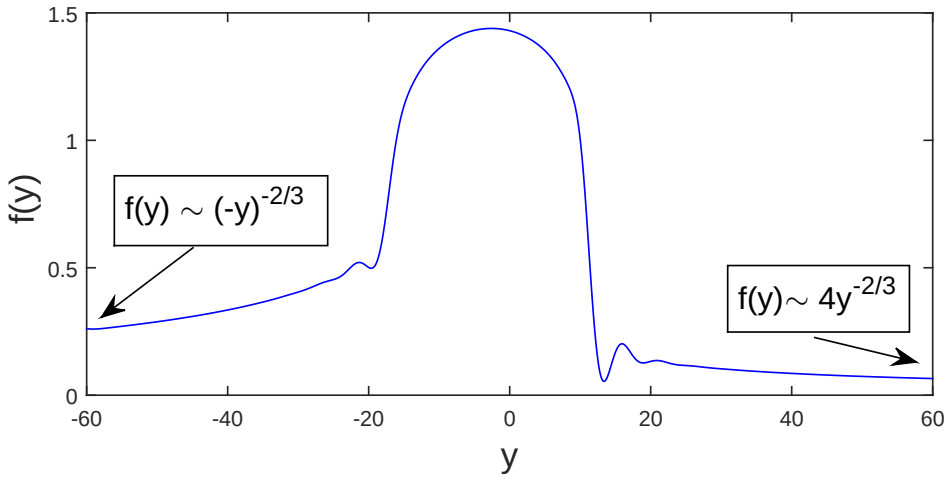

Figure 4-10: A non-symmetric self-similar profile with algebraic decay

Chapter 5

Cahn-Hiliard Equation with a Fourth Order Nonlinearity

5.1. Preliminaries

Equations involving the fourth order nonlinear term $\Delta^2|u|^{p-1}u$ are less common in the literature than the second order equivalent $\Delta|u|^{p-1}u$. It can be considered as a different generalization of the Porous Medium equation (1.2.17) than the better understood Thin Film equation (1.2.18); we refer to [69] as one of the relatively few serious studies of it. While the regularizing affect of including the higher order Δ^3 operator negates some of the more difficult features of the pure fourth order Porous Medium equation, e.g. oscillatory finite interfaces, it still makes many aspects of the analysis much harder compared to the second order nonlinearities considered in Chapters 2 and 4. Indeed, while some analysis carries over from the simpler cases without many changes, we have made only preliminary progress in understanding those areas where this case differs, and we rely even more heavily on numerics to guide us. While shallow, these results are nonetheless an intriguing glimpse into the the range of behaviours higher order equations can possess. We focus only on the $N = 1$ case as we found higher dimensions almost intractable numerically.

For convenience, we collapse our study of the stable and unstable versions into one chapter. Thus, we consider

$$\begin{aligned} u_t = \Delta^3 u \pm \Delta^2\left(|u|^{p-1}u\right) \quad \text{in} \quad \mathbb{R}_+ \times \mathbb{R}^n, \\ u(x,0) = u_0(x), \end{aligned} \tag{5.1.1}$$

where the '+' case makes the nonlinearity destabilizing and we expect solutions

can blow-up in finite time or exist globally, and the '-' case has solutions that are global in time for any reasonable class of initial data. We will not consider more abstract questions like e.g. the effects different functional settings have on the problem, focusing almost entirely on the self-similar solutions, the importance of which cannot be overstated. However, we do turn up some interesting non-existence/instability results in the blow-up case. The assumption that $u_0 \to 0$ as $x \to \infty$ 'sufficiently quickly' will be more than enough for our purposes.

We remind ourselves that in the '+' case, blow-up can easily be seen to occur by writing the equation as the pseudo-parabolic equation

$$\left((-\Delta)^{-1}\right)^2 u_t = \Delta u + |u|^{p-1}u,$$

which is in the form (1.2.25), and so Levine's concavity method provides that blow-up occurs for initial data u_0 satisfying

$$\frac{1}{2}||\nabla u_0||_{L^2}^2 - \frac{1}{p+1}||u_0||_{L^{p+1}}^{p+1} < 0.$$

Moreover, the pseudo-parabolic form can be used to demonstrate that (5.1.1) is a gradient system in H^{-2} which gives a number of strong results on local existence of weak solutions and, in the '-' case, the coercivity extends this to global existence, see Chapter 4 Section 1. Finally, the integral equation equivalent to (5.1.1)

$$u(x,t) = b(t) * u_0 \pm \int_0^t \Delta^2 b(t-s) * |u|^{p-1}u(s)\mathrm{d}s,$$

where $b(x,t)$ is the fundamental solution of (1.3.36) can be used to establish local existence of classical solutions; potential issues with regularity due to the $\Delta^2|u|^{p-1}u$ term demanding higher derivatives of a not-necessarily-regular function (especially for $p < 4$ where the term can become singular) are resolved by the smoothness of b. However, this may in part contribute to the difficulties for smaller $p = 1$ with the elliptic equation determining self-similar solutions (5.1.4) for which this interpretation of solutions is unavailable.

5.1.1. Similarity Solutions: Proceeding in the same way as in section 2.2.2, we perform the scalings

$$x = \lambda_1 \bar{x}, \quad t = \lambda_2 \bar{t}, \quad u = \lambda_3 \bar{u},$$

which give the rescaled equation

$$\frac{\lambda_3}{\lambda_2}\bar{u}_{\bar{t}} = \frac{\lambda_3}{\lambda_1^6}\bar{\Delta}^3\bar{u} \pm \frac{\lambda_3^p}{\lambda_1^4}\bar{\Delta}^2\left(|\bar{u}|^{p-1}\bar{u}\right), \tag{5.1.2}$$

suggesting that for invariance, we require $\lambda_1 = \lambda_2^{\frac{1}{6}}$ and $\lambda_3 = \lambda_2^{-\frac{1}{3(p-1)}}$, giving the desired one-parameter family of scalings

$$u(x,t) = [\sigma(T-t)]^{-1/(3(p-1))}\theta(y,\tau), \quad y = x[\sigma(T-t)]^{-\frac{1}{6}}, \quad \tau = -\sigma\ln([\sigma(T-t)]),$$

where θ satisfies

$$\theta_\tau = \mathbf{A_4}(\theta) = \Delta^3\theta \pm \Delta^2\left(|\theta|^{p-1}\theta\right) - \frac{\sigma}{6}y\cdot\nabla\theta - \frac{\sigma}{3(p-1)}\theta, \tag{5.1.3}$$

with $\sigma = 1$ in the case where solutions blow up and $\sigma = -1$, $T = 0$ for global solutions. Of course, for the stable PDE with the negative sign, only the latter can occur.

The stationary solutions of this equation correspond to the self-similar solutions of (5.1.1),

$$u_S(x,t) = [\sigma(T-t)]^{-1/(3(p-1))}f(y),$$

which are independent of τ solutions of the elliptic equation

$$\mathbf{A_4}(f) = 0 \quad \text{in } \mathbb{R}^N. \tag{5.1.4}$$

Again, we seek radially symmetric, integrable solutions by imposing the boundary conditions

$$f'(0) = f'''(0) = f^{(\mathrm{v})}(0) = 0, \qquad f(y) \to 0 \quad as \quad y \to \infty, \tag{5.1.5}$$

And so (5.1.4) is a sixth order ODE.

(5.1.1) is conservative as long as u decays quickly enough to zero as $x \to \infty$. (5.1.3) does not necessarily have this property, but we can see from taking the time derivative of the identity

$$\int_{\mathbb{R}^N} u_S(x,t)\mathrm{d}x = [\sigma(T-t)]^{-1/(3(p-1))+N/6}\int_{\mathbb{R}^N} f(y)\mathrm{d}y,$$

that the property will hold for integrable solutions either if

$$p = p_0 = 1 + \frac{2}{N}, \tag{5.1.6}$$

or $\int_{\mathbb{R}^N} f(y)\mathrm{d}y = 0$. As such, only solutions of (5.1.1) with zero mass are described by self-similar profiles unless p takes the critical value p_0. See Section 2.3.1 for further comments.

5.1.2. WKBJ analysis of the Similarity Profiles as $y \to \infty$: The large-y behaviour of the similarity profiles can be established in the same manner as in Section 2.2.4; the linearization of (2.2.15) and (5.1.4) differ only in the coefficient of the last term and so we only sketch the arguments here. We apply the WKBJ method in the appropriate regime (y large and f small) to the linearization of (5.1.4) in radial coordinates around the zero solution:

$$\begin{aligned}\mathbf{A_4}'(0)f = f^{(\mathrm{vi})} + \frac{3(N-1)}{y}f^{(\mathrm{v})} + \frac{3(N-1)(N-3)}{y^2}f^{(\mathrm{iv})} + \\ \frac{(N-1)(N-3)(N-8)}{y^3}f''' - \frac{3(N-1)(N-3)(N-5)}{y^4}f'' + \\ \frac{3(N-1)(N-3)(N-5)}{y^5}f' - \frac{\sigma}{6}yf' - \frac{\sigma}{3(p-1)}f = 0. \quad (5.1.7)\end{aligned}$$

Note the similarity with (2.2.19). We introduce a small parameter via the scaling $Y = \theta y$, $\theta \ll 1$ and expand via the ansatz

$$f(Y) \sim \exp\,[\frac{1}{\delta}\sum_{n=0}^{\infty}\delta^n g_n(Y)].$$

Here, we again find the θ-δ balance is found for $\theta = \delta^{5/6}$, so the leading order behaviour is governed by the relationship between the $g_0^{(\mathrm{vi})}$ and the $-\frac{\sigma}{6}Yg_0'$ terms at $\mathcal{O}(\delta^{-1})$, giving

$$g_0(Y) = \beta(\sigma)^{1/5}Y^{6/5},$$

where $\beta = 5/6^{6/5}$. This means that to leading order, we have

$$f(y) = C\exp\,(\beta\sigma^{1/5}y^{6/5})(1 + o(1)) \quad \text{as} \quad y \to \infty \qquad (5.1.8)$$

and so the exponential-type controlling factor is identical to the earlier case (2.2.25).

Again, we seek only integrable profiles (which correspond to viable solutions of (5.1.1) and so we must have $\mathrm{Re}\,(\sigma^{1/5}) < 0$. As such we can conclude that (5.1.7) has

- a three dimensional stable exponential bundle for the global case $\sigma = -1$;

- a two dimensional stable exponential bundle for the blow-up case $\sigma = 1$.

The term at the next order down, $\mathcal{O}(1)$, is slightly different. The balance here is

$$\frac{5}{6}Yg_1' + \frac{N}{2} - \frac{1}{3(p-1)} = 0,$$

giving that

$$g_1(Y) = -\frac{3}{5}\left(N - \frac{2}{3(p-1)}\right)\ln(Y),$$

up to a constant term.

Therefore, the full leading order exponentially decaying behaviour is given by

$$f(y) = \sum_{\mathrm{Re}(\sigma^{1/5})<0} C_\sigma y^{(-3/5)(N-2/(3(p-1)))} \exp(\beta\sigma^{1/5}y^{6/5})(1+o(1)) \quad \text{as} \quad y \to \infty, \tag{5.1.9}$$

where the C_σ are unknown constants.

We also pick up an algebraic mode of decay from the balance $-\frac{\sigma}{6}yf' \sim \frac{\sigma}{3(p-1)}f$, which gives that f can have the form

$$f(y) = A|y|^{-2/(p-1)}(1+o(1)) \text{ as } y \to \infty. \tag{5.1.10}$$

As in Chapter 2, the requirement that f be integrable imposes that $A = 0$ for $p = p_0$.

5.2. Blow-up Solutions

5.2.1. The p_0 critical case: For the rest of the chapter, we focus exclusively on the $N = 1$ case. Now, the p_0 critical serves as a good entry point for our analysis since we can integrate up (5.1.4) once to derive an ODE with only three terms:

$$f^{(\mathrm{v})} + (f^3)''' - \frac{1}{6}yf = 0, \tag{5.2.11}$$

with symmetric boundary conditions at $y = 0$:

$$f'(0) = f'''(0) = 0, \tag{5.2.12}$$

and a two-parameter asymptotic bundle (5.1.9), which becomes:

$$f(y) \sim Cy^{-2/5}\exp(ay^{6/5}) \cdot \cos(by^{6/5} + k), \tag{5.2.13}$$

where C, k are our parameters and $a = (5/6^{6/5})\cos(\frac{4}{5}\pi)$, $b = (5/6^{6/5})\sin(\frac{4}{5}\pi)$. We take this (and four derivatives at y sufficiently large for carrying out the shooting procedure numerically) as initial data for some y sufficiently large and then shoot to pick up symmetry conditions at the origin, more precisely, we attempt to identify all pairs (C, k) such that $f(y; C, k)$ satisfies (5.2.11) with asymptotic behaviour (5.2.13) and the functions

$$R(C, k) = f'(0; C, k) = 0,$$

and

$$S(C, k) = f'''(0; C, k) = 0.$$

The analytic dependence of R and S on C and k can be proved by a similar method as in Section 2.3.2, and Lemma 2.2 can be applied directly to (5.2.11) after suitable rescaling in the $C \to 0$ limit.

The most significant qualitative difference between this shooting problem and the one stemming from the PDE with the second order nonlinearity considered in Chapter 2 is that now the shooting profiles exist globally in y for any C and k combination. There is no mechanism for singularity formation, since the leading order behaviour for large f is given by

$$f^{(\mathrm{v})}(y) = -(f^3(y))'''(1 + o(1)),$$

which does not admit blow-up solutions, hence $f(y; C, k)$ is well defined for all $y \in \mathbb{R}^N$ independent of the choice of $C \in \mathbb{R}_+$ and $k \in [0, 2\pi]$. This really presents a further complication, as it is less obvious how to restrict our search to a more manageable subset of the entire C, k space. It does turn out this is possible in much the same way as before, but our justification is entirely empirical.

5.2.2. Numerical Investigation of the Blow-up Profiles: Figure 5.2.2 shows quantity $\sqrt{f'(0; C, k)^2 + f'''(0; C, k)^2}$ for $C \in [0, 2]$ and $k \in [0, 2\pi]$. The minimum corresponding to the first (positive) admissible even blow-up profile can be seen at $C = 1.90...$, $k = 3.34...$. However, it is impractical to continue this computation for larger values of C, since the the surface can change so quickly that very fine resolution is required to detect its zeroes.

However, we once again find that for each C we can narrow down the range of k for which even solutions can possibly occur to only two values exactly π apart (corresponding to f and $-f$) by constructing a 'maximally oscillatory' profile as

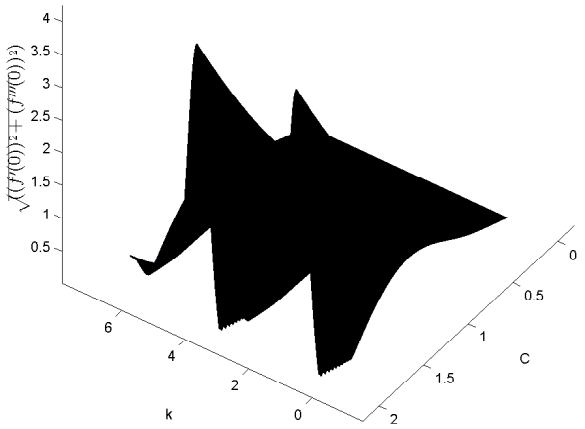

Figure 5-1: C, k dependence of normed odd derivatives of f at zero.

a separatrix. Here we mean oscillatory in the sense of having infinitely many zeros for $y < 0$ rather than merely sequences of alternating local maxima and minima, which occurs for any k.

To elaborate, we find that the generic behavior of $f(y; C, k)$ as $y \to -\infty$ is an asymptotically monotone growing/decreasing profile generated by the balance between the last two terms of (5.2.11) with damped oscillations about it. The presence of the $(f^3)'''$ term means that no exact solutions of even the asymptotic simplifications seems possible, without which a proper understanding cannot really be achieved and it does not seem tractable to even narrow down potential behaviours. This difficulty plagues all our attempts at analyzing (5.2.11) and all related equations stemming from (5.1.4); see further comments in the next section. We reiterate that the description we give here is merely what has been observed, although we have seen no deviations from it whatsoever over a wide range of experiments.

The asymptotic sign of these generic profiles changes only twice as k goes from 0 to 2π, and at these values of k we observe the appearance of 'maximally oscillatory' solutions described by the full balance between the three terms of (5.2.11). In general, these have (increasing as $y \to \infty$) amplitude function parameterized by $C(k)$, and the even blow-up profiles will be exactly the ones

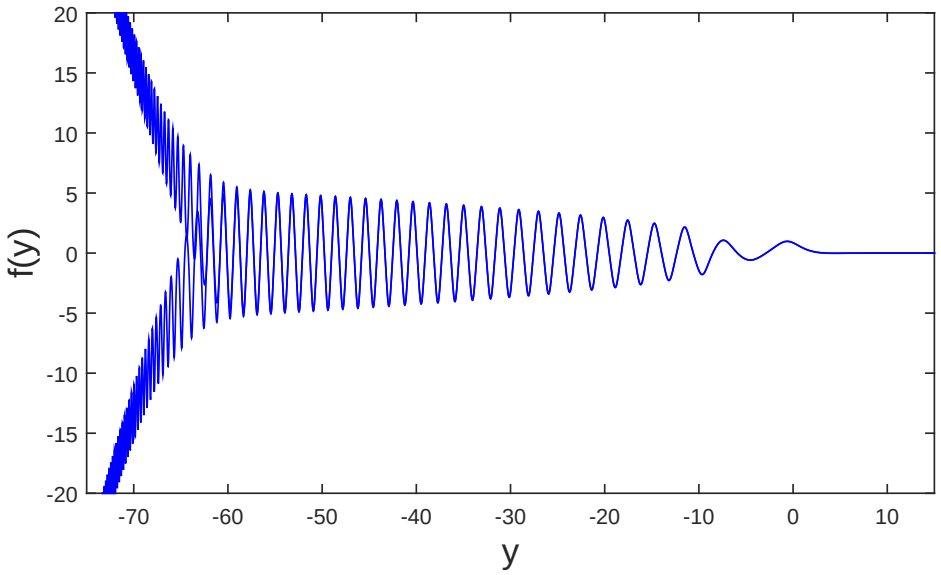

Figure 5-2: Constructing the maximally oscillatory profile for $C = 1$ as a separatrix.

where this amplitude function is identically zero $\iff$ $f'(0) = f'''(0) = 0$ and the behaviour as $y \to \infty$ is instead given by the reflection of (5.2.13). There is a direct analogy with the separatrix construction given in Chapter 2, except instead of the asymptotic signs of singularities that profiles develop we look instead at asymptotic signs of globally existent profiles in a different limit. This process is illustrated for two values of k to within 10^{-14} of the value giving a maximally oscillatory profile in Figure 5.2.2, one too large and the other too small. Observe how they follow the maximally oscillatory profile for along way before diverging to the growing/decreasing behaviours.

We can iterate this procedure for selected values of C to look for profiles with the correct symmetry conditions at $y = 0$. This is shown in Figure 5-3, where we have plotted $\arctan(f'(0;, C(k), k))$ and $\arctan(f'''(0; C(k), k))$ for the values of k established as above. We choose to present the results in this way since $f'''(0; C(k), k)$ quickly becomes much larger than $f'(0; C(k), k)$ and so compression of the ranges is required to see both simultaneously. The distortion for large values this causes is not particularly an issue since it is when these quantities are both zero that concerns us. It is immediately obvious how much less regular they are than the equivalent quantities for (2.3.35) shown in Figure 2-4. However, we again have the beginning of what proves to be a countable, discrete set of solutions of (5.2.11) as both intersect at every zero of either. Once again, if we denote the minimal profile by f_1, which is shown in Figure 5-4, then

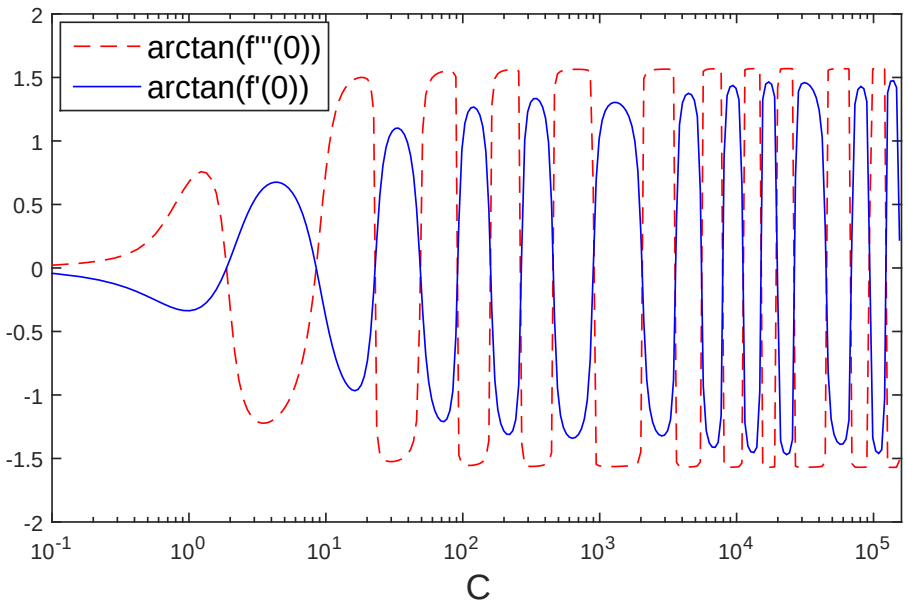

Figure 5-3: C-Dependence of symmetry conditions for the most oscillatory solution.

each new profile f_k is characterized by having precisely k local extremal points in the interval $[0, y_0]$, where here we use y_0 to denote the first zero of f. As in Chapter 2, the profiles presented here are the result of using the profiles gained by numerically shooting with ODE15s as initial guesses in the BVPsuite solver for enhanced accuracy. Figures 5-5-5-7 show profiles f_2 to f_4. However, we also find as C increases that more than one extremal point appear occurs between y_0 and y_1, the second zero of f, which is a new phenomenon not observed for (2.3.35) or indeed for self-similar solutions of (2.1.1) for any $p > 1$. The appearance of these extra 'humps' correlates with the wider gaps between consecutive profiles in Figure 5-3, though we have not been able to establish any pattern that might be able to predict when they appear.

Figures 5-8–5-9 detail the 20th and 21st profiles respectively, both showing three extra humps for negative f before the large y behaviour (5.2.13) dominates. These are the last two we managed to detect by this method within Matlab's default working precision. Continuing the pattern numerically with higher precision libraries should have high priority for future work. We include an example of a non-symmetric profile with very large C in Figure 5-10 to illustrate the complicated, oscillatory-on-multiple-scales structure the solutions take on in this regime, suggesting that the three region asymptotic regime for $C \to \infty$ discussed in Section 2.3.3 for (2.3.35) will not generalize easily to (5.2.11) and multiple rounds

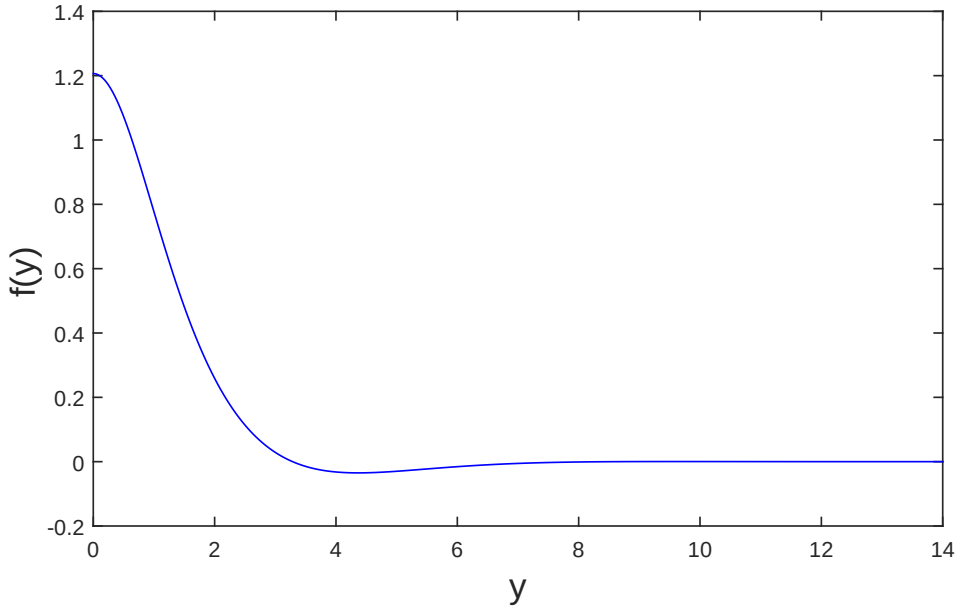

Figure 5-4: The first even blow-up profile.

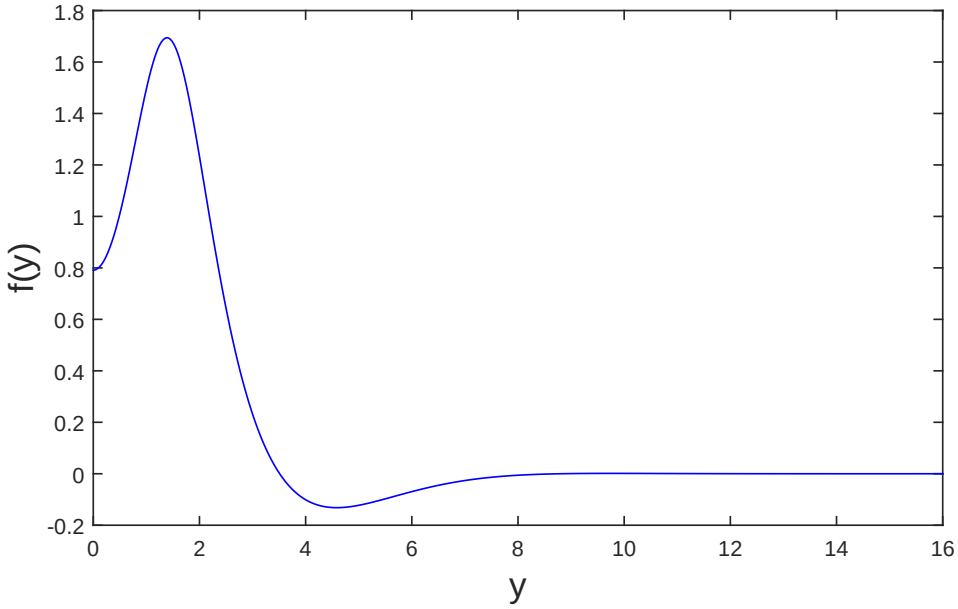

Figure 5-5: Profile f_2.

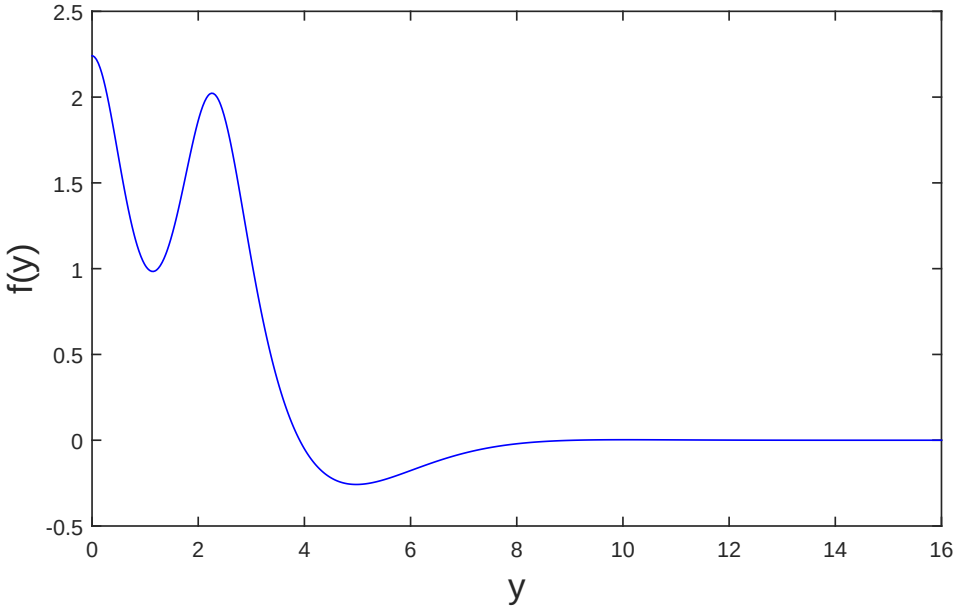

Figure 5-6: Profile f_3.

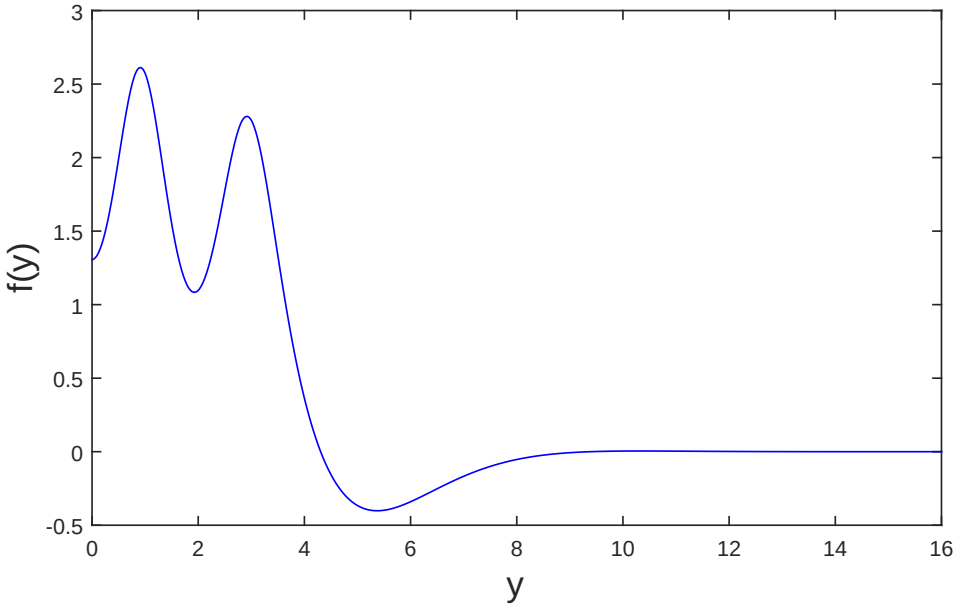

Figure 5-7: Profile f_4.

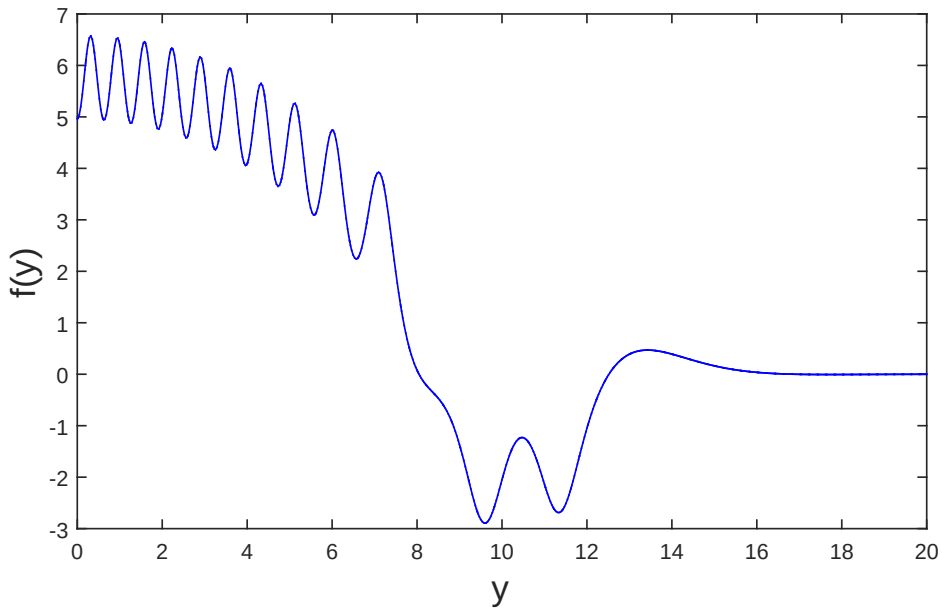

Figure 5-8: Profile f_{20}.

of matching will be required if the approach can be made to work at all. We lay some groundwork for this enterprise in the next section, highlighting some of the problems that will have to be overcome for a proper understanding of this problem to be attained.

5.2.3. Towards an asymptotic construction of a countable set of similarity solutions: We now explore the possibility of applying the procedure that so successfully allowed us to describe solutions to the critical similarity ODEs for (1.1.9), see [56], Chapter 4, and (2.1.1) earlier in this thesis.

We recast (5.2.11) as a singular perturbation problem using the scalings

$$f(y) = ag(z), \qquad y = a^{\frac{1}{2}}z,$$

which gives the equation

$$\varepsilon g^{(\mathrm{v})}(z) + (g^3(z))''' - \frac{1}{6}zg(z) = 0, \quad g(0) = 1, \quad g'(0) = g'''(0) = 0,$$

Where $\varepsilon = a^{-3} << 0$ for C large.

The unperturbed problem is then a third order ODE:

$$(g_0^3(z))''' = \frac{1}{6}zg_0(z), \quad g(0) = 1,\ g'(0) = 0. \tag{5.2.14}$$

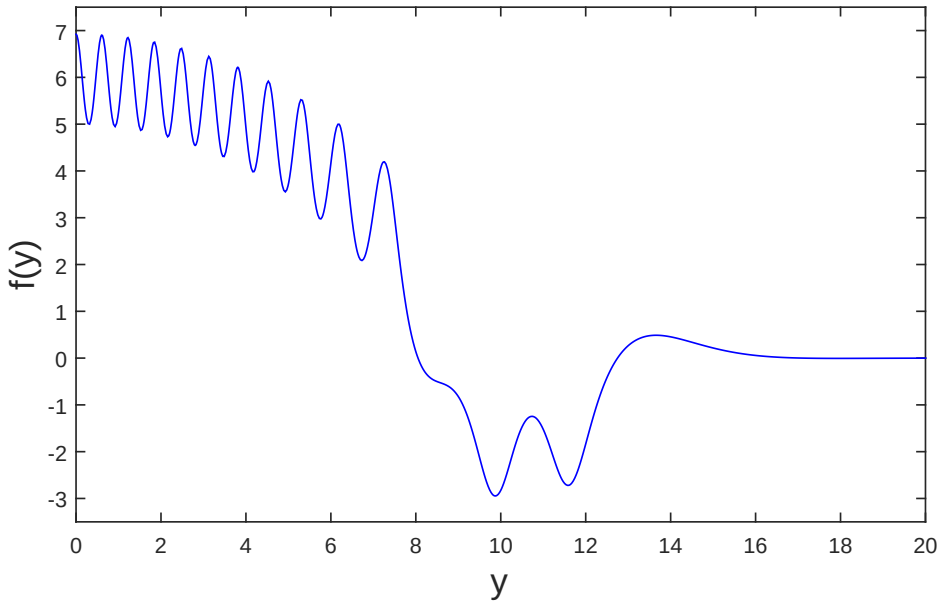

Figure 5-9: Profile f_{21}.

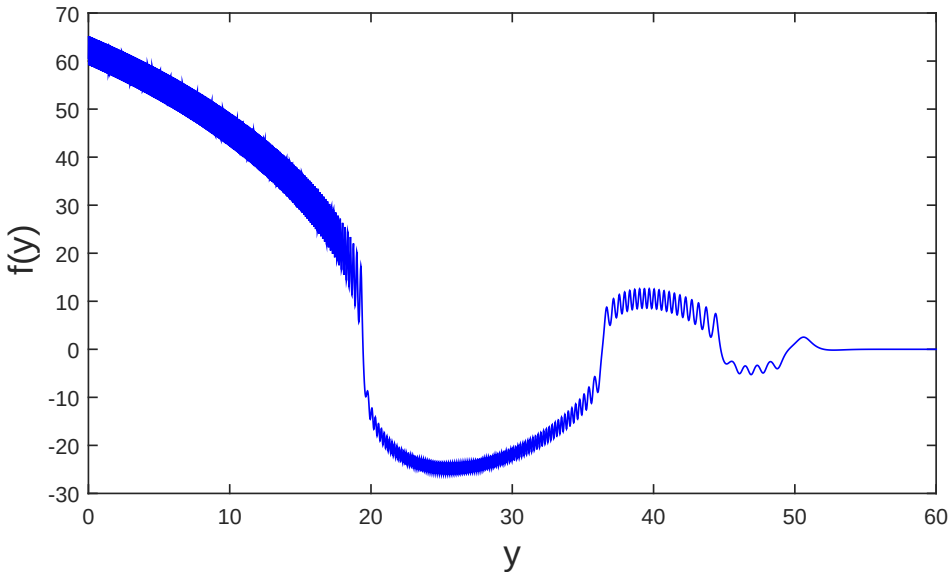

Figure 5-10: A (non-symmetric) shooting profile with $C = 10^{24}$, $k = 0$.

This does not have an exact solution, and moreover the problem seems to be under determined lacking an obvious specification for $g_0''(0)$. This presents a significant difficulty in the construction and accounts for the more complicated behaviour observed in the numerics. It is clear that there will have to be a finite $z_0 > 0$ such that $g_0(z_0) = 0$ in order for this to correspond to a blow-up profile with eventual exponential decay. Using the substitution $g_0 = G_0^{1/3}$ so that (5.2.14) becomes

$$G_0''' = \frac{1}{6} z G_0^{1/3},$$

it is clear that this will occur for sufficiently large (negative) $g''(0)$. However, z_0 will not be fixed and will have to be determined by the matching. Moreover, the numerical profiles for large C, see Figure 5-10, suggest that after this first zero, there may be further regions where the solution is still large and not described by (5.2.13) the comprise additional matching regions. This will necessitate studying (5.2.14) starting at z_0 with conditions $g(z_0) = 0$, $g'(z_0)$ and $g''(z_0)$ to be determined. These values will be fixed according to conditions on g_0 at a second point $z_1 > z_0$ where the solution again crosses zero, followed by a perhaps arbitrarily large sequence of subsequent zeros at which subsequent outer regions can be matched, before a final matching region between an outer solution and the fair field behaviour (5.2.13).

We stress that this is conjecture and we have not been able to determine if this scenario occurs. It may be, for example, that the number of outer regions is finite. Regardless, it does seem we will be required to carry information across multiple matching regions in in which all solutions will be described by difficult nonlinear ODEs.

We are able to describe possible behaviours of g_0 near z_0, although in fact this will apply to any subsequent non-far-field zero of g as well. We pose $g_0(z) \sim A(z_0 - z)^q$ as $z \to z_0$ and substitute into (5.2.14):

$$-A^3 3q(3q-1)(3q-2)(z_0 - z)^{3q-3} \approx \frac{1}{6} A z_0 (z_0 - z)^q,$$

which gives us three possible values of q. If the equation is non-degenerate, then we can equate powers of $(z_0 - z)$ to get $q = 3/2$. However, two alternative, degenerate possibilities exist for $q = 1/3$ or $q = 2/3$. We can conclude that

depending on z_0, we have one of

$$\begin{aligned} g_0(z) &\sim A_0(z_0 - z)^{3/2}, \\ g_0(z) &\sim A_1(z_0 - z)^{1/3} + B_1(z_0 - z)^{10/3}, \text{ or} \\ g_0(z) &\sim A_2(z_0 - z)^{2/3} + B_2(z_0 - z)^{11/3}. \end{aligned} \tag{5.2.15}$$

Which of these occurs will have to be determined via matching.

We can begin to see how each of these behaviours interact with the matching region by zooming in around z_0 via the scalings

$$z = z_0 + \varepsilon^{1/5}\bar{z}, \quad g = \varepsilon^{3/10}R.$$

We thus find that the governing behaviour there is dictated by the equation

$$R^{(\mathrm{v})} + (R^3)''' - \frac{1}{6}(z_0 + \varepsilon^{1/5}\bar{z})R = 0.$$

Matching then requires looking a the limits of large $\bar{z}$ and $-\bar{z}$, although it is clear this remains a difficult problem. We leave our exploration at this point, although we suggest that this would be an extremely interesting, though challenging, near-term research problem.

5.2.4. Solutions for general p: (5.1.1) preserves four quantities during the flow: the mass and the first three moments $\frac{\mathrm{d}}{\mathrm{d}t}\int x^l u \mathrm{d}x = 0$, $l = 0, \ldots, 3$. For the rescaled equation (5.1.3), this only holds for certain values of $p = p_l$, suggesting that only at these values can the self-similar solutions have non-trivial lth moment. If u is exactly self-similar, then we have

$$\frac{\mathrm{d}}{\mathrm{d}t}\int_{\mathbb{R}^N} x^l u \mathrm{d}x = \left(-\frac{1}{3(p-1)} + \frac{N+l}{6}\right)(T-t)^{-1/3(p-1)+(N+l)/6-1}\int_{\mathbb{R}^N} y^l f(y)\mathrm{d}y = 0.$$

Thus, we conclude that $\int_{\mathbb{R}^N} y^l f(y)\mathrm{d}y \equiv 0$ unless $p = p_l = 1 + \frac{2}{N+l}$. Note that these are the first four p-bifurcation points (5.3.19) where non-trivial spreading solutions branch from the trivial solution.

The first moment case $p = p_1$ has a clear analogue with the equation considered in Section 2.3.5. As there, we can multiply (5.1.4) with y and integrate to obtain the equation

$$yf^{(\mathrm{v})} - f^{(\mathrm{iv})} + y\left(|f|f\right)''' - \left(|f|f\right)'' - \frac{1}{6}y^2 f = -f^{(\mathrm{iv})}(0) - \left(|f|f\right)''(0) = \frac{1}{6}A, \tag{5.2.16}$$

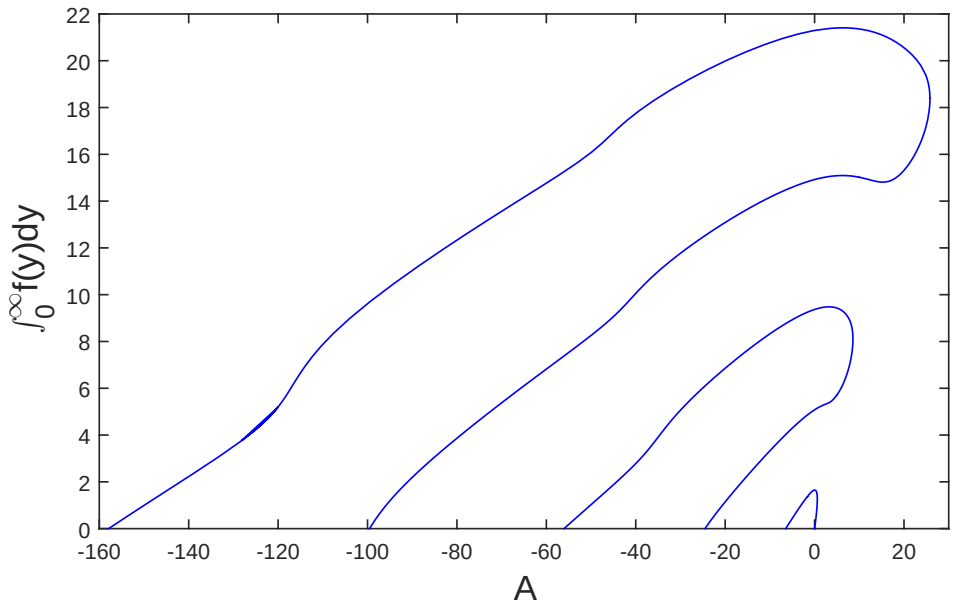

Figure 5-11: Continuation in A of candidate even solutions against mass for $p = p_1$.

where A is the coefficient of algebraic decay from (5.1.10), here having the form $f(y) \sim Ay^{-2}$ as $y \to \infty$.

The equivalent of Lemma 2.4 holds and we can find even solutions of (5.2.16) by solving the equation with $f'(0) = f'''(0) = 0$ and following the solutions in A until we find arrive at one with zero mass. These branches are shown in Figure 5-11 and the corresponding zero mass solutions in Figure 5-12. The qualitative aspects of this problem do not differ significantly from those set out in Section 2.3.5, so we refer the reader to there for details, only drawing attention to the emergence of extra humps for $f < 0$ that do not appear in Figure 2.3.5.

The third moment case $p = p_3$ is more novel. Now, we multiply (5.1.4) with y^3 and integrate to obtain the equation

$$y^3 f^{(\mathrm{v})} - 3y^2 f^{(\mathrm{iv})} + 6yf''' - 6f'' + y^3 \left(|f|f\right)''' - 3y^2 \left(|f|f\right)'' + 6y \left(|f|f\right)' - 6 \left(|f|f\right) - \frac{1}{6} y^4 f = -6f''(0) - 6 \left(|f|f\right)(0) = -\frac{1}{6} A.$$

To find solutions of this equation, with the algebraic decay $f(y) \sim Ay^{-4}$, we repeat the procedure outlined above and more extensively in Section 2.3.5. The result of starting from $A = 0$ and decrementing is shown in Figure 5-13. The branch clearly intersects the zero mass line at $A \approx -1.7$, and the corresponding

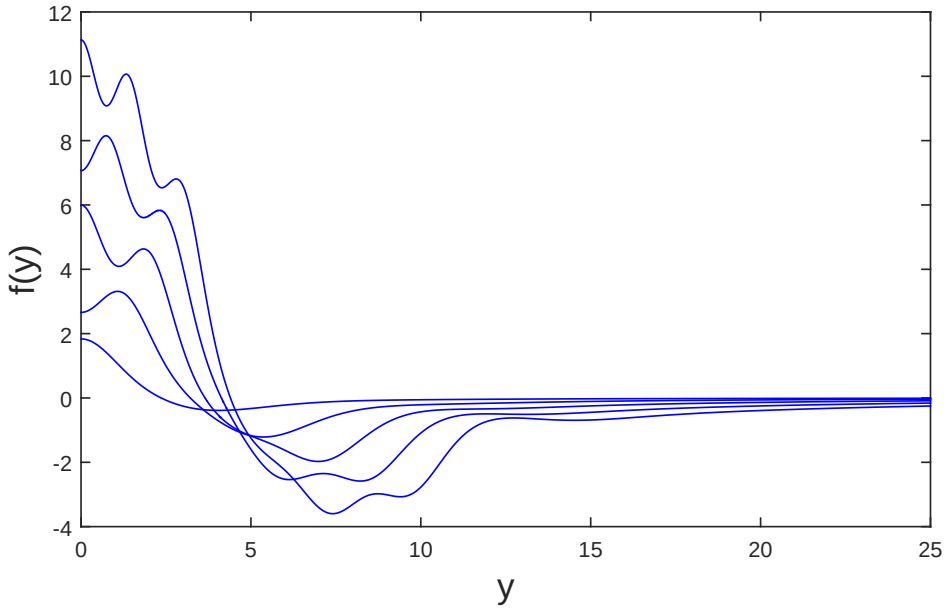

Figure 5-12: Admissible even blow up profiles for $p = p_1$.

profile in shown in Figure 5-14. However, we find this a bit suspicious; in order for the BVPsuite solver to converge even for very small values of A, we used the regularization

$$|f(y)|^{p-1} f(y) \to \left(f(y)^2 + \varepsilon^2\right)^{(p-1)/2} f(y), \quad \varepsilon = 10^{-4}, \tag{5.2.17}$$

and the regularizing parameter is only one order of magnitude smaller than the solution itself. Further investigation is needed to determine whether this profile is a genuine solution of (5.1.4) or a spurious result of our approximation of the problem.

For $p = p_2$ we conjecture the following, surprising negative result:

Proposition 5.1. *There do not exist even, integrable solutions of* (5.1.4) *for* $N = 1$, $p = p_2 = \frac{5}{3}$.

Our evidence to support this is as follows. We multiply (5.1.4) by y^2 and integrate over $[0, y]$ to give

$$y^2 f^{(\mathrm{v})} - 2y f^{(\mathrm{iv})} + 2f''' - f'''(0) + y^2 \left(|f|f\right)''' - 2y \left(|f|f\right)'' + 2 \left(|f|f\right)' - 2 \left(|f|f\right)'(0) - \frac{1}{6} y^3 f = 0. \tag{5.2.18}$$

The asymptotic behaviour of f as $y \to \infty$ for bounded solutions is given by

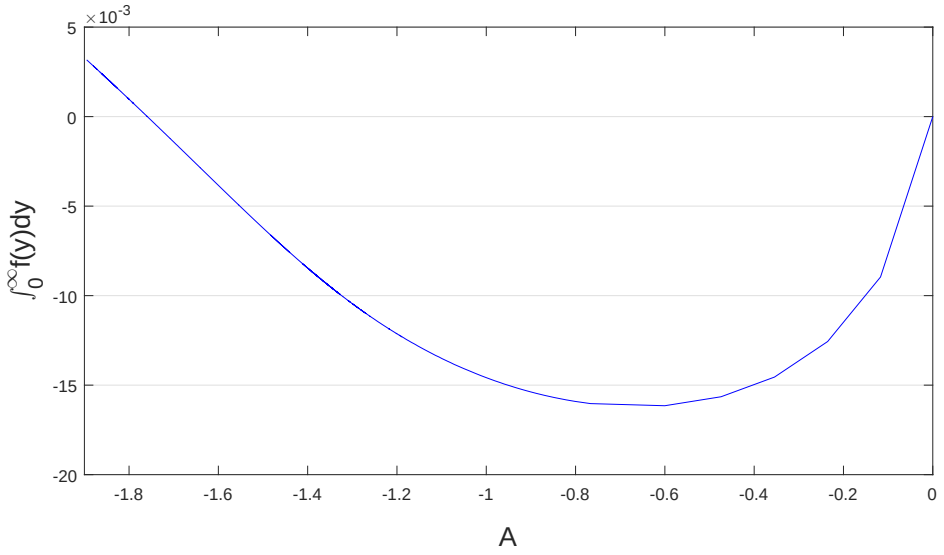

Figure 5-13: Continuation in A of a candidate even solution against mass for $p = p_3$.

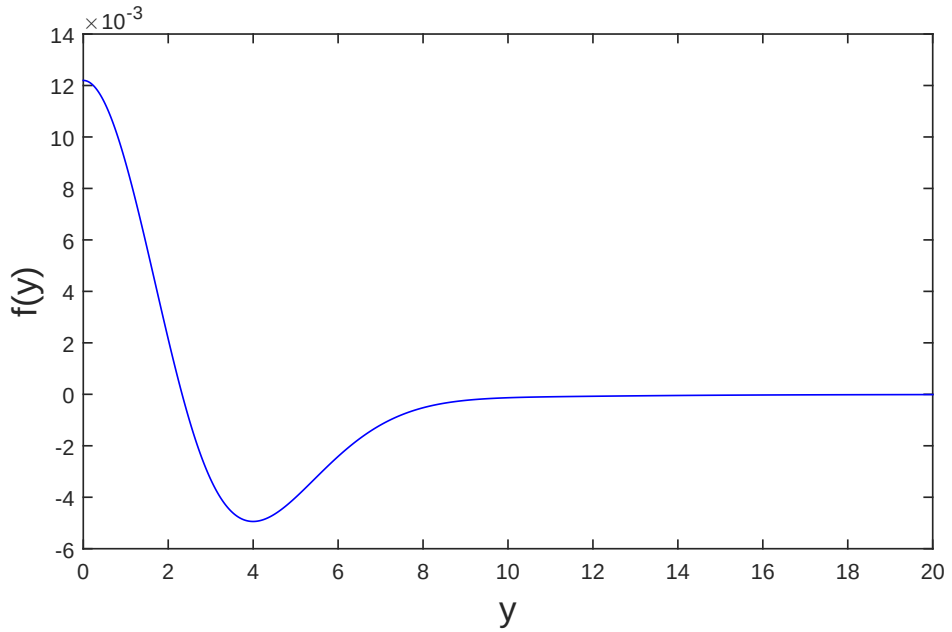

Figure 5-14: An admissible even blow up profile for $p = p_3$.

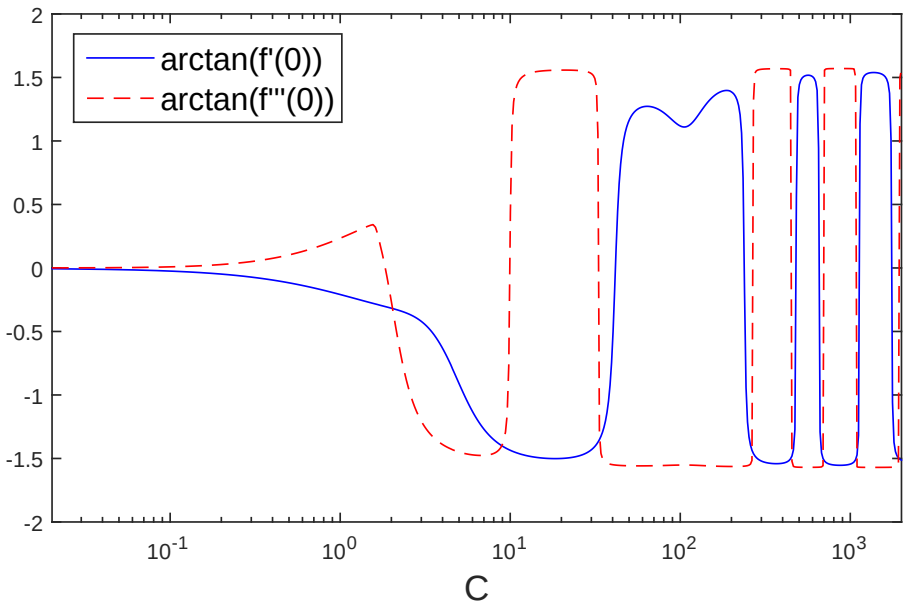

Figure 5-15: Even Symmetry conditions at the origin for $p = p_2$.

(5.1.10) $f(y) \sim Ay^{-3}$, $A \in \mathbb{R}$. Since (5.2.18) must hold for all y, we look at the $y \to \infty$ limit to conclude that $-\frac{1}{6}A = f'''(0) + 2\left(|f|f\right)'(0)$. But the assumption that f is even implies that $f'(0) = f'''(0) = 0$, and so we must have $A = 0$.

Therefore, the large y behaviour of f is given by (5.1.9), which contains only two free parameters. This means there are not enough degrees of freedom to simultaneously satisfy both $f'(0) = f'''(0) = 0$ and the third condition, either $f^{(\mathrm{v})} = 0$ or $\int_0^\infty f(y)\mathrm{d}y = 0$ that must hold for all even solutions of (5.1.4).

To justify that an unexpected dimensional reduction does not occur, we show the results of constructing maximally oscillatory profiles f for each value of C, and recording the values of $f'(0)$ and $f'''(0)$ they take at the origin, in Figure 5-15. Any even solution must lie in this subclass, see discussion in Section 5.2.2. However, we can see that at no point are both quantities simultaneously zero.

Our final evidence comes from using the conservative numerical scheme discussed in Section 3.2.1 to simulate the PDE for $p = p_2$ and $p = p_3$. Starting from bell-shaped initial data, we can see in Figures 5-16 and 5-17 similar, quite irregular patterns form rapidly in both cases. These are not self-similar; when the self-similar scaling $g = \max_x u^{3(p-1)}$ was used for the Sundman transform (3.1.9) the ODE solver stepped past the singularity and the simulation halted early. To produce these figures, we found by trial and error that the transform $g = \max_x u^{6(p-1)}$ resulted in the computational time variable adapting quickly

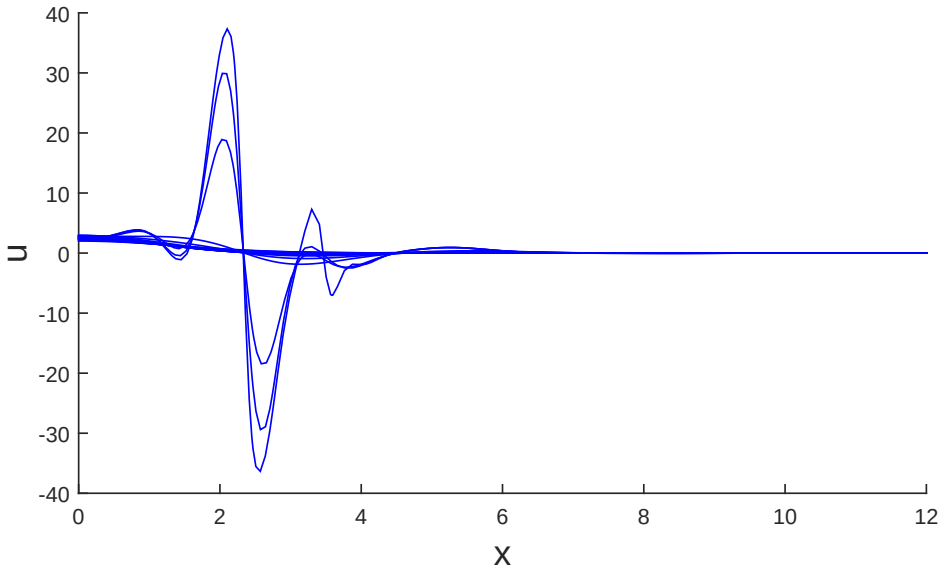

Figure 5-16: Evolution of (5.1.1) with bell-shaped initial data for $p = p_2$.

enough to resolve the singularity and significantly smaller exponents were insufficient. This suggests to us that for these values of p, (5.1.1) is in a sense 'too unstable' for self-similar patterns to emerge before the singularity forms. We are not able to explain the patterns we do observe and recommend that this too will make an interesting future research project.

5.3. Spreading Solutions

While there are a few cosmetic changes, the bifurcation theory used to investigate spreading self-similar solutions for the unstable PDE in Chapter 2 and the stable PDE in Chapter 4 is the same in essence for spreading self-similar solutions of (5.1.1). These correspond to solutions of (5.1.4) with $\sigma = 1$. We therefore do not repeat the analysis here, but we do feel the numerical continuation of the branches makes for an interesting and tantalizing conclusion to the thesis.

In analogy to Sections 2.4.3 and 4.2.1, we find a continuous branch of solutions for $p = p_0$ parameterized by mass. These are shown in Figures 5-18 for the '+' unstable case, and 5-19 in the '-' stable case. Note that in comparison to Figure 2-35, the former exhibits more regions of more drastic non-monotonicity in the mass variable. The latter remains monotone in both the mass and $f(0)$, but we note that the geometric properties of the profiles become more exotic as they increase compared with those seen in Figure 4-3; we have included a sample in

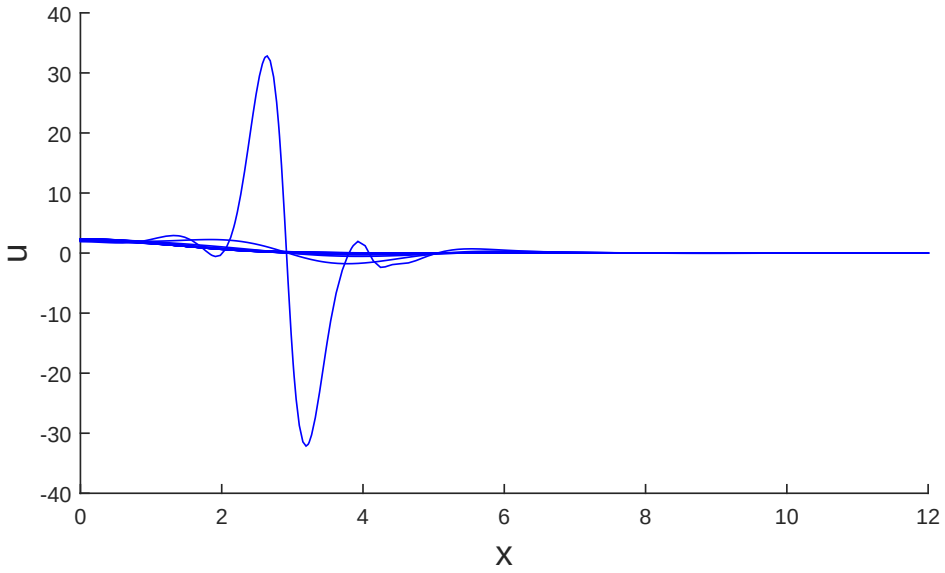

Figure 5-17: Evolution of (5.1.1) with bell-shaped initial data for $p = p_3$.

Figure 5-20.

For general p, we can find branches of solutions according to the bifurcation theory developed in Sections 2.4.4 and 4.2.4. The bifurcation points in this case are are given by the formula

$$p = p_l = 1 + \frac{2}{N + l}, \tag{5.3.19}$$

$l = 0, 1, 2, \ldots$, and the quantities $\kappa_l = \langle \psi_l, \Delta^2 \psi_l^* \rangle$ that determine the instantaneous direction of the branch (refer to 4.2.45) have been found numerically to be

- $\left\langle \psi_2^{5/3}, \Delta^2 \psi_2^* \right\rangle = 0,$
- $\left\langle \psi_4^{7/5}, \Delta^2 \psi_4^* \right\rangle \approx 1.014980364694009e-04,$
- $\left\langle \psi_6^{9/7}, \Delta^2 \psi_6^* \right\rangle \approx 5.046429900578624e-04,$
- $\left\langle \psi_8^{11/9}, \Delta^2 \psi_8^* \right\rangle \approx 9.838148316871605e-04.$

Note that even though κ_2 is zero and the branch leaves the bifurcation point vertically, the global behaviour of the branch is not purely vertical unlike for p_0. This has been established numerically, although we have not been able to explain it analytically.

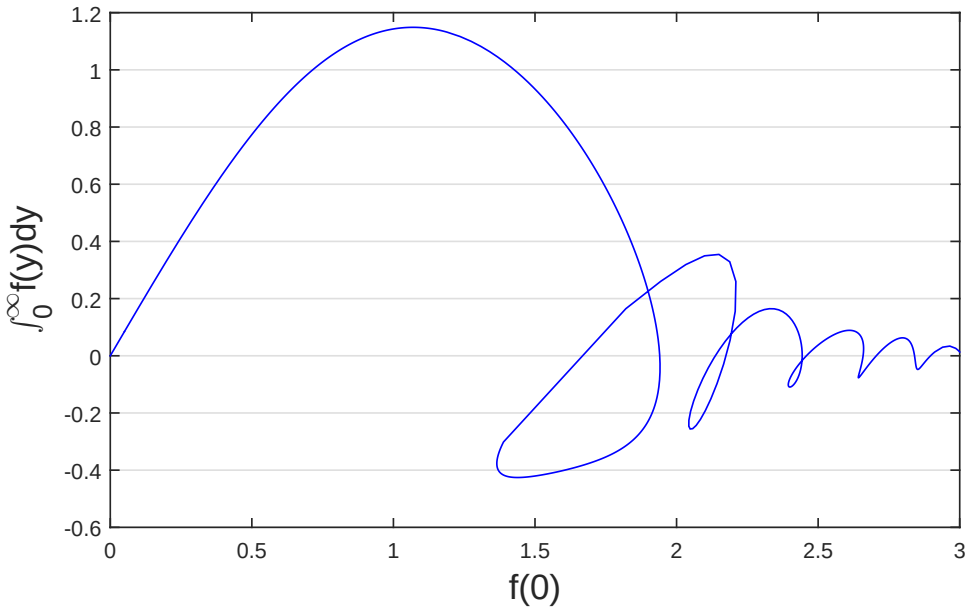

Figure 5-18: The mass bifurcation diagram for the continuous branch of solutions for $p = 3$.

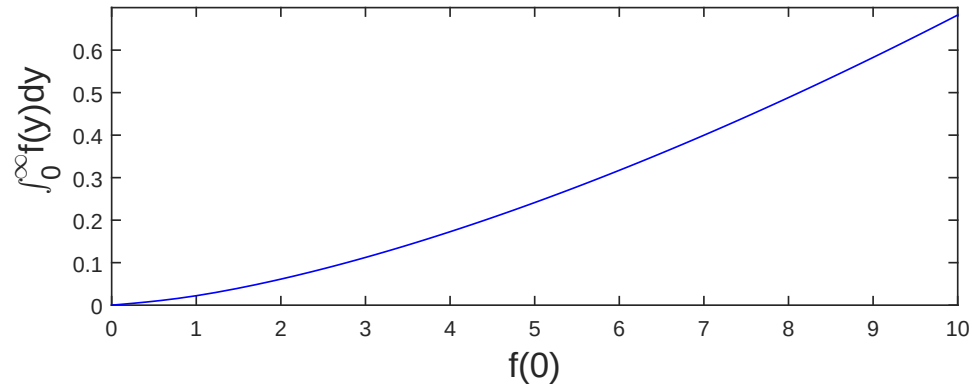

Figure 5-19: The mass bifurcation diagram for the continuous branch of solutions for $p = 3$.

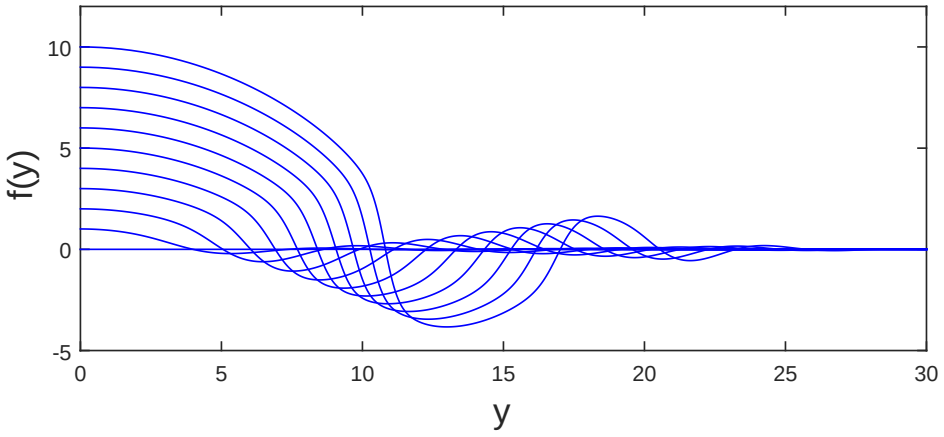

Figure 5-20: Sample solutions on the continuous mass branch for $p = 3$.

Even the numerics have proved impossible to complete in the '+' unstable case; in Figure 5-22 we show the results of following the solutions in p using AUTO starting from the zero-mass solutions indicated in Figure 5-18. We were able to follow the branches to the right indefinitely, however, for p decreasing we were unable to follow the branches beyond what we have shown regardless of the combinations of AUTO parameters we tried.

We were able to pick up the branch near the bifurcation points p_l, these are shown in Figure 5-21. These branches seem to connect to each other and become extinct, suggesting they do not join up with the branches coming from the critical mass branch. There is a precedent for this, see Figure 2-43 which shows the same phenomenon for (2.2.15) the $N = 3$ radial regime. However, note that to pick these branches up we used the regularization (5.2.17) with $\varepsilon = 10^{-4}$. Since the regularizing parameter is not much smaller than the solutions, we are not confident our numerical approximations reflect the true behaviour and so we leave this open.

For the '-' stable case, we had more success, and were able to resolve the p_2 and p_4 branch with AUTO. The bifurcation diagram in shown in Figure 5-23, and two sample profiles can be seen in Figure 5-24. Again the comparison with solutions of (4.2.18) and the corresponding p-bifurcation diagram shown in Figures 4-6 and 4-5 respectively.

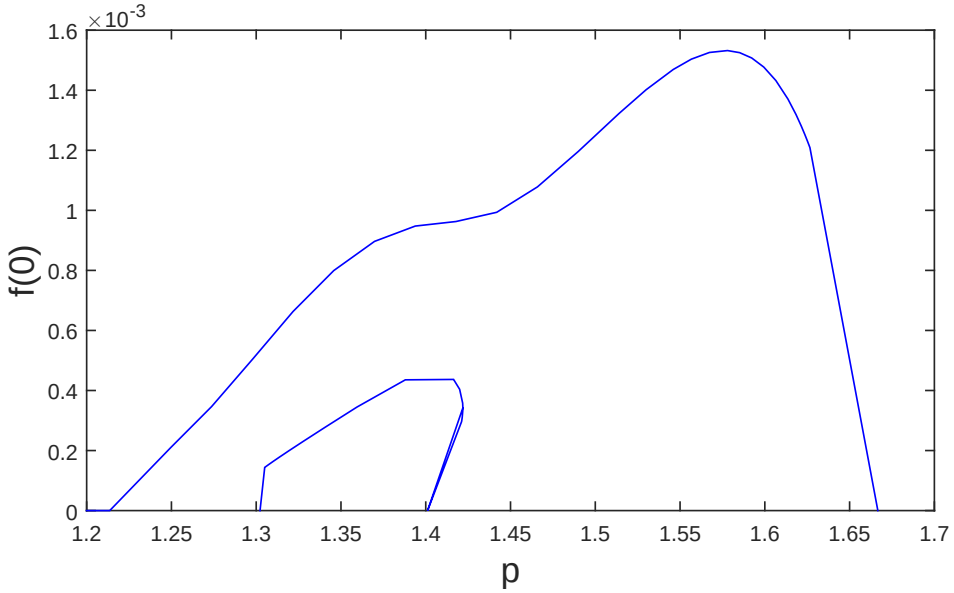

Figure 5-21: The p-bifurcation diagram near the bifurcation points p_l.

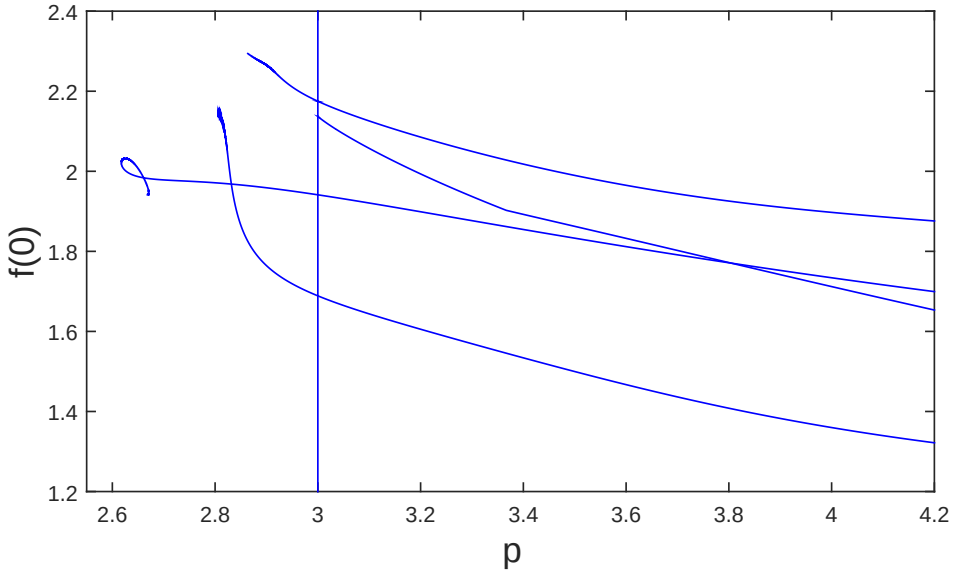

Figure 5-22: The p-bifurcation diagram around the continuous mass-branch shown in Figure 5-18.

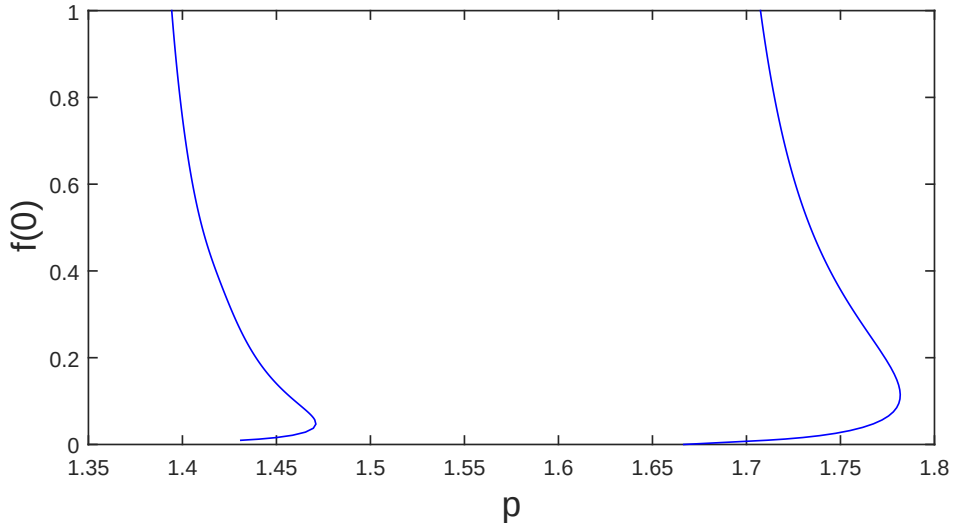

Figure 5-23: The p-bifurcation diagram.

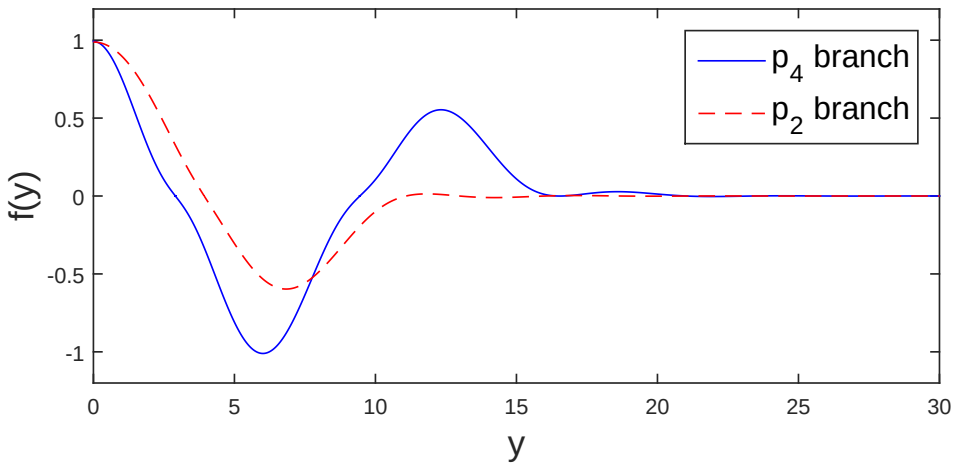

Figure 5-24: Sample solutions from the p-branches with $f(0) = 1$.

Chapter 6

Discussion

The PDEs we have considered in this thesis are, from one perspective, quite simple, being semilinear with quite 'mild' nonlinear terms, having only three terms (or four for the similarity equations), and admitting self-similar solutions. In terms of abstract existence/unqiueness/regularity questions, the machinery is sufficiently advanced to be applicable to classes of equations much harder than these without excessive trouble. A lot has been done for equations of arbitrary order. That is not to say that the field doesn't still hold intriguing mysteries and we expect it to provide novel and interesting research opportunities for the future. Indeed, the simple generalization from (1.1.1) to the class of Thin Film equations

$$u_t = \nabla \cdot \left(|u|^n \nabla \Delta^2 u \right) \pm \Delta^m \left(|u|^{p-1} u \right), \quad n > 0,\ p > 1,\ m = 1, 2,$$

with a relatively simple quasilinear term, presents a number of extremely interesting problems. Questions of optimal regularity, dependence on n and development of a 'nonlinear Hermitian spectral theory' (see [51] for some related discussion for a fourth order equation) are still unresolved. We highlight this generalization as a particularly important direction for future research.

Many of these questions cannot be answered without a thorough understanding of the geometric properties of solutions, and that is where higher order PDEs become much harder than their classical, second order counterparts. Some tentative steps have been taken to develop weakened comparison principles, see [78] for a promising line of inquiry involving good approximations for integral kernels, and [60] for an examination of the phenomenon of 'eventual local positivity' of fourth order linear parabolic equations. We expect that extending and refining these, and applying them in combination with the kinds of numerics and asymptotics

developed in this thesis, will remain and important and active area of research. However, we do not expect anything so powerful and widely applicable as the maximum principle to exist for higher order equations.

We take this opportunity to list what we believe to be the next logical steps to take to extend this research, in roughly increasing order of anticipated difficulty.

First, we believe that the matched asymptotic construction in Section 2.3.3 can be generalized in not only N, the spatial dimension, but also the order of the equation. That is, we believe we can extend those arguments to describe radial solutions self-similar solutions of

$$u_t = -\left(-\Delta\right)^m u - \Delta\left(|u|^{p-1}u\right), \quad m \geq 2,\ p = 1 + \frac{2(m-1)}{N}.$$

Indeed, this is already underway although regrettably has not been completed in time to include in this thesis. It will be interesting to see if the existence of a countable set of such solutions persists over the entire range of m and N.

It also seems natural to ask if we can extend Movcol6 to higher orders. We believe the stability modification will make this extension more plausible, although at some point we do expect there will come diminishing returns and other numerical techniques will become necessary. An extension to higher dimensions will be a harder task, although some results for general moving mesh schemes in dimension greater than one do exist, see for example [26]. We hope that even as it is the scheme will prove useful for more complicated sixth order equations than those considered in this thesis.

Returning to asymptotic constructions in sixth order equations, we are very interested to see whether the beginnings of the approach described in Section 5.2.3 can be made to bear fruit. If not, it may yet be possible to perform something similar on (2.2.15) in the general p case, although this is complicated considerably by not being able to integrate the equation.

One of the more valuable open problems in terms of putting the results of this thesis on a more rigorous footing concerns the spectral theory of linearized operators like those that appear in equations (2.3.60), (2.3.72) and (4.2.28). Knowing, or at least having some information about these spectra would be useful in a number of contexts. For example, for (2.3.60) we would be able to prove asymptotic stability results rather than relying on simulations. For (2.3.72) the spectra would be useful in determining turning points and saddle-node bifurcations in the μ-branches of solutions. Without this we have no hope of systematically understanding how these branches behave, which is vital if we want to be able to

prove multiplicity results for a fixed, non-zero value of μ. Similarly, if we want to understand the p-branches of solutions of (4.2.44), then we must first know the spectrum

$$\sigma\left(\mathbf{I} + (1+c_p)\mathbf{C}^{-1} + p\mathbf{C}^{-1}\Delta\left(|f|^{p-1}\mathbf{I}\right)\right),$$

for any f, p that solve the equation. Only from there can we begin to make conclusions about the global structure of the p-branches using implicit function theorem and its corollaries, rather than relying on finding them numerically.

In all of these cases, the obstacle that must be overcome concerns the linearization of the nonlinear term, typically of the form $\Delta\left(|f|^{p-1}\mathbf{I}\right)$. The function f is itself the solution of a nonlinear PDE and can have quite complicated structure. When we are able to find asymptotic approximations to f, then we can use this to estimate the spectra; this is what we do with (2.3.60). However, absent this we know of no way of recovering spectral information, and so we would encourage extensive research in this direction.

A final research direction prompted directly from results in this thesis concerns extension of solutions past the blow-up time. In Section 2.4.5, we show some preliminary results suggesting that a Leray Scenario does not occur for (2.1.1), at least in the cases $N = 1$, $p = 3, 5$. Even within this context, there is much that can be done, and further investigation numerically across wider parameter ranges would be valuable. Furthermore, simulating the PDE with the truncated nonlinear term (2.4.77) using the methods in Chapter 3 might provide some interesting insights, especially for ε very small. It is developing an extended semigroup representation as $\varepsilon \to 0$ that presents the most intriguing challenge, though. While it is not clear to us at the moment whether some of the geometric techniques mentioned earlier (i.e. comparison against a majorizing kernel or exploiting eventual local positivity, or indeed even some variant of the scaling argument used to prove uniform L^∞ bounds in Chapter 4) might be useful in this endeavour, the possibility that they or some suitable generalizations might is nonetheless some incentive.

We conclude by listing a few research directions that don't stem directly from our results but nonetheless seem natural enough in the context of neighbouring research. There is still much that can be done for the models we've considered, especially concerning non-self-similar blow up. See [71] for a discussion of types of blow-up in higher order models; especially for $N > 1$ we suspect that our equations can exhibit wide ranges of behaviours we have barely encountered.

Quaslinear generalizations of (1.1.1) outside of the Thin Film equation posed

above have received almost no attention, e.g equations like

$$u_t = \Delta^3 \left(|u|^{m-1} u \right) + f(u), \quad m > 0,$$

for some nonlinearity $f(u)$. We expect these to exhibit a number of interesting features typical of quasilinear equations, e.g. compactly supported solutions, rupturing, oscillatory interfaces etc.

Another avenue to explore involved posing the equation in more interesting domains than the whole of $\mathbb{R}^N$, the very beginnings of which are considered in Appendix C. Ultimately it might be interesting to pose the equations on general manifolds, although given the difficulties we've encountered in flat space this could be a formidable task.

Finally, we suggest that some of the approaches we've adopted can apply equally well to hyperbolic equations, e.g the sixth order Boussinesq equation

$$u_{tt} = \Delta^3 \left(|u|^{n-1} u \right), \quad n > 0.$$

We refer to [85] for discussion of a wide range of higher order models.

Bibliography

[1] Helmut Abels, Stefano Bosia, and Maurizio Grasselli. Cahn-Hilliard equation with nonlocal singular free energies. *Ann. Mat. Pura Appl. (4)*, 194(4):1071–1106, 2015.

[2] Helmut Abels, Daniel Depner, and Harald Garcke. On an incompressible Navier-Stokes/Cahn-Hilliard system with degenerate mobility. *Ann. Inst. H. Poincaré Anal. Non Linéaire*, 30(6):1175–1190, 2013.

[3] A. D. Aleksandrov. Certain estimates of solutions of the Dirichlet problem. *Vestnik Leningrad. Univ.*, 22(7):19–29, 1967.

[4] P. Álvarez-Caudevilla, J. D. Evans, and V. A. Galaktionov. The Cauchy problem for a tenth-order thin film equation II. Oscillatory source-type and fundamental similarity solutions. *Discrete Contin. Dyn. Syst.*, 35(3):807–827, 2015.

[5] P. Álvarez-Caudevilla, J. D. Evans, and V. A. Galaktionov. Towards optimal regularity for the fourth-order thin film equation in $\mathbb{R}^N$: Graveleau-type focusing self-similarity. *J. Math. Anal. Appl.*, 431(2):1099–1123, 2015.

[6] Pablo Álvarez-Caudevilla, Jonathan D. Evans, and Victor A. Galaktionov. The Cauchy problem for a tenth-order thin film equation I. Bifurcation of oscillatory fundamental solutions. *Mediterr. J. Math.*, 10(4):1761–1792, 2013.

[7] Pablo Álvarez-Caudevilla and Victor A. Galaktionov. Steady states, global existence and blow-up for fourth-order semilinear parabolic equations of Cahn-Hilliard type. *Adv. Nonlinear Stud.*, 12(2):315–361, 2012.

[8] U. Ascher, R. Mattheij, and R. Russell. *Numerical Solution of Boundary Value Problems for Ordinary Differential Equations*. Society for Industrial and Applied Mathematics, 1995.

[9] G. I. Barenblatt. On some unsteady motions of a liquid and gas in a porous medium. *Akad. Nauk SSSR. Prikl. Mat. Meh.*, 16:67–78, 1952.

[10] Grigory Isaakovich Barenblatt. *Scaling, self-similarity, and intermediate asymptotics*, volume 14 of *Cambridge Texts in Applied Mathematics*. Cambridge University Press, Cambridge, 1996. With a foreword by Ya. B. Zeldovich.

[11] Carl M. Bender and Steven A. Orszag. *Advanced mathematical methods for scientists and engineers. I.* Springer-Verlag, New York, 1999. Asymptotic methods and perturbation theory, Reprint of the 1978 original.

[12] Melvin S. Berger. *Nonlinearity and functional analysis*. Academic Press [Harcourt Brace Jovanovich, Publishers], New York-London, 1977. Lectures on nonlinear problems in mathematical analysis, Pure and Applied Mathematics.

[13] F. Bernis and J. B. McLeod. Similarity solutions of a higher order nonlinear diffusion equation. *Nonlinear Anal.*, 17(11):1039–1068, 1991.

[14] Francisco Bernis and Avner Friedman. Higher order nonlinear degenerate parabolic equations. *J. Differential Equations*, 83(1):179–206, 1990.

[15] A. J. Bernoff and T. P. Witelski. Linear stability of source-type similarity solutions of the thin film equation. *Appl. Math. Lett.*, 15(5):599–606, 2002.

[16] A. Berti and I. Bochicchio. A mathematical model for phase separation: a generalized Cahn-Hilliard equation. *Math. Methods Appl. Sci.*, 34(10):1193–1201, 2011.

[17] A. L. Bertozzi and M. C. Pugh. Long-wave instabilities and saturation in thin film equations. *Comm. Pure Appl. Math.*, 51(6):625–661, 1998.

[18] Bilgesu A. Bilgin and Varga K. Kalantarov. Blow up of solutions to the initial boundary value problem for quasilinear strongly damped wave equations. *J. Math. Anal. Appl.*, 403(1):89–94, 2013.

[19] George W. Bluman and Sukeyuki Kumei. *Symmetries and differential equations*, volume 81 of *Applied Mathematical Sciences*. Springer-Verlag, New York, 1989.

[20] Alberto Bressan. Stable blow-up patterns. *J. Differential Equations*, 98(1):57–75, 1992.

[21] H. Brezis, L. A. Peletier, and D. Terman. A very singular solution of the heat equation with absorption. *Arch. Rational Mech. Anal.*, 95(3):185–209, 1986.

[22] Haïm Brézis and Avner Friedman. Nonlinear parabolic equations involving measures as initial conditions. *J. Math. Pures Appl. (9)*, 62(1):73–97, 1983.

[23] C. J. Budd and V. A. Galaktionov. On self-similar blow-up in evolution equations of Monge-Ampère type. *IMA J. Appl. Math.*, 78(2):338–378, 2013.

[24] C. J. Budd, V. A. Galaktionov, and J. F. Williams. Self-similar blow-up in higher-order semilinear parabolic equations. *SIAM J. Appl. Math.*, 64(5):1775–1809, 2004.

[25] C. J. Budd, B. Leimkuhler, and M. D. Piggott. Scaling invariance and adaptivity. *Appl. Numer. Math.*, 39(3-4):261–288, 2001. Special issue: Themes in geometric integration.

[26] C. J. Budd and J. F. Williams. Parabolic Monge-Ampère methods for blow-up problems in several spatial dimensions. *J. Phys. A*, 39(19):5425–5444, 2006.

[27] C.J. Budd and J.F. Williams. How to adaptively resolve evolutionary singularities in differential equations with symmetry. *Journal of Engineering Mathematics*, 66(1-3):217–236, 2010.

[28] Luis A. Caffarelli and Avner Friedman. Blowup of solutions of nonlinear heat equations. *J. Math. Anal. Appl.*, 129(2):409–419, 1988.

[29] Gunduz Caginalp and Paul Fife. Higher-order phase field models and detailed anisotropy. *Phys. Rev. B (3)*, 34(7):4940–4943, 1986.

[30] John W Cahn. On spinodal decomposition. *Acta Metallurgica*, 9(9):795 – 801, 1961.

[31] John W. Cahn and John E. Hilliard. Free energy of a nonuniform system. i. interfacial free energy. *The Journal of Chemical Physics*, 28(2):258–267, 1958.

[32] Laurence Cherfils, Alain Miranville, and Sergey Zelik. The Cahn-Hilliard equation with logarithmic potentials. *Milan J. Math.*, 79(2):561–596, 2011.

[33] David Clark. A variant of the lusternik-schnirelman theory. *Indiana Univ. Math. J.*, 22:6574, 1973.

[34] Earl A. Coddington and Norman Levinson. *Theory of ordinary differential equations*. McGraw-Hill Book Company, Inc., New York-Toronto-London, 1955.

[35] Charles Collot. Non radial type ii blow up for the energy supercritical semilinear heat equation, 2016.

[36] Shangbin Cui. Local and global existence of solutions to semilinear parabolic initial value problems. *Nonlinear Anal.*, 43(3, Ser. A: Theory Methods):293–323, 2001.

[37] C. M. Dafermos and Milan Pokorný, editors. *Handbook of differential equations: evolutionary equations. Vol. IV*. Handbook of Differential Equations. Elsevier/North-Holland, Amsterdam, 2008.

[38] Carl de Boor. Good approximation by splines with variable knots. In *Spline functions and approximation theory (Proc. Sympos., Univ. Alberta, Edmonton, Alta., 1972)*, pages 57–72. Internat. Ser. Numer. Math., Vol. 21. Birkhäuser, Basel, 1973.

[39] Arnaud Debussche and Lucia Dettori. On the Cahn-Hilliard equation with a logarithmic free energy. *Nonlinear Anal.*, 24(10):1491–1514, 1995.

[40] G. T. Dee and Wim van Saarloos. Bistable systems with propagating fronts leading to pattern formation. *Phys. Rev. Lett.*, 60:2641–2644, Jun 1988.

[41] Klaus Deimling. *Nonlinear functional analysis*. Springer-Verlag, Berlin, 1985.

[42] Eusebius J. Doedel, Thomas F. Fairgrieve, Bjrn Sandstede, Alan R. Champneys, Yuri A. Kuznetsov, and Xianjun Wang. Auto-07p: Continuation and bifurcation software for ordinary differential equations. Technical report, 2007.

[43] E. A. Dorfy and L. Drury. Simple Adaptive Grids for 1-D Initial Value Problems. *jcp*, 69:175–195, 1987.

[44] A. Eden and V. K. Kalantarov. The convective Cahn-Hilliard equation. *Appl. Math. Lett.*, 20(4):455–461, 2007.

[45] Yu. V. Egorov, V. A. Galaktionov, V. A. Kondratiev, and S. I. Pohozaev. Global solutions of higher-order semilinear parabolic equations in the supercritical range. *Adv. Differential Equations*, 9(9-10):1009–1038, 2004.

[46] Yuri V. Egorov, Victor A. Galaktionov, Vladimir A. Kondratiev, and Stanislav I. Pohozaev. On the necessary conditions of global existence to a quasilinear inequality in the half-space. *C. R. Acad. Sci. Paris Sér. I Math.*, 330(2):93–98, 2000.

[47] S. D. Èĭdel′man. *Parabolic systems*. Translated from the Russian by Scripta Technica, London. North-Holland Publishing Co., Amsterdam, 1969.

[48] S. D. Èĭdel′man. Parabolic equations. *Modern Problems of Math. Fundam. Achiev.*, 63:244, 1991.

[49] G. G. Elenin, S. P. Kurdyumov, and A. A. Samarskiĭ. Nonstationary dissipative structures in a nonlinear heat-conducting medium. *Zh. Vychisl. Mat. i Mat. Fiz.*, 23(2):380–390, 1983.

[50] Charles M. Elliott and Zheng Songmu. On the cahn-hilliard equation. *Archive for Rational Mechanics and Analysis*, 96(4):339–357, 1986.

[51] J. D. EVANS and V. A. GALAKTIONOV. On continuous branches of very singular similarity solutions of a stable thin film equation. i the cauchy problem. *European Journal of Applied Mathematics*, 22:217–243, 6 2011.

[52] J. D. EVANS, V. A. GALAKTIONOV, and J. R. KING. Blow-up similarity solutions of the fourth-order unstable thin film equation. *European Journal of Applied Mathematics*, 18:195–231, 4 2007.

[53] J. D. EVANS, V. A. GALAKTIONOV, and J. R. KING. Source-type solutions of the fourth-order unstable thin film equation. *European Journal of Applied Mathematics*, 18:273–321, 6 2007.

[54] J D Evans, V A Galaktionov, and J R King. Unstable sixth-order thin film equation: I. blow-up similarity solutions. *Nonlinearity*, 20(8):1799, 2007.

[55] J D Evans, V A Galaktionov, and J R King. Unstable sixth-order thin film equation: Ii. global similarity patterns. *Nonlinearity*, 20(8):1843, 2007.

[56] J. D. Evans, V. A. Galaktionov, and J. F. Williams. Blow-up and global asymptotics of the limit unstable Cahn-Hilliard equation. *SIAM J. Math. Anal.*, 38(1):64–102, 2006.

[57] J. D. Evans, A. B. Tayler, and J. R. King. Finite-length mask effects in the isolation oxidation of silicon. *IMA J. Appl. Math.*, 58(2):121–146, 1997.

[58] L.C. Evans. *Partial Differential Equations*. Graduate studies in mathematics. American Mathematical Society, 2010.

[59] R. S. Fernandes and V. A. Galaktionov. Eigenfunctions and very singular similarity solutions of odd-order nonlinear dispersion PDEs: toward a "nonlinear airy function" and others. *Stud. Appl. Math.*, 129(2):163–219, 2012.

[60] Alberto Ferrero, Filippo Gazzola, and Hans-Christoph Grunau. Decay and eventual local positivity for biharmonic parabolic equations. *Discrete Contin. Dyn. Syst.*, 21(4):1129–1157, 2008.

[61] Stathis Filippas and Robert V. Kohn. Refined asymptotics for the blowup of $u_t - \Delta u = u^p$. *Comm. Pure Appl. Math.*, 45(7):821–869, 1992.

[62] R. A. FISHER. The wave of advance of advantageous genes. *Annals of Eugenics*, 7(4):355–369, 1937.

[63] J. C. Flitton and J. R. King. Moving-boundary and fixed-domain problems for a sixth-order thin-film equation. *European J. Appl. Math.*, 15(6):713–754, 2004.

[64] Avner Friedman. *Partial differential equations*. Robert E. Krieger Publishing Co., Huntington, N.Y., original edition, 1976.

[65] Avner Friedman and Luc Oswald. The blow-up time for higher order semilinear parabolic equations with small leading coefficients. *J. Differential Equations*, 75(2):239–263, 1988.

[66] H. Fujita. On the blowing up of solutions of the cauchy problem for $u_t = \Delta u + u^{1+\alpha}$. *Journal of the Faculty of Science, University of Tokyo. Sect. 1, Mathematics, astronomy, physics, chemistry*, 13(2):109–124, 1966.

[67] V. A Galaktionov. On a spectrum of blow-up patterns for a higher-order semilinear parabolic equation. *Proc. R. Soc. Lond. A*, 457:1623–1643, July 2001.

[68] V. A. Galaktionov. On interfaces and oscillatory solutions of higher-order semilinear parabolic equations with non-Lipschitz nonlinearities. *Stud. Appl. Math.*, 117(4):353–389, 2006.

[69] V. A. Galaktionov. Countable branching of similarity solutions of higher-order porous medium type equations. *Adv. Differential Equations*, 13(7-8):641–680, 2008.

[70] V. A. Galaktionov. On blow-up space jets for the Navier-Stokes equations in $\mathbb{R}^3$ with convergence to Euler equations. *J. Math. Phys.*, 49(11):113101, 28, 2008.

[71] V. A. Galaktionov. Five types of blow-up in a semilinear fourth-order reaction-diffusion equation: an analytic-numerical approach. *Nonlinearity*, 22(7):1695–1741, 2009.

[72] V. A. Galaktionov. Incomplete self-similar blow-up in a semilinear fourth-order reaction-diffusion equation. *Studies in Applied Mathematics*, 124(4):347–381, 2010.

[73] V. A. Galaktionov. Vast multiplicity of very singular self-similar solutions of a semilinear higher-order diffusion equation with time-dependent absorption. *J. Math. Sci. Univ. Tokyo*, 17(4):323–358 (2011), 2010.

[74] V. A. Galaktionov and P. J. Harwin. Non-uniqueness and global similarity solutions for a higher-order semilinear parabolic equation. *Nonlinearity*, 18(2):717–746, 2005.

[75] V. A. Galaktionov and P. J. Harwin. On center subspace behavior in thin film equations. *SIAM J. Appl. Math.*, 69(5):1334–1358, 2009.

[76] V. A. Galaktionov, S. P. Kurdyumov, and A. A. Samarskiĭ. Letter to the editors: "Asymptotic 'eigenfunctions' of the Cauchy problem for a nonlinear parabolic equation" [Mat. Sb. (N.S) **126**(**168**) (1985), no. 4, 435–472; MR0788082 (86i:35064)]. *Mat. Sb. (N.S.)*, 131(173)(3):413, 1986.

[77] V. A. Galaktionov, E. Mitidieri, and S. I. Pohozaev. On global solutions and blow-up for Kuramoto-Sivashinsky-type models, and well-posed Burnett equations. *Nonlinear Anal.*, 70(8):2930–2952, 2009.

[78] V. A. Galaktionov and S. I. Pohozaev. Existence and blow-up for higher-order semilinear parabolic equations: majorizing order-preserving operators. *Indiana Univ. Math. J.*, 51(6):1321–1338, 2002.

[79] V. A. Galaktionov and S. A. Posashkov. An approximate self-similar solution of a nonlinear equation of heat conduction with absorption. In *Mathematical modeling (Russian) (Moscow, 1984)*, pages 103–122, 306. "Nauka", Moscow, 1989.

[80] V. A. Galaktionov and A. E. Shishkov. Saint-Venant's principle in blow-up for higher-order quasilinear parabolic equations. *Proc. Roy. Soc. Edinburgh Sect. A*, 133(5):1075–1119, 2003.

[81] V. A. Galaktionov and J. F. Williams. On very singular similarity solutions of a higher-order semilinear parabolic equation. *Nonlinearity*, 17(3):1075–1099, 2004.

[82] Victor A. Galaktionov. Critical global asymptotics in higher-order semilinear parabolic equations. *Int. J. Math. Math. Sci.*, (60):3809–3825, 2003.

[83] Victor A. Galaktionov. *Geometric Sturmian theory of nonlinear parabolic equations and applications*. Chapman & Hall/CRC Applied Mathematics and Nonlinear Science Series, 3. Chapman & Hall/CRC, Boca Raton, FL, 2004.

[84] Victor A. Galaktionov and John R. King. Stabilization to a singular steady state for the Frank-Kamenetskii equation in a critical dimension. *Proc. Roy. Soc. Edinburgh Sect. A*, 135(4):777–787, 2005.

[85] Victor A. Galaktionov, Enzo L. Mitidieri, and Stanislav I. Pohozaev. *Blow-up for higher-order parabolic, hyperbolic, dispersion and Schrödinger equations*. Monographs and Research Notes in Mathematics. CRC Press, Boca Raton, FL, 2015.

[86] Victor A. Galaktionov and Juan L. Vazquez. Continuation of blowup solutions of nonlinear heat equations in several space dimensions. *Communications on Pure and Applied Mathematics*, 50(1):1–67, 1997.

[87] Victor A. Galaktionov and Juan L. Vázquez. The problem of blow-up in nonlinear parabolic equations. *Discrete Contin. Dyn. Syst.*, 8(2):399–433, 2002. Current developments in partial differential equations (Temuco, 1999).

[88] Victor A. Galaktionov and Juan Luis Vázquez. Continuation after blow-up of solutions of nonlinear heat equations. *C. R. Acad. Sci. Paris Sér. I Math.*, 321(5):569–574, 1995.

[89] Filippo Gazzola and Hans-Christoph Grunau. Radial entire solutions for supercritical biharmonic equations. *Math. Ann.*, 334(4):905–936, 2006.

[90] Filippo Gazzola, Hans-Christoph Grunau, and Guido Sweers. *Polyharmonic boundary value problems*, volume 1991 of *Lecture Notes in Mathematics*. Springer-Verlag, Berlin, 2010. Positivity preserving and nonlinear higher order elliptic equations in bounded domains.

[91] B. Gidas, Wei Ming Ni, and L. Nirenberg. Symmetry and related properties via the maximum principle. *Comm. Math. Phys.*, 68(3):209–243, 1979.

[92] Yoshikazu Giga and Robert V. Kohn. Asymptotically self-similar blow-up of semilinear heat equations. *Comm. Pure Appl. Math.*, 38(3):297–319, 1985.

[93] I. C. Gohberg and M. G. Kreĭn. *Introduction to the theory of linear non-selfadjoint operators*. Translated from the Russian by A. Feinstein. Translations of Mathematical Monographs, Vol. 18. American Mathematical Society, Providence, R.I., 1969.

[94] Gene H. Golub and John H. Welsch. Calculation of Gauss quadrature rules. *Math. Comp. 23 (1969), 221-230; addendum, ibid.*, 23(106, loose microfiche suppl):A1–A10, 1969.

[95] G. Gompper and M. Schick. Correlation between structural and interfacial properties of amphiphilic systems. *Phys. Rev. Lett.*, 65:1116–1119, Aug 1990.

[96] Ruihan Guo, Yan Xu, and Zhengfu Xu. Local discontinuous Galerkin methods for the functionalized Cahn-Hilliard equation. *J. Sci. Comput.*, 63(3):913–937, 2015.

[97] Morton E. Gurtin. Generalized Ginzburg-Landau and Cahn-Hilliard equations based on a microforce balance. *Phys. D*, 92(3-4):178–192, 1996.

[98] Jack K. Hale. *Asymptotic behavior of dissipative systems*, volume 25 of *Mathematical Surveys and Monographs*. American Mathematical Society, Providence, RI, 1988.

[99] Alain Haraux and Fred B. Weissler. Nonuniqueness for a semilinear initial value problem. *Indiana Univ. Math. J.*, 31(2):167–189, 1982.

[100] Kantaro Hayakawa. On nonexistence of global solutions of some semilinear parabolic differential equations. *Proc. Japan Acad.*, 49:503–505, 1973.

[101] Mark H. Holmes. *Introduction to perturbation methods*, volume 20 of *Texts in Applied Mathematics*. Springer, New York, second edition, 2013.

[102] B. Hu. *Blow-up Theories for Semilinear Parabolic Equations*. Lecture Notes in Mathematics. Springer Berlin Heidelberg, 2011.

[103] Weizhang Huang, Yuhe Ren, and Robert D. Russell. Moving mesh methods based on moving mesh partial differential equations. *J. Comput. Phys*, 113:279–290, 1994.

[104] Weizhang Huang, Yuhe Ren, and Robert D. Russell. Moving mesh partial differential equations (MMPDES) based on the equidistribution principle. *SIAM J. Numer. Anal.*, 31(3):709–730, 1994.

[105] Weizhang Huang and Robert D. Russell. A moving collocation method for solving time dependent partial differential equations. *Appl. Numer. Math.*, 20(1-2):101–116, 1996. Workshop on the method of lines for time-dependent problems (Lexington, KY, 1995).

[106] Weizhang Huang and Robert D. Russell. *Adaptive moving mesh methods*, volume 174 of *Applied Mathematical Sciences*. Springer, New York, 2011.

[107] Josephus Hulshof. Similarity solutions of the porous medium equation with sign changes. *J. Math. Anal. Appl.*, 157(1):75–111, 1991.

[108] Josephus Hulshof and Juan Luis Vázquez. The dipole solution for the porous medium equation in several space dimensions. *Ann. Scuola Norm. Sup. Pisa Cl. Sci. (4)*, 20(2):193–217, 1993.

[109] James M. Hyman, Basil Nicolaenko, and Stéphane Zaleski. Order and complexity in the Kuramoto-Sivashinsky model of weakly turbulent interfaces. *Phys. D*, 23(1-3):265–292, 1986. Spatio-temporal coherence and chaos in physical systems (Los Alamos, N.M., 1986).

[110] Arieh Iserles. On the global error of discretization methods for highly-oscillatory ordinary differential equations. *BIT Numerical Mathematics*, 42(3):561–599, 2002.

[111] S. Kamin and M. Ughi. On the behaviour as $t \to \infty$ of the solutions of the Cauchy problem for certain nonlinear parabolic equations. *J. Math. Anal. Appl.*, 128(2):456–469, 1987.

[112] Stanley Kaplan. On the growth of solutions of quasi-linear parabolic equations. *Comm. Pure Appl. Math.*, 16:305–330, 1963.

[113] Ioannis G. Kevrekidis, Basil Nicolaenko, and James C. Scovel. Back in the saddle again: a computer assisted study of the Kuramoto-Sivashinsky equation. *SIAM J. Appl. Math.*, 50(3):760–790, 1990.

[114] J. R. King. The isolation oxidation of silicon: the reaction-controlled case. *SIAM J. Appl. Math.*, 49(4):1064–1080, 1989.

[115] J. R. King. Two generalisations of the thin film equation. *Math. Comput. Modelling*, 34(7-8):737–756, 2001.

[116] G. Kitzhofer, O. Koch, G. Pulverer, Ch. Simon, and E. B. Weinmüller. The New Matlab code `bvpsuite` for the solution of singular implicit BVPs. *JNAIAM. J. Numer. Anal. Ind. Appl. Math.*, 5(1-2):113–134, 2010.

[117] Kusuo Kobayashi, Tunekiti Sirao, and Hiroshi Tanaka. On the growing up problem for semilinear heat equations. *J. Math. Soc. Japan*, 29(3):407–424, 1977.

[118] M. Korzec, P. Nayar, and P. Rybka. Global weak solutions to a sixth order cahn–hilliard type equation. *SIAM Journal on Mathematical Analysis*, 44(5):3369–3387, 2012.

[119] M. Korzec and P. Rybka. On a higher order convective cahn–hilliard-type equation. *SIAM Journal on Applied Mathematics*, 72(4):1343–1360, 2012.

[120] M. D. Korzec, P. Nayar, and P. Rybka. Global attractors of sixth order PDEs describing the faceting of growing surfaces. *J. Dynam. Differential Equations*, 28(1):49–67, 2016.

[121] M.A. Krasnosel'skii, M.A. Krasnoselskiĭ, and P.P. Zabreĭko. *Geometrical methods of nonlinear analysis*. Grundlehren der mathematischen Wissenschaften. Springer-Verlag, 1984.

[122] Y. Kuramoto and T. Tsuzuki. Persistent propagation of concentration waves in dissipative media far from thermal equilibrium. *Progr. Theor. Phys.*, 55:365, 1976.

[123] S. P. Kurdyumov, G. G. Malinetskiĭ, A. B. Potapov, and A. A. Samarskiĭ. Structures in nonlinear media. In *Computers and nonlinear phenomena (Russian)*, Kibern. Neogranich. Vozmozhn. Vozmozhn. Ogranich., pages 5–43. "Nauka", Moscow, 1988.

[124] R. S. Laugesen and M. C. Pugh. Linear stability of steady states for thin film and Cahn-Hilliard type equations. *Arch. Ration. Mech. Anal.*, 154(1):3–51, 2000.

[125] Howard A. Levine. Some nonexistence and instability theorems for solutions of formally parabolic equations of the form $Pu_t = -Au + \mathcal{F}(u)$. *Arch. Rational Mech. Anal.*, 51:371–386, 1973.

[126] Howard A Levine and Lawrence E Payne. Nonexistence theorems for the heat equation with nonlinear boundary conditions and for the porous medium equation backward in time. *Journal of Differential Equations*, 16(2):319 – 334, 1974.

[127] Howard A. Levine and Grozdena Todorova. Blow up of solutions of the Cauchy problem for a wave equation with nonlinear damping and source terms and positive initial energy. *Proc. Amer. Math. Soc.*, 129(3):793–805, 2001.

[128] Shengtai Li, Linda Petzold, and Yuhe Ren. Stability of moving mesh systems of partial differential equations. *SIAM J. Sci. Comput.*, 20(2):719–738 (electronic), 1998.

[129] A. E. Lindsay. An asymptotic study of blow up multiplicity in fourth order parabolic partial differential equations. *Discrete and Continuous Dynamical Systems - Series B*, 19(1):189–215, 2014.

[130] J.-L. Lions. *Quelques méthodes de résolution des problèmes aux limites non linéaires*. Dunod; Gauthier-Villars, Paris, 1969.

[131] Changchun Liu and Zhao Wang. Optimal control problem for a sixth-order Cahn-Hilliard equation with nonlinear diffusion. *Electron. J. Differential Equations*, pages No. 127, 13, 2012.

[132] Changchun Liu and Zhao Wang. Optimal control for a sixth order nonlinear parabolic equation. *Math. Methods Appl. Sci.*, 38(2):247–262, 2015.

[133] Alessandra Lunardi. *Analytic semigroups and optimal regularity in parabolic problems*. Progress in Nonlinear Differential Equations and their Applications, 16. Birkhäuser Verlag, Basel, 1995.

[134] Alain Miranville. Asymptotic behavior of a sixth-order Cahn-Hilliard system. *Cent. Eur. J. Math.*, 12(1):141–154, 2014.

[135] Alain Miranville. Sixth-order Cahn-Hilliard equations with singular nonlinear terms. *Appl. Anal.*, 94(10):2133–2146, 2015.

[136] B. Nicolaenko, B. Scheurer, and R. Temam. Some global dynamical properties of a class of pattern formation equations. *Comm. Partial Differential Equations*, 14(2):245–297, 1989.

[137] Amy Novick-Cohen and Lee A. Segel. Nonlinear aspects of the Cahn-Hilliard equation. *Phys. D*, 10(3):277–298, 1984.

[138] H. Ockendon and J.R. Ockendon. *Viscous Flow*. Cambridge Texts in Applied Mathematics. Cambridge University Press, 1995.

[139] W. F. Osgood. Beweis der Existenz einer Lösung der Differentialgleichung $\frac{dy}{dx} = f(x, y)$ ohne Hinzunahme der Cauchy-Lipschitz'schen Bedingung. *Monatsh. Math. Phys.*, 9(1):331–345, 1898.

[140] V.A. Galaktionov P. Álvarez-Caudevilla, J.D. Evans. Countable families of solutions of a limit stationary semilinear fourth-order cahn–hilliard equation i. mountain pass and lusternik-schnirel'man patterns in R^N, 2014.

[141] Jacques Papon, Pierre; Leblond and Paul Meijer. *The Physics of Phase Transitions*. Springer, 2006.

[142] R. E. Pattle. Diffusion from an instantaneous point source with a concentration-dependent coefficient. *Quart. J. Mech. Appl. Math.*, 12:407–409, 1959.

[143] I. Pawlow and W. M. Zajaczkowski. A sixth order cahn-hilliard type equation arising in oil-water-surfactant mixtures. *Communications on Pure and Applied Analysis*, 10(6):1823–1847, 2011.

[144] L. A. Peletier and H. C. Serafini. A very singular solution and other self-similar solutions of the heat equation with convection. *Nonlinear Anal.*, 24(1):29–49, 1995.

[145] L. A. Peletier and D. Terman. A very singular solution of the porous media equation with absorption. *J. Differential Equations*, 65(3):396–410, 1986.

[146] L. A. Peletier and W. C. Troy. *Spatial Patterns*. Progress in Nonlinear Differential Equations and their Applications, 45. Birkhäuser Boston, Inc., Boston, MA, 2001. Higher order models in physics and mechanics.

[147] Linda R. Petzold. A description of DASSL: a differential/algebraic system solver. In *Scientific computing (Montreal, Que., 1982)*, IMACS Trans. Sci. Comput., I, pages 65–68. IMACS, New Brunswick, NJ, 1983.

[148] S. I. Pohožaev. On the eigenfunctions of the equation $\Delta u + \lambda f(u) = 0$. *Dokl. Akad. Nauk SSSR*, 165:36–39, 1965.

[149] P. Poláčik. Examples of bounded solutions with nonstationary limit profiles for semilinear heat equations on $\mathbb{R}$. *J. Evol. Equ.*, 15(2):281–307, 2015.

[150] R. D. Russell, J. F. Williams, and X. Xu. Movcol4: A moving mesh code for fourth-order time-dependent partial differential equations. *SIAM J. Scientific Computing*, 29(1):197–220, 2007.

[151] A.A. Samarskiĭ. *Blow-up in Quasilinear Parabolic Equations*. De Gruyter expositions in mathematics. De Gruyter, 1995.

[152] T. V. Savina, A. A. Golovin, S. H. Davis, A. A. Nepomnyashchy, and P. W. Voorhees. Faceting of a growing crystal surface by surface diffusion. *Phys. Rev. E*, 67:021606, Feb 2003.

[153] Giulio Schimperna and Irena Pawłow. A Cahn-Hilliard equation with singular diffusion. *J. Differential Equations*, 254(2):779–803, 2013.

[154] G. I. Sivashinsky. *Ann. Rev. Fluid Mech.*, 15:179–199, 1983.

[155] N. F. Smyth and J. M. Hill. High-order nonlinear diffusion. *IMA J. Appl. Math.*, 40(2):73–86, 1988.

[156] M. Struwe. *Variational Methods: Applications to Nonlinear Partial Differential Equations and Hamiltonian Systems, Third Edition*. 3]. Springer, 2000.

[157] J. Swift and P. C. Hohenberg. Hydrodynamic fluctuations at the convective instability. *Phys. Rev. A*, 15:319–328, Jan 1977.

[158] Tao Tang. Moving mesh methods for computational fluid dynamics. In *Recent advances in adaptive computation*, volume 383 of *Contemp. Math.*, pages 141–173. Amer. Math. Soc., Providence, RI, 2005.

[159] M.E. Taylor. *Partial Differential Equations III: Nonlinear Equations*. Applied Functional Analysis: Applications to Mathematical Physics. Springer, 2011.

[160] Roger Temam. *Infinite-dimensional dynamical systems in mechanics and physics*, volume 68 of *Applied Mathematical Sciences*. Springer-Verlag, New York, 1988.

[161] S.I. Pohozaev V.A. Galaktionov, E. Miditieri. Variational approach to complicated similarity solutions pf higher-order nonlinear pdes. i, 2009.

[162] M. M. Vaĭnberg and V. A. Trenogin. *Theory of branching of solutions of non-linear equations*. Noordhoff International Publishing, Leyden, 1974. Translated from the Russian by Israel Program for Scientific Translations.

[163] Peter E. Van Keken, David A. Yuen, and Linda R. Petzold. DASPK: a new high order and adaptive time-integration technique with applications to mantle convection with strongly temperature- and pressure-dependent rheology. *Geophys. Astrophys. Fluid Dynam.*, 80(1-2):57–74, 1995.

[164] Juan Luis Vázquez. *The porous medium equation*. Oxford Mathematical Monographs. The Clarendon Press, Oxford University Press, Oxford, 2007. Mathematical theory.

[165] Zhao Wang and Changchun Liu. Some properties of solutions for the sixth-order Cahn-Hilliard-type equation. *Abstr. Appl. Anal.*, pages Art. ID 414590, 24, 2012.

[166] Fred B. Weissler. Single point blow-up for a semilinear initial value problem. *J. Differential Equations*, 55(2):204–224, 1984.

[167] Fred B. Weissler. Rapidly decaying solutions of an ordinary differential equation with applications to semilinear elliptic and parabolic partial differential equations. *Archive for Rational Mechanics and Analysis*, 91(3):247–266, 1986.

[168] T. P. Witelski, A. J. Bernoff, and A. L. Bertozzi. Blowup and dissipation in a critical-case unstable thin film equation. *European J. Appl. Math.*, 15(2):223–256, 2004.

[169] Ya. B. Zel'dovich and A. S. Kompaneets. On the theory of propagation of heat with the heat conductivity depending upon the temperature. In *Collection in Honor of the Seventieth Birthday of Academician A. F. Ioffe*, pages 61–71. Izdat. Akad. Nauk SSSR, "Moscow", 1950.

Chapter 7

Appendices

Appendix A. How many boundary conditions?

We can use perturbation techniques to see how much information an asymptotic description is 'worth', i.e. how many constraints it puts on the behaviour of a function. This number is equivalent to a number of standard boundary conditions, for example of Dirichlet or Neumann type.

As $y \to \infty$, the leading order behaviour of (2.3.35) has been shown to be

$$f_\infty(y) = Cy^{-2/5}\exp(ay^{6/5}) \cdot \cos(by^{6/5} + k) \tag{A.1}$$

By adding a small perturbation $\epsilon g(y)$ to $f_\infty(y)$, $\epsilon << 1$, and substituting this back into (**??**), we can derive how the equation demands g behave, and each separate behaviour of g as $y \to \infty$ that diverges from f_∞ will count as one constraint.

At order ϵ, substituting $f_\infty(y) + \epsilon g(y)$ into (2.3.35) gives

$$g^{(\mathrm{v})}(y) - (5f_\infty^4(y)g(y))' - \frac{1}{6}yg(y) = 0 \tag{A.2}$$

To determine the controlling factor, we make the typical substitution $g(y) = \exp(S(y))$, and with again typical assumption on the relative sizes of $S(y)$ and its derivatives as y approaches the *irregular singular* point at infinity, where the higher derivatives are asymptotically smaller, we can find a balance between the highest order terms of

$$(S'(y))^5 = \frac{1}{6}y \tag{A.3}$$

and so it naturally follows that $g(y) \sim \bar{C}\exp(\frac{5}{6^{6/5}}(1)^{1/5}y^{6/5})$. Upon some thought, it should come as no surprise that f_∞ doesn't appear in the controlling factor -

it appears only in the nonlinear term and so will have only a small effect.

This expression of the dominating term in the behaviour has three possible modes - for each of the positive fifth roots of unity - that grow as $y \to \infty$, each of which correspond to a constraint on ways $f(y)$ is allowed to behave as it approaches the bundle (A.1).

Appendix B. Movcol2

For completeness we sketch some aspects of a Gauss collocation moving mesh codes equivalent to that written about in [105]. In part this is a simple way to exhibit the minor alterations in the approach we've made adopted for our work, but also it can be useful to our scheme in the context of initialization, where stability can become and issue. Thus, we describe here only a Gaussian collocation scheme; it is not a stretch to see how the original conservative scheme works from there. With this example and the schemes presented in Chapter 3, is should also be straightforward to reconstruct Movcol4 [150]. In all instances the moving mesh PDEs are discretized as we have done in 3.2.1.

Movcol2 involves approximating the solution in between grid points (at which u_i and $u_{x,i}$ are specified) with cubic Hermite polynomials; the solution is interpolated like

$$u(x,t) \approx V_i(x,t) := u_i(t)\phi_{0,0}(s) + u_{x,i}(t)h_i(t)\phi_{0,1}(s) + u_{i+1}(t)\phi_{1,0}(s) + u_{x,i+1}(t)h_i(t)\phi_{1,1}(s) \quad \text{(B.1)}$$

where the functions ϕ of the local coordinate $s = (x - x_i)/h_i$ are the cubic Hermite polynomials

$$\begin{aligned} \phi_{0,0}(s) &:= (1+2s)(1-s)^2, & \phi_{0,1}(s) &:= s(1-s)^2, \\ \phi_{1,0}(s) &:= (3-2s)s^2, & \phi_{1,1}(s) &:= (s-1)s^2. \end{aligned}$$

Then we can approximate derivatives of u between the mesh points with the formulae

$$u_x(x,t) \approx \frac{\partial}{\partial x} V_i(x,t) := (1/h_i(t)) \left(u_i(t)\phi'_{0,0}(s) + u_{x,i}(t)h_i(t)\phi'_{0,1}(s) + u_{i+1}(t)\phi'_{1,0}(s) + u_{x,i+1}(t)h_i(t)\phi'_{1,1}(s) \right), \quad \text{(B.2)}$$

and

$$u_t(x,t) \approx \frac{\partial}{\partial t}V_i(x,t) := u_i'(t)\phi_{0,0}(s) + (u_{x,i}'(t)h_i(t) + u_{x,i}(t)h_i'(t))\phi_{0,1}(s) + u_{i+1}'(t)\phi_{1,0}(s) + (u_{x,i+1}'(t)h_i(t) + u_{x,i+1}(t)h_i'(t))\phi_{1,1}(s) - \frac{\partial}{\partial x}V_i(x,t)(x_i'(t) + s^{(i)}h_i'(t)), \quad \text{(B.3)}$$

etc. Note that this discretization is different (beyond being of different order) to the one we use in Section 3.2.1, including the terms $u_{x,i}(t)h_i'(t)\phi_{0,1}(s)$ and $u_{x,i+1}(t)h_i'(t)\phi_{1,1}(s)$. If stability issues occur in this scheme for second order equations, we recommend omitting them, though we have never seen this happen in practice.

The $2N$ equations needed to supplement the mesh equations and boundary conditions come from imposing the PDE/auxiliary problem at the two Gauss points in $[0,1]$ given by

$$\rho_1 = \frac{1}{2}\left(1 - \frac{1}{\sqrt{3}}\right), \quad \rho_2 = \frac{1}{2}\left(1 + \frac{1}{\sqrt{3}}\right). \quad \text{(B.4)}$$

This method is $\mathcal{O}(h^4)$ accurate.

Appendix C. Zeroth Order Nonlinearity - Blow Up Multiplicity in Bounded Domains

We include the beginnings of a research project into the sixth order equivalent of [129], which has some independent interest although we had insufficient time to complete.

Preliminaries: In this section we consider the problem

$$u_t = \Delta^3 u + f(u) \quad \text{(C.1)}$$

$$u(x,0) = 0 \quad \text{for} \quad x \in \Omega, \quad \text{(C.2)}$$

$$u(x,t) = 0 \quad \text{for} \quad x \in \partial\Omega \times (0,T) \quad \text{(C.3)}$$

on bounded domains $\Omega \subset \mathbb{R}^N$, with convex nonlinearities f such that $f(0) = 1$. We will mostly be concerned with how the geometry of the domain affects the location and number of blow-up points, examining the small time behaviour to see where the singularities begin to emerge. It may also prove of interest to examine

the connection, if any, between these results and those on the multiplicity of blow-up profiles on unbounded domains examined in [24].

To lay the groundwork we first take the homogeneous initial condition (C.2), as we expect that the ways in which u evolves under (C.1) to in general depend heavily on initial data. The homogeneity means that away from the boundary, the behaviour will be governed by the nonlinear ODE $u_t = f(u)$ and the effects of the tri- Laplacian operator Δ^3 will only be observed in a boundary layer so that we can impose (C.3). As time passes, the boundary layer behaviour will spread through the domain and the interactions with the homogeneous behaviour will determine if, when and where blow-up will occur.

This is really a continuation of the equivalent work on the second and (primarily) fourth order equations discussed in [129], which contrasts the relatively well-behaved second order model with the less predictable effects bestowed on the system by a fourth order operator. In particular, The maximum principle for second order equations ensures that the local maxima of u, which are candidates for blow-up points, will manifest exactly at points in Ω which are farthest away from the boundary. Whether these are unique or not will of course depend on the domain. However, the fourth order operator ensures that behaviour in the boundary layer is not monotone and the interplay of the local maxima that occur in it as it spreads leads to a far more diverse array of possibilities for blow-up. Delicate asymptotic analysis is required to describe this process.

Sixth order operators are more exotic still and we expect this line of inquiry will unearth some interesting results.

One Dimensional Geomteries: To begin with, we consider the problem posed on the one-dimensional strip $[-L, L]$. Here, the only notion of geometry is the length of the strip, so we examine the dependence of the solution on $\varepsilon = L^{-1}$, giving us the singular perturbation problem

$$\begin{aligned} u_t = \varepsilon^6 u_{xxxxxx} + f(u), \quad -1 < x < 1, \quad 0 < t < T_c(\varepsilon) \\ u(\pm 1, t) = u_x(\pm 1, t) = u_{xx}(\pm 1, t) = 0, \quad u(x, 0) = 0, \end{aligned} \tag{C.4}$$

where $T_c(\varepsilon)$ is the blow-up time, which depends on the length of the domain.

It is immediately clear that the outer solution, away from the boundaries, is given by

$$\frac{\mathrm{d}u_0}{\mathrm{d}t} = f(u_0), \quad 0 < t < t_c, \quad u_0(0) = 0, \tag{C.5}$$

where t_c is the blow-up time of the homogeneous system (ensured to be finite by

the convexity of f). In the small-time regime, this gives us that

$$u_0(t) = u_0(0) + tu_0'(0) + O(t^2) = tf(u_0(0)) + O(t^2) \approx t. \tag{C.6}$$

We cannot impose the anchoring conditions at either side of the interval on this solution and so we introduce boundary layers via looking for a solution of the form

$$u(x,t) = u_0(t)v(\eta) \tag{C.7}$$

where we choose $u_0(t)$ as the time dependent term so the scale of the solutions in the inner (boundary layer) and outer regions agree. Then, on the rightmost boundary, the variable $\eta = \frac{1-x}{\phi(t)}$ is chosen to pick up the desired behaviour, the scaling ϕ depending on t to reflect the spreading of the boundary layer as the solution evolves. We determine $\phi(t)$ by plugging (C.7) into (C.4) to get

$$f(u_0(t))v(\eta) - \eta u_0(t)\frac{\phi'(t)}{\phi(t)}v_\eta(\eta) = \frac{\varepsilon^6}{\phi^6(t)}u_0(t)v^{(\mathrm{vi})}(\eta) + f(u_0(t)v(\eta)). \tag{C.8}$$

For small solutions, $f \approx 1$, and so we can pick $\phi(t) = \varepsilon u_0^{1/6}(t)$ to give the fullest balance for an equation in η, and in the small time regime where $u_0(t) \approx t$ this means η resembles a similarity variable. The equation for $v(\eta)$ is then

$$v^{(\mathrm{vi})}(\eta) + \frac{\eta}{6}v'(\eta) - v(\eta) = 1, \tag{C.9}$$

with boundary conditions

$$v(0) = v'(0) = v''(0) = 0, \quad v(\eta) \to 1 \text{ as } \eta \to \infty. \tag{C.10}$$

The relevant dynamics occur at the large η limit, and so we introduce the rescaled variable $\xi = \theta\eta,\ \theta \ll 1$ to give the equation

$$\theta^6 v^{(\mathrm{vi})}(\xi) + \frac{\xi}{6}v'(\xi) - v(\xi) = 1 \tag{C.11}$$

and then make the customary WKBJ substitution

$$v(\xi) \sim 1 + \exp[\frac{1}{\delta}\sum_{k=0}^{\infty}\delta^k\psi_k(\xi)], \quad \delta \ll 1, \tag{C.12}$$

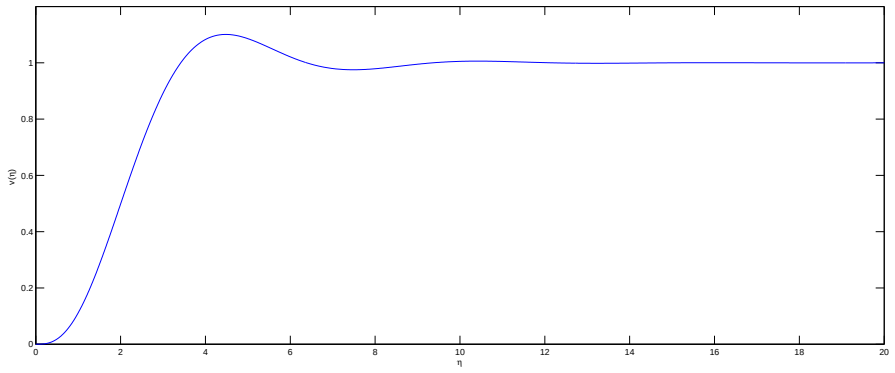

Figure 7-1: Behaviour in the Boundary Layer.

so (C.11) becomes, to leading order,

$$\left(\frac{\theta^6}{\delta^6}(\psi_0'(\xi))^6 + \frac{1}{\delta}\frac{1}{6}\xi\psi_0'(xi)\right)\exp(\psi_0/\delta) - 1 - \exp(\psi_0/\delta) \sim 1. \tag{C.13}$$

The balance given by $\theta = \delta^{5/6}$ gives that the behaviour is governed by the expression

$$(\psi_0'(\xi))^6 = -\frac{1}{6}\xi\psi_0'(\xi) \implies \psi_0 \sim (-1)^{1/5}\frac{5}{6^{6/5}}\xi^{6/5}. \tag{C.14}$$

Since the solutions in the inner region must match up with those in the outer, only solutions which decay as $\eta \to \infty$ are permitted. This demands that $(-1)^{1/5}$ must take the values $\exp(3\pi i/5)$, $\exp(\pi i)$, or $\exp(7\pi i/5)$, giving that v is approximated by the three parameter family

$$\begin{aligned} &v(\eta) \sim 1 + \left[A\exp\left(e^{3\pi i/5}\beta\eta^{6/5}\right) + B\exp\left(e^{\pi i}\beta\eta^{6/5}\right) + C\exp\left(e^{7\pi i/5}\beta\eta^{6/5}\right)\right], \\ &A, B, C \in \mathbb{R},\ \beta = \frac{5}{6^{6/5}}. \end{aligned} \tag{C.15}$$

This can be presented in a more illuminating manner using Euler's identity:

$$\begin{aligned} &v(\eta) \sim 1 + B\exp(-\beta\eta^{6/5}) + D\exp(a\eta^{6/5})\cos(b\eta^{6/5} + E) \text{ as } \eta \to \infty, \\ &B, D, E \in \mathbb{R},\ a = \beta\cos(3\pi/5),\ b = \beta\sin(3\pi/5). \end{aligned} \tag{C.16}$$

This clearly shows that in the boundary region, the damped oscillatory behaviour gives rise to various local maxima, the nature of which will determine the way in which blow-up manifests. This is represented pictorially in figure 7-1. The inherent symmetry of the problem means that the left hand boundary behaviour is simply a reflection of this behaviour, and so the small- time asymptotic representation has first order term given by, loosely speaking, a superposition of both

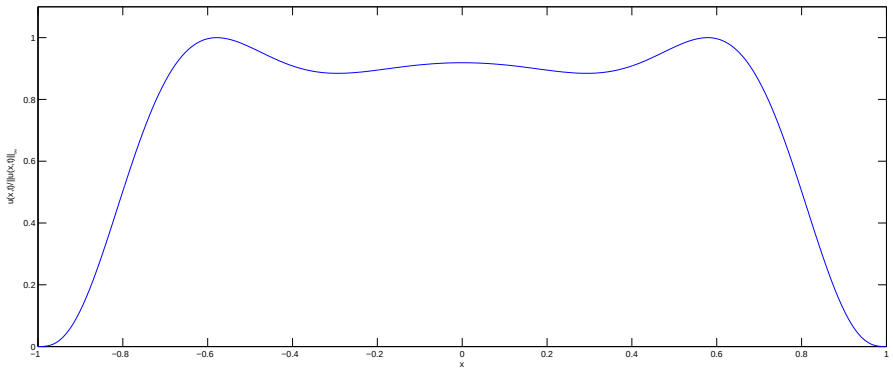

Figure 7-2: Asymptotic approximation of u for $\varepsilon = 0.1$.

boundary layer solutions minus a constant to account for their overlap:

$$u(x,t) \sim u_0(t) + u_0(t)\left[v\left(\frac{1-x}{\varepsilon u_0^{1/6}(t)}\right) + v\left(\frac{1+x}{\varepsilon u_0^{1/6}(t)}\right) - 2\right]. \tag{C.17}$$

Figure 7-2 shows this with the approximation for u scaled such that $||u||_\infty = 1$, an arbitrary but somewhat natural choice as the η variable is (approximately) scale invariant for sufficiently small t. When we compare with numerical simulations of the full problem, we can see they appear close to what we see in this figure under the same scaling for any t up to the point where the $O(t^2)$ term becomes non-negligible compared to $u_0(t)$.

We observe this in 7-3, where the qualitative behaviour is very similar to our asymptotic approximation (the relatively more pronounced peaks, though, suggest that even at $t = 0.5$, the $O(t^2)$ term is too big to be ignored).

Like in the fourth order case, then, the multiplicity of blow up points depends on whether the local maxima that appear in the boundary regions have time to meet before the blow-up time. The speed at which these maxima propagate is described by the $\varepsilon u_0^{1/6}(t)$ term, and so if the location of the local maximum is given by η_0, then we have one, central blow up point if $1 \leq \eta_0 \varepsilon u_0^{1/6}(T)$, where T is the blow up time, otherwise we have two separate points which blow up distributed symmetrically about the origin. Numerical simulations give us a rough estimate for the critical value of $\varepsilon \approx 0.173$ below which the latter occurs.

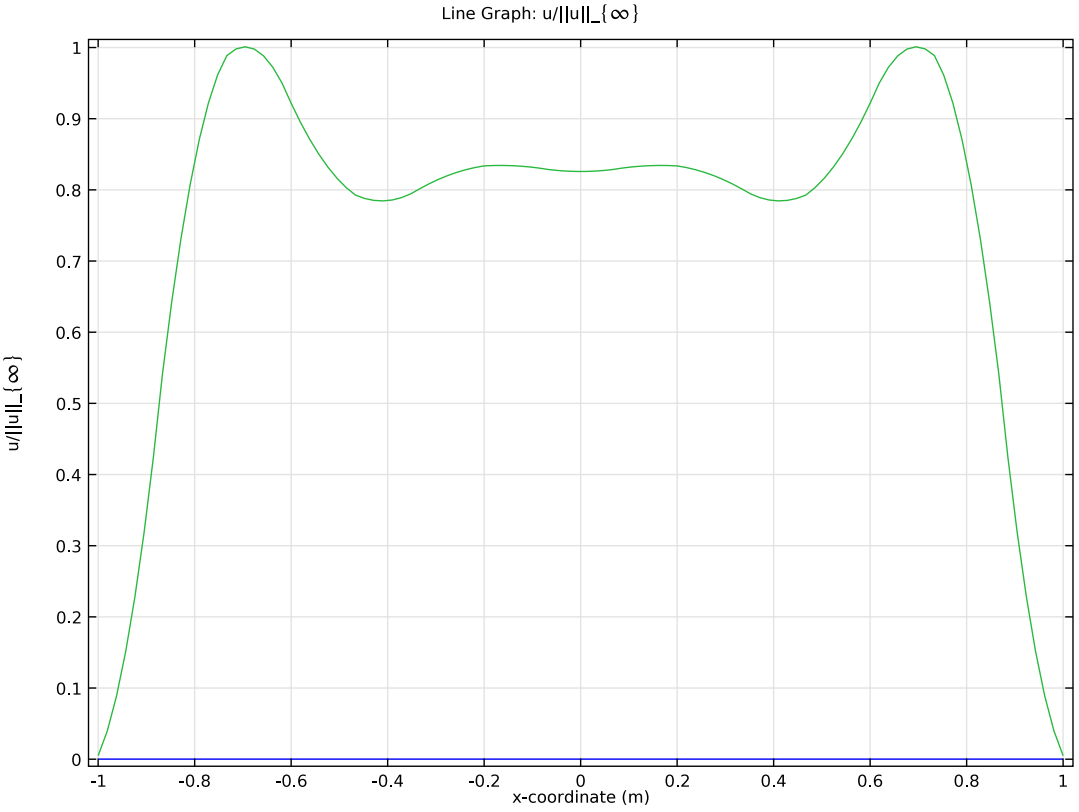

Figure 7-3: Numerical solution of (C.4) for $\varepsilon = 0.1$, $t = 0.5$.